



**HAL**  
open science

# Adsorption and organisation of molecules at the solid/liquid interfaces on nanostructure materials

Marwa Assaf

► **To cite this version:**

Marwa Assaf. Adsorption and organisation of molecules at the solid/liquid interfaces on nanostructure materials. Material chemistry. Université Montpellier, 2021. English. NNT : 2021MONTTS104 . tel-03639156

**HAL Id: tel-03639156**

**<https://theses.hal.science/tel-03639156>**

Submitted on 12 Apr 2022

**HAL** is a multi-disciplinary open access archive for the deposit and dissemination of scientific research documents, whether they are published or not. The documents may come from teaching and research institutions in France or abroad, or from public or private research centers.

L'archive ouverte pluridisciplinaire **HAL**, est destinée au dépôt et à la diffusion de documents scientifiques de niveau recherche, publiés ou non, émanant des établissements d'enseignement et de recherche français ou étrangers, des laboratoires publics ou privés.

# THÈSE POUR OBTENIR LE GRADE DE DOCTEUR DE L'UNIVERSITÉ DE MONTPELLIER

En Chimie des matériaux

École doctorale : Sciences Chimiques Balard

Unité de recherche : Institut Charles Gerhardt de Montpellier UMR 5253

## Adsorption et organisation de molécules aux interfaces solide/liquide dans des matériaux nanostructurés

Présentée par Marwa ASSAF

Le 10 decembre 2021

Sous la direction de Benedicte PRELOT du Directeur de thèse  
et Gaelle GASSIN du co-Directeur de thèse  
Devant le jury composé de

Isabelle BEURROIES, Prof, Université de Aix Marseille, MADIREL

Emmanuel BENICHOU, Prof, Université Claude Bernard Lyon 1

Alexander SACHSE, CR, IC2MP de Poitiers

Didier TICHIT, DR, Université de Montpellier, ICGM

Sandrine DOURDAIN, DR, ICSM CEA Marcoule

Benedicte PRELOT, DR, Université de Montpellier, ICGM

Gaelle GASSIN, MC, Université de Montpellier, ICGM

Rapportrice

Rapporteur

Examineur

Président du jury

Invité

Directrice de thèse

Co-directrice de thèse



UNIVERSITÉ  
DE MONTPELLIER



## Acknowledgments

During my Ph.D. studies, I have thought a lot about science and life, but I have never thought of the moment of writing the acknowledgements of my thesis. At this moment, after finishing writing all chapters of my thesis, I realize the acknowledgment is probably one of the most difficult parts for me to complete. I have got support and help from so many people, and it is hard to put all my gratitude into words. This thesis cannot be accomplished without them.

First of all, I would like to thank the AIME (Agregates, Interfaces and Materials for Energy) team of and the MPH (Hybrid and Porous Material) department, of the Charles Gerhardt Institute of Montpellier (ICGM) and its directors, Jerzy Zajac, Laure Monconduit, the head of the D3 department (Porous and Hybrid Materials), Corine Gerardin and the head of the doctoral school Jean Jacques Vasseur for welcoming me during all this time.

I would like to express my sincere thanks to my thesis director Benedicte Prelot and my co-director Gaelle Gassin at the ICGM laboratory for their welcome. I would like to express my gratitude to them for their support, interest, and availability during these three years and the trust they have placed in me throughout this work, especially during the most difficult times. I thank them so much for their scientific contribution and their wise advice. I thank them for their optimism, enthusiasm, daily help, and advice, especially when writing this manuscript. I hope they find, beyond these few words, the testimony of my sincere gratitude and admiration. A special thanks to Benedicte for being not only the director of my thesis but also a parent to me, thanks for her invitation to home, she encouraged me every day to do better, she always said: "I trust you".

A part of this work took place at ICGM-Galera with the MACS team where I was welcomed by Anne Galarneau whom I thank for this opportunity. This collaboration has brought me a precious openness thanks to the help of Jeremy Rodriguez, in the post-synthesis of zeolite.

I would like to thank Pierre-Marie Gassin for his valuable help and regular discussions in the field of non-linear optics as well as his help in writing articles.

I thank the members of the jury, Isabelle Beurroies and Emmanuel Benichou who agreed to be rapporteurs and to judge my manuscript, as well as Sandrine Dourdain, Alexander Sachse and Didier Tichit for their participation in my thesis jury.

I would also like to thank Mr. Jerzy Zajac for his advice and his valuable help, especially with the ITC part. Thanks also to Phillipe Gaveau and Emmanuel Fernandez for their help in Si-solid state NMR measurements and for discussing the results. Also, thanks to Amine Geneste for his valuable help in ITC measurements.



I would like to thank my parents and parents in law who still have pushed and encouraged me during my studies which made me have the best education possible.

I would also like to thank my colleagues, in building 15 and 17, which allowed me to decompress and avoid thinking about the various worries that I may have met during these three years of the thesis.

I would like to thank Fabrice, Moulay, Nicolas Louvain for their support. I can't forget Marie-Pierre for her standing with me all the time by giving always positive vibes.

A big thanks to all my friends, for all the good moments spent with you Nina, Hanna, Salma, Hao, Lotfi and Ali (with whom I have pleasantly shared the office during these years) thank you for having been present in the difficult moments, for all the laughter and delighted to count you among my friends, I wish you all the best. Especial thanks to Maha Ismail for her support. Thanks to all people I met during these years. A special thanks to Nina for her standing beside me and helping me a lot.

The last word will be for my love, Mustafa, there are no words can explain my thanks for him for being always beside me especially in the hard moment and for his daily encouragement, his patience, understanding and ability to make me laugh the moment I expect it less.



## Résumé

La pollution des eaux, souvent le résultat des activités humaines, est une question récurrente, une problématique de santé publique, à la fois environnementale et stratégique. Les polluants organiques (colorants, pesticides, médicaments...) sont souvent de nature complexe et difficilement dégradables. Certains processus de décontamination reposent sur des adsorbants présentant des propriétés spécifiques telles qu'une forte capacité d'adsorption et une grande accessibilité, ce qui est le cas des matériaux nanostructurés comme les zéolithes.

Notre objectif était de comprendre les mécanismes d'adsorption aux interfaces solide/liquide. En particulier, il s'agissait de déterminer l'impact de la porosité sur les mécanismes d'interactions, avec des matériaux ayant une capacité d'adsorption élevée et différents niveaux de porosité, et d'étudier l'effet du rapport Si/Al et du solvant sur le processus d'adsorption. Une zéolite de type faujasite (FAU) a été sélectionnée en raison de la possibilité de décliner à partir de ce matériau de départ une série de faujasites dites hiérarchiques. Les faujasites modifiées ont été préparées par post-synthèse en utilisant un traitement alcalin en présence d'agent structurant. Plusieurs méthodes de caractérisation (structurales, texturales, ...) ont été réalisées telles que la physisorption d'azote ( $N_2$ ), la spectroscopie RMN- $^{29}Si$ , la fluorescence et la diffraction des Rayons-X (DRX).

Les conditions expérimentales (préparation des suspensions, temps d'équilibre, solvant et rapport solide/liquide) sont des éléments importants pour sélectionner les conditions finales pour réaliser les isothermes d'adsorption. Ces expériences ont été réalisées avec un colorant linéaire (sDiA hemicyanine) adsorbé sur la faujasite commerciale.

L'enthalpie de déplacement associée à l'adsorption des molécules de colorant a été déterminée par Calorimétrie Isotherme de Titration. Cette approche permet d'évaluer directement l'effet de la porosité, et de la chimie de surface sur les effets enthalpiques. En outre, la diffusion de seconde harmonique (SHS) a été utilisée comme technique locale pour évaluer l'interaction et l'organisation de colorant à l'interface.

Une capacité d'adsorption élevée est obtenue pour le colorant linéaire contrairement aux colorants volumineux (Basic Fushin). Pour la série de zéolithe poreuse, la capacité de sorption de sDiA reste constante sauf pour la FAU plus modifiée dont la capacité est plus faible. En revanche, pour le Basic Fushin, cette capacité augmente progressivement avec l'augmentation de la porosité. D'autres études ont été réalisées pour sDiA sur la faujasite initiale, et en présence de différents solvants. La capacité d'adsorption en présence de solvants non aqueux est plus faible que dans l'eau. Cette

diminution est due à la différence d'activité de l'acide de Bronsted qui conduit à des molécules moins organisées aux interfaces.

L'analyse des mesures SHS permet de quantifier les corrélations dans un système moléculaire. L'analyse permet de mettre en évidence un indicateur appelé  $i_4$  fortement lié aux interactions et à l'organisation moléculaire. Ce paramètre  $i_4$  est élevé pour le colorant linéaire dans les conditions suivantes : solvant aqueux et le solide microporeux, ce qui indique alors une forte corrélation entre molécules. En outre, la valeur absolue élevée de l'enthalpie de déplacement révèle une forte interaction entre ce colorant et le matériau. Ces valeurs deviennent moins importantes dans la faujasite la plus mésoporeuse. Cependant, dans le cas des molécules volumineuses, le paramètre  $i_4$  n'est pas significatif. Pour ce qui concerne l'enthalpie de déplacement, elle est similaire pour les 2 colorants sur la faujasite mésoporeuse, mais n'a pas pu être déterminée pour la faujasite initiale.

Ainsi, nous avons réussi à combiner des approches à la fois macroscopiques et locales pour mettre en évidence, de façon innovante, les effets du confinement lors des processus d'adsorption.

**Mots-clés** : Physicochimie ; Optique non linéaire ; Adsorption ; Confinement ; Matériaux nanostructurés ; Organisation moléculaire

## Abstract

Water pollution is one of our most strategic recurring problems that are usually a result of human activities. The source of these contaminants is mostly the organic pollutants (dyes, pesticides, phenols, drugs...) that are considered complex and poorly degradable. The decontamination processes are often based on the use of adsorbents with specific properties such as high adsorption capacity and accessibility, which is the case of nanostructure materials such as zeolites, clays, porous silica....

Our objectives were to study in details the fundamental physicochemical and adsorption mechanisms at the solid liquid interface. Particularly, we focus on the impact of porosity on the interactions with materials having high sorption capacity, the different levels of porosity (micro and meso), the effect of the material Si/Al ratio and the solvent on the adsorption process. A well-known faujasite type zeolite (FAU) has been selected due to its possibility to obtain hierarchical faujasite. Thus, modified faujasite was post synthesized using an alkaline treatment in the presence of surfactant (structuring agent). Several characterization methods have been carried out such as N<sub>2</sub>-Sorption-Isotherm, <sup>29</sup>Si-NMR, X-ray fluorescence, and X-ray diffraction to evaluate structural and textural properties.

Several organic molecules were chosen for their properties of size, charge, functional group to determine their sorption efficiency. Cationic molecules showed the highest adsorption capacity compared to the neutral and anionic molecules.

The experimental conditions tested (isotherm protocols with the suspension preparation, equilibrium times, solvents, and Solid/liquid ratio) are essential steps to select the conditions to carry out the adsorption isotherm. These experiments have been performed for linear dye adsorption onto commercial Faujasite.

The displacement enthalpy associated with the adsorption of the dye molecules was estimated using Isothermal Titration Calorimetry (ITC). This approach offers the possibility to evaluate the effect of porosity, and the surface chemistry (hydrophilicity) using direct measurements as a function of the loading. In addition, Second Harmonic Scattering (SHS) has been used as a local technique to evaluate the interaction and organization of the dyes at the interface.

A high sorption capacity is obtained for the linear dye (sDiA hemicyanine) in contrast to the bulky dyes (Basic Fushin) towards the commercial FAU. The sorption capacity of sDiA remains constant except for the highly modified FAU which becomes lower. However, for BF, this capacity increases progressively with increasing the porosity. Other studies were performed for sDiA onto FAU in the presence of various solvents. The adsorption capacity in the presence of solvents is lower than in

water. This decrease is probably due to the difference in the activity of the Bronsted acid which leads to less organized molecules at FAU surfaces.

The SHS measurements analysis allows to quantify the correlations in the molecular system. The analysis puts in evidence the indicator called  $i_4$  highly related to molecular interactions and organization. This  $i_4$  parameter is high for the linear dye for conditions: water solvent and microporous solid, which indicates a high correlation between the dye's molecules. In addition, the high absolute value of the displacement enthalpy reveals a strong interaction between this dye and FAU material. These values become less significant in mesoporous FAU. However, in the case of bulky molecules, the  $i_4$  is not significant for both FAUs, and the displacement enthalpy was not determined for FAU and its similar to sDiA in the case of mesoporous FAU.

Finally, the confinement effect on the adsorption of sDiA and Basic Fushin has been highlighted when the enthalpy and the  $i_4$  indicator become more negative. Thus, we succeed to combine such macroscopic and local approaches to evidence the effect of confinement on the sorption behavior.

**Key words:** Physical chemistry; Non-linear Optics; Confinement; Adsorption; Molecular organization; Nanostructured materials



## List of abbreviation

C<sub>1</sub>DiA or sDiA: trans-4-[4-(Dimethylamino)styryl]-1-methylpyridinium iodide

C<sub>4</sub>DiA: trans-4-[4-(Dibutylamino)styryl]-1-methylpyridinium iodide

C<sub>16</sub>DiA: 4-Di-16-ASP (4-[4-(Dihexadecylamino)styryl]-N-Methylpyridinium Iodide)

BF: Basic fuchsin

BP: Blue patent

BG: Brilliant green

CV: Crystal violet (CV)

AO: Auramine-O

MG: Malachite green

MB: Methylene blue

Rh-B: Rhodamine-B

MO: Methyl orange

OTC: Oxytetracycline HCl

MT: Morantel tartrate Hydrate

C<sub>18</sub>TAB: Octadecyltrimethylammonium bromide surfactants

SC: supercage

BAS: Bronsted acid site

$\Delta H$ : Enthalpy change

$\Delta S$ : entropy change

$\Delta G$ : Gibbs free energy change

Mw: Molecular weight

FAU: Faujasite

FAU-0: commercial Faujasite (CBV720)

FAU-1: modified FAU with NaOH/Si = 0.075

FAU-2: modified FAU with NaOH/Si = 0.095

FAU-2a: modified FAU with NaOH/Si = 0.125



FAU-2b: modified FAU with NaOH/Si = 0.15

FAU-3: modified FAU with NaOH/Si = 0.25

DMSO: dimethyl sulfoxide

S/L: solid/liquid ratio

IUPAC: international union of pure and applied chemistry

$\lambda$ : wavelength

$S_{\text{ext}}$ : external surface

$V_{\text{micro}}$ : microporous volume

$V_{\text{meso}}$ : mesoporous volume

TGA: thermogravimetric analysis

SEM: scanning electron microscopy

XRD: X-ray fluorescence

DLS: Dynamic Light Scattering

$\zeta$ : Zeta potential

XRF: Wavelength-dispersive X-Ray fluorescence

BET: Brunauer-Emmett-Teller

SHS: Second Harmonic Generation

SHG: Second Harmonic Generation

HRS: Hyper-Rayleigh Scattering

ITC: Isothermal Titration Calorimetry

$^{29}\text{Si-NMR}$ : silicon solid state nuclear magnetic resonance

UV: Ultra Violet



## Table of contents

Acknowledgments .....	3
List of abbreviation.....	11
List of figures .....	19
Résumé étendu .....	25
General introduction .....	42
Chapter I: State of the art.....	48
1 Colored molecules and Dyes .....	48
1.1 Dyes in our civilization.....	48
1.2 Natural and synthetic dyes.....	48
1.3 Probe organic molecules .....	49
1.4 Processes for dyes removal.....	50
1.4.1 Coagulation-flocculation method.....	50
1.4.2 Biological method.....	51
1.4.3 Membrane filtration.....	51
1.4.4 Chemical oxidation .....	51
1.4.5 Photodegradation.....	51
1.4.6 Adsorption processes .....	52
1.4.7 Adsorption of dyes .....	53
2 Zeolites .....	54
2.1 Introduction to zeolites .....	54
2.2 Classification of zeolite.....	55
2.3 Applications of zeolites.....	55
2.3.1 Ionic exchange .....	56
2.3.2 Adsorption and separation.....	57
2.3.3 Heterogeneous catalysis .....	57
2.4 History and characteristic of zeolite Y (Faujasite-type).....	58
2.5 Hierarchical zeolites .....	60
2.5.1 Definition and properties of hierarchical zeolites.....	60
2.5.2 Synthesis of hierarchical faujasite material via mixed route .....	61
3 Physicochemical phenomena inside nanometric structures .....	69
3.1 Confinement effect .....	70
3.2 Selectivity between host and guest .....	71
4 Experimental approaches to probe adsorption and interfacial phenomena.....	72
4.1 Thermodynamic approaches of the adsorption and the particular case of calorimetric measurements.....	72

4.1.1	Enthalpy of adsorption or enthalpy of displacement.....	73
4.1.2	Study of molecular adsorption in a confined system.....	73
4.2	The molecular approach: Non-Linear Optics.....	78
4.2.1	Second Harmonic Generation (SHG).....	78
4.2.2	Second Harmonic Scattering (SHS).....	79
4.2.3	Hyper Rayleigh Scattering (HRS).....	80
4.2.4	Properties probed using interfacial second harmonic processes .....	80
5	Conclusion .....	83
6	The objectives of this work, choice of material, and strategy of the thesis.....	84
Chapter II: Experimental part.....		92
Molecules.....		92
1.1	Outlook.....	92
1.2	2 D molecules .....	92
1.3	3D molecule.....	94
1.4	UV-visible spectroscopy characterization .....	94
Faujasites.....		96
1.5	Commercial Faujasite .....	96
1.6	Synthesis of modified faujasites.....	96
1.7	Characterization methods for solids .....	98
1.7.1	Scanning electron microscopy (SEM) .....	99
1.7.2	Dynamic Light Scattering (DLS).....	100
1.7.3	Zeta ( $\zeta$ ) potential.....	101
1.7.4	X-Ray diffraction (XRD).....	103
1.7.5	Wavelength-dispersive X-Ray fluorescence (XRF).....	104
1.7.6	Nitrogen-sorption isotherm at 77K .....	105
1.7.7	$^{29}\text{Si}$ solid state NMR.....	111
1.7.8	Thermogravimetric analysis (TGA) .....	113
Adsorption isotherms determination.....		113
1.8	By UV-Visible spectrometry.....	114
1.9	By SHS.....	116
Titration calorimetry measurements .....		117
1.10	Generalities .....	117
1.11	Theory.....	117
1.12	Instrument.....	118
1.13	Protocol .....	119
1.14	Data treatment.....	120

Second Harmonic Scattering measurement.....	121
1.15 Introduction to non-linear optics.....	121
1.15.1 Basic introduction.....	121
1.15.2 Molecular view.....	122
1.16 Second Harmonic Generation (SHG).....	123
1.17 Hyper-Rayleigh Scattering (HRS).....	124
1.17.1 HRS Principle.....	124
1.18 Second Harmonic Scattering (SHS).....	125
1.18.1 SHS Principle.....	125
1.18.2 Properties probed.....	125
1.18.3 Coherence between molecules.....	125
1.18.4 Experimental setup of SHS.....	126
Conclusions.....	129
Chapter III: Characterization of zeolite and selection of the conditions for the adsorption process .	135
1 Characterization techniques of zeolitic materials.....	135
1.1 X-Ray fluorescence.....	135
1.2 Thermogravimetric analysis (TGA).....	136
1.3 N <sub>2</sub> -sorption isotherm.....	137
1.4 X-Ray diffraction.....	139
1.5 <sup>29</sup> Si-NMR.....	140
2 Selection of experimental conditions of the procedure performed for sDiA adsorption onto commercial Faujasite.....	142
2.1 Effect of isotherm preparation.....	143
2.2 Effect of solid/liquid ratio (S/L ratio).....	144
2.2.1 In water medium.....	144
2.2.2 In ethanol medium.....	145
2.2.3 By SHS.....	146
2.3 Effect of time on the stability of FAU suspension.....	149
2.3.1 In water for solid/liquid ratio 0.25 g/l.....	149
2.3.2 For solid / liquid ratio 0.05 g/l in water and in ethanol.....	150
2.4 Effect of contact time on sDiA and FAU suspension.....	156
2.4.1 In water medium.....	156
2.4.2 In ethanol medium.....	160
2.4.3 In 50% water- 50% ethanol medium.....	163
2.5 Effect of sonication.....	165
2.6 Effect of ionic strength.....	166

2.7	Effect of the presence of particles on SHS plot .....	168
3	Adsorption of organic molecules onto Faujasite.....	169
3.1	Organic molecules panel .....	170
3.2	Charge impact.....	174
3.3	Size effect .....	175
3.4	Effect of counter ion on Malachite green adsorption.....	176
3.5	Effect of ethanol on sDiA adsorption to FAU .....	177
4	Comparison between FAU-3 and Al-MCM-41.....	178
5	Comparison between adsorption of dyes using ITC approach.....	180
6	Conclusion .....	182
Chapter IV: The Driving Forces of Cationic Dye Adsorption, Confinement and Long Range Correlation in Zeolitic Materials .....		187
1	Written manuscript submitted in Langmuir Journal .....	188
Conclusion .....		209
Chapter V: Effect of modification of the porosity of Zeolite FAU on the adsorption of dyes: contribution of global and local techniques.....		211
1	Written manuscript submitted in Journal of colloid and interface science .....	212
Conclusion .....		255



## List of figures

Figure 1: Histogramme montrant la capacité d'adsorption de différentes molécules organiques sur FAU (Si/Al=15) en fonction de leur état ionique. Blue patent (BP), Brilliant green (BG), Crystal violet (CV), Auramine-O (AO), Malachite green (MG), Methylene blue (MB), Rhodamine-B (Rh-B), Methyl orange (MO), Oxytetracycline HCl (OTC) and Morantel tartrate Hydrate (MT).....	34
Figure 2: Enthalpies d'adsorption (cercle plein $\Delta H$ pour 1DiA, carré pour BF) et $I_4$ (cercle vide $I_4$ pour 1DiA) à la charge maximale de colorants. ....	37
Figure 3: 1) Faujasite frame with highly organized channels structures. In gray a zoom for 2), 3), 4). Zeolite structure consists of Si, Al, O and negative charge obtained after Si substitution with Al that is compensated with cation form. 2) Representation of a possible molecular distribution in a pore with protons water molecules. Negative sites of the Faujasite frame are in red. 3) Representation of a possible configuration for two interacting dyes within the Faujasite pore. 4) Representation of a second possible configuration for two interacting dyes within the Faujasite pore. The blue dotted line represents an interaction. ....	44
Figure 4 : DiA structure $(14.5+n) \text{ \AA}/4.3\text{ \AA}$ for length/height ratio with $n=1, 4,$ and $16,$ with their charge transfer through double bonds. ....	50
Figure 5 : 3D Zeolite network showing the interconnectivity of the channels taken from Zeolyst website. ....	55
Figure 6 : Ion exchange mechanism between cationic molecules and zeolite compensating ions. ....	56
Figure 7 : A Faujasite framework with only the tetrahedral central atoms (Si or Al) <sup>20</sup> .....	59
Figure 8 : Mechanism of desilication involved during alkaline treatment <sup>57</sup> .....	64
Figure 9 : Diagram showing the influence of the Si / Al ratio on desilication process <sup>27</sup> .....	65
Figure 10 : Schematic summary of the steps in the recrystallization of zeolite.....	66
Figure 11 : Representation of the possible phenomena that can occur at the interface. ....	69
Figure 12 : Effect of pore size on the adsorption of methylene blue onto titania nanotubes at low coverage ( $\Theta = 30\%$ ) and high coverage where the monolayer is completely filled ( $\Theta = 100\%$ ) <sup>95</sup> .....	75
Figure 13 : Effect of pore size on the heat of adsorption of various alkanes on 5 types of zeolites (FER, TON, MFO, MOR and FAU). R eported from reference <sup>96</sup> . ....	76
Figure 14 : A schematic interpretation of the result obtained from the reference <sup>119</sup> . SHS intensity for the adsorption of MO onto LDH-CO <sub>3</sub> and LDH-NO <sub>3</sub> with lateral adsorption and intercalation for LDH-CO <sub>3</sub> and LDH-NO <sub>3</sub> respectively.....	82
Figure 15 : On the left, magnitude of $I_4$ for the control molecule DiA and water. On the right, $I_4$ for different KCl (square) and NaCl (round) concentrations taken from the reference <sup>122</sup> . ....	83
Figure 16 : General structure of C <sub>n</sub> DiA molecule .....	93
Figure 17 : Molecular representation of dye molecules and their sizes a) C <sub>1</sub> DiA b) C <sub>4</sub> DiA and c) C <sub>16</sub> DiA using Avogadro's software. ....	93
Figure 18 : The molecular representation of Basic fuchsin molecule and its size using Avogadro's software.....	94
Figure 19 : Experimental photo absorbance UV-Visible of commercial Faujasite (Si/Al = 15), dye alone in water solvent, dye in the presence of FAU particles and after adsorption and after filtration (supernatant).....	95
Figure 20 : Procedure used for the modification of FAU material via mixed route (desilication process by NaOH in the presence of structuring agent CTAB). ....	98
Figure 21 : SEM image for commercial FAU (FAU-0) (Si/Al = 15) of trade name CBV-720 purchased from Zeolyst international .....	99



Figure 22 : DLS for two faujasite sample (FAU-0) prepared in suspension with ultra-pure water (a) after 30 min of preparation while (b) after 24 h with Pdl 0.5 and 0.7 respectively. Green peak corresponds to the population in the fresh suspension (as prepared) while the red corresponds to the new population. ....	101
Figure 23 : Schematic representation of zeta potential <sup>126</sup> .....	102
Figure 24 : Representative diagram of the X-ray diffraction phenomenon .....	103
Figure 25 : Diffractogram for FAU (Si/Al = 15).....	104
Figure 26 : Classification of physisorption isotherm, according to IUPAC <sup>131</sup> .....	106
Figure 27 : t-plot for the N <sub>2</sub> sorption isotherm at 77 K for FAU-2 (obtained after modification of commercial FAU by NaOH/Si = 0.095) which contain both micro and mesoporosity. ....	110
Figure 28 : N <sub>2</sub> adsorption-desorption isotherm of Faujasite sample (FAU-0) degassed at 200 °C overnight. The filled and empty symbols correspond to the adsorption and desorption isotherms, respectively. ....	111
Figure 29 : Example of solid-state <sup>29</sup> Si NMR spectrum of a FAU-0 with their chemical shifts of species Si (nAl) .....	113
Figure 30 : Experimental procedure of adsorption isotherm.....	116
Figure 31 : Major phenomena of the global enthalpy due to adsorption, desorption and displacement (hydration –dehydration).....	118
Figure 32 : Schematic representation of the ITC experiment together with the experimental thermogram obtained for sDiA adsorption onto commercial FAU.....	119
Figure 33 : Representative scheme of SHG where two photons at the fundamental frequency produce one photon at doubled frequency. ....	124
Figure 34 : Principle of Hyper Rayleigh Scattering (HRS) .....	124
Figure 35 : Principle of SHS experimental set-up .....	127
Figure 36 : Polarization-resolved SHS signal diagram sDiA alone in water medium.....	127
Figure 37 : TGA thermograms recorded on material (FAU; the black curve), material after dye adsorption (FAU + sDiA; the red curve) and dye alone (sDiA alone; the green curve). ....	137
Figure 38 : Nitrogen sorption isotherm for modified FAU, FAU-0.125 (FAU-2a; red points) and FAU-0.15 (FAU-2b; blue points). The filled and empty symbols correspond to the adsorption and desorption branches, respectively.....	138
Figure 39 : Nitrogen sorption isotherm for modified FAU, FAU-0.25 (red points) and Al-MCM-41 (black points). The filled and empty symbols correspond to the adsorption and desorption branches, respectively. ....	139
Figure 40 : Diffractogram for FAU-2a and FAU-2b with NaOH/Si = 0.125 and 0.15 respectively at a) large angle and b) small angle.....	140
Figure 41 : Si-NMR spectra for FAU-2a and FAU-2b.....	141
Figure 42 : Schematic representation showing two different protocols to prepare adsorption isotherm. ....	143
Figure 43 : Adsorption isotherm of sDiA onto commercial FAU (Si/Al = 15) prepared using the powdered form of 5 mg in 20 ml system and suspension form for 0.25 g/l in water solvent. ....	144
Figure 44 : Adsorption isotherm of sDiA onto commercial FAU (Si/Al = 15) prepared using the suspension form for 0.05, 0.15 and 0.25 g/l experiments in water solvent with their corresponding error bar. ....	145
Figure 45 : Adsorption isotherm of sDiA onto commercial FAU (Si/Al = 15) prepared using the suspension form for 0.05, 0.15 and 0.25 g/l experiments in ethanol solvent with evaluation of the error bar. ....	146

Figure 46 : Effect of S/L ratio of FAU on the adsorption of sDiA onto commercial FAU (Si/Al = 15) 0.05 g/l (orange), 0.1 g/l (red), 0.15 g/l (green), 0.2 g/l blue), 0.25 g/l (pink) in aqueous medium at sDiA different concentrations. a) 10 $\mu$ M b) 20 $\mu$ M c) 40 $\mu$ M d) 60 $\mu$ M. ....	148
Figure 47 : Adsorption isotherm of sDiA onto 0.25 g/l commercial FAU (Si/Al=15) prepared in water medium at different contact time between FAU and water 30 min, 2 hr and 24 hr. ....	149
Figure 48 : DLS measurements of 0.1 g/l FAU (Si/Al = 15) prepared after 30 min and night in water a) and c) and ethanol medium b) and d) respectively.....	151
Figure 49 : Effect of contact time between commercial FAU (Si/Al = 15) and solvent on the adsorption capacity of sDiA dye after 30 min and 2 days in water (W) and ethanol (Eth) using a) UV-Vis spectroscopy and b) SHS. ....	152
Figure 50 : Spectra of 100 $\mu$ M sDiA dye alone (calibration) (black spectrum), supernatant after 30 min (red spectrum) and 2days (blue spectrum) of contact time between 0.05 g/l commercial FAU (Si/Al = 15) suspension in a) water solvent and b) ethanol solvent obtained by UV-Vis spectroscopy. ....	153
Figure 51 : SHS plots for sDiA with 0.05 g/l commercial FAU (Si/Al = 15) in ethanol after 30 min and 2 days on a) and b) respectively and in water after 30 min and 2 days on c) and d) respectively. ....	155
Figure 52 : $I_4$ parameter calculated for sDiA adsorbed onto commercial FAU (Si/Al = 15) (blue and dark blue dotted curve) in water and in ethanol (orange and brown dotted curve) after 30 min and 2 days, respectively. ....	156
Figure 53 : Effect of time on the adsorption capacity of sDiA onto 0.05 g/l commercial FAU (Si/Al = 15) in water medium using UV-Vis spectrometry. ....	157
Figure 54 : Effect of time on the adsorption capacity of sDiA onto 0.05 g/l commercial FAU (Si/Al = 15) in water medium using SHS.....	158
Figure 55 : SHS plots of four different concentration of sDiA adsorbed onto 0.05 g/l commercial FAU (Si/Al = 15) measured at different time in water medium; a) 10 $\mu$ M, b) 20 $\mu$ M, c) 40 $\mu$ M and d) 60 $\mu$ M. ....	159
Figure 56 : Effect of time on the adsorption capacity of sDiA onto 0.05 g/l commercial FAU (Si/Al = 15) in ethanol medium using SHS.....	161
Figure 57 : SHS plots of four different concentration of sDiA adsorbed onto 0.05 g/l commercial FAU (Si/Al = 15) measured at different time in ethanol medium; a) 10 $\mu$ M, b) 20 $\mu$ M, c) 40 $\mu$ M and d) 60 $\mu$ M. ....	162
Figure 58 : Effect of time on the adsorption capacity of sDiA onto 0.05 g/l commercial FAU (Si/Al = 15) in mixture of 50% water-50% ethanol medium using SHS.....	163
Figure 59 : SHS plots of four different concentration of sDiA adsorbed onto 0.05 g/l commercial FAU (Si/Al = 15) measured at different time in mixture of 50% water- 50% ethanol medium; a) 10 $\mu$ M, b) 20 $\mu$ M, c) 40 $\mu$ M and d) 60 $\mu$ M. ....	164
Figure 60 : SHS plot of sDiA adsorbed onto 0.05 g/l commercial FAU (Si/Al = 15) prepared in water medium at two different sDiA concentrations with and without sonication. The measurement done for suspension and supernatant, the solid line and the dotted line respectively. ....	165
Figure 61 : Adsorption isotherm of sDiA on commercial FAU (Si/Al = 15) prepared in Ultra-Pure water or in sodium nitrate (NaNO <sub>3</sub> ) at various ionic strengths. ....	167
Figure 62 : SHS for sDiA 20 $\mu$ M in suspension with 0.05 g/l commercial FAU (Si/Al = 15) prepared in Ultra-Pure water or in sodium nitrate (NaNO <sub>3</sub> ) at various ionic strengths.....	168
Figure 63 : SHS plots for sDiA supernatant after filtration at different concentration.....	169
Figure 64 : Adsorption isotherms of organic molecules prepared using protocol 1 in water solvent. The symbols representing the isotherms are: ■ for BP, ● for BG, ▲ for CV, ▼ for AO, ◆ for MG.Oxalate, ◀ for MB, ▶ for Rh-B, ● for MG.Cl, ★ for MO, ● for MT, ● for OTC, ■ for sDiA.....	172
Figure 65 : Histogram showing the adsorption capacity of different organic molecules onto FAU (Si/Al=15) depending on their ionic state. ....	174

Figure 66 : Comparison between the adsorption isotherm of neutral OTC and MT and anion MO compounds towards FAU. ....	175
Figure 67 : Effect of counterion on the adsorption isotherm of MG towards FAU.....	177
Figure 68 : Effect of solvents (water, ethanol, and mixture of 50% water 50% ethanol) on the adsorption capacity of sDiA onto commercial FAU of Si/Al ratio 15.....	178
Figure 69 : Sorption isotherm for sDiA towards FAU-3 (the highly modified material) and Al-MCM-41 (mesoporous material) in water medium, red and black curves respectively.....	179
Figure 70 : SHS polarization plot for 20 $\mu$ M sDiA adsorbed onto FAU-3 and Al-MCM-41, orange and dark red plots respectively. ....	179
Figure 71 : Adsorption isotherm of sDiA and auramine-O with commercial FAU (Si/Al = 15).....	181
Figure 72 :The enthalpy of displacement of dyes calculated from ITC. The experimental conditions are 2.4 mM of Auramine-O (red) and sDiA (black) onto 1mg FAU at free pH.....	181
Figure 73: Schematic representation of the three various elements (adsorbate, adsorbent and solvent) involved in the modulation of the adsorption processes and studied in the present work. The hemicyanine dye is referred as sDiA dye molecule in the following.....	190
Figure 74: A) sDiA in water adsorption isotherm onto the three Faujasite, B) Corresponding ITC measurement, C) SHS polarization plot measured at the concentration given by the arrow in A), D) the adsorption thermodynamic quantities for the three Faujasite, at high coverage. On right, a microscopic picture to illustrate the interaction or not between the neighboring dyes.....	194
Figure 75: A) Adsorption isotherm for sDiA onto FAU720 with different solvents: water (brown), acetonitrile (green), ethanol (red) and DMSO (blue). B) SHS polarization plot performed at the isotherm shoulder, as indicated with the arrow on graph A. C) Scheme to depict active or inactive Bronsted Acid Site depending on the solvent used. D) Evolution of free enthalpy during the adsorption process. .	197
Figure 76: A) Adsorption isotherm for sDiA onto FAU400, FAU720 and FAU780 in ethanol, B) SHS polarization plot performed at the isotherm shoulder, as indicated with the arrow on graph A. ....	198
Figure 77: I4 parameters deduced from SHS experiments for sDiA adsorption onto the different Faujasites and various solvent. The acronym in horizontal axis gives the material and solvent (W=Water, E=Ethanol, D=DMSO and A=Acetonitrile).....	199
Figure 78: XRD patterns (high angles) of commercial H-FAU-Y (FAU-0) and hierarchical faujasite named FAU-1,2 and 3, XRD pattern (high angles) of FAUmes prepared with different NaOH/Si ratios. Inset, magnification of (220) XRD peak of FAU-Y.....	222
Figure 79: Nitrogen sorption isotherm at 77 K for commercial H-FAU-Y (Si/Al = 15) (CBV720) named FAU-0 and hierarchical FAU named FAU-1,2 and 3, synthesized from H-FAU-Y and C <sub>18</sub> TAB surfactants with NaOH/Si ratios 0.075, 0.095 and 0.25 respectively. The filled and empty symbols correspond to the adsorption and desorption isotherms, respectively. ....	224
Figure 80: <sup>29</sup> Si-NMR spectra for parent FAU (FAU-0) and modified FAU (FAU-1,2 and 3).....	225
Figure 81: Q <sup>n</sup> contribution corresponds to Si(nSi, n-1Al) environment obtained from Si-NMR analysis using DMFIT.....	225
Figure 82: Adsorption isotherm for sDiA (left and BF (right) onto hierarchical FAU with water solvent using UV-Vis spectrometer.....	226
Figure 83: Adsorbed amount of dyes (sDiA and BF) as a function of (a) micropore surface areas, (b) mesopore and external surface areas, (c) micropore volumes and (d) mesopore volumes for FAU-0, FAU -1, FAU-2, FAU-3. ....	227
Figure 84: a SHS polarization plot for sDiA adsorbed onto FAU-0 and hierarchical FAU; b normalized i4 (I4 parameters) deduced from SHS experiment for sDiA adsorption onto pristine FAU and hierarchical FAU. ....	230

Figure 85: Curves of heat displacement change against the equilibrium adsorbed amount for adsorption of a) sDiA dye and b) BF on the parent FAU and hierarchical FAU adsorbent at free pH values at 25 °C ..... 232

Figure 86: Enthalpies of adsorption (plain circle  $\Delta H$  for sDiA, square for BF) and I4 (empty circle I4 for sDiA) at the maximum dyes loading..... 235

Figure 87 : Schematic overview of the objectives achieved in the framework of this PhD thesis. It shows the adsorption behavior of 2D dyes at the solid/liquid interface. The adsorption of 2D dye molecules (purple flash) on an active site is associated with a loss of water molecules around it forming an enthalpy of dehydration (red flash). These dyes, enter the FAU pore and become confined and thus forming the enthalpy of adsorption. The global enthalpy of adsorption, the organization of molecules as well as the confinement effect decreases with increasing FAU porosity. .... 259



# Résumé étendu

## Introduction

La pollution des eaux est un problème récurrent, et représente désormais une question stratégique. Cette pollution est due au rejet de composés, plus ou moins dangereux, comme des hydrocarbures, des composés phénoliques, des métaux lourds, des colorants, des insecticides, etc. Ces produits chimiques proviennent des activités anthropiques, de l'agroalimentaire et de diverses industries telles que la chimie, le textile, la tannerie, l'agroalimentaire, la pharmacie, etc. De nombreuses méthodes de décontamination de l'eau ont été développées et optimisées depuis plusieurs décennies. Parmi ces techniques, on recense les procédés de précipitation chimique, de floculation, d'échange d'ions, d'électrolyse, les procédés membranaires et l'adsorption. Les travaux étudiés dans cette thèse reposent sur ces phénomènes d'adsorption qui offrent de nombreux avantages en particulier concernant l'efficacité des procédés. Outre les travaux relatifs à l'optimisation des performances, de nombreuses études portent aussi sur la compréhension des mécanismes et des forces motrices de l'adsorption. Les phénomènes d'adsorption sont impactés par les propriétés des matériaux adsorbants utilisés, par celles des espèces à adsorber, et dans le cas des effluents liquides, on considérera aussi l'influence du solvant.

Parmi les caractéristiques intéressantes des solides, la surface disponible pour l'adsorption, et plus généralement les propriétés texturales, sont des critères souvent retenus comme importants pour améliorer l'efficacité. Pour augmenter la surface disponible, les matériaux choisis sont souvent des matériaux poreux, présentant parfois différents niveaux de porosité, avec des micropores (de taille inférieure à 2nm), ou des mésopores (de taille comprise entre 2 et 50 nm). Cependant, à l'intérieur des micropores et dans les petits mésopores, les caractéristiques de l'adsorption ne peuvent être considérées comme similaires au cas des surfaces planes. La courbure de la surface, la proximité du mur opposé, le voisinage entre les sites de sorption, ... modifient l'adsorption, mais aussi très probablement les propriétés du solvant lui-même, en interaction avec la surface, et avec les molécules cibles à adsorber. L'ensemble de ces modifications est désigné sous le terme très général d'effet de confinement, terme qui englobe de nombreuses contributions, sans qu'elles soient toujours clairement explicitées et comprises.

Originellement initié dans le contexte d'application à la dépollution, ce travail avait pour objectif plus fondamental de comprendre les mécanismes d'interactions au sein des matériaux nanostructurés. La littérature montre qu'un nombre important d'approches et de techniques ont été développées pour caractériser l'adsorption et explorer ces interactions impliquées dans les processus d'adsorption. Il peut s'agir de méthodes dites globales ou macroscopiques, décrivant les quantités adsorbées, par gramme de matériaux, ou dans certains cas, ces quantités sont rapportées à l'aire surfacique pour

s'affranchir des effets de surface accessible, ou disponible pour l'adsorption. On parlera ici de la mesure d'isotherme d'adsorption. Dans des approches plus spécifiques, on discutera des affinités d'adsorption voire on déterminera des constantes d'adsorption afin de quantifier les interactions. Ces approches thermodynamiques globales sont parfois complétées par des mesures calorimétriques plus spécifiques, afin d'accéder à l'évaluation des contributions enthalpiques, voire pour établir un bilan complet entre enthalpie et entropie. Néanmoins, même quantifiées précisément, ces mesures ne permettent pas une observation directe des phénomènes, ne donnent pas de vision in situ ni d'informations locales sur l'interface. En particulier, concernant les espèces adsorbées, les distances et les distributions vis-à-vis de la surface, l'orientation des molécules, entre elles ou vis-à-vis de la surface, ... sont des indications qui ne sont pas accessibles par ces approches dites globales ou macroscopiques. Si les approches de modélisations, et en particulier avec les développements de la considération explicite des solvants, donnent accès à des données spécifiques aux zones interfaciales, elles nécessitent des approximations et sont loin des systèmes réels, comme par exemple les défauts de surface, les nanostructurations, des hétérogénéités énergétiques, ... Il s'avère que les observations des interfaces, à l'échelle du nanomètre, sont beaucoup plus complexes à mettre en place d'un point de vue méthodologique. Les difficultés proviennent de la taille réduite de la zone à observer, de la faible quantité de la matière (espèces adsorbées), de la présence solvant plus ou moins structuré au niveau de l'interface... Il s'agit donc d'identifier la ou les techniques donnant accès à des caractéristiques mesurables, spécifiques de la zone interfaciale, et corrélables aux différentes caractéristiques de l'adsorbat et de l'adsorbant, et des interactions mises en jeu

De très nombreux paramètres influencent ces interactions. Concernant les matériaux (ou adsorbants), on relèvera, outre les effets de texture évoqués ci-dessus (surface accessible, nanostructuration, volume poreux et diamètre de pores ...), tous les effets de chimie de surface (charge variable / permanente, hydrophilie / hydrophobie,...). A ces effets relatifs aux solides viennent se rajouter les caractéristiques des espèces à adsorber, avec la charge, la taille, la polarité, ... Il s'agissait donc de déterminer en quoi ces deux types de caractéristiques modifient d'une part les propriétés macroscopiques de l'adsorption, mais aussi les comportements à l'échelle locale. Devant la multiplicité des paramètres en jeu, l'approche développée dans ce travail devait cibler les paramètres clés pour lesquelles des variations de comportement seraient mesurables et en lien avec les modulations du système.

### **Objectifs de la thèse et structure du manuscrit**

L'objectif de cette thèse est d'étudier l'adsorption et l'organisation des molécules en utilisant deux approches complémentaires à différentes échelles afin d'avoir une vue d'ensemble des

phénomènes d'adsorption se produisant à l'interface solide/liquide. Nous avons associé d'une part une approche globale, à partir de la détermination des isothermes d'adsorption et de l'évaluation des contributions enthalpiques par mesures calorimétriques, et d'autre part une approche locale utilisant l'optique non linéaire et plus particulièrement la diffusion de seconde harmonique.

Pour cela, le système d'étude choisi devait reposer sur un matériau déjà couramment étudié en raison de ses propriétés connues d'adsorption et de rétention des polluants, ainsi que de la possibilité de modifier la texture ou la chimie de surface. Une série de matériaux zéolithiques a été retenue, zéolithes pour lesquelles la physicochimie interfaciale resterait a priori similaire, mais au sein de laquelle la microporosité serait combinée à de la mésoporosité. Cette zéolite Y ou faujasite (FAU) a été choisie comme matériau de départ, et matériau modèle en raison de son faible coût, de sa bonne stabilité thermique et hydrothermale, de ses propriétés structurales intéressantes, en particulier son volume microporeux élevé. Elle possède en outre une capacité de sorption élevée et la littérature a montré la possible modification de porosité.

Un autre volet de ce travail était de pouvoir mettre en évidence l'impact de la nanostructuration du matériau sur les mécanismes d'interactions aux interfaces, d'une part d'un point de vue thermodynamique de l'adsorption, et d'autre part d'un point de vue de l'organisation locale des espèces adsorbées. A cette fin, l'objectif était de définir la meilleure méthodologie pour modifier les caractéristiques texturales du matériau initial, afin de disposer d'un matériau à multiples porosités (micro et mésoporeuse), tout en conservant les propriétés intrinsèques de la zéolithe de départ.

A partir de cette famille de matériau, le but était de déterminer en quoi l'évolution des différents niveaux de porosité impacte les propriétés des molécules confinées dans ces réseaux poreux. Pour cela, une série de molécules a été choisie, présentant différentes caractéristiques en vue de mettre en évidence l'influence de la structure, de la charge, de la taille, ... sur les phénomènes interfaciaux. L'enjeu était de pouvoir étudier localement leur organisation et/ou orientation à l'interface solide/liquide. Pour cela, la méthode retenue afin d'obtenir des informations in situ et en conditions réelles (en présence de solvant) était basée sur les méthodes d'optique non linéaire, et plus particulièrement en diffusion de seconde harmonique. Le choix de molécules à adsorber s'est porté sur différents types de colorants. Ces colorants, du fait de la présence de liaisons  $\pi$  conjuguées et leur valeur d'hyperpolarisabilité peuvent être activés en SHS, et ont ainsi pu être utilisés comme des molécules sondes des interfaces. Compte tenu de la capacité d'échange cationique des zéolithes, ce sont surtout des colorants cationiques qui ont été retenus, mais quelques études spécifiques ont été menées avec des espèces anioniques, zwitterioniques, voire neutres. Des colorants de différentes structures (plus ou moins linéaire ou plus compacte), mais aussi de différentes tailles ont été sélectionnés afin d'étudier les propriétés d'adsorption.



Le manuscrit de la thèse est structuré de la manière suivant, avec une introduction générale, cinq chapitres dont deux sont des articles soumis ou à soumettre, et enfin une dernière partie comprenant une conclusion et des perspectives.

Le **premier chapitre** est un état de l'art sur la problématique de notre étude. Il décrit tout d'abord des généralités sur les systèmes étudiés, avec les colorants, les différentes méthodes couramment mises en œuvre pour la dépollution, et enfin les zéolithes, qui sont des matériaux de choix dans les procédés d'adsorption. Par ailleurs, les différentes méthodes de modification de zéolithes en vue d'obtenir un matériau hiérarchique sont décrites. Enfin, après quelques généralités sur l'adsorption et les 'effets de confinement'. Enfin, un aperçu bibliographique illustre les deux approches majeures mises en œuvre dans cette thèse pour établir la caractérisation physico-chimique précise des interfaces. Ceci inclut d'une part l'approche dite globale avec les isothermes de l'adsorption et la thermodynamique associée par des mesures calorimétriques en mode titrage (ou ITC pour *Isotherm Titration Calorimetry*), et une approche locale en vue de déterminer in situ l'organisation des molécules de colorants à l'interface solide/liquide en utilisant la diffusion de seconde harmonique (ou SHS pour *Second Harmonic Scattering*).

Le **deuxième chapitre** décrit par la partie expérimentale de ce travail. Il présente tout d'abord les systèmes étudiés, avec les principaux colorants, et la série de matériaux adsorbants de type zéolithe. La synthèse de faujasites hiérarchiques par modification post-synthèse (désilication-recristallisation) de matériaux commerciaux est décrite en détail. Ensuite, l'ensemble des techniques expérimentales de caractérisation des solutions et des solides est décrit. Enfin, nos deux techniques principales sont présentées en détail, avec la description des différents dispositifs, les protocoles expérimentaux, ainsi que les procédures relatives à l'analyse des données.

Le **troisième chapitre** est consacré d'une part à des analyses complémentaires sur les matériaux, et d'autre part à une étude détaillée des conditions expérimentales appliquées lors de la réalisation des isothermes d'adsorption (effets de solvant, impact du rapport solide/liquide, temps de solvation du matériau, cinétique de sorption, effet de température, effet de force ionique, ...). Ensuite, des isothermes d'adsorption de différentes molécules organiques sur le matériau initial de type faujasite ont été réalisées. Enfin, des études plus spécifiques, combinant les approches globales et locales, sont décrites pour certains systèmes.

Le **quatrième chapitre** vise à présenter la première publication qui traite l'étude de l'effet la chimie de surface et de l'effet de confinement de plusieurs colorants à l'interface solide/liquide. Différents matériaux adsorbants commerciaux, présentant différents rapports Si/Al, ont été utilisés. Des colorants de type hémicyanines, ou nDiA diffèrent les uns des autres par leur chaîne alkyle (avec  $n = 1, 4, \text{ et } 16$ ) ont été utilisés comme molécules sondes. Les isothermes d'adsorption en présence de différents solvants ont été établies. En outre, l'étude à l'échelle locale a également été réalisée pour évaluer les processus de sorption, l'organisation interfaciale des molécules et les possibles effets de corrélation. La combinaison des deux approches permet de sonder les molécules confinées à l'intérieur du matériau zéolitique.

L'effet de différents niveaux de porosités des zéolithes sur les propriétés d'adsorption des colorants a fait l'objet du **cinquième chapitre** qui est une seconde publication à soumettre prochainement. Quatre échantillons de faujasite ont été caractérisés en détail afin de mettre en évidence l'évolution des caractéristiques structurales et texturales en fonction du degré de modification. Deux molécules sondes, le 1DiA (colorant linéaire) et la fuchsine basique (colorant volumineux) sont utilisées. Des mesures de capacité d'adsorption, d'enthalpies de déplacement par ITC et de corrélation par SHS ont été réalisées et comparées sur ces 2 colorants.

Enfin, le manuscrit se termine par une conclusion qui permettra de mettre en évidence tous les résultats de ce travail, suivie de suggestions pour les perspectives à la poursuite de ce travail.

## Chapitre I

Même si les dommages causés par les activités humaines sur l'environnement sont déjà connus et médiatisés, la quantification précise des impacts sur la santé humaine ou les écosystèmes est quasiment impossible, avec des nouvelles pathologies, des contaminants émergents et la constante diminution des ressources naturelles. Les pollutions environnementales sont croissantes, en particulier celles des eaux, et de ce fait ces ressources précieuses et indispensables à la vie sont de plus en plus fragilisées. Les molécules organiques, en particulier les colorants, font partie des polluants qui constituent un risque élevé pour l'environnement et la santé humaine en raison de leur résistance à la biodégradabilité, de leur accumulation et de leur utilisation dans de nombreux domaines en particulier les industries textiles et les teintures. Un enjeu environnemental et sociétal important est de limiter la diffusion de ces polluants et donc de développer des méthodes qui permettent de préserver les écosystèmes et les ressources en eau. Plusieurs procédés de traitement ont été développés pour

réduire les quantités de ces contaminants dans les milieux aquatiques. Le procédé d'adsorption est l'une des méthodes ayant déjà montré une grande rentabilité pour l'élimination des contaminants comme les polluants organiques (pesticides, colorants, médicaments, composés phénoliques...).

L'optimisation des procédés repose sur le développement de nouveaux adsorbants mais aussi sur des recherches plus fondamentales pour comprendre les mécanismes qui gouvernent l'adsorption. Dans ce contexte, les matériaux poreux présentent un intérêt particulier en raison de l'importante surface accessible et disponible pour retenir les polluants cibles. Cette propriété est à l'origine de l'utilisation de ces matériaux non seulement dans les domaines de l'adsorption, y compris l'échange d'ions, mais aussi les applications en catalyse. Parmi la très large gamme de matériaux poreux disponibles dans la littérature, les aluminosilicates microporeux comme les zéolithes, font l'objet de nombreuses études puisqu'elles sont relativement peu coûteuses, stables thermiquement et d'un point de vue hydrothermale. Leur structure leur confère des caractéristiques texturales très intéressantes avec d'importants volumes poreux (notamment microporeux), de grandes surfaces spécifiques, et de ce fait des capacités de sorption élevée. La cristallographie et l'organisation des structures quadri-connectées de  $AlO_4$  et de  $SiO_4$  tétraédriques est telle que le matériau présente un déficit de charge compensé par des cations dits cations échangeables. Ce réseau poreux et ces capacités d'échanges d'ions en font de matériaux de choix. Dans ce travail, la zéolite Y de forme faujasite (FAU) a été sélectionnée comme matériau modèle. Cependant, les matériaux zéolitiques présentent des inconvénients liés à la diffusion en raison de leur porosité étroite. Ceci peut avoir un impact négatif sur l'applicabilité des zéolithes et réduit leur efficacité d'adsorption des molécules volumineuses.

Il a été démontré que les matériaux hiérarchiques combinant différentes porosités permettent de surmonter ces problèmes. Ces matériaux peuvent être produits en utilisant deux types d'approches. La première est appelée "bottom up" ou "constructive" tandis que la seconde est "top down" ou "destructive" et correspond à un traitement post-synthèse. La première méthode est moins utilisée en raison de la présence de réactifs et d'agents structurants souvent coûteux. La formation de mésopores par post-synthèse est cependant difficile à contrôler car le processus est rapide et la mésoporosité résultante présente une large distribution en taille.

La recristallisation est un traitement post-synthèse qui combine les voies destructives et constructives. En effet, la zéolithe utilisée comme source de silice-alumine est dissoute en présence d'une solution basique. Puis, dans des conditions hydrothermales, la zéolithe dissoute peut recristalliser autour des micelles formées par l'agent structurant pour donner un matériau micro-mésoporeux. Cela permet d'obtenir des zéolithes avec une mésoporosité ordonnée, une taille de mésopores contrôlée, et les propriétés du matériau initial.

La modification de la taille des pores contribue à des variations du comportement de la phase liquide au sein de la porosité, à des modifications des molécules dans ce solvant, à des changements dans les interactions entre la surface et les molécules adsorbées. On parle d'effets de confinement, ce terme étant utilisé pour signifier une modification des propriétés physico-chimiques (par exemple, la structuration du solvant, la mobilité moléculaire, les caractéristiques d'adsorption, ...) des espèces confinées dans l'espace poral. Dans le système confiné, les molécules pourraient être modifiées, plus ou moins organisées que dans le système non confiné. Pour confirmer cette hypothèse, notre attention s'est portée sur deux techniques principales pour tenter de mieux décrire et quantifier ces effets.

L'étude de la littérature montre que parmi les approches utilisées dans l'étude des phénomènes d'adsorption, les données thermodynamiques apportent de nombreux renseignements. Les déterminations de l'enthalpie et de l'entropie apportent des informations macroscopiques sur le confinement. Ces données peuvent être obtenues par des modélisations, par des mesures d'isothermes à différentes températures et l'application d'un traitement de Van't Hoff, ou par des mesures de calorimétries d'adsorption. Dans notre étude, nous souhaitons réaliser des mesures directes de l'enthalpie globale d'adsorption (ou de déplacement) dans des zéolithes présentant des variations de porosités, et ainsi comprendre l'interaction des molécules adsorbées sur ou dans le matériau. A l'interface solide / liquide, parmi les techniques utilisées, la calorimétrie par titrage isotherme (ou ITC pour Isotherm Titration Calorimetry) occupe une place importante, en raison de sa capacité à fournir une description thermodynamique complète du phénomène étudié. En effet, l'ITC permet une mesure directe de l'enthalpie d'interaction à une température donnée, sans variation de température, sans nécessité de faire des hypothèses sur le modèle d'adsorption, ou les variations des capacités thermiques entre les espèces libres et associées. Cette approche donnant une vision uniquement globale, une méthodologie basée sur une technique locale a été associée aux mesures des isothermes et des enthalpies afin d'avoir un aperçu de l'organisation des espèces aux interfaces, en particulier en se basant sur la réponse optique des molécules adsorbées. Pour cela, le choix des espèces adsorbées s'est porté sur des colorants moléculaires.

L'optique non linéaire, plus particulièrement le processus de double fréquence, est adapté pour sonder les propriétés de la matière molle ou condensée à des échelles proches de la longueur d'onde utilisée. En effet, en raison de la cohérence de la réponse de génération de seconde harmonique, il est possible de distinguer les réponses non linéaires spatialement corrélées de celles non corrélées. Ainsi, en particulier dans le cas de ce travail, la diffusion de seconde harmonique (ou SHS pour Second Harmonic Scattering), a été appliquée pour étudier in-situ des particules de zéolithes en suspension, les possibles auto-organisation entre molécules dans l'espace porale, les phénomènes aux interfaces

solide/liquide, l'adsorption, les interactions molécule-solide et l'organisation moléculaire des colorants à cette interface.

Ainsi, la force de ce travail repose sur le couplage de l'approche thermodynamique et l'approche moléculaire, et le travail présenté dans ce manuscrit se base sur une vision multi technique et multi-échelle, sur un système judicieusement choisi pour répondre aux questions posées.

## **Chapitre II**

Dans ce chapitre, nous présentons les molécules, les matériaux et les méthodes réalisées pour caractériser le matériau ainsi que les approches utilisées pour étudier les phénomènes d'adsorption à l'interface solide / liquide.

Concernant le matériau adsorbant, notre choix s'est donc porté sur des zéolithes de type Faujasite noté FAU, et leur déclinaison avec une série de matériaux hiérarchiques (designées FAU-0 FAU-1, FAU-2a , FAU-2b, FAU-3). La fabrication de ces FAU hiérarchiques a été réalisée par post-synthèse, qui semblait ici un moyen efficace de produire suffisamment d'adsorbant et d'accéder à des caractéristiques, et en particulier améliorer la diffusion en créant un réseau des mésopores homogènes en nature et en taille, tout en préservant les propriétés intrinsèques de la faujasite initiale. Notre stratégie était basée sur la modification de matériaux commerciaux, avec une voie hybride entre méthode destructive et méthode constructive, par une approche de désilication-recristallisation, utilisant NaOH en présence d'un agent structurant de type CTAB.

Les techniques de caractérisation utilisées dans cette thèse ont également été décrites. Le but de toutes ces techniques est d'analyser la structure, la texture, la morphologie, la composition, l'environnement chimique, la chimie de surface et la réactivité des matériaux utilisés dans cette thèse. Cela a permis de mieux appréhender les différentes caractéristiques du matériau et de disposer des informations nécessaires en vue de corréler les spécificités des solides et leurs propriétés d'adsorption. Ce chapitre décrit ensuite le protocole d'adsorption et la méthode d'étude de la stabilité de la suspension.

Enfin, les dispositifs et les procédures expérimentales des mesures en ITC et en SHS, et les traitements de données associés, sont décrites. Les mesures ITC donnent accès à l'enthalpie globale de déplacement. Et en dernier lieu, des mesures SHS permettent d'une part de déterminer les isothermes à une échelle locale, et d'autre part de mettre en évidence la corrélation entre les molécules adsorbées et d'identifier l'organisation et/ou l'orientation des molécules à l'interface solide/liquide.

### Chapitre III

Les résultats majeurs de cette thèse sont donnés dans deux articles soumis ou à soumettre, comme décrit dans les chapitre IV et V. Au préalable dans ce chapitre III, des résultats complémentaires sont donnés. La caractérisation de matériaux additionnels est tout d'abord réalisée, suivie de l'évaluation des performances d'adsorption des colorants en fonction de différents paramètres expérimentaux. Les résultats de différents tests d'adsorption du 1DIA sur la FAU sont présentés, en analysant en particulier les différents milieux, les différents solvants (eau, éthanol, mélange 50% - 50 eau - éthanol), et suivant différents paramètres (temps de contact, rapport solide/liquide, ...). La comparaison entre les faujasites fortement modifiées et un matériau mésoporeux classique dopé à l'aluminium nous permettra de mettre en évidence les relations entre les propriétés texturales et les performances de sorption. Enfin, une étude thermodynamique a été réalisée pour deux colorants ayant une capacité de sorption similaire afin de quantifier l'aspect enthalpique des interactions adsorbant/adsorbat.

L'analyse complémentaire de FAU, FAU-2a, FAU-2b et Al-MCM-41 prouve que la modification de FAU par traitement alcalin affecte le matériau et en particulier sa texture. On observe une diminution du volume microporeux, une augmentation du volume mésoporeux, tout en conservant une certaine cristallinité. Le réseau de porosité est ordonné, sauf pour le matériau le plus modifié FAU 3. En parallèle, on relève la diminution des environnements  $Q^4$  et l'augmentation des environnements  $Q^3$ , en lien avec une perte de cristallinité. La possibilité de contrôler la porosité, tout en conservant les autres propriétés physicochimiques, est ce que nous recherchions afin d'étudier l'impact de la porosité (éventuellement hiérarchique), en particulier sur l'organisation des molécules aux interfaces.

Plusieurs paramètres ont un impact sur le comportement d'adsorption. La présence du solvant éthanol conduit à une diminution de la capacité de sorption. L'effet du rapport solide/liquide, de la sonication, de la force ionique est étudié. Une diminution de la capacité est observée dans l'eau pour les rapports solide / liquide élevés, alors qu'il n'y a pas d'effet dans l'éthanol. Par ailleurs, la sonication ou la modification de la force ionique n'a pas d'impact sur l'adsorption. L'étude de ces différents paramètres du protocole a montré que le rapport solide/ liquide de la suspension à 0.1 g/l est celui le plus adapté pour notre étude.

De manière générale, ces résultats montrent que la faujasite commerciale possède une capacité d'adsorption intéressante pour la rétention de molécules organiques. Cette conclusion est valable qu'il s'agisse de cations positifs ou neutres à condition que leur taille des molécules soit plus petite par rapport à la taille des pores (Figure 1). Dans le cas des molécules volumineuses cationiques comme le

vert de malachite, le cristal violet, ou la rhodamine B, la capacité d'adsorption est de l'ordre de 100 à 150  $\mu\text{mol/g}$  alors que pour les petites molécules la capacité de sorption atteint 650 et 800  $\mu\text{mol/g}$  pour l'auramine-O et le bleu de méthylène respectivement. Une faible capacité est observée pour le méthyl orange, un colorant négatif, en raison de la répulsion électrostatique entre la surface négative de la zéolithe et le colorant. En outre, dans le cas de molécule neutre, la capacité de sorption varie avec la taille, avec 100 et 350  $\mu\text{mol/g}$  pour l'oxytétracycline HCl et le tartrate de morantel Hydrate respectivement.

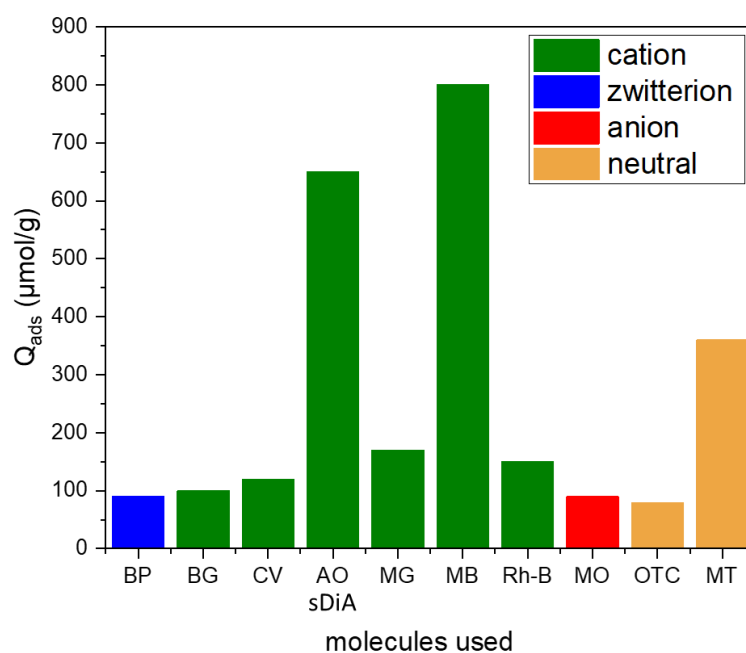


Figure 1: Histogramme montrant la capacité d'adsorption de différentes molécules organiques sur FAU (Si/Al=15) en fonction de leur état ionique. Blue patent (BP), Brilliant green (BG), Crystal violet (CV), Auramine-O (AO), Malachite green (MG), Methylene blue (MB), Rhodamine-B (Rh-B), Methyl orange (MO), Oxytetracycline HCl (OTC) and Morantel tartrate Hydrate (MT).

Les résultats de cette recherche ont été comparés aux résultats publiés dans le même domaine, et jugés en accord avec la plupart d'entre eux.

Les études thermodynamiques sur l'adsorption par FAU de deux colorants (1DiA et auramine-O), présentant des capacités d'adsorption similaire, suggèrent des processus d'adsorption exothermiques. Pour les faibles taux de recouvrement, les valeurs d'enthalpies sont similaires, mais pour des recouvrements plus élevées, l'enthalpie d'interaction entre la surface et le colorant semble légèrement plus élevée pour le 1DiA. Cela démontre une interaction plus forte entre le 1DiA et la faujasite et de ce fait, une meilleure organisation à l'interface solide / liquide.

En outre les Al-MCM-41 (matériaux intrinsèquement mésoporeux) présentent un comportement similaire à celui des FAU-3 (les solides hautement modifiés), y compris la structure, la performance et les propriétés de sorption.

## Chapitre IV

Les résultats présentés dans ce chapitre concernent l'étude de la force motrice de l'adsorption à l'interface solide/liquide. Des faujasites présentant différentes propriétés de surface ont été sélectionnées. Il s'agit d'une série de matériaux commerciaux avec différents rapports Si/Al, de 2.55, 15 et 40 appelées FAU400, FAU720 et FAU780 respectivement. L'objectif était de mettre en évidence l'effet de la chimie de surface et l'impact sur le confinement des molécules dans la porosité, et sur la corrélation à longue portée dans le matériau zéolithique.

Trois molécules sondes ont été choisies ; il s'agit de colorants n-DiA, qui diffèrent entre eux par la longueur de la chaîne alkyle et leurs propriétés hydrophobes. Quatre solvants différents : eau, éthanol, acétonitrile et DMSO ont été utilisés. Les capacités d'adsorption ont été évaluées, et des corrélations ont été établies.

Nous avons montré que la combinaison d'une série de matériaux bien définis et de molécules sonde bien adaptées permet d'identifier les contributions de différents effets. Ceux-ci incluent le rapport Si/Al, la longueur de la chaîne alkyle du colorant hémicyanine, les sites acides de Bronsted et la solvatation des protons. La capacité d'adsorption élevée révèle que l'adsorption des colorants se produit à l'intérieur de la porosité de la zéolite. Grâce aux mesures SHS, il a été possible de sonder l'effet de confinement des colorants, avec la mise en évidence de la corrélation entre les molécules d'une part, et l'organisation des molécules à l'interface solide/liquide d'autre part.

La capacité d'adsorption obtenue suit la tendance suivante : FAU400 > FAU720 > FAU780 ce qui est lié à la capacité d'échange cationique (CEC) du matériau. De plus, dans le cas du FAU720, cette capacité varie avec les solvants, allant de l'eau, ayant les sites d'acidité de Bronsted les plus élevés, à l'acétonitrile suivi de l'éthanol puis du DMSO. Il est important de noter que c'est pour le matériau FAU720 que le paramètre  $I_4$ , déterminé par les mesures SHS comme étant un indicateur de corrélation moléculaire dans le système, est le plus élevé en valeur absolue en présence de solvant aqueux. Cette analyse permet de mettre en évidence des interactions importantes entre les molécules et/ou avec l'interface solide. Elle permet en particulier de conclure à un degrés d'organisation augmenté dans le système.

Sur la base de ces résultats, nous pouvons conclure que la variation des corrélations à plus ou moins longue distance est principalement liée à la microporosité et aux variations de chimie de surface,



induisant des changements dans le confinement. L'effet de confinement peut être expliqué par le mouvement figé des colorants à l'intérieur des pores. Le mouvement des colorants dépend de la charge présente du matériau, en lien avec le rapport Si/Al.

Dans le système confiné, le remplissage (ou recouvrement) à l'intérieur du matériau est optimal de manière à remplir l'ensemble des pores et neutraliser au mieux, sans pour autant modifier la conformation des molécules. Cela conduit à une organisation élevée des molécules à l'interface et donc à une corrélation élevée entre les molécules.

## Chapitre V

Dans cette partie, une série de matériaux hiérarchiques a été préparée à partir d'une faujasite commerciale comme matériau de départ (CBV-720). Ils ont été synthétisés par post-synthèse en milieu basique (NaOH) en présence du tensioactif C<sub>18</sub>TAB. Ces matériaux ont été désignés par FAU-0, 1, 2 et 3 pour un rapport Si/NaOH de 0, 0.075, 0.095 et 0.25, respectivement.

Les quatre matériaux ont été caractérisés en utilisant des techniques complémentaires. La diffraction des rayons X a montré la présence d'une structure FAU pour tous les matériaux, avec une forte diminution de l'intensité des pics pour le FAU-3, qui est finalement proche de matériau mésoporeux comme les MCM-41 dopés à l'aluminium, avec toujours la présence de quelques nanocristaux de FAU dispersés, d'une taille de 50 nm.

La composition chimique des zéolithes hiérarchiques a été déterminée par fluorescence X. Le ratio Si/Al pour la faujasite initiale est égal à 15. Ce rapport est constant pour les 2 zéolithes les moins modifiées. Pour la faujasite hautement modifiée, une réduction du rapport Si/Al de 15 à 13 a été observée. Les diagrammes DRX à faible angle montrent pour FAU-1 et FAU-2 la présence de mésopores ordonnés, ce qui n'est pas observé pour FAU-3. La RMN MAS <sup>29</sup>Si montre des spectres similaires pour FAU-0, -1, -2, indiquant que FAU-1 et FAU-2 sont construits sur la base de la structure de la faujasite de départ, et les mésopores creusés dans la structure initiale. Un léger changement dans le rapport Q<sup>3</sup>/Q<sup>4</sup> est observé pour FAU-2 avec une légère augmentation de Q<sup>3</sup> suggérant une distorsion ou une certaine dégradation du réseau de zéolithe dans FAU-2. En revanche, FAU-3 est principalement une structure amorphe. L'isotherme d'adsorption d'azote montre une diminution continue du volume des micropores et en parallèle une augmentation continue du volume des mésopores en passant de FAU-0 à FAU-3.

L'adsorption de la 1DiA montre une affinité très élevée pour le matériau initial et les matériaux hiérarchiques. Le 1DiA est en effet assez petit pour entrer dans les supercages de FAU. La capacité d'adsorption maximale de FAU-1 et FAU-2 est égale à la capacité d'adsorption de FAU-0 (0.6 mmol/g).

L'enthalpie d'adsorption mesurée par ITC montre des modifications en fonction du taux de recouvrement et du niveau de porosité (voir le résumé des données sur la Figure 2). Les valeurs sont identiques pour les faibles quantités adsorbées. Pour les recouvrements plus élevés, les échantillons les plus microporeux (FAU-0 et FAU-1) présentent des enthalpies plus élevées, suggérant que les colorants adsorbés dans les supercages sont en forte interaction avec la surface. Les mesures de SHS et les valeurs de  $I_4$  confirment de fortes interactions.

Pour le solide micro et mésoporeux (FAU-2), l'enthalpie d'adsorption de 1DiA est plus faible que pour le matériau le plus mésoporeux, ce qui suggère une interaction plus faible avec la surface. Les mesures SHS et les valeurs  $I_4$  montrent de très faibles interactions entre les sondes, suggérant un grand degré de liberté à la surface des supercages pour FAU-2.

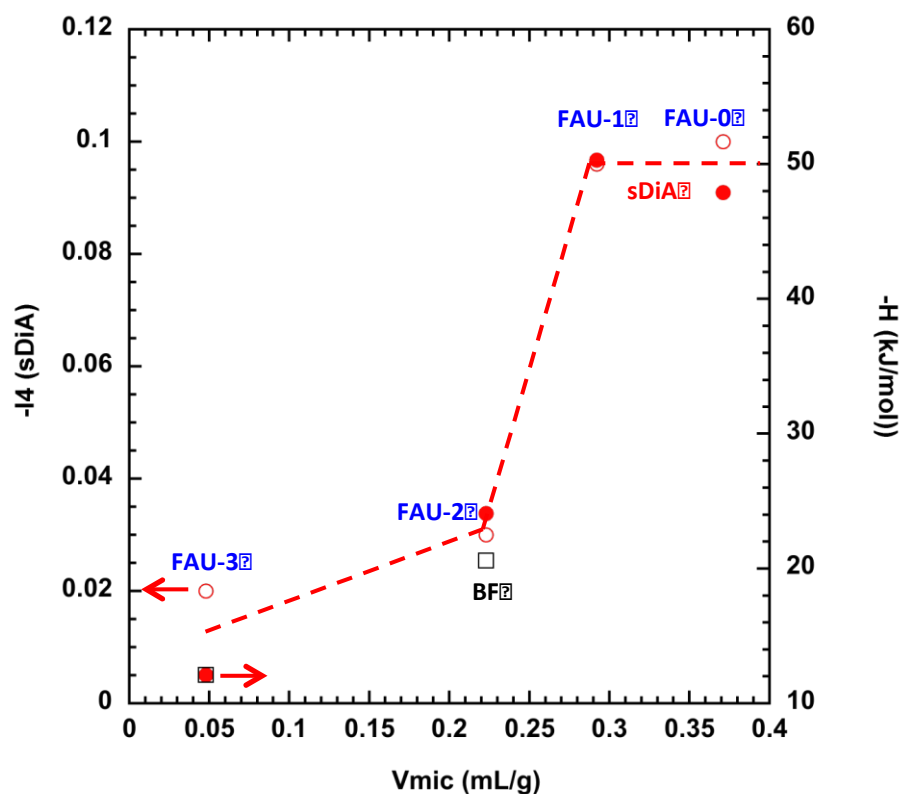


Figure 2: Enthalpies d'adsorption (cercle plein  $\Delta H$  pour 1DiA, carré pour BF) et  $I_4$  (cercle vide  $I_4$  pour 1DiA) à la charge maximale de colorants.

Les isothermes d'adsorption de la Basic Fuchsin (ou BF) montrent de plus faibles quantités adsorbées et de faibles affinités avec la surface du matériau initial ou des matériaux hiérarchiques. En

effet, le BF est trop volumineux pour pénétrer dans les micropores de la Faujasite. Cependant, une augmentation linéaire de la quantité adsorbée de colorants de 0,05 à 0,4 mmol/g est observée pour FAU-0 à FAU-3 respectivement, en lien avec l'augmentation des mésopores et des surfaces externes, les mésopores ayant un diamètre suffisamment grand pour adsorber ces molécules plus volumineuses. L'enthalpie d'adsorption est faible révélant de faibles interactions avec la surface. Les valeurs de  $l_4$  calculées à partir des mesures SHS sont très faibles, montrant de très faibles interactions entre la surface et les colorants et suggérant un grand degré de liberté des molécules à la surface des mésopores. L'adsorption d'un colorant plus volumineux, à la surface des mésopores et sur les surfaces externes, est caractérisée par une faible enthalpie d'adsorption et une faible interaction entre les molécules et la surface.

Ces deux types de colorants ont donc permis de sonder cette famille de faujasites présentant différents niveaux de porosités. Le colorant sDiA permet de sonder l'intégrité des supercages des FAU et le colorant BF permet de sonder les mésopores et la surface externe.

## **Conclusion**

L'idée initiale de cette thèse de doctorat était d'étudier l'adsorption et l'organisation des molécules aux interfaces solide-liquide. Pour mener à bien ce travail, deux approches ont été proposées et combinées. La première approche consistait à adsorber les molécules de colorants afin de déterminer la capacité d'adsorption à partir de l'isotherme d'adsorption et d'évaluer les interactions entre les molécules et les matériaux en mesurant l'enthalpie globale par calorimétrie de titrage isotherme (ITC). Cette approche est appelée étude à l'échelle macroscopique. La deuxième approche a été développée pour évaluer la corrélation et l'organisation des molécules à l'échelle locale en utilisant l'optique non linéaire (ONL), en particulier la diffusion de seconde harmonique (SHS).

Différents paramètres du protocole d'adsorption ont été étudiés afin de déterminer l'impact de plusieurs conditions expérimentales : rapport solide/liquide, sonication de la suspension de faujasite, temps de contact entre le colorant et le FAU, temps d'équilibre, et force ionique. La capacité d'adsorption des molécules organiques varie en fonction des propriétés de la molécule adsorbée (taille, charge et groupe fonctionnel), de la propriété du matériau (mésoporosité, microporosité et rapport Si/Al) et du solvant.

Les résultats de cette étude montrent que la faujasite commerciale a une capacité d'adsorption intéressante pour la rétention de molécules organiques, qu'il s'agisse d'espèces cationiques ou neutres à condition qu'elles aient une taille plus petite par rapport à la taille des pores.

Tous les paramètres testés (rapport solide/liquide, température, mode de préparation de la suspension, force ionique, type de solvant) ont un impact plus ou moins important sur le comportement d'adsorption. En particulier, la présence d'éthanol conduit à une diminution de la capacité de sorption. Cette partie de notre étude a permis de définir les conditions opératoires optimales pour la mise en œuvre des approches expérimentales spécifiques de la suite de ce travail.

Le choix du protocole de synthèse pour générer des mésopores dans une série de zéolites, à savoir par désilication - recristallisation, a permis d'obtenir une famille de faujasite. Les différentes caractérisations ont montré que la composition et la microporosité de la faujasite de départ sont conservées. La diffraction des rayons X et les isothermes de sorption de N<sub>2</sub> ont mis en évidence la diminution du volume microporeux, l'augmentation du volume mésoporeux, et le caractère relativement organisé de la phase mésoporeuse. Le rapport Si/Al est évalué entre 15 et 13.

Les changements structuraux vus en DRX ont été confirmés par <sup>29</sup>Si-NMR en analysant l'environnement du silicium et révélant la transformation de l'environnement Q<sup>4</sup> en Q<sup>3</sup> d'une part, et l'augmentation de la contribution Q<sup>4</sup> amorphe, ceci étant due à la dissolution de la zéolithe.

L'introduction d'un réseau secondaire de mésopores dans la faujasite par la méthode de désilication - recristallisation améliore la capacité d'adsorption des molécules volumineuses en augmentant l'accessibilité des sites actifs. La fuchsine basique (BF), colorant volumineux de taille supérieure à celle des micropores, présente une adsorption majoritairement sur la surface externe, et avec l'augmentation de la mésoporosité, cette capacité augmente.

Le colorant linéaire, 1DiA, présente une capacité d'adsorption plus élevée, ce qui révèle que l'adsorption a lieu à l'intérieur des pores. Ce colorant est confiné à l'intérieur des pores de la faujasite, ce qui se traduit par une enthalpie d'adsorption élevée de l'ordre de -50 kJ / mol, une forte organisation des molécules à l'interface et une corrélation entre les molécules elles-mêmes. Pour la série de faujasite présentant des volumes poreux de plus en plus élevés, la capacité de sorption reste constante sauf pour la faujasite hautement modifiée qui présente une légère diminution. Ceci est dû au volume poreux élevé. Dans la mesure où l'espace disponible est plus important, les molécules ont plus de liberté, sont moins organisées et moins corrélées à l'interface comme cela est aussi observé en ITC avec une enthalpie plus faible, et en SHS, avec un facteur de corrélation moins élevé.

La capacité d'échange cationique du matériau, la nature du solvant et la capacité des molécules à pénétrer dans les porosités peuvent modifier les caractéristiques de l'adsorption. La nature des interactions adsorbat / adsorbant et leur modification en fonction rapport Si/Al du matériau, du solvant et la de taille des molécules adsorbées ont été étudiées sur une série de faujasites présentant différents rapports Si/Al, avec trois molécules sondes de tailles différentes, 1-DiA, 4-DiA et 16-DiA, et

pour certains systèmes, en présence de différents solvants (eau, acétonitrile, éthanol, DMSO). La capacité d'adsorption et l'organisation de 1-DiA sur la faujasite à Si/Al = 15 montre la corrélation la plus élevée et évolue de la manière suivante : eau > acétonitrile > éthanol > DMSO. Ceci est en lien avec les propriétés des sites actifs, pour lesquels le proton des sites échangeurs est plus actif dans l'eau que dans l'éthanol ou les autres solvants. Pour le colorant le plus grand, 16-DiA, la capacité de sorption est faible en raison de la faible accessibilité dans les pores.

Les colorants sont plus organisés lorsque la capacité d'échange est la plus élevée (faible rapport Si/Al). Il existe cependant un optimum prenant aussi en considération la quantité de sites acide de Bronsted, qui, s'ils sont trop nombreux, peuvent modifier la conformation du colorant, et donner lieu à moins de corrélation.

Ainsi, nous avons réussi à combiner des approches à la fois macroscopiques et locales pour mettre en évidence, de façon innovante, les effets du confinement lors des processus d'adsorption.



## General introduction

Water pollution is one of our most strategic recurring problems and most difficult because it is associated with humans' lifestyles. As a result, water pollution accidentally or intentionally becomes a universal scourge that leads to environmental degradation, reduction in the quality of water, and poses a threat to public health. It is currently attracting major forces from various operators (suppliers, scientists, legislators, associations, etc.).

This pollution is due to the release of certain hazardous chemical compounds which may or may not be biodegradable (hydrocarbons, phenolic compounds, heavy metals, dyes, insecticides, etc.). These chemicals originate from various industries such as chemicals, textiles, tannery, food processing, pharmaceuticals, etc. The impact of these industrial effluents on wildlife and plants is very harmful. Raising the awareness of socio-economic actors and the public, accompanied by strict regulations concerning discharges, would contribute to the fight against this drift and thus would make it possible to save what can still be.

Many methods and techniques for water decontamination have been developed in recent years. Among these techniques, the chemical precipitation processes, flocculation, ion exchange, electrolysis, membrane processes, and adsorption. The process of adsorption has been studied in this thesis.

Adsorption on activated carbon is the most widely used and recommended for wastewater treatment processes. Despite its effectiveness, activated carbons are rarely found naturally and remain expensive materials. Hence, the search for new products that come from a cheap and available source, is useful.

Zeolites are microporous crystallized solids, containing a regular and organized network of channels, giving them unique properties of activity and selectivity, making them a material of choice in the industry as catalysts, adsorbents or supports. Faujasite, from the family Zeolites, is one of the most studied materials because of their well-known properties of adsorption and retention of pollutants as well as the possibility of their textural modification and/or their functionalization. The description of their structure makes it possible to understand the molecular adsorption properties. In general, we studied the adsorption capacity of the materials established by the measurements of isotherms, and sometimes other characterizations are made such as kinetics.

The molecular interactions phenomena are at the basis of many biological processes and chemical applications. Therefore, understanding these phenomena is a recurring scientific question, especially at the quantitative level. Thus, evaluation of intermolecular affinities is necessary to rationalize any non-covalent chemical phenomenon.

As the interactions result in a rather intense modification of the properties of the materials of species involved, it is possible to exploit any physicochemical technique to stabilize the supramolecular structures concerned. A considerable number of techniques, protocols, and data processing have thus been developed and exploited in the literature. While this diversity results in a rich panel of tools available to the experimenter, the approaches do not facilitate the task of physical chemists and can hinder the comparative reading of the works in the literature. Significant differences can be observed for the same interaction when it is investigated by different techniques.

The thermodynamic values due to the adsorption of organic molecules within zeolite are very important for understanding well the process of adsorption. For this reason, calorimetric measurement must be done. For this purpose, we chose isothermal titration calorimetry ITC which allows a direct measurement of the interaction enthalpy at a given temperature, whereas the other techniques require data acquisition of isotherm at various temperatures, and then the application of the van't Hoff equation. Nevertheless, as this type of treatment generally neglects the variation of heat capacities between free and associated species, the enthalpy obtained by this way might be distorted, thus reinforcing the validity of the ITC. Therefore, once the adsorption measurement is performed, the ITC method is developed to examine the global enthalpy of adsorption as well as to evaluate the interaction between molecules and materials.

Understanding phenomena that occur at the microscopic level in interface geometry and dynamics is crucial for many systems. An interface represents a boundary separating two media of different physical and chemical constitutions. The asymmetry of the forces which exist there as well as the bidirectional geometry are at the origin of very specific properties. In chemistry and materials physics, interfaces are already widely exploited concerning electrocatalysis (environmental electrochemistry, fuel cells), electrodialysis, and the development of barrier layers for example. In addition to the global approach (isotherms and ITC), we elaborate the strategy of this study to get an insight into the organization of molecular dyes, this strategy is being based on the optical response of the adsorbed molecules.

Nonlinear optics, and more specifically the double frequency process, can be very useful for probing the properties of soft or solid matter at sub-wavelength scales. Indeed, due to the coherence of the second harmonic generation response, particularly the second harmonic scattering, it is possible to distinguish spatially correlated from uncorrelated nonlinear sources. Thus, second harmonic scattering has been applied to study the solid/liquid interface of zeolites particles dispersed in solvent, and the molecular organization of dyes at this interface.



Finally, thermodynamic and microscopic approaches are complementary techniques used to produce a complete study of the interface. The global approach probes the interaction between host and guest by measuring the global enthalpy of adsorption which consists of hydration/dehydration and adsorption/desorption. Furthermore, the local one probes the organization of molecules at the solid/liquid interface. Therefore, they can provide an overview of the confinement behavior occurring in the system as summarized in Figure 3.

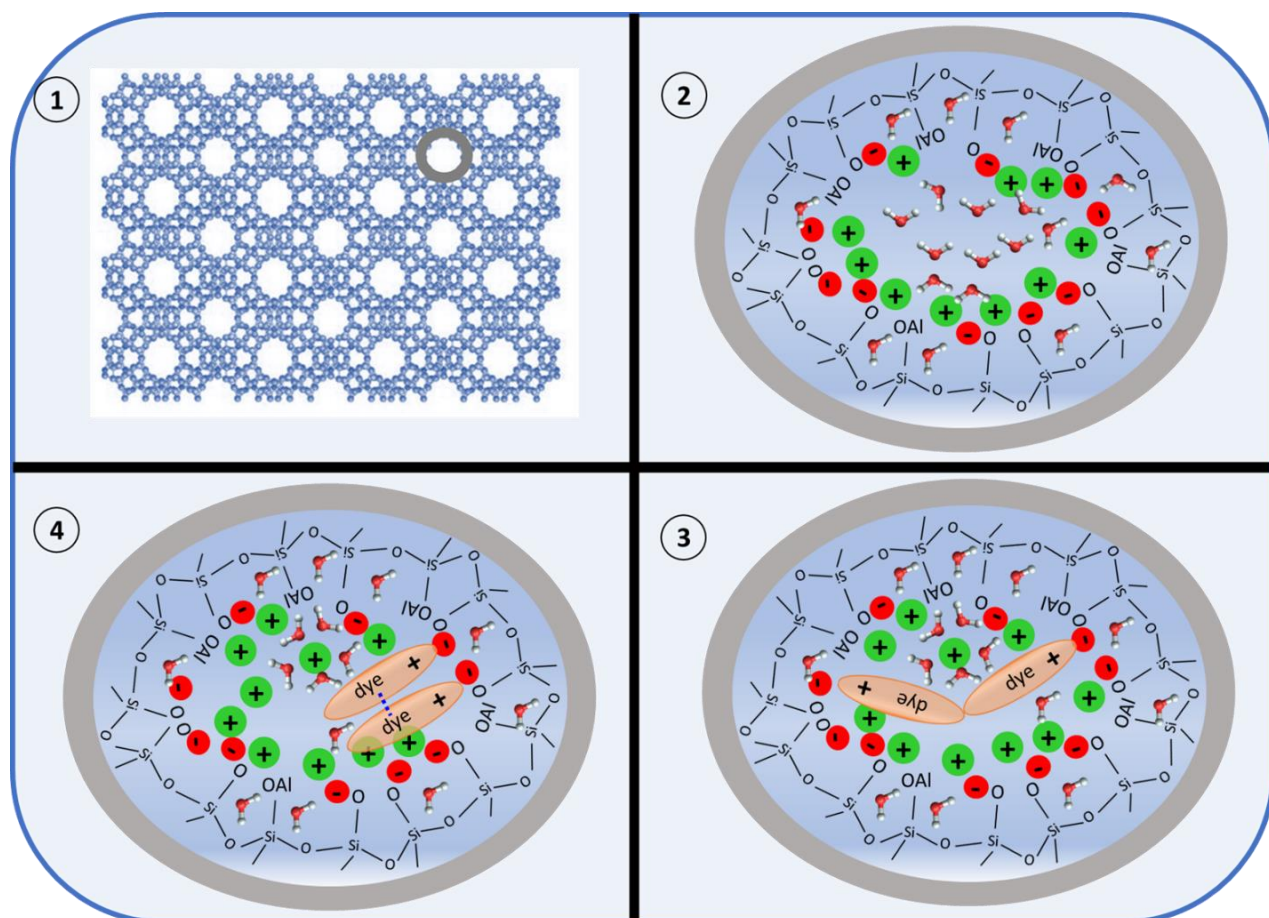


Figure 3: 1) Faujasite frame with highly organized channels structures. In gray a zoom for 2), 3), 4). Zeolite structure consists of Si, Al, O and negative charge obtained after Si substitution with Al that is compensated with cation form. 2) Representation of a possible molecular distribution in a pore with protons water molecules. Negative sites of the Faujasite frame are in red. 3) Representation of a possible configuration for two interacting dyes within the Faujasite pore. 4) Representation of a second possible configuration for two interacting dyes within the Faujasite pore. The blue dotted line represents an interaction.

Figure 3 represents the possible configurations occurring at the solid/liquid interface. 1) represents the zeolite structure with highly organized channels. 2) show the adsorption of water molecules. 3) the adsorption of dye molecule towards zeolite active site with a possible configuration for two interacting dyes. 4) another possibility of adsorption showing the organization of molecules at solid/liquid interface with high interaction between the adsorbing dyes.

In order to properly treat our subject, we have divided it into five chapters:

The first chapter describes the state of art on the material selectivity for dyes adsorption and the modification of its porosity by post-synthesis. After a bibliographic overview, the techniques used for accurate physicochemical characterization have been described. This includes the two main approaches used in the present work with a global approach such as isotherms and thermodynamics of adsorption using ITC, and a local approach by determining the organization of dye molecules at solid/liquid interface using nonlinear optics, particularly second harmonic scattering.

The second chapter is the experimental part. It will present first the molecules and then the description of the material preparation. Our strategy was based on a post-synthesis modification of commercial material. Second, the standard characterization techniques are described. Finally, a detailed technical description of our two main experimental methods is given, with the thermodynamic global approach, together with the local optic approach. These parts contain the different experimental setup, the experimental protocols developed to carry out the different studies, as well as the procedure followed for the data analysis.

The third chapter is devoted to the key parameters for assessing a detailed study on analysis of the chosen material. This part is complementary to the fourth and the fifth chapters which will give detailed analyses of the sorption behavior. The experimental selection of a 1D hemicyanine dye, adsorption onto FAU has been reviewed under various conditions. Then adsorption isotherms of different organic molecules on FAU material have been carried out. Moreover, global and local studies for some systems are detailed.

The fourth chapter presented through a first publication deals with the study of the confinement effect of several dyes at solid/liquid interface. Various commercial adsorbents bearing different Si/Al ratios were applied. A hemicyanine dye molecules that differ from each other by their alkyl chain, and consequently by their hydrophobicity and size, were used as probe molecules. Adsorption isotherms, based on a global scale, have been measured in the presence of different solvents. In addition, based on a local scale, the organization/correlation of molecules during sorption processes has been evaluated. The combination of both approaches allows probing the confined molecules inside zeolitic material.

The effect of modification of faujasite porosity on the adsorption behavior of dyes has been the subject of the fifth chapter, which is presented as a second publication. In this section, unmodified and chemically modified faujasites having different porosity levels were used. The behavior of the linear

and the bulky dye are compared in this chapter. Different results concerning the adsorption, the global enthalpy, and the SHS measurement of two dyes have been described.

And the manuscript ends with a conclusion that allows us to highlight all the results of this work followed by suggestions for future work.



## Chapter I: State of the art

This first part is a synthesis of the state of the art related to this thesis work. In this chapter, we first describe briefly the contamination of water by dyes and the process for their removal. A general presentation of zeolites is then given. We then discuss the different methods of improving the accessibility of the active sites in zeolites, with the various routes to synthesize zeolite with specific morphologies and textures. We then focus on the work done on the thermodynamics of adsorption as a macroscopic approach, to study the molecular adsorption in confined systems. The local approach is also used and based on non-linear optical techniques, in particular second harmonic scattering. These techniques allow to quantitatively determine the correlation and organization of the molecules at the interface. We will show during this thesis that the coupling of these various techniques allows access to complementary information, essential to better understand interfacial phenomena.

### 1 Colored molecules and Dyes

#### 1.1 *Dyes in our civilization*

The use of dyes in human everyday life dates back to ancient times. Primitive populations used the paints for body decorations. Ancient Egyptians also used dyes to dye rocks and ceramics. At the time, the coloring materials used were of natural origin extracted either from plants such as indigo or animals like carmine. The use of these natural dyes continued until the first half of the 19th century. After, they have been gradually replaced by synthetic dyes. Today, dyes are considered as basic materials in many industries such as textile, leather, paper, plastic, pharmaceutical, cosmetic... etc. The global production of dyes hits records with approximately 700000 tons/year.

The release of dyes into the environment (soils, aquatic media, ...) is a critical issue. The presence of such contaminants in water highly impacts ecosystems. Numerous studies have shown that exposure to dyes causes negative effects on human health.

#### 1.2 *Natural and synthetic dyes*

Dyes designate products capable of dyeing a substance in a durable way. It is characterized by an assembly of chromophoric groups, auxochromes and conjugated aromatic structures. These groups have the property of interacting and sometimes absorbing a part of the white light in the visible spectrum (from 380 to 750 nm) and diffusing a colored light. For example, the absorption band of the carbonyl group ( $=C=O$ ) occurs at a wavelength of 270-280 nm. The chromophores are groups of atoms that carry at least one double bond and they form a conjugated sequence with the rest of the molecule.

These groups are responsible for the coloring of the molecule. Table 1 presents a list of the main chromophore classified by their functional group. An auxochrome is a group of ionizable atoms capable of changing the absorption frequency of a chromophore. They allow the fixation of the dyes on the material. Most of the dyes are toxic, persistent and non-biodegradable. The notion of dyeing is considered when it comes to color textiles using water-soluble products; the insoluble dyes are called pigments.

A natural dye is a coloring material derived from natural sources such as plants, animals and minerals. Most natural dyes come from the roots, berries, bark, leaves or wood of dye plants, or from biological sources like fungi or lichens. A synthetic dye is produced by chemical synthesis from organic molecules. They are widely used in textile dyeing, cosmetics, leather, paper printing, food, and pharmaceutical industries. They are used in large scale production.

Table 1 : The main chromophore classified by their functional group<sup>1</sup>

Chromophore		Auxochrome	
	Functional group		Functional group
Azo	(-N=N-)	Amino	(-NH <sub>2</sub> )
Nitroso	(-NO or -N-OH)	Methylamine	(-NHCH <sub>3</sub> )
Carbonyl	(=C=O)	Dimethylamine	(-N(CH <sub>3</sub> ) <sub>2</sub> )
Vinyl	(-C=C-)	Hydroxyl	(-HO)
Nitro	(-NO <sub>2</sub> or =NO-OH)	Alkoxy	(-OR)
Sulphur	(>C=S)	Electron donor groups	

### 1.3 Probe organic molecules

In the present work, dyes will also be used to locally probe adsorption phenomena, since (i) they will be adsorbed in our selected systems and conditions, and (ii) they will be detectable using non-linear optics (described below). The main probe molecules used in this thesis are DiA molecules. DiA is a cationic amphiphilic molecule. It has a polar hydrophilic head centered on the positive charge which has a strong affinity for water. The other part is hydrophobic and formed by two aromatic rings to which are attached to two apolar aliphatic chains of *n* carbons as shown in Figure 4. When the number of carbons in the aliphatic chains increases, the molecule becomes more hydrophobic. Therefore, the solubility of these molecules depends on the length of the alkyl chain.

DiA molecule has the useful property of having a strong nonlinear optical response due to its "donor-acceptor" structure.<sup>2</sup> These compounds are also called "push-pull" forming a delocalized  $\pi$ -electron system. The nitrogen atom has an electron pair not involved in a chemical bond. It is thus

called the neutral form of the compound, i.e. without charge transfer. When the transfer takes place, one of the two electrons of the lone pair is moved towards the carbon atom of the aromatic ring. From one to the other, due to the alternation of the conjugated bonds, a negative charge is towards the positive charge of the pyridinium group called the acceptor group while the donor group is uncharged. The organic compound thus takes a form called zwitterionic: the compound keeps globally its initial positive charge but a strong dipole is established by charge separation.

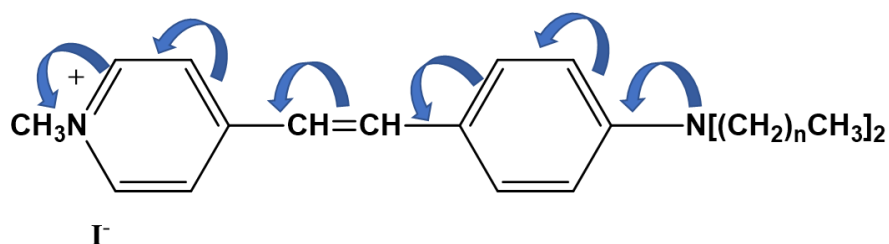


Figure 4 : DiA structure  $(14.5+n) \text{ \AA}/4.3 \text{ \AA}$  for length/height ratio with  $n=1, 4,$  and  $16$ , with their charge transfer through double bonds.

## 1.4 Processes for dyes removal

The intense and irrational use of dyes and the massive risks posed to the environmental quality and human health have been at the origin of studies to identify methods to remove these pollutants from the environment, or at least decrease their concentration. Various processes, such as biological, physical and chemical procedures were developed to eliminate dyes from aquatic environments. Some of these processes are coagulation-flocculation method, biological method, membrane filtration, solid phase extraction, and the classical adsorption on specific materials.

### 1.4.1 Coagulation-flocculation method

Coagulation-flocculation is a physico-chemical method of water treatment. Its principle is based on the charge neutralization and further agglomeration of colloidal particles. These particles are characterized by a small diameter and generally negative charge which generates repulsion between colloids. This produces a stable colloidal system that hardly settles down. The addition of a coagulant, often iron or aluminum salts in the case of negatively charged colloids, allows charge neutralization of these particles, decrease of the repulsion and finally the formation of agglomerates which can then be eliminated by decantation and/or filtration.

### 1.4.2 Biological method

This method consists in breaking the organic pollutants present in the water using microorganisms. There are two modes for this type of treatment:

-Aerobic treatment method takes place in a basin made up of active sludge on which organic pollutants will undergo biodegradation by bacteria and other microorganisms. After purification, the sludge is separated from the wastewater by sedimentation in a decantation system. Part is recycled and the excess is discharged after pressing or centrifugation.

-Anaerobic treatment method is based on the degradation of organic pollutants by microorganisms in the absence of oxygen. It leads to the formation of carbon dioxide, methane and water.

### 1.4.3 Membrane filtration

Membrane separation filtration is considered amongst the most important in the field of water treatment. In addition to their efficiency and their respect for the environment, this type of treatment is achieved without the addition of any chemicals. Membranes are extremely fine filters capable of filtering water and therefore removing existing contaminants depending on the properties of pollutants and the cutoff membranes. The disadvantages of this technique are the following: it is very expensive due to the cost of membranes, and requires significant means of operation or maintenance, in addition to the need for water remineralization after treatment.

### 1.4.4 Chemical oxidation

Chemical oxidation techniques consist in using the oxidizing power of chemical substances to transform or destroy pollutants. The oxidizing substances are multiple (ozone, halogens, hydrogen peroxide). These treatment processes, unlike physical processes, are capable of eliminating the pollutants until they are eventually mineralized. The disadvantages of these techniques are the formation of intermediate compounds of oxidation that can present toxicity as high as their precursor.

### 1.4.5 Photodegradation

Photodegradation is a process for the degradation of photodegradable molecules to produce small molecules. This process is performed by photon absorption, especially wavelengths of sunlight like visible light, ultraviolet light, infrared radiation. Oxidation and hydrolysis are usually used in photodegradation. In the case of organic dyes, photodegradation plays a dominating role, but it is not the only factor. The composition of its environment also plays an important role, too high or too low humidity, or strong episodic variations, the storage temperature, hot-cold cycles, an oxygen-rich



atmosphere or a closed environment, the presence of atmospheric pollutants, bacteria or fungi, are all factors that can impact the kinetics and nature of a degradation. The disadvantage of this technique is the destruction of the dye molecules, which leads to the loss of their physical properties.

#### 1.4.6 Adsorption processes

Adsorption has been known since ancient times. The adsorbent properties of materials like clays, sand, charcoal and zeolites were used by the Phoenicians, the Assyrians, the Egyptians, the Greeks, ... These processes included desalination of the water, clarification of fats and purification of water. This phenomenon is currently still the object of many researches.

##### 1.4.6.1 Brief history about adsorption

The phenomena of adsorption have been studied quantitatively by a large number of scientists from the 18th century. The first quantitative studies of gas retention on certain forms of active carbon seem to be made by Scheele in 1773 and by Priestley in 1775<sup>3</sup>. The first attempts concerning the relationship between the quantity adsorbed and pressure were then made by Chappuis and Kayser in 1881. In the same year, Kayser has effectively applied the terms "adsorption" and "isothermal" to his measurements<sup>3</sup>. Later, in 1907, Freundlich was one of the first researchers to conceive the notion of the adsorption capacity of solid surface.<sup>4</sup> He proposed a general mathematical relation for the well-known isotherm now known as the "Freundlich isotherm". During the last century, adsorption studies become countless. The most important developments in theoretical interpretation of gas adsorption data were made by Zsigmondy, Polanyi, then Langmuir, during the first years of the twentieth century. In particular, the work of Langmuir, in 1916<sup>5</sup>, brought a radical change in the approach of surface science. Indeed, he quickly suggested that adsorption onto solid surfaces involved the formation of a monolayer. In retrospect, it may be considered that Langmuir's theory produced a real revolution in surface science.

Another milestone in the history of gas adsorption was the work of Emmet and Brunauer which preceded the publication of Brunauer-Emmet-Teller (BET) in 1938. In 1934, they<sup>6</sup> made their first attempt of nitrogen adsorption on an iron catalyst at low temperature. Then they developed a method for determining the specific area from these experimental data. This so-called BET method is now accepted as a standard procedure for the determination of the specific surface area of a wide range of fine powders and porous materials. However, it is important to point out that their equation is based on a very simplified multilayer adsorption model. Therefore, it is essential to verify that several conditions are met so that its use is valid. Otherwise, precaution must be taken when this method is used due to the lack of a rigorous theoretical background, i.e. the case of zeolites where it could only be used in the qualitative analysis of their pores<sup>7</sup>.

### 1.4.6.2 Definition of adsorption

The contact of two phases A and B forms an interface. The lack of symmetry of intermolecular forces at the interface of phases A and B, for example, solid–liquid, causes a change in the properties of A and B directly nearby from the interface.

The molecules at the surface level of the phase of A and B do not have the same environment within solid A or liquid B, which implies the existence of a surface field, which will attract molecules to be adsorbed onto the surface. The phenomenon is called "adsorption", the solid is "the adsorbent" and the other phase is "adsorbate". Sorption term is also used to refer to both adsorption and desorption. We can consider that the immediate space located on both sides of the interface, in which the properties vary, forms a new phase called the adsorbed phase. Within this phase, links or lateral interactions may exist between the molecules adsorbed themselves, especially when the coverage ratio is high.<sup>7</sup>

The solid might be covered with a molecular layer at low pressure or concentration which is called a "monolayer". Whereas, when the surface of the solid remains attractive despite the deposition of the first layer, other layers can be formed: this is called "multilayer" adsorption. The curve which describes the quantity of molecules adsorbed on the surface of the solid as a function of equilibrium concentration or pressure, for a given temperature, is called an "adsorption isotherm".

The first layer of molecules is in direct contact and interaction with the surface and the nature of forces between the adsorbed molecules and the surface determines the nature of the bond. If the type of adsorption involves weak interactions such as van der Waals interaction, the adsorption phenomenon is said to be "physisorption". This phenomenon is reversible. In contrast, if strong chemical bonds between the adsorbed molecules and the surface are formed, the process is noted chemisorption, with high energy interaction, and irreversible behavior.

### 1.4.7 Adsorption of dyes

Adsorption on solid materials is considered an efficient method for dyes removal due to the chemical stability of these dyes and the difficulty of their degradation.<sup>8</sup> In comparison with other processes listed above, the sorption process has been chosen because the design and the operating conditions are flexible and the adsorption process does not generate any new pollutant. Due to the possible reversibility of the process, there are options for the sorbent to be regenerated. Many materials have shown considerable retention capacities for these pollutants. Activated carbon is among the most used adsorbents. Their large specific surface, their richness in active sites, allow to absorb pollutants such as organic compounds<sup>9</sup>, methylene blue, and azo disperse dyes. However, this

family of materials makes the adsorption process costly since the activated carbon is expensive and difficult to regenerate depending on the type of activated carbon and the nature of the targeted pollution. Hence there is a need to develop other alternatives. Rafatullah et al.<sup>10</sup> have listed in a review the different low-cost adsorbents (including zeolite) used to adsorb methylene blue since it has been identified as a model for organic removal due to its high adsorption capacity towards activated carbon. Dai et al.<sup>11</sup> reported in their article the efficiency of graphene oxide aerogel supported by polyvinyl alcohol material for Congo red and methylene blue removal. The zeolites MCM-22<sup>12</sup> and MCM-41<sup>13</sup> were used to adsorb organic basic dyes from waste effluents. Methylene blue, crystal violet, and rhodamine-B were studied in the case of MCM-22 and malachite green, crystal violet, and rhodamine-B in the case of MCM-41. Due to the high removal efficiency of zeolite toward most dyes compared to others, zeolites were selected in this thesis as reference material.

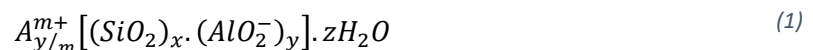
Industrial dyes removal is a key issue for the environment. The adsorption process is one of the most interesting techniques in terms of efficiency, flexibility, and cost...

## 2 Zeolites

### 2.1 Introduction to zeolites

Zeolites are an important class of porous materials with Aluminum Silicate well-defined crystalline structures. They are composed mainly of aluminum, silicon and oxygen. These elements are arranged in tetrahedral structures of  $\text{SiO}_4$  and  $\text{AlO}_4$  which in turn form various types of three-dimensional zeolitic frameworks depending on their arrangement leading to an unlimited variety of zeolite structures.<sup>14</sup> The substitution of silicon atoms by aluminum creates a negative charge within the zeolite structure which is counterbalanced by the presence of compensating cations, often alkaline metals or alkaline-earth metals. It is also possible to substitute Si or Al atom with other elements such as phosphorus or germanium. The materials obtained are then grouped under the name of zeotypes. These cations are quite mobile in the lattice and thus can be exchanged with other cations leading to the ion exchange property of zeolites.<sup>15</sup> During the sorption or exchange, the molecule diffuses progressively in the zeolitic channels until it reaches a preferential adsorption site. Bronsted acid is produced when the negative charge is compensated by proton. However, Lewis acid is generated when water is lost at a high temperature.

The general chemical composition of a zeolite is represented by the following formula:



Where

- A is a cation with the charge m
- (x+y) is the number of tetrahedral per crystallographic unit cell
- x/y is the framework silicon to aluminum ratio (Si/Al)
- z depends on the degree of hydration

## 2.2 Classification of zeolite

Over 255 types of structures (natural and synthetic) have been identified by International Zeolite Association (IZA). They assign a three-letter code to each structural topology. This is applied for material identification and does not refer to any aspect of the chemical composition. The most commercialized zeolites are zeolites A (structural type LTA), Beta (\*BEA), ZSM-5 (MFI), mordenite (MOR), ferrierite (FER), X and Y (FAU). Zeolites structures are composed of internal voids like pores, cavities and channels. They are classified according to the microporosity and channel system. The size of the pores of a zeolite is related to the number of tetrahedra that create the channels or the openings. There are for example zeolites with small pores (around 4 Å) with channels of 8 tetrahedra, medium pore zeolites (around 5.5 Å) with channels of 10 tetrahedra and zeolites with large pores (around 7.5 Å) made up of channels of 12 tetrahedra. Finally, the porous network of a zeolite can be of 1, 2 or 3 dimensions (L zeolite, mordenite, Y zeolite respectively) depending on the interconnectivity or not of these channels (Figure 5).

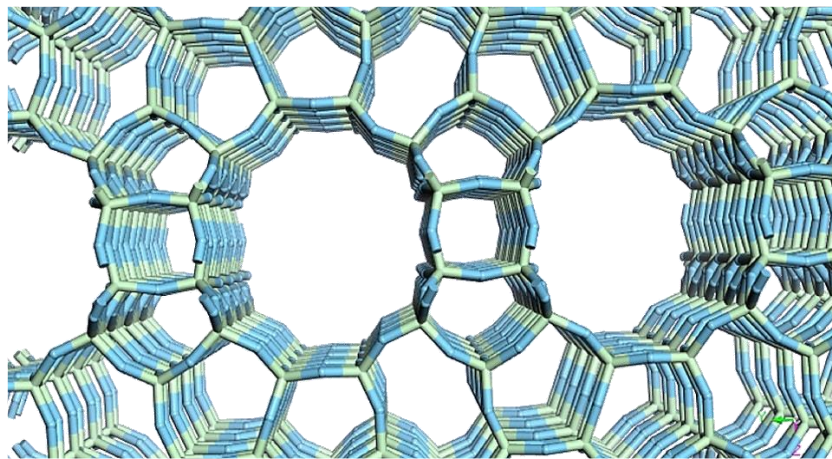


Figure 5 : 3D Zeolite network showing the interconnectivity of the channels taken from Zeolyst website.

## 2.3 Applications of zeolites

The remarkable physico-chemical properties of zeolites are at the origin of their three applications: ion exchange, adsorption and catalysis. For industrial use, natural zeolites are by far the most widely used. However, because of their heterogeneity of structure and significant presence of

impurities, they are only used as base products in high-tonnage, low-value-added applications. Concerning synthetic materials, only about twenty of the existing structures (i.e. 8%) are used for commercial operations, including the famous BEA, FAU, FER, MFI and MOR zeolites, called the "Big Five" zeolites, which are frequently used in the catalysis industries.

### 2.3.1 Ionic exchange

As presented in the previous section, zeolites possess charge-compensating cations occluded in the porosity of the crystalline framework which can be exchanged in equilibrium with the surrounding solution. The modification of the nature of the cations present in the zeolite allows to control its acid character (Brønsted acidity if the cation is a proton, Lewis acidity if the cation is an alkaline), basic (with an alkaline cation, the tetrahedrons ( $\text{AlO}_4^-$ ) and the anionic oxides of the network are basic sites) or even its stability (by the size of the cation in comparison to the size of the pores).<sup>16</sup> This remarkable exchange property is also used to modify a medium by trapping certain ions. For example, in detergency, which is the most important application concerning 78% of the zeolites synthesized for industrial purposes, the aim of the process is to trap the calcium and magnesium ions contained in water in order to soften it and improve the efficiency of the washing agents. This is achieved by ion exchange with i.e. the sodium ions initially present in the zeolite. This exchange property is also used for soil fertilization (exchange of ammonium ions) and also the elimination of heavy metals (copper, nickel and zinc) in wastewater or radioactive cations present in the environment due to wastewater discharges.<sup>17</sup> This was notably the case during the Chernobyl nuclear disaster, where a large quantity of clinoptilolite and chabazite was spread in order to trap the elements cesium and strontium released in nature. The ionic exchange mechanism is represented in the figure below (Figure 6).

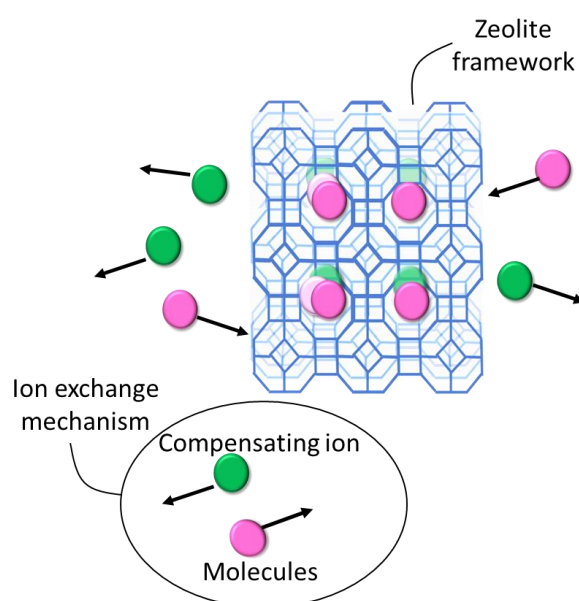


Figure 6 : Ion exchange mechanism between cationic molecules and zeolite compensating ions.

### 2.3.2 Adsorption and separation

Depending on their crystallographic structures, zeolites have pores and channels of well-defined sizes, sometimes close to the size of molecules, which gives them the name of molecular sieve. Their adsorption properties are based on two types of contributions, the size differences between the molecules and the porosity, and the interaction of adsorbates with the internal surface of the zeolite. This kind of selective adsorptions allows the use of zeolites in various applications such as dehydration or purification. For example, by playing on the silicon to aluminum ratio of the zeolite framework, its affinity with water varies (the more the material is rich in silica, the more hydrophobic it is), which directly increases or decreases the capacity of adsorption of organic molecules according to their intrinsic affinity with water molecules in comparison with their affinity for the surface.

Historically, the first use was for water capture to preserve organic solvents and gases from air humidity (desiccant). Today, zeolites continue to be used extensively as desiccants in formulations such as resins, polyurethanes, sealants, etc.

Zeolites are also used for drying natural gas and cracked gases and for the removal of sulfur compounds from natural gas and LPG (liquefied petroleum gas). In petrochemicals, they are used for the separation of xylenes as well as for the separation by molecular sieving of linear and branched paraffins.<sup>18</sup> Thanks to zeolites, one can also produce oxygen with 93-95% purity from the air by pressure swing adsorption (PSA) or vacuum swing adsorption (VSA), in which nitrogen is preferentially adsorbed.<sup>18</sup> Finally, a large quantity of natural zeolites (mainly clinoptilolite) is used in cat litter to adsorb ammonia from urine and thus limit odors.

### 2.3.3 Heterogeneous catalysis

Zeolites play a major role in heterogeneous catalysis, which is not the most used application but it is, by far, the one with the greatest added value. A catalyst is a chemical species, regenerable, which makes it possible to accelerate the speed and to increase the selectivity of a chemical reaction without participating in the reaction balance. In particular, heterogeneous catalysis is based on a mechanism of diffusion - adsorption - reaction - desorption - diffusion of reactants and products on the surface and within a catalyst. These interactions modify the reaction path and lower the energy barrier of the chemical reaction, which allows the conversion of reactants into products more quickly and under milder conditions. Nowadays, more than 85% of industrial processes use a heterogeneous catalyst, which represents a total market of 16 billion dollars in 2008.<sup>19</sup> Indeed, the intrinsic properties of zeolite make it a material of choice for catalysis by offering numerous advantages:

- A regular porous structure of molecular size in which the active sites are located, where the reactions take place.
- A wide range of structures offering different active centers, pore sizes and shapes and openings inducing different transformation speeds, stabilities and selectivities.
- An adaptability of the active centers allowing them to be shaped as needed for an acidic basic, redox or bifunctional (metal-acid) catalysis.
- The use of clean, atomic and energy-saving processes. The reactions being more selective with zeolites, the economic profitability increases and fewer pollutant discharges of pollutants linked to the separation steps are to be expected. In addition, these materials do not present any danger for the health.

Zeolites thus become an essential component of the most widely used catalysts in oil refining. They are also widely used in petrochemicals for the production of essential aromatics for the chemical industry: benzene, paraxylene, alkylbenzenes (ethylbenzene, cumene) and the production of ethylene and propene from methanol.

#### ***2.4 History and characteristic of zeolite Y (Faujasite-type)***

Existing in its natural state and discovered by the mineralogist Faujas de Saint-Fond from Montile, faujasite remains a rare natural mineral which is not subject to any exploitation project. However, it has been widely studied in the 1950's in order to synthesize an isostructural compound.

The faujasite structure (FAU), as is depicted in Figure 7, consists of 24  $\text{TO}_4$  tetrahedra connected to form eight rings with six-tetrahedra and six rings with four-tetrahedra, which form a cube-octahedron called sodalite cage or  $\beta$  cage. The structure can be described as an assembly of cube-octahedra connected to each other by hexagonal prisms. This assembly reveals a large polyhedral cavity with 26 faces called supercage (or  $\alpha$  cage) which constitutes the basic unit of the microporosity of this zeolite. The supercages are assimilated to pseudo-spheres of 13 Å in diameter and about 850 Å<sup>3</sup> of volume. They are connected with each other through openings with 12 oxygen atoms (7.4 Å in diameter), which allows access to many molecules. The  $\beta$ -cage has a diameter of 7 Å and a volume of 160 Å<sup>3</sup> approximately. It is connected to the supercage by openings with 6 oxygen atoms of 3 Å in diameter.

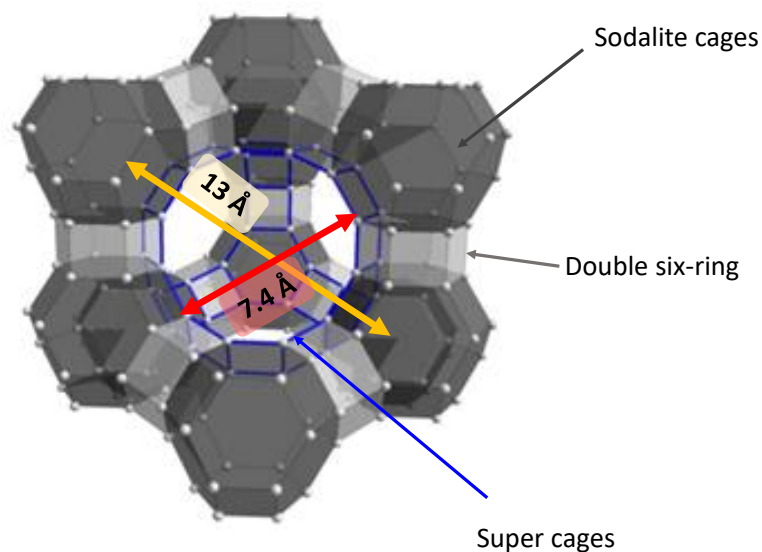


Figure 7 : A Faujasite framework with only the tetrahedral central atoms (Si or Al)<sup>20</sup>

The elementary unit cell of faujasite consists of 8  $\alpha$  cages and 16 hexagonal prisms, forming a face-centered cubic structure. Its lattice parameter varies from 24.2 to 24.8 Å depending on the aluminum number in the frame and the compensation cations (nature and number). There are two types of faujasite zeolites (lattice formula  $\text{Na}_x\text{Al}_x\text{Si}_{192-x}\text{O}_{384}$  with  $x$  the number of aluminum and sodium in the structure) according to the composition and the Si / Al ratio. FAU-X and FAU-Y have the same structure but differ from each other by their Si/Al ratio (amount of aluminum substituting silicon), both containing 120 water molecules. In zeolite X, the Si/Al ratio ranged between 1–1.5, whereas in zeolite Y it is higher than 1.5. In terms of industrial applications, zeolite Y (FAU) is one of the most zeolites used in catalysis. This is due to its structure, allowing the adsorption of a variety of molecules, thus a good candidate for a large molecule such as dye, pesticides, drugs, ... In addition to its remarkable thermal stability, it allows multiple structural modifications to be made as required.

Nevertheless, these materials suffer from their own microporous structure, indeed this generates a diffusion limitation which does not allow the reagents/products to migrate readily to the active sites and then to the exterior of the particles<sup>21</sup>. Microporosity over a long path causes diffusion complications. Indeed, the transport of a molecule in a pore having a similar size is difficult. Moreover, the small size of the micropores makes the zeolite inaccessible to a wide variety of molecules that can allow them to react only at the external surface. Finally, these diffusional limitations are caused by restricted access and slow transport to the active sites confined in the micropores, thus inducing a low utilization of the material for adsorbing large molecules. So, hierarchical materials offer increased accessibility of their active sites located in the micropores and improve diffusion problems by building



large pores (meso or macropores) connected to the micropores. These hierarchizations can be prepared in various ways.

Zeolites are the most used material in the adsorption process due to their unique properties such as high cationic exchange capacity, thermal and hydrothermal stability, shape selectivity... However, bulky molecules can block the pores and limit their diffusion toward the materials, therefore, reduce its efficiency. Nowadays, the use of hierarchical zeolites is of interest to many adsorption processes that can overcome or decrease these limitations.

## 2.5 Hierarchical zeolites

### 2.5.1 Definition and properties of hierarchical zeolites

As mentioned by Schwieger et al.<sup>22</sup> the material is called “hierarchical” if it achieves two criteria. First, the structural elements have to be characterized by more than one length scale. Second, each of these structural elements must have a very distinct but complementary function. Hierarchy can be found in many aspects of daily life, from the simplest cell to the complex systems like electricity, butterfly wings, water, lungs and blood circuit in the human body. Hierarchical porous materials or, micro–mesoporous materials are defined as porous materials having a wide distribution of interconnected pore sizes, spanning several orders of sizes. The interest of these materials lies in their ability to combine a large specific surface and an improved mass transfer property. In addition, it enables the improvement of sorption processes which is the driving force for the development of hierarchical materials. Indeed, their very large specific surface area gives them a large number of active sites and their hierarchical structure gives them a transport of fluid and increased access to all sites. These materials have a very potential for the treatment of polluted water under flow. In fact, if the hierarchization is efficient, it allows to considerably reduce the effects of pressure drop through the material.

Hierarchical zeolites combine micropores (below 2 nm), which are the characteristic of zeolites and ordered mesopores (between 2 and 50 nm) or even macropores (above 50 nm) that can be either restricted to the external layer of the zeolite crystal or connected to the microporosity. The characteristics of the additional porosity such as pore size and pore connectivity are governed by the synthesis pathways. These materials began to attract attention in the 2000<sup>s</sup> and numerous reviews have been devoted to them.<sup>23-27</sup>

Two main methods are commonly used for building porosities to obtain hierarchical zeolites, with “**bottom up**” or “constructive” and “**top down**” or “destructive” approach, both of which being described in the following sections.

## 2.5.2 Synthesis of hierarchical faujasite material via mixed route

In literature, a large number of methods are available for the preparation of porous materials bearing hierarchical properties. In this context, we will present the current state of knowledge relating to the preparation of hierarchical faujasite by using a mixed route (desilication-recrystallization synthesis) related to the physicochemical properties of the zeolites required.

In recent years, numerous research teams have focused their efforts on the development of physical or chemical techniques to hierarchize zeolitic materials<sup>28-30</sup> by generating a secondary network of porosity (mesoporosity and/or macroporosity). The amount of information from this work provides an access to a wide range to the future studies which allows the improvement of the experimental conditions to hierarchize a given zeolite class.

### 2.5.2.1 The constructive route

The first category is called “assembly” or “bottom up” or “constructive”. It works constructively and consists of introducing the porosity at the time of the synthesis of the zeolite. It is considered to be more challenging as it often involves complicated templating routes, such as hard- and soft-templating.<sup>29</sup>

- *The “zeolitisation” of amorphous mesoporous materials*

This method consists in crystallizing the walls of an ordered amorphous mesoporous material<sup>31</sup>,<sup>32</sup> or not<sup>33,34</sup> using molecular structuring agents. This technique leads in most cases to heterogeneous composite materials, with well crystallized zeolite phases and amorphous phases. Moreover, the conditions of crystallization of zeolites (high temperature and high alkalinity) are incompatible with the stability of amorphous mesoporous materials and can lead to a collapse of the mesostructure.

- *The synthesis of materials with simultaneous creation of micropores and mesopores*

This approach requires the use of a mixture of “soft” or “hard” structuring agents for the formation of micropores and mesopores, as well as aluminosilicates precursors.<sup>31, 34, 35</sup>

Synthesis using soft structuring agents can be done in one<sup>34, 35</sup> or two steps<sup>31, 35</sup> but most often leads to a heterogeneous mixture of the mesoporous and zeolite phases. Indeed, the two structuring agents act rather competitively and the control of the interactions between (i) the surfactant and the

silica for the formation of the mesopores on the one hand and (ii) between the molecular structuring agent and the silica for the formation of micropores on the other hand is very delicate.

In order to avoid competition between the two structuring agents, the team of Holland et al.<sup>36</sup> replaced the soft structuring agent for the formation of mesopores by a hard structuring agent, in the case polystyrene beads. After calcination of the polymer, a macroporous material with zeolitic microporous walls was obtained. The conditions of impregnation are essential to obtain homogeneous materials. Indeed, the impregnation of the zeolite must take place only in the interstitial pores of the substrate to avoid the formation of purely microporous zones. For that, it is preferable to proceed by successive impregnations of the substrate by the zeolite gel synthesis. This method allows to obtain micro-mesoporous materials of which it is possible to control the size, the shape and the connectivity of the mesopores according to the choice of the structuring agent.

Generally, the advantage of this approach is to possibly control the size, the morphology and the ordering of mesopores<sup>37</sup> depending on the use of the template and when tuning the length of the template used. However, there are a lot of disadvantages behind this category depending on the path used, such as the disordered nature of mesoporosity, the low control on the mesopore size, the cost and thus the lower attractivity for large scale use.<sup>23, 28, 30, 38</sup>

### 2.5.2.2 The destructive route

The zeolites framework being made up of silicon and aluminum surrounded by oxygen atoms, the destructive methods for the creation of mesopores consist in the selective elimination of silicon or aluminum atoms. These demetallization techniques are called desilication and dealumination.

- ***Dealumination***

Dealumination is one of the first methods of creating mesoporosity in zeolites and is the most widely used demetallization technique in the industry.<sup>39, 40</sup> It is carried out either by steam treatment (steaming) or by acid treatment. Some common methods by heat treatment<sup>41-43</sup> or chemical treatment<sup>40, 44</sup> are also described in the literature but are less used. The steaming treatment is the most used method for the generation of mesopores in zeolites. It is carried out at a high temperature, generally above 500°C, under steam flow. The acid treatment uses concentrated solutions of acids to hydrolyze the Si-O-Al bonds. The nature of the acid used and the structure of the zeolite have a great influence on the efficiency of the method. Giudici et al.<sup>45</sup> studied the effect of acid on the dealumination process. They found that oxalic acid is more effective than nitric acid which can be explained by the double nature of oxalic acid. It can act as hydrolyzing and chelating agent that is capable to form trioxalato aluminum complex as well as it has a large effect on Si/Al.

However, in addition to the modification of the porosity of the materials, this method causes a decrease in the density of acidic sites. Indeed, the elimination of aluminum from the network is responsible, among other things, for the loss of Brønsted acid sites. Moreover, dealumination tends to create an accumulation of aluminum atoms outside the network, which can cause an increase in the number of Lewis acid sites. Generally, a second steaming treatment or acid wash under milder conditions is applied to the material to avoid this problem.

- *Desilication*

Desilication is the second method of demetallization used for the creation of mesopores in zeolites. It is a technique that is now fairly well described in the literature and which consists this time in selectively extracting the silicon atoms from the zeolite lattice using a basic solution.

Desilication, or basic treatment, was first introduced in the late 1960s.<sup>46</sup> It is a simple method experimentally. The experimental conditions depend on several parameters: the concentration of the base, the temperature and the time of treatment. Generally, the alkaline solution used for the extraction of silicon is sodium hydroxide (NaOH). The formation of additional pores is obtained after Si removal from the framework by selectively hydrolyzing Si-O-Si bonds.

There are also works reporting the use of organic bases such as tetrapropylammonium hydroxide (TPAOH) on ZSM-5<sup>47, 48</sup> and tetrabutylammonium hydroxide (TBAOH) on \*BEA<sup>49, 50</sup> have shown that the activity of these molecules during desilication allows the creation of mesoporosity while preserving the microporosity. Desilication, in comparison with dealumination, alters to a lesser extent the composition of the material and subsequently its acidic properties, since in theory this method does not remove any aluminum atoms.

Ogura's team used the desilication route on ZSM-5 ( $\text{SiO}_2/\text{Al}_2\text{O}_3=39.4$ ) in the early 2000s.<sup>51</sup> They find that the selective removal of silicon from the lattice of zeolite does not lead to any structural change. However, the dissolved silicon is easily precipitated on the surface of the ZSM-5 crystals, forming a layer of amorphous silica and leading to pore blockage. The use of lower NaOH concentrations and shorter reaction times tend to reduce this problem.

It has been shown by Ogura's team<sup>51, 52</sup> that the amount of Si removed increases progressively with the duration of the treatment. The quantity of Al eliminated is significantly lower than Si and goes through a maximum before decreasing for longer reaction times. We can therefore conclude that the alkaline treatment of the zeolite leads to selective extraction of silicon from the lattice. This quantity of silicon removed during the alkaline treatment is then quantified and it corresponds approximately to the volume of the mesopores formed.

Concerning the porosity of the material after desilication, the analysis of the nitrogen adsorption-desorption curves proves that the microporosity is preserved. At constant NaOH concentration, the increase of the reaction time amplifies the diameter of the mesopores. However, if the treatment conditions used are too extreme, a decrease in microporous volume is obtained. In addition to the impact on the microporosity, the use of severe zeolite treatment conditions (high NaOH concentration, long treatment times) induces a significant change in the morphology of the crystals. There is indeed the formation of cracks and defects on the surface, and then the edges of the grains appear as "melted", and finally the collapse of the grains is observed.<sup>52</sup> Under optimal desilication conditions, the fact that there is no intrinsic modification of the microporosity of the zeolite, while the external surface increases considerably, shows that the mesopores are created following the destruction of the network, from the outside to the inside of the crystal.<sup>53, 54</sup>

The same effect as that observed on ZSM-5 was found by Li and his team with mordenite.<sup>55</sup> The X-ray diffraction peaks for the modified MOR gave a broad peak with a decrease in their intensity which reflects that the grain size of the zeolite decreases after desilication due to the Si removal. Defects and cracks are also observed on the surface of the grains, which leads to the partial collapse of the large particles, to give particles of smaller sizes.

Subsequently, the team of Groen et al.<sup>56</sup> carried out the majority of the studies on desilication. They showed that desilication was an effective method for the creation of extra-porosity. After working on MFI-type zeolites, they studied the behavior of mordenite and BEA during desilication. In addition, they obtained in 2007 the first mordenites with intra-crystalline mesoporosity that retained their acidity. It was also that demonstrated by this team the existence of an optimal Si/Al ratio of the zeolite lattice between 25 and 50 to obtain the best desilication results, i.e. a controlled mesoporosity, conservation of microporosity and acidity. To obtain such a value of Si/Al ratio, preliminary treatment of dealuminating the zeolite is often necessary before desilication.<sup>55</sup> Thus, to control independently the porosity and the acidity of the zeolite, several combinations of desilication and dealumination were tested starting with ZSM-5.

Figure 8 shows the mechanism involved in the desilication process reported from the reference.<sup>57</sup>

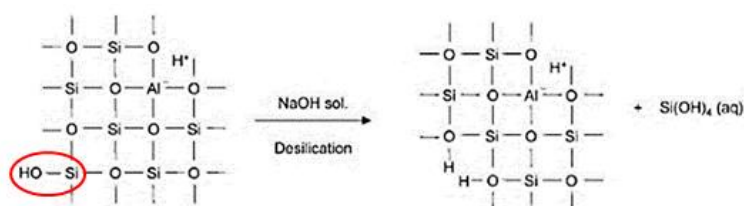


Figure 8 : Mechanism of desilication involved during alkaline treatment<sup>57</sup>

Nevertheless, the preservation of the Si/Al ratio of the framework and the creation of mesoporosity by alkaline treatment also depends on the Si/Al ratio of the pristine material. According to the literature<sup>24, 29, 58</sup>, if the Si/Al ratio is too low, the aluminum therefore excessively protects the structure against hydroxide ions and thus the formation of mesopores is limited due to the ineffective desilication. On the other hand, if the Si/Al ratio is too high, the desilication is then excessive and leads to the formation of macropores. So, it was noticed that the desilication process is favorable when the Si/Al ratio is optimal  $\sim 25$ -50.<sup>23, 59-61</sup> The effect of the Si/Al ratio on the desilication process is illustrated in Figure 9.

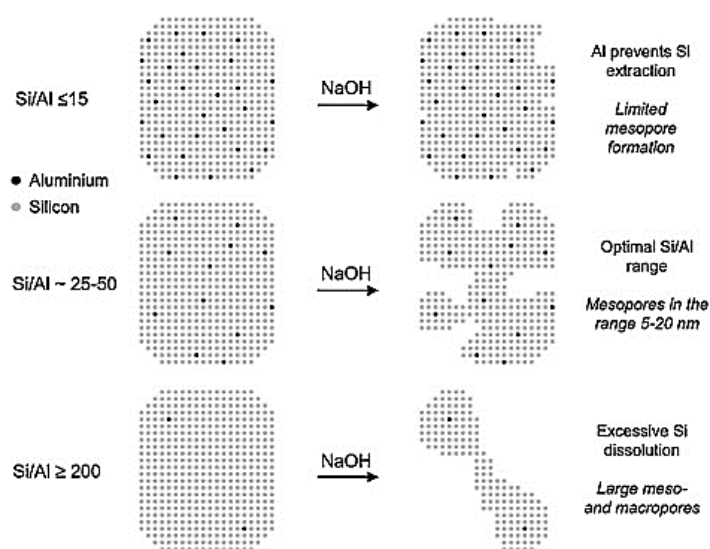


Figure 9 : Diagram showing the influence of the Si / Al ratio on desilication process<sup>27</sup>

Recently the desilication of low Si/Al (<10) mordenites has been reported by Van Laak et al.<sup>48</sup> Inter-crystalline mesoporosity can be created if high concentrations of NaOH, typically 1M, with reaction times of 30 min. Under these conditions, there is then a risk of altering the microporosity. The compromise is to use high concentrations of NaOH but with a low reaction time.

Desilication is therefore a method that has developed rapidly in recent years and applies to a large number of various zeolites. However, some of them require more severe treatment conditions, for example ferrierite and ZSM-22. The formation of mesopores by desilication is nevertheless difficult to control (in terms of the size distribution of the mesopores and their spatial distribution) because the process is rapid, i.e. already achieved after about ten minutes. The resulting mesoporosity is usually distributed in a very broad pattern, centered at 10 nm.

- *Recrystallization route*

Recrystallization is a post-synthesis treatment that combines destructive and constructive ways. Indeed, the zeolite used as a source of silica-alumina is dissolved in the presence of an alkaline solution.

Then, under hydrothermal conditions, the dissolved zeolite can recrystallize around the micelles formed by the structuring agent to give a micro-mesoporous material. It allows to obtain zeolites with ordered mesoporosity.

This method takes place in several steps represented for a model case in Figure 10. In the first step, the zeolite is partially dissolved in an alkaline solution at room temperature. A surfactant used as a mesopore structuring agent is then added to the medium and the mixture undergoes a hydrothermal treatment under one to several hours. During this step, the dissolved zeolite recrystallizes around the micelles of the surfactant. After cooling at room temperature, the solid is recovered by filtration, washing and drying. The removal of the organic structuring agent in the material is performed by calcination to finally obtain the microporous/mesoporous composite material.

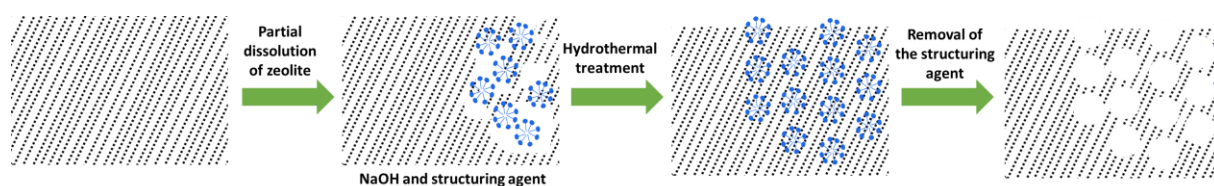


Figure 10 : Schematic summary of the steps in the recrystallization of zeolite

The first materials prepared by zeolite recrystallization were obtained by Goto et al. in 2002.<sup>62</sup> The starting zeolites used were ZSM-5, mordenite or faujasite. The dissolution step was done with soda solution and structuring agent which is CTACl (hexadecyltrimethylammonium chloride). The presence of micropores and mesopores for ZSM-5 and mordenite is confirmed by nitrogen adsorption-desorption technique. The formation of mesoporous structure seems to be formed around the zeolite crystals and the obtained materials are composites of zeolite and purely mesoporous materials. These synthesized materials seem however different from simple physical mixtures of microporous and mesoporous solids and present a better catalytic activity than the starting zeolites for the cracking of n-hexane.

Later, Ivanova et al<sup>63</sup> studied the preparation of micro/mesoporous mordenites using the two techniques of dealumination (in order to increase the Si/Al ratio) in combination with the recrystallization techniques. The recrystallization step is done in the presence of soda and surfactant, CTAB (hexadecyltrimethylammonium bromide). The structure of the mordenite is preserved after dealumination. On the other hand, recrystallization has an effect on the structure and the texture of the material, more or less, depending on the concentration of the soda used. A high concentration (1.6 M of NaOH) leads to the increase in the mesoporous volume by the appearance of a phase of type MCM-41, but also the destruction of the zeolite and the development of amorphous phase in the

structure, while lower concentrations (0.3 M NaOH) allow to keep the microporosity but lead to lower development of the mesoporosity.

Thus, according to Ivanova et al.<sup>64</sup> it seems that the most important parameter of the recrystallization of zeolite is the concentration of soda. There would be an optimal concentration of NaOH corresponding to optimal proportions of micropores and mesopores. The importance of the Na/Si ratio in the recrystallization process of mordenite was also highlighted by the team of Wang et al.<sup>64</sup> the same year.

Concerning the acidity, some recrystallized samples show an inversion of the proportions of the weak and strong acid sites compared to the starting zeolite. Ivanova et al.<sup>63</sup> indeed noted after the recrystallization treatment an increase in the number of weak acid sites and a decrease in strong acid sites. It has also been shown that the total acidity of the recrystallized zeolite can become greater than that of the starting material, which, according to this team, suggests that there is not only a simple mixture of micro and mesoporous structures but also a homogeneous material at the nanometric scale.

Similar work was conducted by Ordonsky et al.<sup>65</sup> on BEA zeolite. They show that the use of mild conditions does not affect the acidity of the sample but on the other hand, under more severe conditions of alkaline treatment (2M NaOH), the amount of Brønsted acid sites decreases while the number of Lewis acid sites increases. These same trends were later demonstrated by Ivanova et al.<sup>66</sup> on mordenite.

The size of the mesopores is a parameter that can also be controlled during recrystallization unlike desilication. According to Ying et al.<sup>67</sup> it is sufficient to change the length of the aliphatic chain of the surfactant used. This patent, mentions the preparation of mesoporous zeolites starting from ZSM-5, mordenite or faujasite, in presence of CTAB. TEM (Transmission Electron Microscopy) images confirm that the mesopores and micropores are in the same phase and that it is not a simple physical mixture. However, their method of extraction of CTAB requires a massive quantity of organic solvents such as ethanol, methanol or acetone in the presence of strong acids (HCl, H<sub>2</sub>SO<sub>4</sub>). Moreover, only a part of the structuring agent is extracted.

Finally, the study of Chal<sup>68</sup> on Y zeolite clearly shows that recrystallization in the presence of CTAB leads to the formation of mesoporosity within the zeolite crystals, while keeping an important part of the initial microporosity. The structure thus has a co-localized bimodal porosity with a very narrow mesopore size distribution centered at 4 nm. This size is adjusted by varying the length of the aliphatic chain.



Thus, although the recrystallization technique has only been studied recently, many teams have obtained conclusive results leading to zeolites with controlled hierarchical porosity. A recent review by Ivanova et al.<sup>69</sup> gives an overview of the studies on the recrystallization of zeolites and the different processing conditions used to obtain them.

In this review, Ivanova classifies recrystallized micro-mesoporous materials into three groups according to their degree of recrystallization, (i) mesostructured zeolite crystal covered by a mesoporous phase film, (ii) composite material made up of two co-existing phases of zeolite and mesoporous material and (iii) mesoporous material containing only small fragments of zeolites in its walls. According to the textures obtained after recrystallization, the synthesized materials can be classified in one of these categories. The objective is to obtain materials as homogeneous as possible to be used in catalysis and thus be able to establish a correlation between structure and catalytic properties.

Sachse et al.<sup>70</sup> gave an overview of the various strategies to obtain a hierarchical zeolite by designing the obtained mesopores. Each step in the process of building the mesoporosity was analyzed using different techniques in order to see the mechanism of this process as well as different properties of the product in addition to their application especially in the catalysis field. Al-Ani et al.<sup>71</sup> mentioned in their work that the presence of the surfactant helps in the formation of regular mesopores zeolites during the desilication process. Furthermore, Sachse and his coworkers<sup>72</sup> explained in detail the mechanism of the mesoporous formation firstly by hydrolyzing the Si-O bonds to induce negative charge defect size in order to attract CTA<sup>+</sup>. Secondly, micelles formed by reassembling the silica around it thus forming an ordered mesoporous system. Recently, the same team<sup>73</sup> was able to illustrate the influence of the hierarchization of zeolite material in which they observe an increase in the mesoporous volume as well as the specific surface area while the microporous volume remains constant. This was explained by the fact that the desilication preferentially destroyed the hemicages of MCM material which has been studied by the adsorption of n-nonane.

Several parameters are highlighted as having an influence on the formation of mesopores, such as the type of base used and its concentration, the type and the quantity of surfactant, the duration of the hydrothermal treatment or the Si/Al ratio of the starting zeolite.

Currently, the most convenient method to prepare hierarchical zeolites is the post-synthesis method that starts from commercial zeolites. The obtained material helps in improving the adsorption properties, first by keeping the intrinsic properties of the pristine material then by enhancing the adsorption of bulky molecules. This opens a new door to study the different interfacial phenomena occurring due to adsorption of molecules on modified zeolite bearing different porosity.

### 3 Physicochemical phenomena inside nanometric structures

Particle size has a great impact on the interfacial phenomena including adsorption, reactivity on the surface and thermodynamics. In addition, the crystallinity of the particles can also affect interfacial reactivity. The variation in size is sometimes in correlation with the morphology of the particle thus affecting its interfacial reactivity. This was studied by Jolivet et al.<sup>74</sup> on boehmite particles. When the size of particles changes, the shape might change and the ratio of the XRD faces varies. This exposure of various crystallographic faces induces a modification in the surface energy and electrostatic surface charge density. Therefore, the interfacial reactivity can be adjusted by controlling particle size and shape. Moreover, arsenic (III) adsorption toward iron oxide showed an augmentation in the capacity when the particle size decrease. This was due to the change in the surface structure that produce new adsorption sites.<sup>75</sup> Therefore, different interfacial phenomena can be extracted depending on the chosen system. In the case of zeolitic material, many of these interfacial phenomena can occur as displayed in the figure below.

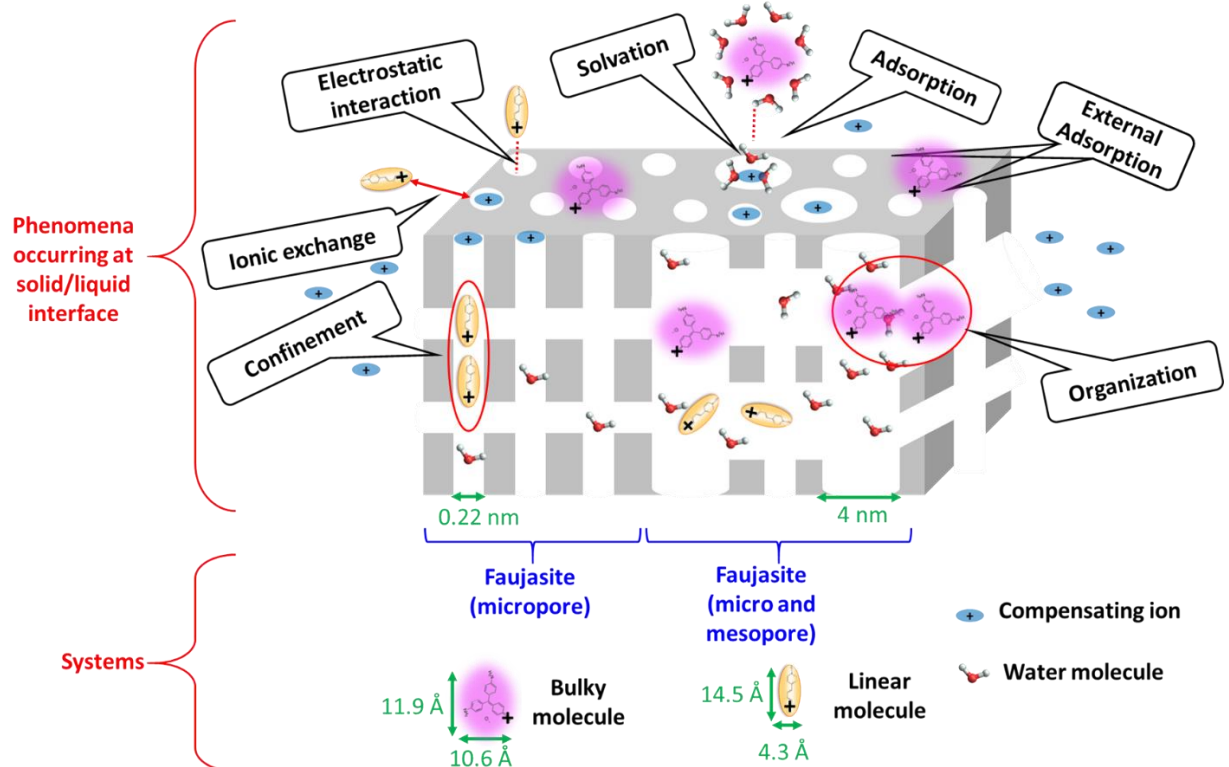


Figure 11 : Representation of the possible phenomena that can occur at the interface.

### 3.1 Confinement effect

In the case of molecules confined in a solid material, the confinement term is used to mean a modification in the physico-chemical properties (e.g., phase behavior, molecular mobility, the adsorption characteristics) of the species confined in the pore space.<sup>76</sup> Thus, it might influence the reactivity due to the different behavior of the adsorbed species and the solvents inside the zeolite pores. The confinement effect may be observed when the pore size of the particle is comparable with the size of the molecule.<sup>77</sup> This makes the molecules trapped inside the pores and prevents their release.

Most of the studies related to confined systems were made on the water or the solvent<sup>78, 79</sup> confinement in the pore space with the help of molecular simulations. There are three factors in which the confinement effect can influence the adsorption phenomena. These factors are (i) size, (ii) shape, and (iii) interaction of guest species with the boundaries of the confined space.<sup>80</sup> In the large pores the surface curvature becomes almost flat which makes the interactions between molecules and the surface not affected by any type of confinement.

The confinement arises from the interaction between attractive long-range interactions and repulsive short-range interactions. In the late eighties, a new concept of confinement effect was introduced by Derouane et al.<sup>81</sup> This concept depends on the non-covalent interactions between the molecules located in the pores and the zeolitic framework. The attractive van der Waals force operates in the long-range (3–5 Å), while the repulsive Pauli reaction operates in the short term (< 2 Å). These two types of interaction are responsible for the confinement effect. Therefore, the origin of this effect depends on the curvature of the channels, cages, and external "pockets" of the zeolite.<sup>82</sup>

Senapati and Chandra<sup>83</sup> measured the dielectric constant of water in the spherical nanocavity having three different sizes of the cavity. They deduced that the dielectric constant of water decreases with decreasing the cavity size. They notice that this reduction is due to the confinement effect since the cavity surface is neutral i.e. the electrostatic interaction is null. Moreover, Mizota et al.<sup>84</sup> were interested in the entropy of confined water. They obtained, at 298 K, a molar entropy of confined water in a saturated zeolite A, of 3 J.K<sup>-1</sup>.mol<sup>-1</sup>. This value reveals the organization of water within the microporous volumes of zeolites A since it is lower than 42 J.K<sup>-1</sup>.mol<sup>-1</sup>, molar entropy of ice at 273 K.

In previous studies performed by Hureau et al.<sup>85</sup> and Luchez et al.<sup>86</sup>, trans-stilbene and phenothiazine molecules were adsorbed into the porosity of zeolites of type FER, ZSM-5, and MOR zeolites in order to highlight the action of the topology on the charge transfers. The results of spectral data and molecular modeling calculations show that the probe molecules adsorb in the vicinity of the charge-compensating cations in both zeolites in the FER type zeolites constituted by the narrowest

channels ( $0.42 \times 0.54 \text{ nm}^2$ ) as well as in the slightly wider channels of ZSM-5 ( $0.53 \times 0.56 \text{ nm}^2$ ) and especially in MOR ( $0.67 \times 0.79 \text{ nm}^2$ ). The confinement effect is notably highlighted during the adsorption of trans-stilbene in the FER exchanged with  $\text{Na}^+$ . This spontaneously leads to the ionization of the molecule whereas a photonic excitation is necessary if the same molecule is incorporated in NaZSM5 or NaMOR. Moreover, it has been shown that the processes of charge transfer and recombination in zeolites depend not only on acid zeolites but also on the confinement effect. These processes were strongly slowed down when the confinement increased from MOR to ZSM-5 and then to FER. Indeed, despite similar Si/Al ratios close to 10, the radical cation formed in large quantities after ionization of trans-stilbene in the HFER remains stabilized for several months and evolves very weakly only towards the electron-hole pair. On the contrary, the radical cation is only an intermediate reaction in the MFI where it is clearly observed and in HMOR where it is hardly detected because its lifetime is very short<sup>85</sup>.

The host-guest interaction, the size of molecules in comparison with the size of the pores, and the topology have a great impact on the confinement system- The molecules could be more organized in the confined system due to the lack of free space and various types of surface reactivity. Such interfacial or confined molecules display different properties compared to the bulk.

### 3.2 Selectivity between host and guest

Zeolite framework composed of tetrahedrons  $\text{TO}_4$  ( $\text{T}=\text{Si}^{4+}, \text{Al}^{3+}$ ) carries an anionic charge which is compensated by cations located in the channels, free and easily exchangeable. Thanks to the important electrostatic field in the cavities and their regular geometry, zeolites can adsorb host molecules with a selectivity that can be modified (controlled) by changing the charge compensating cation. Another selection criterion that enters into the specification of the adsorbents is their pore size distribution. This one acts on the selectivity of the adsorbent towards the adsorbates. Similarly, the polarity of an adsorbent will affect the adsorption selectivity.

The knowledge of the selectivity of molecules within the material is very important for the study of the adsorption process. The selectivity represents the preferential encapsulation of either one molecule over another or a type of cage compared to another. Thus, it depends on different aspects such as the steric factor, the thermodynamic conditions of adsorption and the solubility in water.

In the literature, Chu et al.<sup>87</sup> showed that the cyclohexanone oxime Beckmann rearrangement reaction can be catalyzed by H-ZSM-5 zeolite more effectively due to the perfect fitting between zeolite pores and the cyclohexanone oxime size. Regarding the stability of adsorbate in the confined zeolite, Song et al.<sup>77</sup> investigate the stability of hydrocarbon species in the confined microporous zeolite framework based on the analysis of H-ZSM-5 theoretical models using energy decomposition analysis

(EDA). Also, they investigated that the zeolite pore confinement effect is different for different hydrocarbon species depending on their charge, HOMO and LUMO, host/guest interactions, and electrostatic interaction for the charged species. Also, the confinement model permits the diffusional mass transfer of hydrocarbons in zeolites to be rationalized according to the size and shapes of pores and channels. This shows the decrease in the diffusion transfer due to the increase in the sticking force.<sup>88</sup>

It is worth noting that the dye molecules are flexible so they can change their conformation to permit the diffusion of the molecules to the host framework even if the molecule is oversized for example the methyl viologen,<sup>89</sup> or cyanine dyes<sup>90</sup>. Therefore, flexibility might avoid the molecules from blocking configurations, however, if it is the reverse case and the blocking molecules cooperate, they lead to the channel plugging.<sup>91</sup> In addition, Hennessy et al.<sup>89</sup> studied the adsorption of methyl viologen in the zeolite L channels. They removed the adsorbed molecules from the outer surface. Therefore, the adsorbed molecules were intercalated inside the channels. This was proved by IR where  $MV^{2+}$  gave four peaks and Raman which indicate that the pyridyl rings of  $MV^{2+}$ -L zeolites were twisted.

Selectivity between host and guest is affected by steric factor, polarity of an adsorbent, electrostatic interactions, geometry and size conformation.

## 4 Experimental approaches to probe adsorption and interfacial phenomena

In many systems, the presence of probed molecules depends on the nature of the material used (hydrophilic and hydrophobic surfaces) as well as on its porosity. Such interfacial or confined molecules display different properties compared to the bulk. Indeed, the molecular structure is affected by steric limitation via their molecular characteristics such as structure and shape. In this section, the experimental approach used to probe the interfacial phenomena and adsorption will be stated.

### 4.1 *Thermodynamic approaches of the adsorption and the particular case of calorimetric measurements*

The thermodynamic study provides useful information on the spontaneity of the adsorption process as well as the calculation of fundamental thermodynamic parameters, such as  $\Delta G$ ,  $\Delta H$ , and  $\Delta S$ . In the context of phenomena at thermodynamic equilibrium, it is not only interesting to understand the interaction of the adsorbed molecules with the material but also to study the phenomena corresponding to the confinement effect by varying the porosity size.

Different types of calorimeters have been developed since the ice calorimeter of the French chemist Antoine Lavoisier (1789), up to quasi-adiabatic versions such as that of French Pierre Eugène Berthelot's (1864) or Sir James Dewar's (1891). More recently (1922), the isothermal microcalorimeter was developed with thermopiles and Joule Peltier compensation by the French chemist Albert Tian. And it was in Marseille (1947) that the work of his student, Edouard Calvet, will lead to the development of the diathermic microcalorimeter with thermal conduction called Tian-Calvet.

#### 4.1.1 Enthalpy of adsorption or enthalpy of displacement

Isotherms are often used to study the properties of adsorbent materials using various species and are usually characterized by a local technique. Another type of characterization is required which could be fulfilled through simultaneous measurement of adsorption energy. This measurement allows the understanding of the physical and chemical processes when adsorption takes place. The enthalpy of adsorption can provide information about the strength of interaction between adsorbate-adsorbent and adsorbent-adsorbent as well as information about surface composition. It is formed from the heat released when there is the displacement of solvent or adsorbate in the adsorption process. This heat is measured directly using a calorimetric instrument or indirectly by the mean of simulations such as Monte Carlo, DFT calculation, M06-2X method.

The displacement enthalpy of adsorption is a measure of the interaction that takes place during adsorption. Direct calorimetric methods can measure only the total interactions and not the individual interactions i.e. hydrogen bond, electrostatic interaction, dissolution, hydration, dehydration.

In microporous material, the adsorbing molecules of smaller sizes first fill the pores. Then, the adsorption enthalpy varies depending on the fitting between the pore and the molecule size. The effect of material structure and surface chemistry on adsorbent-adsorbate interactions can be measured by changing a single property, for example, by varying the Si/Al ratio, and the effect of compensating cations on the ion exchange process. In addition, it estimates the enthalpy of adsorbate-adsorbate and somehow  $\pi$  bond interactions.

#### 4.1.2 Study of molecular adsorption in a confined system

In this section, some aspects of the adsorption thermodynamics will be presented showing the effects of the porosity and confinement on the enthalpic change. Some information of the confinement effect of molecules on thermodynamics is given in the literature. Most of the thermodynamics of zeolite materials are studied theoretically, by using various types of simulations with the help of different models such as Monte Carlo, DFT, ONIOM. Several parameters may influence the enthalpic properties: (i) the **pore size** of the host and the size of the guest molecule, (ii) the **interaction** between

the confined molecules and the host matrix, (iii) the **topology** of the material. It is also possible to combine two or more factors that lead to the variation of the heat effect depending on the predominant factor.

#### 4.1.2.1 The size effect of both host material and guest molecules

The size effect of the host and guest has a great influence on the confinement. For example, Fu et al.<sup>92</sup>, studied the effect of confinement by evaluating  $\Delta H$  using DFT calculation. Different adsorbents bearing different pore sizes (HY and HZSM-5 zeolites), large series of alkanes with an increasing number of alkyl chains and branched chains have been used. They differ from each other by the pore size where HY has a greater pore size than HZSM-5. For N- alkanes, as N increases,  $\Delta H$  increases in absolute value when the confinement effect increases. While, in the same family of alkanes, as the branch size increases, the confinement effect increases thus  $\Delta H$  increases in the case of HY. However, in the case of HZSM-5, as the branch size increases, the confinement effect decreases which leads to a decrease in the  $\Delta H$  because of their stronger steric repulsion with the zeolite wall, indicating that the pores are too large for the molecules to be stable. A similar observation was obtained by Pantu et al.<sup>93</sup> where thermodynamic adsorption of hydrocarbons into H-FAU and H-MOR zeolite was studied using theoretical methods. Moreover, another simulation method, ONIOM method, was used to calculate the thermodynamic of adsorption of unsaturated aliphatic, aromatic, and heterocyclic compounds in H-ZSM-5 Zeolite by Boekfa et al.<sup>94</sup> that leads to a similar conclusion as mentioned by Pantu et al. and Fu et al. Finally, it can be said that the confinement effect, the perfect fitting between the host pore size and the guest size has a great influence on the enthalpy of adsorption. In another word, when the confinement effect increases, the enthalpic change increases in absolute value.

Hsieh et al.<sup>95</sup>. studied the effect of mesoporosity on the adsorption of methylene blue onto titania nanotubes which were obtained from different calcination temperatures. Variation of isosteric heat ( $q_{st}$ ) calculated from adsorption isotherm was observed when the average pore size of titania nanotubes changes. The heat of adsorption is higher at low coverage compared to complete monolayer. This can be explained by the fact that the adsorption of molecules firstly takes place to increase the Van der Waals attraction energy, and also to achieve the best fit between the molecules (shape and size) and the material. In addition, when the pore size increases the isosteric heat becomes lower as shown in Figure 12. It can be said that at low pore size, the heat of adsorption is higher due to the highly fitting between the size of methylene blue and the narrow pore.

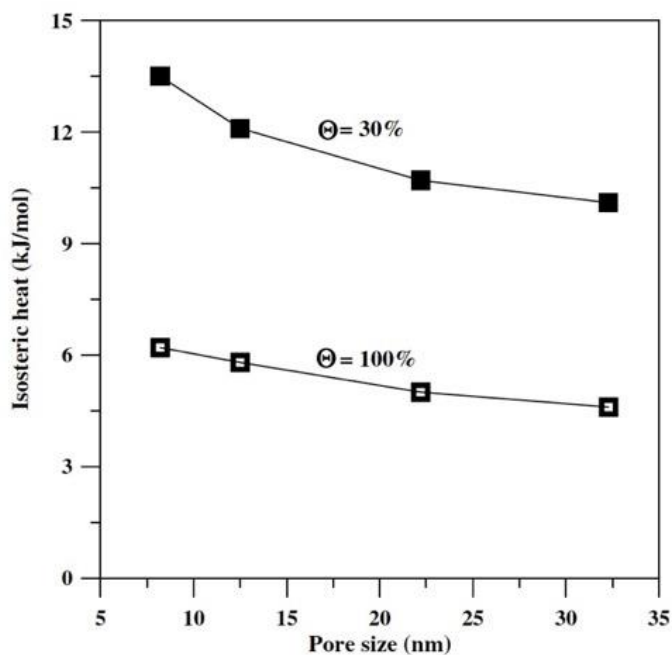


Figure 12 : Effect of pore size on the adsorption of methylene blue onto titania nanotubes at low coverage ( $\Theta = 30\%$ ) and high coverage where the monolayer is completely filled ( $\Theta = 100\%$ )<sup>95</sup>

#### 4.1.2.2 Interaction between host and guest molecule

Eder and Lercher<sup>96</sup> have determined the heat of adsorption of various alkanes onto zeolite bearing different acidity and porosity using gravimetry and calorimetry. They observed that the Brønsted acid sites favor the adsorption of alkanes. The higher heat of adsorption is measured for the maximum coverage where all acid sites of zeolite are occupied. The effect of molecular sieves of zeolite is highly dependent on the high fitting between the size of the alkane and the pore size of zeolite which gives high adsorption enthalpy<sup>96</sup> as shown in Figure 13.



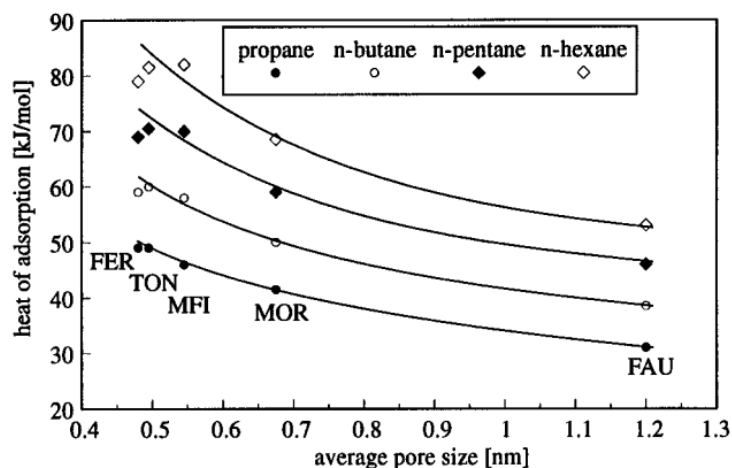


Figure 13 : Effect of pore size on the heat of adsorption of various alkanes on 5 types of zeolites (FER, TON, MFI, MOR and FAU). Reported from reference<sup>96</sup>.

Boekfa et al.<sup>78</sup> studied the acetone adsorption into 3 different zeolites having different pore sizes, H-FER, H-ZSM-5, and H-MCM-22 from smaller to bigger sizes respectively using quantum chemical information, M06-2X method. From H-FER to bigger size H-ZSM-5,  $\Delta H$  becomes more negative since the interaction between acetone and Bronsted acid of zeolite H-FER is stronger. However, from H-ZSM-5 to H-MCM-22,  $\Delta H$  becomes less negative since both have strong interaction but H-MCM-22 is bigger thus the small pore size with high interaction leads to a strong confinement effect. It is considered that there is competition between both factors.

Moreover, the presence of the Bronsted acid in the confined space plays a vital role in the adsorption process. For example, in the work of Gounder et al.<sup>97</sup>, the confinement effect of the monomolecular cracking and dehydrogenation of alkane into the zeolite framework (H-MFI, H-FER, and H-MOR) was studied. These zeolites consist of main channels (12-MR) and side pockets (8-MR) where the monomolecular cracking and dehydrogenation reaction preferentially happened in the 8-MR, the partially confined system. Therefore, a loss of enthalpy is observed due to the presence of a confined system.

Recently, Chai et al. worked on zeolite (Ni@FAU) based on faujasite (FAU) with confined isolated Ni (II) sites to attain high adsorption of alkyne and efficient separations of alkyne/olefin mixtures. A strong and reversible binding between alkynes and open Ni(II) sites was demonstrated by forming metastable complexes  $[\text{Ni}(\text{alkyne})_3]$ .<sup>98</sup> This implies that the confined environment has a high effect on the bonding of molecules.<sup>99</sup>

### 4.1.2.3 Materials topology effect

The effect of topology on the confinement was shown by Janda et al.<sup>100</sup> where they studied by Monte Carlo simulations the adsorption of n-Butane onto zeolite having different structures. They measured the largest cavity diameter (LCD) of zeolite to determine the appropriate nanocavity where the molecules are more constrained. They showed that when LCD increases the confinement effect becomes stronger in some systems which is a reverse result to the aforementioned. This was explained with the material having the same topology, the LCD decrease leads to more constrained molecules, thus more negative enthalpy is obtained. However, even other materials with lower LCD but with different topology such as n-Butane are not confined and have less negative enthalpy. This is due to the shape of the zeolite structure that leads to competition between the size effect and the shape effect.

Similar studies were done to measure the heat of adsorption using direct calorimetric measurements on different materials. The advantage of the direct calorimetric measurements over the others is to offer the possibility to study weak interactions involved in the system. It is also a powerful characterization method capable of measuring with precision the heat released or absorbed by the interactions between two species.

Thach et al.<sup>101</sup> studied the adsorption of chromate onto the ionosilicas synthesized on the one hand from three different oligosilylated ammonium precursors, and on the other hand using various templating agents, with anionic, cationic, or neutral surfactants. The materials having various surface chemistry, exhibit quite a similar sorption capacity, whereas the global enthalpy of the interaction was different. The heat of adsorption is influenced directly by the nature of the cationic substructure, in relationship with the steric hindrance of the alkyl groups that surround the cationic center.

Guil et al.<sup>102</sup> showed that the heat of adsorption measured by microcalorimetry was directly related to the pore size and the interaction between the molecules adsorbed and the host. In the case of the mesitylene molecule, the heat of adsorption is higher compared to n-hexane and toluene molecules. This is due to the fact of the flat position gave maximum interaction, thus, higher heat.

PreLOT et al.<sup>76</sup> investigated the confinement effect on the heat of adsorption of cadmium onto nonporous and four ordered mesoporous silica using flow calorimetry. They found that the enthalpy is higher in the nonporous material compared to the porous one. This is explained not only by the porosity but also by the surface chemistry. In the small pores, the silanol lying on the opposite walls become closer to each other. Thus, the adsorption of molecules to more than one surface site is favored, which leads to a decrease in the heat of adsorption.

Cao et al.<sup>103</sup> expected different mass transfer mechanisms for confined and bulk water. The differences are attributed to the differences in the proton transfer rate. The proton transport happens through a “Zundel-Zundel” ( $\text{H}_5\text{O}^{2+}$ ) mechanism with a low barrier in the case of confined water in one-dimensional channels. However, in the case of bulk water, the proton transfer favors by “Eigen-Zundel-Eigen” mechanism that involves both cations Eigen ( $\text{H}_9\text{O}^{4+}$ ) and Zundel ( $\text{H}_5\text{O}^{2+}$ ). Therefore, the “Zundel-Zundel” mechanism is considered to be a more efficient method.

Accordingly, the aforementioned factors (size, topology, and host-guest interaction) could be effective all together and simultaneously. The confinement effects are then mainly influenced by the predominant one. The enthalpy of adsorption is large in the confined system leading to the high strength of interaction between the guest and host.

The organization and/or orientation of molecules as well as the correlation between molecules at solid/liquid interface is complicated and sometimes impossible to be elucidated using a macroscopical scale. So, complementary techniques are required to provide information about the organization of molecules at the local scale.

## 4.2 *The molecular approach: Non-Linear Optics*

In the present work, non-linear optics (NLO) has been chosen as a local complementary technique to calorimetry. It results from the nonlinearity of the response of a material to the action of an intense electromagnetic field in the optical domain. The first NLO studies closely followed the invention and development of high peak power laser sources delivering very short pulses. In 1962 Armstrong et al.<sup>104</sup> theoretically described most of the physical phenomena related to second order optical interactions.

### 4.2.1 Second Harmonic Generation (SHG)

Historically, Non-Linear Optics (NLO) is a domain that appeared after the invention of the laser and the first observation of Second Harmonic Generation (SHG) by Franken et al. in 1961.<sup>105</sup> Nonlinear optics, and more particularly the second harmonic generation proves to be a very powerful tool for probing the structure of interfaces at a very small scale, below the diffraction limit at wavelengths of the visible optical domain, of the order of a few hundred nanometers. In this elementary process, a virtual absorption of two photons at frequency  $\omega$  is coupled with the emission of a single photon at frequency  $2\omega$ .

SHG process is indeed forbidden in a centrosymmetric medium. Because of the prohibition of the phenomenon within the centrosymmetric media and the breaking of centrosymmetry at an interface between two media. Actually, the rule of centrosymmetry has been widely used to

characterize the interfaces between two centrosymmetric material media such as air/liquid, liquid/liquid, or solid/liquid interfaces. All this is possible at the interface of two media because the symmetry is broken, thus allowing the generation of second harmonics in the interfacial region. In other words, the second harmonic generation is used as a probe for the study of surfaces and interfaces.<sup>106</sup> Indeed, this second order process has the advantage of not being limited to flat interfaces. Structures of size less than the wavelength can also be studied, and this is the case for liposomes and micelles for example. Depending on the size of the object, there is mainly a scattering light.<sup>107</sup>

#### 4.2.2 Second Harmonic Scattering (SHS)

Second Harmonic Scattering (SHS) is a particular case of SHG. The use of SHS for obtaining information on the surface chemistry of particles in liquid medium was demonstrated in 1996 by Eienthal and his group<sup>108</sup>. This study was carried out on MG dye molecules (malachite green) which exhibit a strong non-linear polarization when they are adsorbed on the surface of colloidal particles of polystyrene of micrometric size in an aqueous solution. Another study of the particle / solvent interface in a colloid has opened access to new uses of SHS for the study of many colloidal objects<sup>107, 109</sup>. Some examples of the use of SHS will be briefly described in the following section.

SHS is used as a probe for the study of surfaces and interfaces in bulk medium. Indeed, this signal comes from structures composed of molecules comprising a break in symmetry such as interfaces, aggregates, colloids but also lipid bilayers. This non-linear analysis method provides information on the organization of molecules but also on the different interactions involved.

SHS can be used to probe the interfacial properties of particles in liquid and solid media. It is used to probe objects of size  $< 20 \mu\text{m}$ <sup>107</sup> for example colloidal liquid solution. It enables lower concentration measurement and is used to probe the interactions of molecular species with colloidal particles.

SHS can be also used to study the adsorption phenomena at the particle interfaces<sup>110-112</sup>, to determine the adsorption free energy, and to define the surface potential of suspended colloidal particles<sup>113</sup>. The total intensity of SH light emitted from a large solid angle was only detected by in situ surface studies.

The second harmonic scattering term is reserved for the **coherent** process for which a non-random phase relation exists between the elementary waves which translate the response of a supramolecular structure composed of correlated molecules.

### 4.2.3 Hyper Rayleigh Scattering (HRS)

It is necessary to distinguish the **incoherent** process from the coherent one. In the first case, the non-linear sources participating in the conversion process together form an incoherent source of a harmonic wave. The phases of each of the elementary waves produced by nonlinear sources are random. This process is known as hyper Rayleigh diffusion or harmonic light scattering or Hyper Rayleigh Scattering, HRS. The second harmonic scattering process is referred to the coherent non-random phase.

The signal of SHS arises from the break in symmetry thus it is used to probe surfaces, interfaces, aggregates and colloids. It probes the coherency process in the system that comes from the organization of molecules at the solid/liquid interface.

### 4.2.4 Properties probed using interfacial second harmonic processes

Second harmonic generation is used to probe the interface, **adsorption, organization, diffusion**. Dyes having conjugated bonds and high hyperpolarizability can be used as probe molecules, thus they are SHG active. The diffusion of DAMPI dye (in some articles it referred to sDiA) through films with different thicknesses was studied by Van der Veen et al.<sup>114</sup> The substrate second-order susceptibility  $\chi_{\text{sub}}^{(2)}$  is negligible for both interfaces (film/liquid and substrate/film interface). They interpret the variations in signal intensity between samples to small differences in the alignment of the adsorbed molecules. The  $\chi_{\text{ads}}^{(2)}$  is linearly dependent on the surface concentration at the substrate surface  $q(t)$  of the adsorbate molecule. Thus, the thicker the film, the less dense it is, the lower SHG intensity, therefore, it is a thickness-dependent diffusion.

Another study was done by Eckenrode et al.<sup>115</sup> on the adsorption of positively charged dye, Malachite Green (MG), on three polystyrene microspheres plain surfaces, neutral with no functional group termination, negatively charged (sulfate terminated), and positively charged (amine-terminated). The adsorption was performed at the aqueous interface using second harmonic generation. They concluded that for the sulfate terminated polystyrene, the adsorption is upright with a high rotational degree of freedom due to the electrostatic interaction between the oppositely charged surfaces. And thus, it gives large negative free energy (-12.67 kcal/mol) due to the strong interaction. Whereas in the case of neutral surface, the interaction is weaker than for the oppositely charged surfaces and favored by van der Waals. A slightly lower  $\Delta G$  is observed (-12.39 kcal/mol) and the molecules are more tilted. In the case of positively charged polystyrene, repulsive force exists due to similar charges with a flat molecule and gives low  $\Delta G$  compared to other materials (-10.46 kcal/mol). The highest interaction gives large negative free energy. However, in this article, the free energy for the negative and the neutral surfaces are similar due to the effect of solvation. Therefore, the effect

of solvation must be subtracted in order not to hinder the real effect of interactions between the solid and the guest molecules. Another adsorption of MG was performed on colloidal gold nanoparticles (16 nm) in an aqueous medium by Haber et al.<sup>116</sup>. They observed that MG is adsorbed more strongly and at higher surface density on the gold nanoparticles compared to the result of MG onto polystyrene microparticles or oil droplets in water. This is due to the presence of charged groups that is attributed to a different type of interaction between adsorbent and adsorbate.

Schürer et al.<sup>117</sup> investigated the effect of electrolytes on particle/water interfaces by angle resolved-SHS intensity. In their review, they focused on probing the molecular orientation of water in the presence of salt. They showed that the water molecule is less oriented with lower SHS intensity when the concentration of salt increases. Since the surface charges are affected by their counterions and the depth of penetration of the static electric field into the surrounding water, the SHS intensity is reduced.

SH signal can be a response of dipolar or quadrupolar contributions. The quadrupolar contribution is the response of the molecular micelles or organization. In the work of Revillod et al.<sup>118</sup> the multipolar contribution in the SH response of mixed SDS/4-(4-dihexadecylaminostyryl)-N-methylpyridinium iodide (DiA) molecular micelles was studied with polarization-resolved hyper-Rayleigh scattering. They notice that the SH response of DiA molecule alone is dominated by dipolar contribution, whereas, the SH response is dominated by quadrupolar contribution in the presence of SDS (anionic surfactant) to form micelles when there is a spherical arrangement. However, in the case of DiA in suspension with SDS, the dominant contribution then depends on the concentration of SDS used. At high SDS concentration, the dipolar signal becomes dominant since there are small molecules of DiA per micelle to form the spherical arrangement.

The adsorption and/or intercalation of Methyl Orange (MO) dye was studied to explore the organization and dynamics of CO<sub>3</sub> and NO<sub>3</sub> LDH (layered double hydroxide) colloidal materials. This study was done in our group by Gassin et al.<sup>119</sup> using polarization-resolved SHS. A schematic representation for the results obtained is depicted in Figure 14. The simulation was done with different dipoles with different geometrical distribution and then compared with experiment to see where the adsorption takes place, i.e. if it is on the lateral surface or intercalated within the layers. The interaction and the adsorption onto the lateral surface are demonstrated for LDH-CO<sub>3</sub>, while for the LDH-NO<sub>3</sub>, the intercalation within the interlayer is demonstrated and the organization in the material can be observed from high SHS intensity.

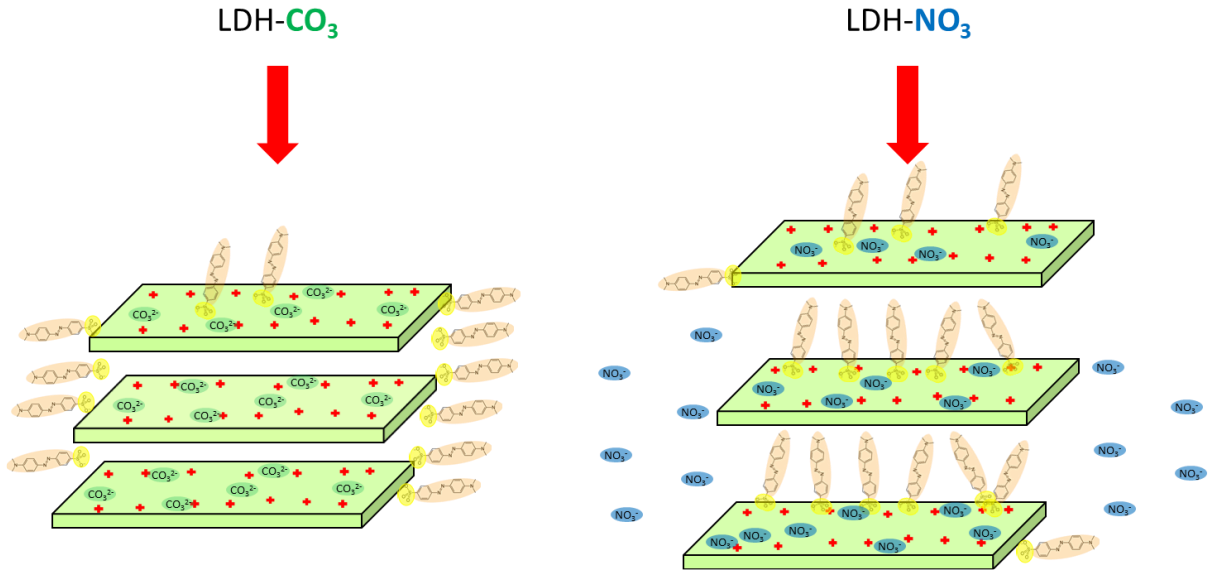


Figure 14 : A schematic interpretation of the result obtained from the reference <sup>119</sup>. SHS intensity for the adsorption of MO onto LDH-CO<sub>3</sub> and LDH-NO<sub>3</sub> with lateral adsorption and intercalation for LDH-CO<sub>3</sub> and LDH-NO<sub>3</sub> respectively.

Furthermore, we have also been able to discriminate between the free molecules (sDiA) in the solution and molecules adsorbed onto the polystyrene particles. A strong wavelength dependence pattern has been observed. This reveals the reorganization of the dye units in the vicinity of polystyrene nanoparticles<sup>120</sup>. Lastly, in a recent work from our group<sup>121</sup>, a program called PySHS has been used to replot the horizontal ( $H_{out}$ ) and vertical ( $V_{out}$ ) polarization plots to confirm the experimental result concerning the organization of DiA-4 dye onto a DOPG liposome membrane. The HRS contribution of the dye alone has been removed from the experimental result to facilitate the comparison between the theoretical model and the experiment.

To extract information from the NLO data acquisition, a mathematical model has been developed to interpret the signal in terms of correlation and orientation. The mathematical expression published by Duboisset et al.<sup>122</sup> is given below:

$$I_{SHS} = i_0 + i_2 \cos(2\alpha) + i_4 \cos(4(\alpha - \alpha_0)) \quad (2)$$

$$I_4 = \frac{i_4 \cos 4\alpha_0}{i_0} \quad (3)$$

where  $i_0$ ,  $i_2$  and  $i_4$  are the amplitudes of the constant, the harmonic  $2\alpha$  and the harmonic  $4\alpha$  terms respectively. The authors consider that the value of  $I_4$  is an indicator to probe correlation

between molecules. A high negative value of  $I_4$  was obtained at a high concentration of salt thus leading to a high correlation of water molecules as shown in Figure 15.

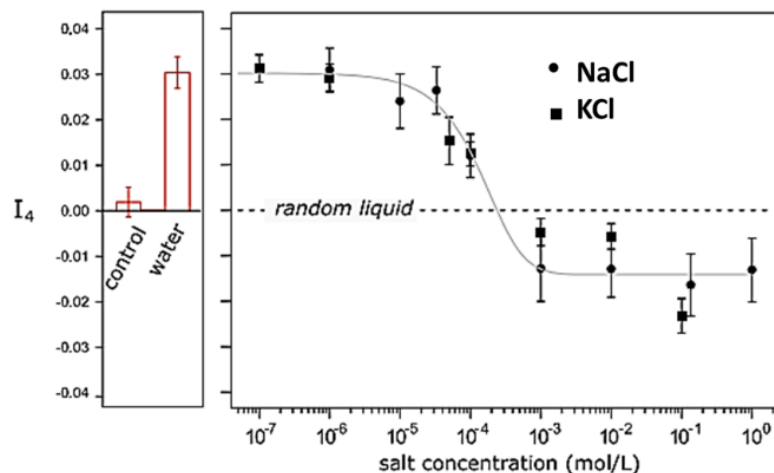


Figure 15 : On the left, magnitude of  $I_4$  for the control molecule DiA and water. On the right,  $I_4$  for different KCl (square) and NaCl (round) concentrations taken from the reference<sup>122</sup>.

The local SHS measurement is an interesting tool that has been used recently to quantify the correlation between molecules, to probe the organization and the orientation of the guest molecules confined within the material. It is also used to evaluate the adsorption isotherm, thus quantifying the adsorption capacity.

## 5 Conclusion

The bibliographic study aimed to collect information about the use of zeolite materials and their application in adsorption processes and the understanding of the different ways to obtain hierarchical material. This has provided a base of knowledge on the main properties of zeolites and their behavior. From the literature, the confinement effects are generally studied theoretically using simulation or few experimental studies that allow extracting the thermodynamic parameters like the global enthalpy of adsorption. Therefore, in order to probe the molecules experimentally at a global scale, Isothermal Titration Calorimetry (ITC) will be utilized in this research.

Taking into consideration that the literature lacked studies of the organization of molecules inside the porous material, the SHS approach will be used to probe molecules specifically at the interface and investigate the degree of **organization** of molecules close to a solid.

Coupling the thermodynamic and the molecular approach, the work presented in this manuscript would benefit from a **multi technique and multiscale** point of view. This represents a



strength to understand interfacial mechanisms during the adsorption of a molecule in solution onto a solid surface.

## 6 The objectives of this work, choice of material, and strategy of the thesis

This thesis aims to study the adsorption and organization of molecules using two approaches at different scales to have an overview of the adsorption phenomena occurring at the solid/liquid interface. The two approaches are: first, the global approach composed of adsorption isotherm and Isothermal Titration Calorimetry (ITC) and the second approach is the local one using non-linear optics, in particular second harmonic scattering. In other words, the general objective of this thesis is to study the adsorption phenomena in order to understand how it is adsorbed at the solid/liquid interface, and to produce particular conditions to induce confinement thus by choosing particular geometries, as well as to produce solids with hierarchical porosity to modulate the conditions of transport/diffusion, VdW or electrostatic interaction, available space, and hydrophilicity/hydrophobicity.

- To achieve this objective, our research strategy proceeded as follows: The first strategy is to define what could be the appropriate **material** that responds to the required specifications. Therefore, Zeolite Y of Faujasite (FAU) form was chosen as a material model because of its low cost, its good stability thermal and hydrothermal, its interesting structural properties such as a large microporous volume compared to others, large surface area, high sorption capacity, and the ability to modify their porosity.
- The second target is to relate the properties of the confined molecules with the different **levels of porosity**. To achieve this goal, a mixed route between destructive and constructive methods, will be used to obtain hierarchical FAU, with a desilication- recrystallization route using NaOH in the presence of CTAB as a structuring agent.
- The final strategy is to choose the molecules to be adsorbed. Molecules with different structures (linear and bulky) will be used in this thesis as probe non-linear molecules to study the interfacial phenomena and their organization and/or orientation at the solid/liquid interface. Because these molecules contain conjugated  $\pi$  bonds in addition to their hyperpolarizability value that allows them to be SHS active. From this family of molecules, cationic molecules will be used due to their high capacity toward negative surfaces zeolites because of the electrostatic interaction. This allows the comparison of adsorption phenomena, their organization, and their behavior at the solid/liquid interface.

## References

1. Guivarch, E. Traitement des polluants organiques en milieux aqueux par procédé électrochimique d'oxydation avancée" Electro-Fenton": application à la minéralisation des colorants synthétiques. Université de Marne-la-Vallée, 2004.
2. Oudar, J. L.; Zyss, J., Structural dependence of nonlinear-optical properties of methyl-(2,4-dinitrophenyl)-aminopropanoate crystals. *Physical Review A* **1982**, 26 (4), 2016-2027.
3. Sing, K. S., Adsorption by active carbons. *Adsorption by powders and porous solids: principles, methodology and applications* **2013**, 321-391.
4. McKay, G.; Porter, J. F.; Prasad, G. R., The Removal of Dye Colours from Aqueous Solutions by Adsorption on Low-cost Materials. *Water, Air, and Soil Pollution* **1999**, 114 (3), 423-438.
5. Langmuir, I., The Constitution and Fundamental Properties of Solids and Liquids. part I. Solids. *Journal of the American Chemical Society* **1916**, 38 (11), 2221-2295.
6. Emmett, P. H.; Brunauer, S., The Adsorption of Nitrogen by Iron Synthetic Ammonia Catalysts. *Journal of the American Chemical Society* **1934**, 56 (1), 35-41.
7. Rouquerol, J.; Rouquerol, F.; Llewellyn, P.; Maurin, G.; Sing, K. S., *Adsorption by powders and porous solids: principles, methodology and applications*. Academic press: 2013.
8. Forgacs, E.; Cserhádi, T.; Oros, G., Removal of synthetic dyes from wastewaters: a review. *Environment International* **2004**, 30 (7), 953-971.
9. Bhatnagar, A.; Hogland, W.; Marques, M.; Sillanpää, M., An overview of the modification methods of activated carbon for its water treatment applications. *Chemical Engineering Journal* **2013**, 219, 499-511.
10. Rafatullah, M.; Sulaiman, O.; Hashim, R.; Ahmad, A., Adsorption of methylene blue on low-cost adsorbents: A review. *Journal of Hazardous Materials* **2010**, 177 (1), 70-80.
11. Dai, J.; Huang, T.; Tian, S.-q.; Xiao, Y.-j.; Yang, J.-h.; Zhang, N.; Wang, Y.; Zhou, Z.-w., High structure stability and outstanding adsorption performance of graphene oxide aerogel supported by polyvinyl alcohol for waste water treatment. *Materials & Design* **2016**, 107, 187-197.
12. Wang, S.; Li, H.; Xu, L., Application of zeolite MCM-22 for basic dye removal from wastewater. *Journal of Colloid and Interface Science* **2006**, 295 (1), 71-78.
13. Lee, C.-K.; Liu, S.-S.; Juang, L.-C.; Wang, C.-C.; Lin, K.-S.; Lyu, M.-D., Application of MCM-41 for dyes removal from wastewater. *Journal of Hazardous Materials* **2007**, 147 (3), 997-1005.
14. Wong, T., *Handbook of zeolites: Structure, properties and applications*. Materials Science and Technolo: 2009.
15. Inglezakis, V. J., The concept of "capacity" in zeolite ion-exchange systems. *Journal of Colloid and Interface Science* **2005**, 281 (1), 68-79.
16. Waheed, A.; Baig, N.; Ullah, N.; Falath, W., Removal of hazardous dyes, toxic metal ions and organic pollutants from wastewater by using porous hyper-cross-linked polymeric materials: A review of recent advances. *Journal of Environmental Management* **2021**, 287, 112360.
17. Townsend, R. P.; Coker, E. N., Chapter 11 Ion exchange in zeolites. In *Studies in Surface Science and Catalysis*, van Bekkum, H.; Flanigen, E. M.; Jacobs, P. A.; Jansen, J. C., Eds. Elsevier: 2001; Vol. 137, pp 467-524.
18. Lutz, W.; Löffler, E.; Zibrowius, B., Increased hydrothermal stability of highly dealuminated Y zeolites by alumination. *Zeolites* **1993**, 13 (8), 685-686.
19. Lutz, W.; Wieker, W.; Müller, D.; Schneider, M.; Rüscher, C. H.; Buhl, J. C., Phase Transformations in Alkaline and Acid Leached Y Zeolites Dealuminated by Steaming. *Zeitschrift für anorganische und allgemeine Chemie* **2000**, 626 (6), 1460-1467.
20. Ojuva, A. Processing and performance of zeolites for efficient carbon dioxide separation. Department of Materials and Environmental Chemistry, Stockholm University, 2015.

21. Tao, Y.; Kanoh, H.; Abrams, L.; Kaneko, K., Mesopore-Modified Zeolites: Preparation, Characterization, and Applications. *Chemical Reviews* **2006**, *106* (3), 896-910.
22. Schwieger, W.; Machoke, A. G.; Weissenberger, T.; Inayat, A.; Selvam, T.; Klumpp, M.; Inayat, A., Hierarchy concepts: classification and preparation strategies for zeolite containing materials with hierarchical porosity. *Chemical Society Reviews* **2016**, *45* (12), 3353-3376.
23. Pérez-Ramírez, J.; Christensen, C. H.; Egeblad, K.; Christensen, C. H.; Groen, J. C., Hierarchical zeolites: enhanced utilisation of microporous crystals in catalysis by advances in materials design. *Chemical Society Reviews* **2008**, *37* (11), 2530-2542.
24. Chal, R.; Gérardin, C.; Bulut, M.; van Donk, S., Overview and Industrial Assessment of Synthesis Strategies towards Zeolites with Mesopores. *ChemCatChem* **2011**, *3* (1), 67-81.
25. Koohsaryan, E.; Anbia, M., Nanosized and hierarchical zeolites: A short review. *Chinese Journal of Catalysis* **2016**, *37* (4), 447-467.
26. Verboekend, D.; Nuttens, N.; Locus, R.; Van Aelst, J.; Verolme, P.; Groen, J. C.; Pérez-Ramírez, J.; Sels, B. F., Synthesis, characterisation, and catalytic evaluation of hierarchical faujasite zeolites: milestones, challenges, and future directions. *Chemical Society Reviews* **2016**, *45* (12), 3331-3352.
27. Zhang, K.; Ostraat, M. L., Innovations in hierarchical zeolite synthesis. *Catalysis Today* **2016**, *264*, 3-15.
28. de Jong, K. P.; Zečević, J.; Friedrich, H.; de Jongh, P. E.; Bulut, M.; van Donk, S.; Kenmogne, R.; Finiels, A.; Hulea, V.; Fajula, F., Zeolite Y Crystals with Trimodal Porosity as Ideal Hydrocracking Catalysts. *Angewandte Chemie International Edition* **2010**, *49* (52), 10074-10078.
29. Li, W.; Zheng, J.; Luo, Y.; Da, Z., Effect of hierarchical porosity and phosphorus modification on the catalytic properties of zeolite Y. *Applied Surface Science* **2016**, *382*, 302-308.
30. Mehlhorn, D.; Rodriguez, J.; Cacciaguerra, T.; Andrei, R.-D.; Cammarano, C.; Guenneau, F.; Gedeon, A.; Coasne, B.; Thommes, M.; Minoux, D.; Aquino, C.; Dath, J.-P.; Fajula, F.; Galarneau, A., Revelation on the Complex Nature of Mesoporous Hierarchical FAU-Y Zeolites. *Langmuir* **2018**, *34* (38), 11414-11423.
31. Huang, L.; Guo, W.; Deng, P.; Xue, Z.; Li, Q., Investigation of Synthesizing MCM-41/ZSM-5 Composites. *The Journal of Physical Chemistry B* **2000**, *104* (13), 2817-2823.
32. Verhoef, M. J.; Kooyman, P. J.; van der Waal, J. C.; Rigutto, M. S.; Peters, J. A.; van Bekkum, H., Partial Transformation of MCM-41 Material into Zeolites: Formation of Nanosized MFI Type Crystallites. *Chemistry of Materials* **2001**, *13* (2), 683-687.
33. Majano, G.; Mintova, S.; Ovsitser, O.; Mihailova, B.; Bein, T., Zeolite Beta nanosized assemblies. *Microporous and Mesoporous Materials* **2005**, *80* (1), 227-235.
34. Kloetstra, K. R.; Zandbergen, H. W.; Jansen, J. C.; van Bekkum, H., Overgrowth of mesoporous MCM-41 on faujasite. *Microporous Materials* **1996**, *6* (5), 287-293.
35. Karlsson, A.; Stöcker, M.; Schmidt, R., Composites of micro- and mesoporous materials: simultaneous syntheses of MFI/MCM-41 like phases by a mixed template approach. *Microporous and Mesoporous Materials* **1999**, *27* (2), 181-192.
36. Holland, B. T.; Abrams, L.; Stein, A., Dual Templating of Macroporous Silicates with Zeolitic Microporous Frameworks. *Journal of the American Chemical Society* **1999**, *121* (17), 4308-4309.
37. Vuong, G.-T.; Do, T.-O., A New Route for the Synthesis of Uniform Nanozeolites with Hydrophobic External Surface in Organic Solvent Medium. *Journal of the American Chemical Society* **2007**, *129* (13), 3810-3811.
38. Wei, Y.; Parmentier, T. E.; de Jong, K. P.; Zečević, J., Tailoring and visualizing the pore architecture of hierarchical zeolites. *Chemical Society Reviews* **2015**, *44* (20), 7234-7261.
39. Garwood, W. E., Conversion of  $C_2$ - $C_{10}$  to Higher Olefins over Synthetic Zeolite ZSM-5. In *Intrazeolite Chemistry*, AMERICAN CHEMICAL SOCIETY: 1983; Vol. 218, pp 383-396.
40. Tabak, S. A.; Krambeck, F. J.; Garwood, W. E., Conversion of propylene and butylene over ZSM-5 catalyst. *AIChE Journal* **1986**, *32* (9), 1526-1531.
41. Wang, S.; Dou, T.; Li, Y.; Zhang, Y.; Li, X.; Yan, Z., A novel method for the preparation of MOR/MCM-41 composite molecular sieve. *Catalysis Communications* **2005**, *6* (1), 87-91.

42. Datema, K. P.; Nowak, A. K.; van Braam Houckgeest, J.; Wielers, A. F. H., In-situ<sup>13</sup>C magic-angle-spinning NMR measurements of the conversion of ethene to aliphatic hydrocarbons over structurally different zeolites. *Catalysis Letters* **1991**, *11* (3), 267-276.
43. Yamamura, M.; Chaki, K.; Wakatsuki, T.; Okado, H.; Fujimoto, K., Synthesis of ZSM-5 zeolite with small crystal size and its catalytic performance for ethylene oligomerization. *Zeolites* **1994**, *14* (8), 643-649.
44. Fărcașiu, D.; Hutchison, J.; Li, L., An analysis of factors that influence shape selectivity in the cracking of long-chain alkanes on zeolite catalysts. *Journal of Catalysis* **1990**, *122* (1), 34-43.
45. Giudici, R.; Kouwenhoven, H. W.; Prins, R., Comparison of nitric and oxalic acid in the dealumination of mordenite. *Applied Catalysis A: General* **2000**, *203* (1), 101-110.
46. Hogan, J., Catalytic polymerization of olefins. *Phillips petroleum company, US* **1957**, 2794842.
47. Caicedo-Realpe, R.; Pérez-Ramírez, J., Mesoporous ZSM-5 zeolites prepared by a two-step route comprising sodium aluminate and acid treatments. *Microporous and Mesoporous Materials* **2010**, *128* (1), 91-100.
48. van laak, A. N. C.; Gosselink, R. W.; Sagala, S. L.; Meeldijk, J. D.; de Jongh, P. E.; de Jong, K. P., Alkaline treatment on commercially available aluminum rich mordenite. *Applied Catalysis A: General* **2010**, *382* (1), 65-72.
49. Holm, M. S.; Hansen, M. K.; Christensen, C. H., "One-Pot" Ion-Exchange and Mesopore Formation During Desilication. *European Journal of Inorganic Chemistry* **2009**, *2009* (9), 1194-1198.
50. Groen, J. C.; Abelló, S.; Villaescusa, L. A.; Pérez-Ramírez, J., Mesoporous beta zeolite obtained by desilication. *Microporous and Mesoporous Materials* **2008**, *114* (1), 93-102.
51. Ogura, M.; Shinomiya, S.-y.; Tateno, J.; Nara, Y.; Kikuchi, E.; Matsukata, M., Formation of Uniform Mesopores in ZSM-5 Zeolite through Treatment in Alkaline Solution. *Chemistry Letters* **2000**, *29* (8), 882-883.
52. Ogura, M.; Shinomiya, S.-y.; Tateno, J.; Nara, Y.; Nomura, M.; Kikuchi, E.; Matsukata, M., Alkali-treatment technique — new method for modification of structural and acid-catalytic properties of ZSM-5 zeolites. *Applied Catalysis A: General* **2001**, *219* (1), 33-43.
53. Paixão, V.; Carvalho, A. P.; Rocha, J.; Fernandes, A.; Martins, A., Modification of MOR by desilication treatments: Structural, textural and acidic characterization. *Microporous and Mesoporous Materials* **2010**, *131* (1), 350-357.
54. van Laak, A. N. C.; Sagala, S. L.; Zečević, J.; Friedrich, H.; de Jongh, P. E.; de Jong, K. P., Mesoporous mordenites obtained by sequential acid and alkaline treatments – Catalysts for cumene production with enhanced accessibility. *Journal of Catalysis* **2010**, *276* (1), 170-180.
55. Li, X.; Prins, R.; van Bokhoven, J. A., Synthesis and characterization of mesoporous mordenite. *Journal of Catalysis* **2009**, *262* (2), 257-265.
56. Groen, J. C.; Sano, T.; Moulijn, J. A.; Pérez-Ramírez, J., Alkaline-mediated mesoporous mordenite zeolites for acid-catalyzed conversions. *Journal of Catalysis* **2007**, *251* (1), 21-27.
57. Groen, J. C.; Peffer, L. A. A.; Moulijn, J. A.; Pérez-Ramírez, J., Mechanism of Hierarchical Porosity Development in MFI Zeolites by Desilication: The Role of Aluminium as a Pore-Directing Agent. *Chemistry – A European Journal* **2005**, *11* (17), 4983-4994.
58. Groen, J. C., Mesoporous zeolites obtained by desilication. **2007**.
59. Groen, J. C.; Moulijn, J. A.; Pérez-Ramírez, J., Desilication: on the controlled generation of mesoporosity in MFI zeolites. *Journal of Materials Chemistry* **2006**, *16* (22), 2121-2131.
60. Abelló, S.; Bonilla, A.; Pérez-Ramírez, J., Mesoporous ZSM-5 zeolite catalysts prepared by desilication with organic hydroxides and comparison with NaOH leaching. *Applied Catalysis A: General* **2009**, *364* (1), 191-198.
61. Yang, S.; Yu, C.; Yu, L.; Miao, S.; Zou, M.; Jin, C.; Zhang, D.; Xu, L.; Huang, S., Bridging Dealumination and Desilication for the Synthesis of Hierarchical MFI Zeolites. *Angewandte Chemie International Edition* **2017**, *56* (41), 12553-12556.
62. Goto, Y.; Fukushima, Y.; Ratu, P.; Imada, Y.; Kubota, Y.; Sugi, Y.; Ogura, M.; Matsukata, M., Mesoporous Material from Zeolite. *Journal of Porous Materials* **2002**, *9* (1), 43-48.

63. Ivanova, I. I.; Kuznetsov, A. S.; Yuschenko, V. V.; Knyazeva, E. E., Design of composite micro/mesoporous molecular sieve catalysts. *Pure and Applied Chemistry* **2004**, *76* (9), 1647-1657.
64. Wang, S.; Dou, T.; Li, Y.; Zhang, Y.; Li, X.; Yan, Z., Synthesis, characterization, and catalytic properties of stable mesoporous molecular sieve MCM-41 prepared from zeolite mordenite. *Journal of Solid State Chemistry* **2004**, *177* (12), 4800-4805.
65. Ordonsky, V. V.; Murzin, V. Y.; Monakhova, Y. V.; Zubavichus, Y. V.; Knyazeva, E. E.; Nesterenko, N. S.; Ivanova, I. I., Nature, strength and accessibility of acid sites in micro/mesoporous catalysts obtained by recrystallization of zeolite BEA. *Microporous and Mesoporous Materials* **2007**, *105* (1), 101-110.
66. Ivanova, I. I.; Kuznetsov, A. S.; Knyazeva, E. E.; Fajula, F.; Thibault-Starzyk, F.; Fernandez, C.; Gilson, J. P., Design of hierarchically structured catalysts by mordenites recrystallization: Application in naphthalene alkylation. *Catalysis Today* **2011**, *168* (1), 133-139.
67. J.Y. Ying, J. G. M., Mesostructured zeolitic materials, and methods of making and using the same. *Massachusetts Institute Of Technology, US*, **2005**, Patent n° US 2005/0239634 A1.
68. Chal, R.; Cacciaguerra, T.; van Donk, S.; Gérardin, C., Pseudomorphic synthesis of mesoporous zeolite Y crystals. *Chemical Communications* **2010**, *46* (41), 7840-7842.
69. Ivanova, I. I.; Knyazeva, E. E., Micro-mesoporous materials obtained by zeolite recrystallization: synthesis, characterization and catalytic applications. *Chemical Society Reviews* **2013**, *42* (9), 3671-3688.
70. Jolivet, J.-P.; Froidefond, C.; Pottier, A.; Chanéac, C.; Cassaignon, S.; Tronc, E.; Euzen, P., Size tailoring of oxide nanoparticles by precipitation in aqueous medium. A semi-quantitative modelling. *Journal of Materials Chemistry* **2004**, *14* (21), 3281-3288.
71. Auffan, M.; Rose, J.; Bottero, J.-Y.; Lowry, G. V.; Jolivet, J.-P.; Wiesner, M. R., Towards a definition of inorganic nanoparticles from an environmental, health and safety perspective. *Nature Nanotechnology* **2009**, *4* (10), 634-641.
72. Song, B.; Chu, Y.; Li, G.; Wang, J.; Lo, A.-Y.; Zheng, A.; Deng, F., Origin of Zeolite Confinement Revisited by Energy Decomposition Analysis. *The Journal of Physical Chemistry C* **2016**, *120* (48), 27349-27363.
73. Prelot, B.; Lantenois, S.; Chorro, C.; Charbonnel, M.-C.; Zajac, J.; Douillard, J. M., Effect of Nanoscale Pore Space Confinement on Cadmium Adsorption from Aqueous Solution onto Ordered Mesoporous Silica: A Combined Adsorption and Flow Calorimetry Study. *The Journal of Physical Chemistry C* **2011**, *115* (40), 19686-19695.
74. Boekfa, B.; Pantu, P.; Probst, M.; Limtrakul, J., Adsorption and Tautomerization Reaction of Acetone on Acidic Zeolites: The Confinement Effect in Different Types of Zeolites. *The Journal of Physical Chemistry C* **2010**, *114* (35), 15061-15067.
75. Varghese, J. J.; Mushrif, S. H., Origins of complex solvent effects on chemical reactivity and computational tools to investigate them: a review. *Reaction Chemistry & Engineering* **2019**, *4* (2), 165-206.
76. Boscoboinik, J. A., Chemistry in confined space through the eyes of surface science-2D porous materials. *J Phys Condens Matter* **2019**, *31* (6), 063001.
77. Derouane, E. G.; André, J.-M.; Lucas, A. A., A simple van der waals model for molecule-curved surface interactions in molecular-sized microporous solids. *Chemical Physics Letters* **1987**, *137* (4), 336-340.
78. Derouane, E. G., The energetics of sorption by molecular sieves: Surface curvature effects. *Chemical Physics Letters* **1987**, *142* (3), 200-204.
79. Senapati, S.; Chandra, A., Dielectric Constant of Water Confined in a Nanocavity. *The Journal of Physical Chemistry B* **2001**, *105* (22), 5106-5109.
80. Mizota, T.; Petrova, N. L.; Nakayama, N., Entropy of Zeolitic Water. *Journal of Thermal Analysis and Calorimetry* **2001**, *64* (1), 211-217.
81. Hureau, M.; Moissette, A.; Legrand, A.; Luchez, F.; Sliwa, M.; Bremard, C., Chemical Control of Photoinduced Charges under Confinement in Zeolites. *The Journal of Physical Chemistry C* **2012**, *116* (16), 9092-9105.

82. Luchez, F.; Carré, S.; Moissette, A.; Poizat, O., Sorption and spontaneous ionization of phenothiazine within channel type zeolites: Effect of the confinement on the electron transfers. *RSC Advances* **2011**, *1* (2), 341-350.
83. Chu, Y.; Ji, P.; Yi, X.; Li, S.; Wu, P.; Zheng, A.; Deng, F., Strong or weak acid, which is more efficient for Beckmann rearrangement reaction over solid acid catalysts? *Catalysis Science & Technology* **2015**, *5* (7), 3675-3681.
84. Derouane, E. G.; Nagy, J. B.; Fernandez, C.; Gabelica, Z.; Laurent, E.; Maljean, P., Diffusion of alkanes in molecular sieves evidence for confinement effects. *Applied Catalysis* **1988**, *40*, L1-L10.
85. Hennessy, B.; Megelski, S.; Marcolli, C.; Shklover, V.; Bärlocher, C.; Calzaferri, G., Characterization of Methyl Viologen in the Channels of Zeolite L. *The Journal of Physical Chemistry B* **1999**, *103* (17), 3340-3351.
86. Insuwan, W.; Rangsiwatananon, K.; Meeprasert, J.; Namuangruk, S.; Surakhot, Y.; Kungwan, N.; Jungsuttiwong, S., Combined experimental and theoretical investigation on Fluorescence Resonance Energy Transfer of dye loaded on LTL zeolite. *Microporous and Mesoporous Materials* **2017**, *241*, 372-382.
87. Viani, L.; Minoia, A.; Cornil, J.; Beljonne, D.; Egelhaaf, H.-J.; Gierschner, J., Resonant Energy Transport in Dye-Filled Monolithic Crystals of Zeolite L: Modeling of Inhomogeneity. *The Journal of Physical Chemistry C* **2016**, *120* (48), 27192-27199.
88. Fu, J.; Feng, X.; Liu, Y.; Yang, C., Effect of pore confinement on the adsorption of mono-branched alkanes of naphtha in ZSM-5 and Y zeolites. *Applied Surface Science* **2017**, *423*, 131-138.
89. Pantu, P.; Boekfa, B.; Limtrakul, J., The adsorption of saturated and unsaturated hydrocarbons on nanostructured zeolites (H-MOR and H-FAU): An ONIOM study. *Journal of Molecular Catalysis A: Chemical* **2007**, *277* (1), 171-179.
90. Boekfa, B.; Choomwattana, S.; Khongpracha, P.; Limtrakul, J., Effects of the Zeolite Framework on the Adsorptions and Hydrogen-Exchange Reactions of Unsaturated Aliphatic, Aromatic, and Heterocyclic Compounds in ZSM-5 Zeolite: A Combination of Perturbation Theory (MP2) and a Newly Developed Density Functional Theory (M06-2X) in ONIOM Scheme. *Langmuir* **2009**, *25* (22), 12990-12999.
91. Hsieh, C.-T.; Fan, W.-S.; Chen, W.-Y., Impact of mesoporous pore distribution on adsorption of methylene blue onto titania nanotubes in aqueous solution. *Microporous and Mesoporous Materials* **2008**, *116* (1), 677-683.
92. Eder, F.; Lercher, J. A., On the Role of the Pore Size and Tortuosity for Sorption of Alkanes in Molecular Sieves. *The Journal of Physical Chemistry B* **1997**, *101* (8), 1273-1278.
93. Gounder, R.; Iglesia, E., Catalytic Consequences of Spatial Constraints and Acid Site Location for Monomolecular Alkane Activation on Zeolites. *Journal of the American Chemical Society* **2009**, *131* (5), 1958-1971.
94. Chai, Y.; Han, X.; Li, W.; Liu, S.; Yao, S.; Wang, C.; Shi, W.; da-Silva, I.; Manuel, P.; Cheng, Y.; Daemen, L. D.; Ramirez-Cuesta, A. J.; Tang, C. C.; Jiang, L.; Yang, S.; Guan, N.; Li, L., Control of zeolite pore interior for chemoselective alkyne/olefin separations. *Science* **2020**, *368* (6494), 1002.
95. Dai, J.; Zhang, H., Recent Advances in Catalytic Confinement Effect within Micro/Meso-Porous Crystalline Materials. *Small* **2021**, *n/a* (n/a), 2005334.
96. Janda, A.; Vlaisavljevich, B.; Lin, L.-C.; Smit, B.; Bell, A. T., Effects of Zeolite Structural Confinement on Adsorption Thermodynamics and Reaction Kinetics for Monomolecular Cracking and Dehydrogenation of n-Butane. *Journal of the American Chemical Society* **2016**, *138* (14), 4739-4756.
97. Thach, U. D.; Prelot, B.; Pellet-Rostaing, S.; Zajac, J.; Hesemann, P., Surface Properties and Chemical Constitution as Crucial Parameters for the Sorption Properties of Ionosilicas: The Case of Chromate Adsorption. *ACS Applied Nano Materials* **2018**, *1* (5), 2076-2087.
98. Guil, J. M.; Perdigón-Melón, J. A.; Brotas de Carvalho, M.; Carvalho, A. P.; Pires, J., Adsorption microcalorimetry of probe molecules of different size to characterize the microporosity of pillared clays. *Microporous and Mesoporous Materials* **2002**, *51* (2), 145-154.

99. Cao, Z.; Peng, Y.; Yan, T.; Li, S.; Li, A.; Voth, G. A., Mechanism of Fast Proton Transport along One-Dimensional Water Chains Confined in Carbon Nanotubes. *Journal of the American Chemical Society* **2010**, *132* (33), 11395-11397.
100. Armstrong, J. A.; Bloembergen, N.; Ducuing, J.; Pershan, P. S., Interactions between Light Waves in a Nonlinear Dielectric. *Physical Review* **1962**, *127* (6), 1918-1939.
101. Franken, P. A.; Hill, A. E.; Peters, C. W.; Weinreich, G., Generation of Optical Harmonics. *Physical Review Letters* **1961**, *7* (4), 118-119.
102. Brevet, P.-F., *Surface second harmonic generation*. PPUR presses polytechniques: 1997.
103. Roke, S.; Gonella, G., Nonlinear Light Scattering and Spectroscopy of Particles and Droplets in Liquids. *Annual Review of Physical Chemistry* **2012**, *63* (1), 353-378.
104. Eisenthal, K. B., Liquid Interfaces Probed by Second-Harmonic and Sum-Frequency Spectroscopy. *Chemical Reviews* **1996**, *96* (4), 1343-1360.
105. Gonella, G.; Dai, H.-L., Second Harmonic Light Scattering from the Surface of Colloidal Objects: Theory and Applications. *Langmuir* **2014**, *30* (10), 2588-2599.
106. Wang, H.; Yan, E. C. Y.; Borguet, E.; Eisenthal, K. B., Second harmonic generation from the surface of centrosymmetric particles in bulk solution. *Chemical Physics Letters* **1996**, *259* (1), 15-20.
107. Wang, H.; Troxler, T.; Yeh, A.-G.; Dai, H.-L., In Situ, Nonlinear Optical Probe of Surfactant Adsorption on the Surface of Microparticles in Colloids. *Langmuir* **2000**, *16* (6), 2475-2481.
108. Eckenrode, H. M.; Dai, H.-L., Nonlinear Optical Probe of Biopolymer Adsorption on Colloidal Particle Surface: Poly-L-lysine on Polystyrene Sulfate Microspheres. *Langmuir* **2004**, *20* (21), 9202-9209.
109. Yan, E. C. Y.; Liu, Y.; Eisenthal, K. B., New Method for Determination of Surface Potential of Microscopic Particles by Second Harmonic Generation. *The Journal of Physical Chemistry B* **1998**, *102* (33), 6331-6336.
110. van der Veen, M. A.; Verbiest, T.; De Vos, D. E., Probing microporous materials with second-harmonic generation. *Microporous and Mesoporous Materials* **2013**, *166*, 102-108.
111. Eckenrode, H. M.; Jen, S.-H.; Han, J.; Yeh, A.-G.; Dai, H.-L., Adsorption of a Cationic Dye Molecule on Polystyrene Microspheres in Colloids: Effect of Surface Charge and Composition Probed by Second Harmonic Generation. *The Journal of Physical Chemistry B* **2005**, *109* (10), 4646-4653.
112. Haber, L. H.; Kwok, S. J. J.; Semeraro, M.; Eisenthal, K. B., Probing the colloidal gold nanoparticle/aqueous interface with second harmonic generation. *Chemical Physics Letters* **2011**, *507* (1), 11-14.
113. Schürer, B.; Wunderlich, S.; Sauerbeck, C.; Peschel, U.; Peukert, W., Probing colloidal interfaces by angle-resolved second harmonic light scattering. *Physical Review B* **2010**, *82* (24), 241404.
114. Revillod, G.; Duboisset, J.; Russier-Antoine, I.; Benichou, E.; Bachelier, G.; Jonin, C.; Brevet, P.-F., Multipolar Contributions to the Second Harmonic Response from Mixed DiA-SDS Molecular Aggregates. *The Journal of Physical Chemistry C* **2008**, *112* (7), 2716-2723.
115. Gassin, P.-M.; Prelot, B.; Grégoire, B.; Martin-Gassin, G., Second-Harmonic Scattering in Layered Double Hydroxide Colloids: A Microscopic View of Adsorption and Intercalation. *Langmuir* **2018**, *34* (40), 12206-12213.
116. Gassin, P.-M.; Bellini, S.; Zajac, J.; Martin-Gassin, G., Adsorbed Dyes onto Nanoparticles: Large Wavelength Dependence in Second Harmonic Scattering. *The Journal of Physical Chemistry C* **2017**, *121* (27), 14566-14571.
117. Boudjema, L.; Aarrass, H.; Assaf, M.; Morille, M.; Martin-Gassin, G.; Gassin, P.-M., PySHS: Python Open Source Software for Second Harmonic Scattering. *Journal of Chemical Information and Modeling* **2020**, *60* (12), 5912-5917.
118. Duboisset, J.; Brevet, P.-F., Salt-induced Long-to-Short Range Orientational Transition in Water. *Physical Review Letters* **2018**, *120* (26), 263001.





## Chapter II: Experimental part

The aim of this chapter is to describe the various materials and the methods used in this thesis. The study of the various properties of initial and synthesized materials is necessary to rationalize information on their structure, morphology, texture, composition, together with the chemical environment of specific elements. A series of experimental techniques used to evaluate their properties are described.

Then, the two main approaches of this thesis will be presented. They allow the study of probe molecules at a solid/liquid interface by combining macroscopical and local levels. The first approach consists of the determination at a global scale of adsorption isotherm to evaluate the capacity and the affinity of the adsorption. This will be completed with calorimetric measurements to evaluate the enthalpic changes during the adsorption process. The second level of our approach is based on local technique, using non-linear optics. In particular, second harmonic scattering experiments will be carried out, to determine in a different way the adsorption isotherm, together with the study of the local environment of adsorbed molecules.

## Molecules

### 1.1 Outlook

The adsorption of molecules depends on the adsorbent materials, and varies from one molecule to another. These variations depend of donor or acceptor group permits the electron delocalization, that is required in our case for Second Harmonic Scattering measurements. This is why we have selected specific molecules.

### 1.2 2D molecules

In this study, three  $C_n$ -DiA (trans-4-[4-(dimethylamino)styryl-1-methyl]pyridinium iodide, named  $C_1$ DiA; trans-4-[4-(Dibutylamino)styryl]-1-methylpyridinium iodide, named  $C_4$ DiA; 4-Di-16-ASP (4-[4-(Dihexadecylamino)styryl]-N-Methylpyridinium Iodide), named  $C_{16}$ DiA) dyes will be used. They are aminostyryl cationic molecules which differ from each other by their hydrocarbon chains of different lengths. Of these three dyes, some of them are hydrophilic and others are lipophilic. These molecules have the advantage of being detectable in UV-Vis spectroscopy and used as probe molecules in SHS.

The general structure of  $C_n$ -DiA is depicted in Figure 16. These dyes are linear dye with 2D form.

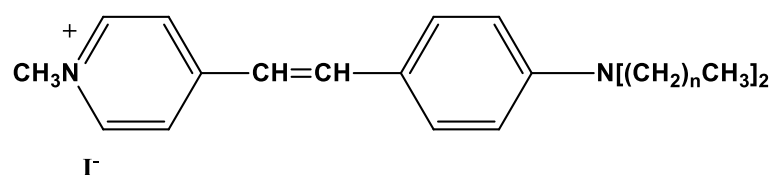


Figure 16 : General structure of C<sub>n</sub>DiA molecule

C<sub>1</sub>DiA is the dye with the shortest hydrophobic chain among those we have used as shown in Figure 17 a). This molecule contains two non-cyclic aliphatic alkane groups connected to the nitrogen atom, with two carbon each. It has the particularity of being hydrophilic.

C<sub>4</sub>DiA, Figure 17 b), has two chains with 4-carbons. Unlike C<sub>1</sub>DiA, this molecule is not soluble in water and has the characteristic of being slightly hydrophobic.

Finally, Figure 17 c) the last dye is C<sub>16</sub>DiA. It has two non-cyclic aliphatic alkane groups of sixteen carbon each, connected to the nitrogen atom. Thus, it gives it the value of the most hydrophobic dye among the three dyes presented above.

In order to study the effect of solvent on adsorption of dyes onto zeolites and on their behavior at solid / liquid interface, different solvents have been used which are dimethyl sulfoxide (DMSO), acetonitrile, methanol, ethanol and water.

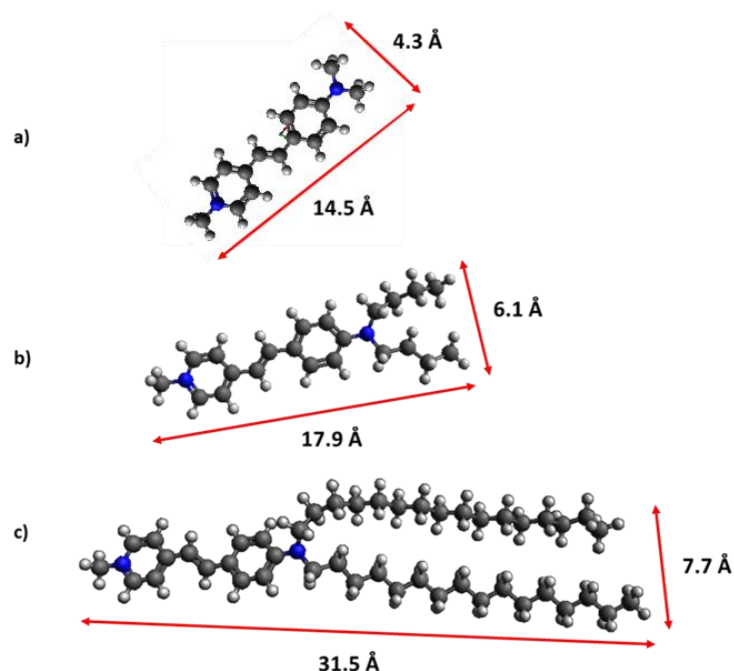


Figure 17 : Molecular representation of dye molecules and their sizes a) C<sub>1</sub>DiA b) C<sub>4</sub>DiA and c) C<sub>16</sub>DiA using Avogadro's software.

Acetonitrile, methanol, ethanol, and DMSO were obtained from Sigma Aldrich of HPLC grade. Ultrapure water has a resistivity of 18 M $\Omega$ , C<sub>n</sub>DiA (C<sub>1</sub>DiA, Mw = 366 g/mol, C<sub>4</sub>DiA Mw = 450 g/mol, and C<sub>16</sub>DiA Mw = 787 g/mol) were purchased from Sigma Aldrich (C<sub>1</sub>DiA and C<sub>4</sub>DiA) and Molecular Probes Invitrogen Company (C<sub>16</sub>DiA).

### 1.3 3D molecule

In addition, basic fuchsin (BF) also has been used in this thesis. Its structure is shown in Figure 18. As seen on the molecular representation, it is a 3D bulky dye compared to C<sub>n</sub>DiA. BF (Mw = 323 g/mol) was purchased from Sigma Aldrich.

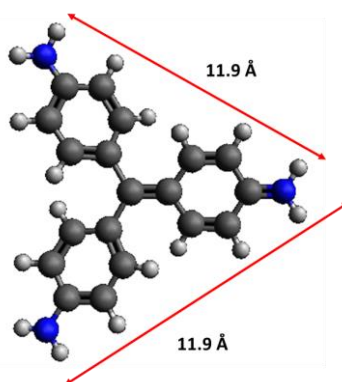


Figure 18 : The molecular representation of Basic fuchsin molecule and its size using Avogadro's software.

### 1.4 UV-visible spectroscopy characterization

The analysis of the UV spectrum permits qualitative and quantitative determination of the analytes by calculating the concentration of the unknown solution. The principle of this method consists in illuminating a solution of molecules or a suspension of particles with a polychromatic light beam and measure the intensity of transmitted light. The basic principle is that each compound absorbs or transmits light over a certain range of wavelength, in our case the wavelength varies depending on the optical property of each dye. Our measurements were performed in the liquid phase in the range of wavelength between 200 and 800 nm for both suspension and supernatant. The suspension measurement was done on the one hand to estimate the contribution of the interaction between dyes and material and on the other hand to know the absorption value at 400 nm for the re-absorption effect (to be explained later).

The measurements were performed using a Spectrophotometer from JASCO (V-670). The light source is a Halogen-Deuterium lamp allowing a wide spectral coverage in the UV and visible domain. The analysis of the zeolites (Faujasite FAU) particles were carried out in two steps. First, the wavelength

spectrum of the transmitted beam was recorded for a cell filled with ultra-pure water. This measurement is used as a reference and corresponds to the intensity transmitted by the cell in the absence of nanoparticles. Then, the absorption spectrum of the nanoparticle suspension was recorded. Finally, the latter spectrum is divided by signal obtained for ultra-pure water. This measurement allows to overcome spectral modulation of the beam of the white lamp. Likewise, a time averaging procedure eliminates time fluctuations.

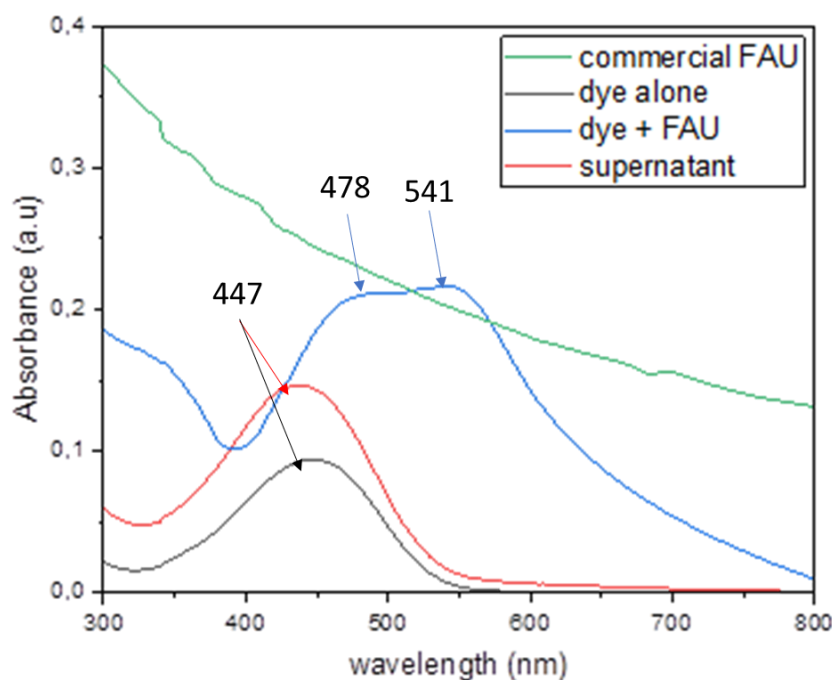


Figure 19 : Experimental photo absorbance UV-Visible of commercial Faujasite ( $Si/Al = 15$ ), dye alone in water solvent, dye in the presence of FAU particles and after adsorption and after filtration (supernatant).

Figure 19 reveals the superposition of UV spectra for the molecule alone, the material alone, the molecules in the presence of particles and the molecules after filtration. The spectrum of the dye alone has one peak at 447 nm. We observe that the spectrum of dye molecule adsorbed on FAU consists of two peaks one at 447 nm and the latter at 541 nm. The peak at 447 nm corresponds to the molecule free in the solution while the second peak at 541 nm reveals the interaction between dye and FAU particles.

## Faujasites

The purpose of this paragraph is to describe the experimental protocols used to modify a starting commercial zeolite (Faujasite) by post-synthesis desilication treatment in the presence of structuring agent.

### 1.5 Commercial Faujasite

Several Zeolites with different Si/Al ratios with hydrogen as the cation form were supplied by Zeolyst International. These zeolites are CBV-400, CBV-720 and CBV-780 with Si/Al, given by the supplier, 2.55, 15 and 40 respectively. These materials were used without any further purification. These materials were used to study the impact of the Si/Al ratio on the adsorption and their behavior with different solvents. The characterization of these zeolites will be then presented in the next parts.

### 1.6 Synthesis of modified faujasites

Our objective in this work is to combine microporosity and mesoporosity in order to study their influence on the adsorption properties. Mesoporosity was incorporated in zeolitic materials by post treatment using a dissolution-recrystallization strategy. This method is based on two main steps. The first step is the dissolution of FAU in an alkaline solution (NaOH). The second step is the recrystallization of the dissolved part in hydrothermal conditions in the presence of alkyltrimethylammonium bromide surfactants (C<sub>18</sub>TAB) as a structuring agent.

Desilication-recrystallization method is used in this thesis to obtain zeolites with hierarchical porosity. The synthesis of modified zeolite was done using the protocol of A. Galarneau et al. (2018)<sup>123</sup>. Zeolite is partially dissolved in the presence of an alkaline solution. In this study, the solution used is soda (NaOH), provided by Sigma-Aldrich in the form of anhydrous pellets. The recrystallization takes place in the presence of a structuring agent. The structuring agent used is octadecyltrimethylammonium bromide (C<sub>18</sub>TAB). This surfactant comes from Sigma-Aldrich with 98% purity.

Different materials having different levels of porosity, different porous volumes and sizes, were obtained by varying the quantity of NaOH used. The following procedure<sup>123</sup> has been followed to obtain 7g of all modified faujasite. Different quantity of NaOH pellets (0.3495; 0.8854; 1.1655 g for NaOH/Si ratio 0, 0.075, 0.095 and 0.25 respectively) was used depending on the mesoporosity we expect. NaOH was mixed with 104.86 g of H<sub>2</sub>O into 250 ml beaker in the presence of magnetic stirrer to achieve the total dissolution. 4.573 g of C<sub>18</sub>TAB was then added to the mixture by keeping the stirring until the total dissolution. When the homogeneity of the mixture was obtained, the magnetic stirrer

was replaced by an endless screw stirrer, under gentler speed to keep the particle size and shape of the initial particles. Then 7 g of pristine FAU (Si/Al = 15) was added to the mixture and stirred for 1-2 h at ambient temperature (25 °C) to get a white homogeneous suspension. After that, the mixture is transferred into a 250 ml Teflon-lined stainless-steel autoclave and kept under constant conditions for 20 hours at 115 °C. Finally, the mixture was filtered and washed several times until the pH become neutral. It is then dried at 80°C in an oven for 12 h and calcined at 550 °C for 8 h with a heating rate of 5 °C/min. The synthesis process is summarized in Figure 20. The modified materials have been renamed in the present work. Depending on the NaOH/Si ratio, for 0, 0.075, 0.095 and 0.25 the materials are referred as FAU-0,1,2 and 3 respectively. Zeolite with various properties is reported in Table 2.

Table 2 : zeolite with different properties used in this thesis

Zeolite used	Si/Al ratio	Referred name	Modified zeolite	
			NaOH/Si ratio	Referred name
CBV400	2.5	FAU400	-	-
CBV720	15	FAU720	0	FAU-0
			0.075	FAU-1
			0.095	FAU-2
			0.125	FAU-2a
			0.15	FAU-2b
			0.25	FAU-3
CBV780	40	FAU780	-	-



Figure 20 : Procedure used for the modification of FAU material via mixed route (desilication process by NaOH in the presence of structuring agent CTAB).

### 1.7 Characterization methods for solids

A series of techniques have been used to characterize the various properties of the prepared zeolites. A brief description of the main fundamentals of X-Ray Diffraction (XRD), X-Ray Fluorescence (XRF), N<sub>2</sub> physisorption, Scanning Electron Microscopy (SEM), Zeta Potential and Dynamic Light Scattering (DLS), <sup>29</sup>Si solid state NMR, Thermogravimetric Analysis (TGA) techniques are presented in this part.

### 1.7.1 Scanning electron microscopy (SEM)

SEM is a commonly used tool to study the morphology of particles. SEM has a lower resolution compared to TEM (Transmission Electron Microscopy). Nevertheless, SEM is appropriate for zeolites allowing to obtain images of a material with a resolution of the order of a few hundred nanometers. It is based on a high energy beam of electrons (from 5-50 eV) which interacts with the sample. According to the principle of electron microscopy, the production of images of sample is the result of surface scanning with a focused beam of electrons. When the beam is small, the resolution is better thanks to the focusing of energy on a small surface. If the sample doesn't absorb the electrons, they are returned back in various types such as X-rays, Auger electrons, secondary electrons and etc<sup>124</sup>.... Depending on the devices and their configuration, samples can be observed in high and low vacuum, in wet conditions and in elevated temperatures.

In the present study, these measurements allowed to evaluate the morphology of the prepared materials. The various zeolites were analyzed by scanning electron microscopy at field emission (FE-SEM) using a Hitachi S-4800 microscope (Hitachi Europe SAS, Velizy, France). The samples were first prepared by depositing a sample amount of around 5 mg on an adhesive carbon tape on a SEM sample holder.

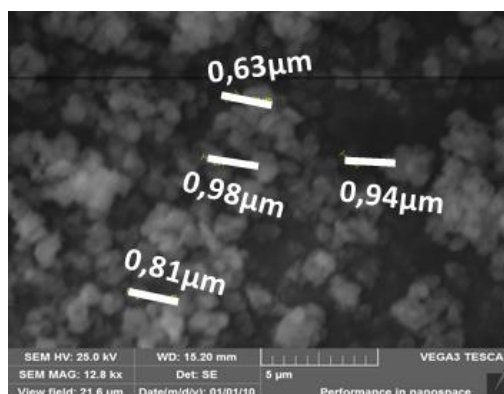


Figure 21 : SEM image for commercial FAU (FAU-0) (Si/Al = 15) of trade name CBV-720 purchased from Zeolyst international

The Figure 21 shows the SEM images corresponding to commercial initial material or FAU-0 zeolite. FAU-0 sample has a typical size estimated by SEM is between 0.7 and 1  $\mu\text{m}$  with aggregation of the particles. To confirm this observation, and the evolution of the size in liquid suspension, additional characterizations are therefore sometimes necessary to identify the actual size of individual nanocrystals, such as Dynamic Light Scattering (DLS).



### 1.7.2 Dynamic Light Scattering (DLS)

Dynamic Light Scattering (DLS) is a non-destructive spectroscopic analysis technique allowing access to the size of particles suspended in a liquid. This analysis technique strongly depends on the suspension stability and viscosity of the medium and the temperature. The diffused intensity is expressed as a function of the size to obtain the size distributions in intensity.

The apparatus used in the present study is a High Performance Particle Sizer (HPPS) (Malvern Instrument, UK) equipped with a 633 nm He-Ne laser. The measurements were carried out at 25 ° C and a scattering angle of 173 °. Samples were prepared by suspending 1mg FAU in 10 ml of either ultra-pure water or other solvents (ethanol, methanol, acetonitrile, DMSO). The suspension is sonicated for 10 min in an ultrasonic bath to ensure homogeneity of the sample and avoid the particle aggregation.

This technique is suitable to determine the monodispersity or polydispersity, the presence of large particles in the sample considered as aggregates by evaluating the size polydispersity index (Pdl). The Pdl is a dimensionless value that gives information on the width of the size distribution in correlation with the homogeneity or heterogeneity of particles size. When its value exceeds 1, this indicates that the sample has too large size distribution and may not be suitable for a DLS measurement.

Figure 22 shows the DLS signals of two suspensions of FAU material (FAU-0) in ultra-pure water, the first one is measured after 30 min of stirring of the prepared sample while the latter is measured after 24 hours of stirring of the prepared sample. The size distribution of FAU is 900 nm which corresponds to one population having a Pdl value of 0.5 as shown in Figure 22 a). However, Figure 22 b) displayed two populations with Pdl value of 0.7 (indication of polydispersity) having a different size between 700 and 1000nm. It is worth noting that the aggregation happened after a while due to the presence of aggregates.

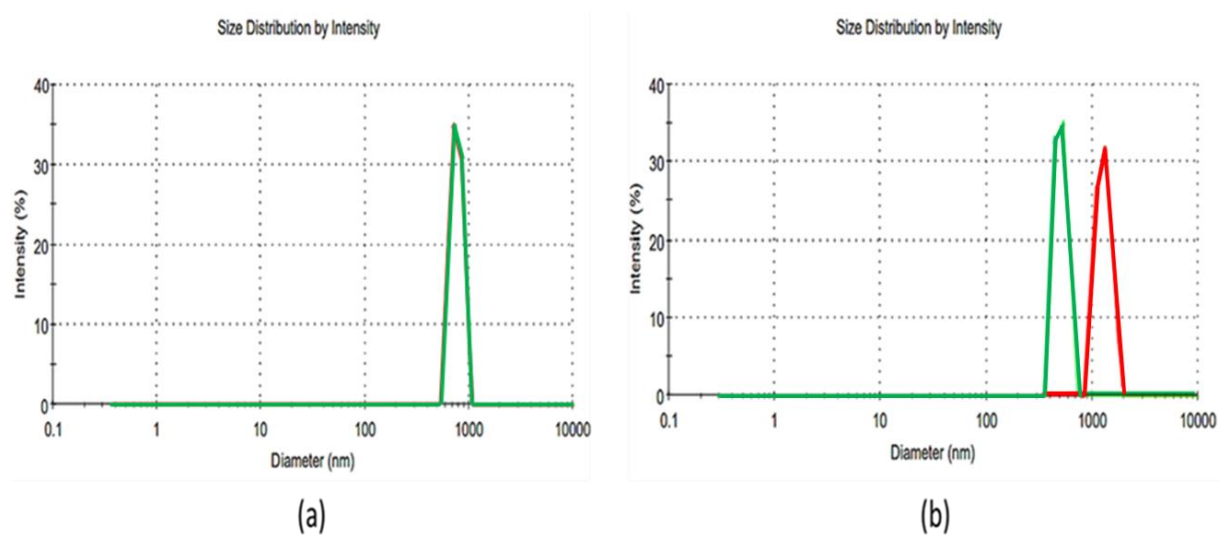


Figure 22 : DLS for two faujasite sample (FAU-0) prepared in suspension with ultra-pure water (a) after 30 min of preparation while (b) after 24 h with Pdl 0.5 and 0.7 respectively. Green peak corresponds to the population in the fresh suspension (as prepared) while the red corresponds to the new population.

### 1.7.3 Zeta ( $\zeta$ ) potential

Zeta potential is defined as electric potential from the shear plane to the bulk solution. The electrophilic mobility is linked to zeta potential.<sup>125</sup> A schematic representation is shown in Figure 23.

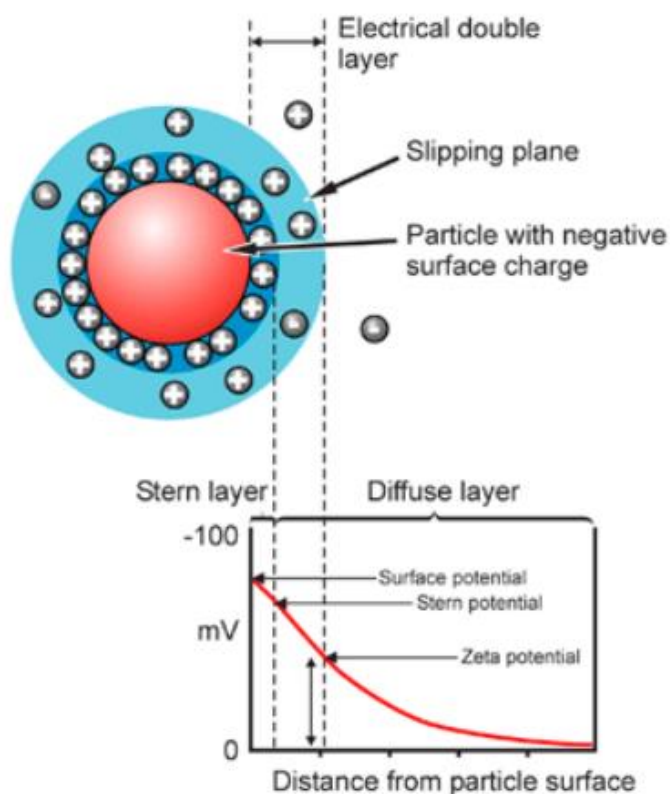


Figure 23 : Schematic representation of zeta potential<sup>126</sup>

Zeta potential varies depending on the conditions of the medium: pH, ionic strength, nature of the electrolyte. When the ionic strength increases, the repulsion of double layers decreases, which can lead to aggregation or coagulation of particles.

Usually, the values of zeta potential are the average of the zeta potential distribution for the overall population on eventual heterogeneous particles. The values are commonly in the range of – 100 mV to 100 mV, and depending on these values, the stability of the suspension is determined. Suspended particles with a zeta potential range near -30 mV or + 30 mV display the best stability.<sup>127</sup> When zeta potential is equal to 0, the particles are said to be at the isoelectric point (IEP) and tend to aggregate and flocculate.

The preparation of samples was done by suspending 1mg FAU in 10 ml either ultra-pure water or other solvents (ethanol, methanol, acetonitrile, DMSO), sonicated for 10 min in an ultrasonic bath to homogenize the sample and then injected to the instrument using a syringe. The apparatus used to characterize the zeta potential is Zeta Sizer 3000 HSA.

### 1.7.4 X-Ray diffraction (XRD)

To verify the structure of zeolites before and after modification of porosity, the X-ray diffraction (XRD) measurement was performed. XRD is the most used technique to identify crystalline solids as well as it can be used for the estimation of the degree of crystallinity. Each material has its own diffraction pattern thus X-ray diffraction data are considered as the fingerprint of the specific material.

The principle of this method is based on the diffraction of an X-rays incident beam through the crystal. This beam is then diffracted in a given direction ( $2\theta$  angle) according to Bragg's law:

$$n\lambda = 2d_{hkl} \sin \theta \quad (4)$$

where:

$n$  the order of interference;

$\lambda$  is the wavelength of the incident radiation used;

$d$  is the interplanar distance with  $(hkl)$  Miller indices;

$\theta$  is the incidence angle.

The diffractogram of X-rays obtained by constructive and destructive interference of X-rays with a family of parallel planes provides information about the characteristic distance and the crystal structure of solid studied (Figure 24).

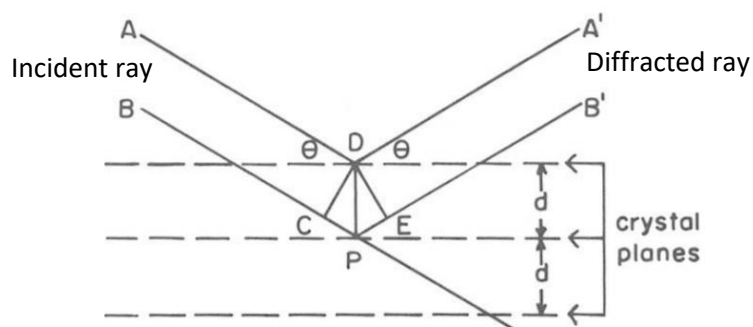


Figure 24 : Representative diagram of the X-ray diffraction phenomenon

The samples were compacted in sample holders. The XRD analyses were carried out on Philips PANalytical X'Pert PRO MPD diffractometer equipped with an X'Celerator Scientific detector. X-Ray diffraction patterns in this thesis were recorded at room temperature with Cu K $\alpha$  radiation ( $\lambda = 1.5406 \text{ \AA}$ ) over the  $2\theta$  diffraction small angles range from  $0.5^\circ$  to  $6^\circ$  for ordered mesoporous materials and from  $3^\circ$  to  $40^\circ$  for all the materials to be used. The scan angular rate was  $0.025^\circ$  with a counting time step of 5s per step. An example of the diffractogram obtained under these analysis conditions is given in Figure 25. From the diffractogram, we notice that the material is well crystallized showing the

structure of FAU as compared to Mehlhorn et al.<sup>30</sup> The detailed description of this diffractogram is stated in chapter 5.

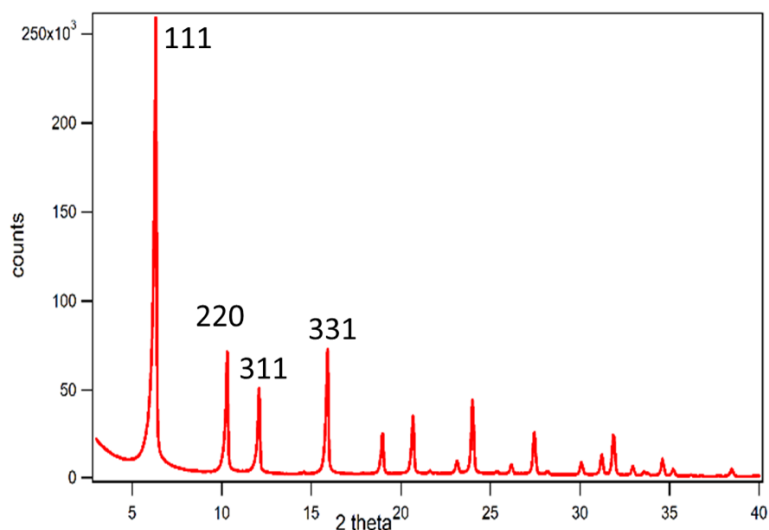


Figure 25 : Diffractogram for FAU (Si/Al = 15)

### 1.7.5 Wavelength-dispersive X-Ray fluorescence (XRF)

Wavelength-dispersive X-ray fluorescence (WDXRF) was used to determine the elemental composition present in samples. XRF is an elemental analysis technique that can be applied to liquids as well as solids. When an atom is excited by an X-ray photon, a constitutive electron of material is ejected. The vacant place left by this electron will be filled by an electron from the upper energy layer. It will then release energy in the form of X photons. This phenomenon is called fluorescence. The energy released is characteristic of each element and will then allow its identification. This method is also quantitative (up to a few ppm), thanks to the intensity of the peak measured by dispersive wavelength analysis (WPS).<sup>128</sup>

The production of X-rays from the spectrometer is applied to excite the atoms present in the solid sample, therefore the emission of X-rays is activated at wavelengths characteristic of the elements present in the structures. The estimation of the concentration and the nature of elements present in the zeolitic structure as well as Si/Al ratio has been evaluated from the intensity and the wavelength of X-rays emission respectively. The spectrometer applied for the XRF analyses was a PANalytical AXIOS Max with an SST-mAX50 X-ray source especially adapted for the detection of light elements.

In this thesis, XRF was performed before and after FAU modification in order to determine the global Si/Al ratio and to ensure the efficiency of alkaline treatment in the presence of a structuring agent. The determination of the zeolite composition was directly analyzed with XRF without any preparation or pretreatment. The samples were prepared in matrices that are pressed by a hydraulic press machine using Specac Atlas 15T manual hydraulic press to obtain flat pellets with a homogeneous representation of the sample and no void spaces. The results obtained in XRF will be shown in chapter 5.

### 1.7.6 Nitrogen-sorption isotherm at 77K

Nitrogen adsorption is widely used to characterize materials in order to know their textural properties, i.e. the specific surface area, the micro- and mesoporous volumes which are essential information for our study.

The measurements are carried out by placing a known mass of the solid degassed in advance in order to free the porosity in a measuring cell. The nitrogen pressure introduced into the doser is measured ( $P_i$ ), then the gas is introduced into the adsorption cell. The pressure decreases gradually due to the adsorption of nitrogen molecules onto the surface and in the porosity of the solid. When the pressure no longer varies, it is measured ( $P_f$ ). For each dose of nitrogen introduced, the quantity of adsorbed gas can be calculated from the  $P_i$  and  $P_f$  values. This method based on the introduction of a succession of doses of nitrogen makes it possible to trace point-by-point the adsorption isotherm, by reporting the quantity adsorbed per gram of adsorbent as a function of the ratio of the equilibrium pressure of the adsorbable gas and its saturating pressure, to the considered temperature (-196 °C, or 77 K).

According to IUPAC, Nitrogen-sorption isotherm are classified into eight different types from I to VI as shown in Figure 26.<sup>129, 130</sup>

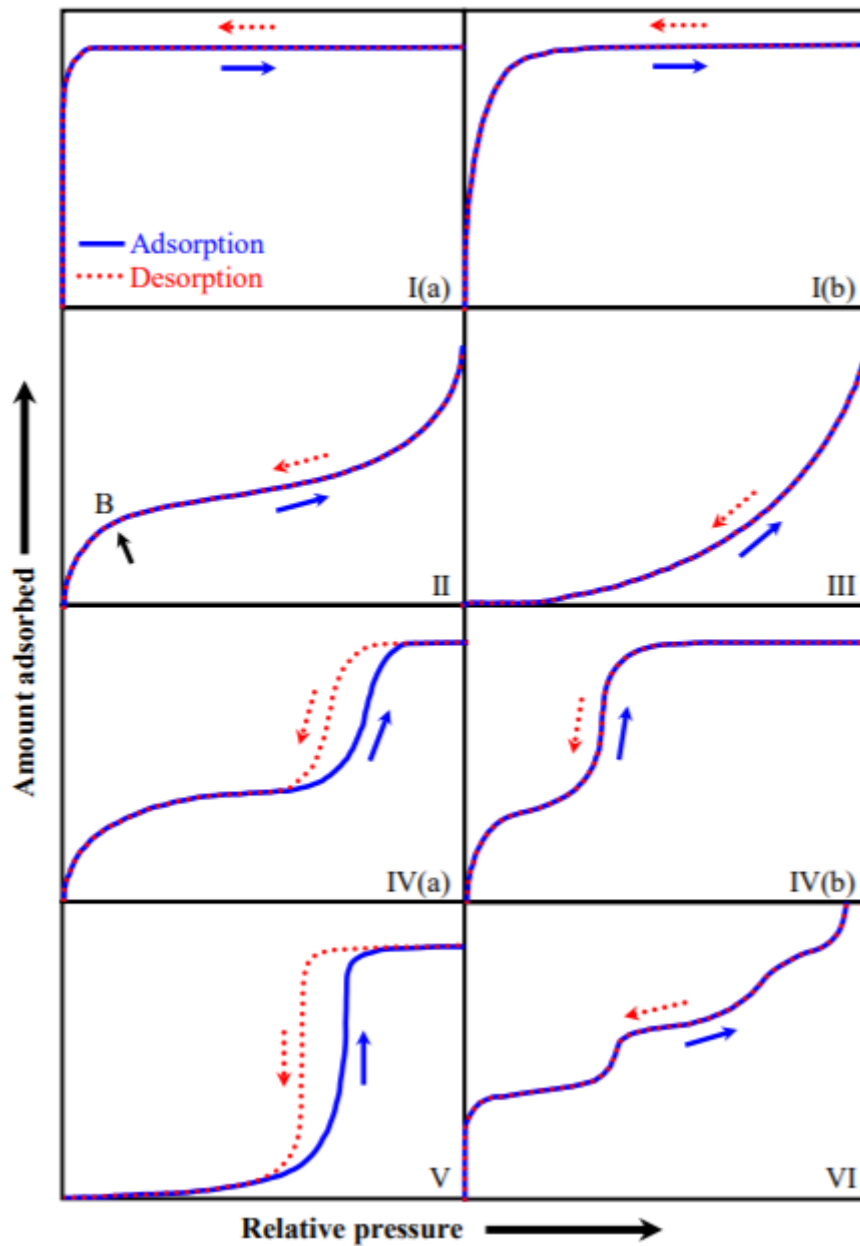


Figure 26 : Classification of physisorption isotherm, according to IUPAC<sup>131</sup>

The different types of isotherms can be translated as follows:

- Type I(a) isotherm is obtained for narrow microporous materials having a pore size  $< \sim 1$  nm.
- Type I(b) isotherm is mainly characterized for monolayer adsorption.
- Type II isotherm is characteristic of non-porous or macroporous material at the surface of which the adsorbed layer gradually increases. Point B represents the ending of the monolayer and the formation of the multilayer.

- Type III and V isotherms are both uncommon types of isotherms with no formation of multilayers meaning that the interactions between adsorbent and adsorbate are weak, thus, the adsorbate-adsorbate interaction plays a crucial role.
- Type IV (a) and (b) differ from each other by the presence of hysteresis loops. Type IV (a) isotherm has a pore width greater than 4 nm while Type IV (b) with pore width lower than 4 nm.
- Type VI isotherm demonstrates the adsorption of layer by layer on a smooth nonporous surface.

The surface areas and the pore volumes were determined by applying Brunauer-Emmett-Teller (BET) and t-plot, using the experimental data of nitrogen sorption isotherm. It was obtained at 77 K with the help of an automated sorption device (Micromeritics 3 Flex). Prior to the experiment, the samples were outgassed at 200 °C overnight under a secondary vacuum to remove surface impurities.

BET model is based on the extension of the theory of covering the surface with adsorbed molecules by forming a monolayer then a multilayer. For low partial pressures ( $0.05 < P / P_0 < 0.35$ ). It should be noted that this method of the BET model is considered to be based on the following assumptions:

- the adsorption is localized,
- the surface is homogeneous from the energy point of view,
- there are no lateral bonds,
- the molecules are indistinguishable,
- the surface can be covered, for an equilibrium pressure  $P$ , with 0, 1, 2, ...  $i$  layers,
- the values of the molar energies of adsorption from the second layer are equal to the molar energy of liquefaction  $E_L$ .

The BET equation can be expressed in a linear form:<sup>132, 133</sup>

$$\frac{P/P_0}{V(1 - P/P_0)} = \frac{1}{V_m C} + \frac{C - 1}{(V_m C)} (P/P_0) \quad (5)$$

With:

$P/P_0$  is the relative pressure

$V$  volume of adsorbed molecule at STP

$V_m$  is the monolayer volume under STP conditions



C is the BET constant related to the enthalpy and heat of vaporization

By plotting  $(P/P_0) / [V(1-P/P_0)]$  as a function of  $P/P_0$ , we obtain a straight line at a certain pressure range where the slope is equal to  $(C - 1)/V_m C$  and a y-intercept is equal to  $1/V_m C$ . We then use these results as well as the cross-sectional area of an adsorbate molecule, to calculate the specific surface of the material and the constant C. The values of  $P/P_0$  for which there is a linearity of the BET curve are found for mesoporous materials, in general, between 0.10 and 0.25.

The specific surface area S of a solid is equal to the area occupied by an adsorbed molecule  $a_m$  multiplied by the number of adsorbed molecules N contained in the volume  $V_m$ :

$$S = a_m \times N \quad \text{or,} \quad S = a_m \times N_a \times n \quad (6)$$

Where,  $N_a$  is the Avogadro's number and  $n$  the number of moles of adsorbate

At standard temperature and pressure conditions (STP conditions) for nitrogen gas having a bulky size equal  $16.26 \text{ \AA}^2$ , the specific surface of a solid (expressed in  $\text{m}^2 / \text{g}$ ) is given by:

$$S_{BET} = 4.35 \times V_m \quad (7)$$

However, as stated in the literature review, Derouane et al.<sup>134</sup> the BET model is not valid for microporous materials, as in the case of zeolites, and to a minimal extent to mesoporous ones. Because the adsorption of nitrogen in microporous zeolite occurs at very low relative pressures, the monolayer capacity deduced from the BET model would actually be in the micropore filling range.<sup>135</sup> Caution is needed in type I and combination between type I and IV or type I and II isotherms since it is complicated to discriminate between monolayer-multilayer adsorption process and micropore filling<sup>136</sup>.

Therefore, the microporous and mesoporous volumes in porous materials in this thesis were determined by t-plot method. This method depends on the thickness of the adsorbed layer (t) as the function of pressure for the same adsorbate and temperature. Generally, t values (in nm) are estimated using the following equations:<sup>137</sup>

$$t = A_1 [1 - \exp(A_2 P/P_0)] + A_3 [1 - \exp(A_4 P/P_0)] \quad (P/P_0 < 0.03)$$

$$t = B_1 (P/P_0)^{B_2} + B_3 (P/P_0)^{B_4} \quad (0.03 \leq P/P_0 < 0.25)$$

$$t = \left[ \frac{C_1}{C_2 - \log(P/P_0)} \right]^{C_3} \quad (0.25 \leq P/P_0 < 0.6) \quad (8)$$

$$t = \left[ \frac{D_1}{D_2 - \log(P/P_0)} \right]^{D_3} \quad (0.6 \leq P/P_0 < 0.9)$$

$$t = E_1(P/P_0)^{E_3} + E_3(P/P_0)^{E_4} \quad (0.9 \leq P/P_0)$$

Where,  $A_1 = 0.1887299$  nm,  $A_2 = -481.3$ ,  $A_3 = 0.182099$  nm,  $A_4 = -23.78$ ,  $B_1 = 0.5675647$  nm,  $B_2 = 0.199735$ ,  $B_3 = 0.4116168$  nm,  $B_4 = 2.00834$ ,  $C_1 = 0.1423566$ ,  $C_2 = 0.1078$ ,  $C_3 = 0.4888$ ,  $D_1 = 0.08309076$ ,  $D_2 = 0.02995$ ,  $D_3 = 0.369$ ,  $E_1 = 1.268066$  nm,  $E_2 = 1.931$ ,  $E_3 = 0.76934$  nm, and  $E_4 = 51.09$ .

The adsorbed volume ( $\text{cm}^3$  STP/g) is then plotted as a function of thickness  $t$  (nm) as shown in Figure 27. The total specific area (mesoporous + external area) is obtained from the calculated slope of the red line. The slope of the purple curve gives the specific surface area of the external surface only. By subtracting the external surface area from the total specific surface area, the mesoporous surface area is obtained. The intercept of the first linear part (the dashed red line) gives the microporous volume, while the intercept of the second linear part obtained after condensation (the dashed purple line) corresponds to the total volume. The mesoporous volume can be estimated from the difference between total and microporous volume.

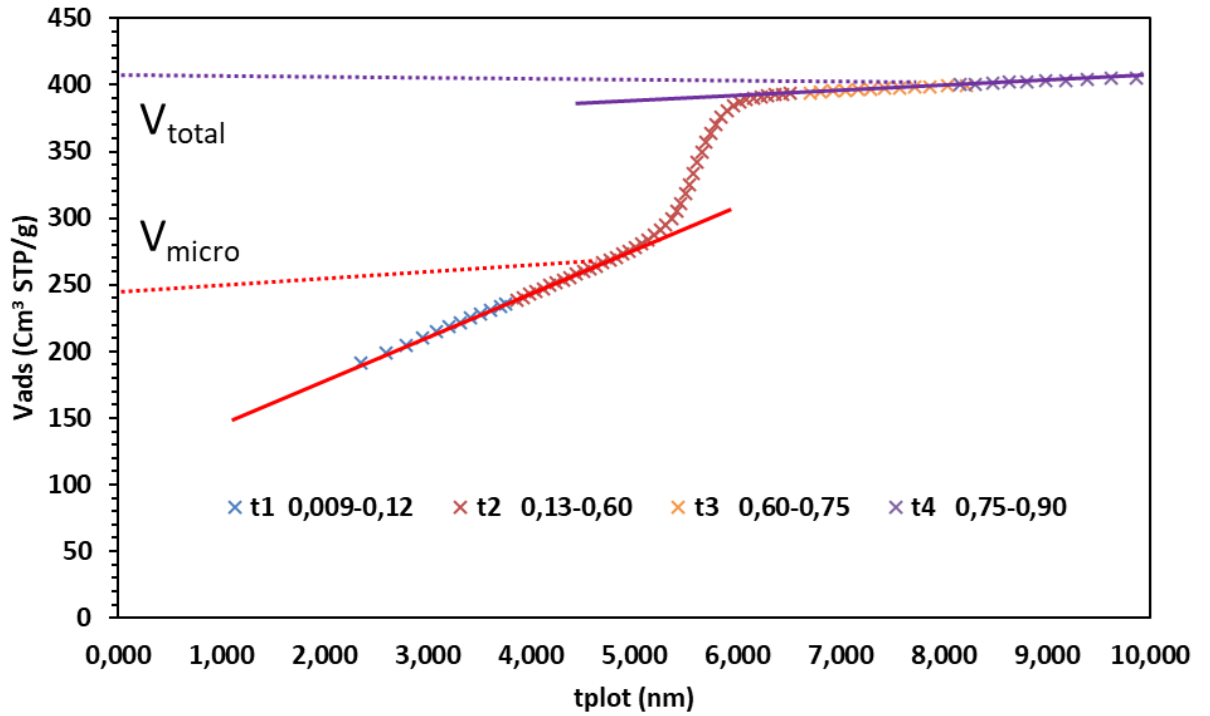


Figure 27 : t-plot for the  $N_2$  sorption isotherm at 77 K for FAU-2 (obtained after modification of commercial FAU by NaOH/Si = 0.095) which contain both micro and mesoporosity.

For faujasite and hierarchical faujasite, it was demonstrated that classical t-plot underestimated micropore volume and overestimated mesopore surface area. Corrections of micropore volume and mesopore surface area were provided by a corrected t-plot method as a function of  $V_{mic}$  and  $V_{total}$  defined by classical t-plot analysis ( $(V_{mic}/V_{tot})_{tpt}$ ) for hierarchical faujasite following the equations:<sup>123,</sup>

137

$$V_{mic}/V_{tot} < 30\% : (S_{mes+ext})_{real} / (S_{mes+ext})_{tpt} = 1 \quad (9)$$

$$30 < (V_{mic}/V_{tot})_{tpt} < 55\% : (S_{mes+ext})_{real} / (S_{mes+ext})_{tpt} = 1.6 - 0.02138(V_{mic}/V_{tot})_{tpt} \quad (10)$$

$$(V_{mic}/V_{tot})_{tpt} > 55\% : (S_{mes+ext})_{real} / (S_{mes+ext})_{tpt} = 0.38 \quad (11)$$

$$(V_{mic}/V_{tot})_{tpt} < 7\% : (V_{mic})_{real} / (V_{mic})_{tpt} = 1 \quad (12)$$

$$7\% > (V_{mic}/V_{tot})_{tpt} < 45\% : (V_{mic})_{real} / (V_{mic})_{tpt} = 0.52947 (V_{mic}/V_{tot})_{tpt}^{0.25334} \quad (13)$$

$$(V_{mic}/V_{tot})_{tpt} > 45\% : (V_{mic})_{real} / (V_{mic})_{tpt} = 1.40 \quad (14)$$

With  $(V_{mic}/V_{tot})_{tpt}$  expressed in %.

Figure 28 shows the example of  $N_2$  adsorption-desorption isotherm for Faujasite sample FAU-0. The obtained isotherm is classified as majority of type I (microporous material) with few mesoporosity.

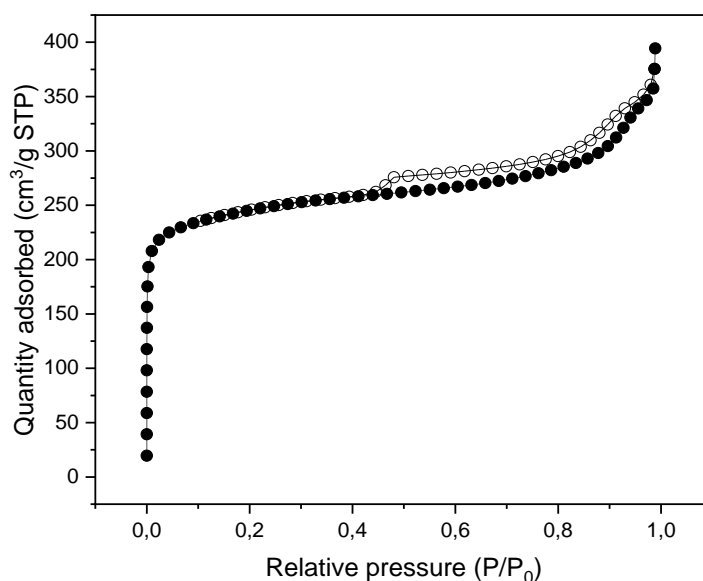


Figure 28 :  $N_2$  adsorption-desorption isotherm of Faujasite sample (FAU-0) degassed at 200 °C overnight. The filled and empty symbols correspond to the adsorption and desorption isotherms, respectively.

### 1.7.7 $^{29}\text{Si}$ solid state NMR

The purpose of using this characterization technique is to determine the local environment (number and type of neighboring atoms) of silicon and indirectly of aluminum.

NMR spectroscopy is suitable for any nucleus that holds a magnetic moment, a nuclear spin. Solid state NMR is a very useful technique for the atom's framework, extra-framework and surface site of solid and of adsorbates and their interaction formed on this solid. Practically, each chemical shift is used to give information about the Si environment that corresponds to a specific number of Al bounded to Si.<sup>138</sup>

In this thesis,  $^{29}\text{Si}$  NMR is performed to ascertain if there is any kind of structural defects. The experiment can be done either by Cross Polarization (CP) or One Pulse (OP). To ensure the high resolution of different sites of  $^{29}\text{Si}$  NMR spectra, CP in the presence of Magic Angle Spinning (MAS) is the best tool, since it decreases the line broadening of the spectra and increases the magnitude of the signal-to-noise ratio. However, One Pulse (OP) experiment is more convenient to obtain the quantitative analysis.

Prior to the experiment, the preparation of the samples was done by filling the NMR rotor with the powder without any treatment. Silicon-29 NMR spectra were obtained at 5 kHz with a Varian

VNMRS 400 spectrometer using a magnetic field strength of 9.4 T. The experiments were performed with One Pulse (OP) sequence, resulting in a quantitative analysis of the spectrum which has done at the p/6 pulse and the 60s recycling delay instead of qualitative analysis.<sup>139</sup> The Si-NMR spectra were modeled using the DMFit program.

<sup>29</sup>Si NMR was used to determine the number of aluminum atoms located in the immediate environment of silicon atoms as well as the possible presence of terminal OH groups. An example of the <sup>29</sup>Si-NMR spectrum is shown in Figure 29. This determination begins with the detection of OH groups using the transfer of polarization of the proton towards silicon. This transfer has the effect of enhancing the silicon NMR signal when an OH group is attached to it. Using this information, it is then possible to assign all bands observed on the <sup>29</sup>Si NMR spectrum. The position of the bands provides information on the number of aluminum atoms linked to silicon via oxygen: the greater the chemical shift (position) close to 0 ppm, the more aluminum there is.

The spectra of FAU-0 shows the standard peaks of FAU-Y at -108 ppm corresponding to Si(4Si, 0Al), abbreviated Q<sup>4</sup> environment, and -102 ppm that related to Si(3Si, 1Al), abbreviated Q<sup>3</sup> environment.

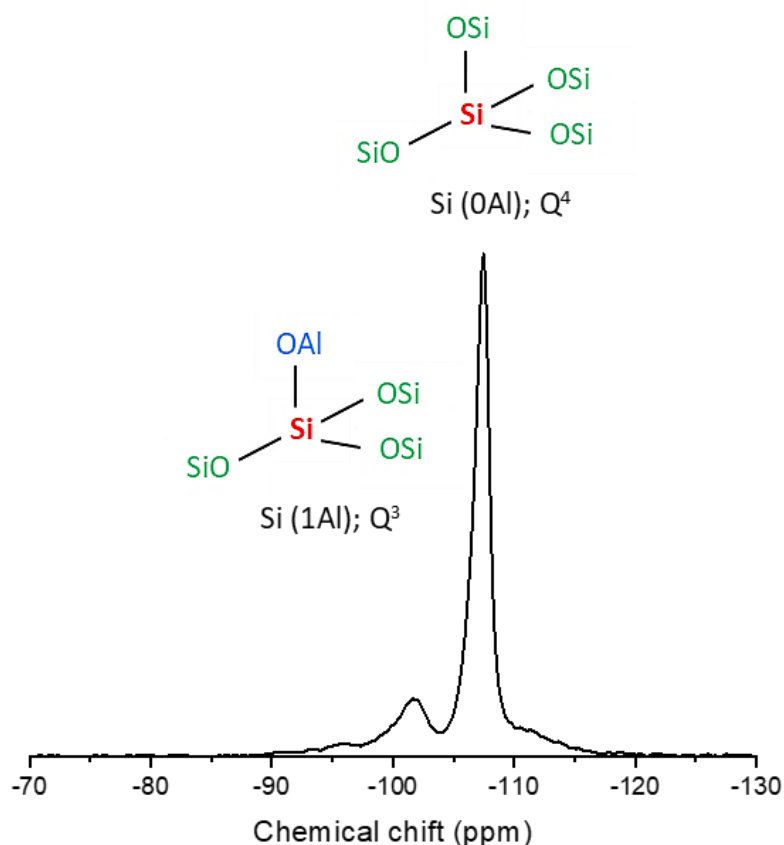


Figure 29 : Example of solid-state  $^{29}\text{Si}$  NMR spectrum of a FAU-0 with their chemical shifts of species Si (nAl)

### 1.7.8 Thermogravimetric analysis (TGA)

Thermogravimetric analysis (TGA) measures the change in mass of a material as a function of temperature and time, in a controlled atmosphere. It might be used to evaluate the volatile content (solvent residue, adsorbed water, etc.), thermal stability or even degradation characteristics. A typical thermogravimetric analyzer consists of a precision balance with a sample cell located inside an oven with a programmable control temperature. The temperature is generally increased at a constant rate to cause a thermal reaction. A variation in the mass of the sample is measured during the temperature ramp (gain in mass by oxidation or loss in mass by evaporation/sublimation, for example). Thermogravimetric analysis was performed on NETZSCH Jupiter STA 449 apparatus. The temperature calibration was carried out using  $\text{Al}_2\text{O}_3$ . Between 10 and 20 mg of samples were heated from 25 to 800°C at 5°C/min under air flow.

### Adsorption isotherms determination

The method most commonly used to study adsorption is based on the depletion of the species to be adsorbed with the particles in the equilibrated state. The thermodynamic representation of the

adsorbed amount of the species versus the concentration at equilibrium is known as adsorption isotherm. In the present work, batch experiments were carried out.

The quantity of adsorbed compounds  $Q_{ads}$  (mmol/g) was calculated using the following equation:

$$Q_{ads} = \frac{V(C_i - C_e)}{m_{solid}} \quad (15)$$

Where  $C_i$  is the initial concentration (mmol/L),  $C_e$  is the equilibrium concentration (mmol/L),  $V$  is the volume of solution (L), and  $m$  is the mass of adsorbent (g).

### 1.8 By UV-Visible spectrometry

To deal with dye molecules, the absorbance spectrum will be measured using UV-Vis spectrometry to quantify the concentration of free molecules in solution and to deduce the amount adsorbed inside the solid.

The following protocol has been applied, and for simplification, the experimental procedure can be seen in Figure 30.

- Contact:

Adsorption tests were carried out using the following procedure. Suspension with 0.1g/l of material was prepared in the appropriate solvent (water, ethanol, methanol, acetonitrile and DMSO). It was added to centrifugation tubes of volume 30 ml and made up of Nalgene™ Oak Ridge High Speed PPCO (Polypropylene copolymer) using different ratios of a concentrated mother solution and solvent with a constant volume of suspension in the tubes. The pH was measured for all suspensions after few minutes of contact and after moderate shaking. The tubes were then stirred on a planetary rotative system at ambient temperature ( $25 \pm 2^\circ\text{C}$ ) for 18 h to ensure adsorption equilibrium and pH was measured again to check the possible pH variation after equilibrium.

- Separation and filtration:

Suspension was then centrifuged at 11000 rpm for 60 minutes. The supernatant was filtered using a syringe filter (polypropylene membrane, 25mm diameter and 0.22 $\mu\text{m}$  porosity).

- Concentration Measurement:

The equilibrium concentration of dyes is measured using a UV-Vis spectrometer. A calibration curve is drawn with 4 or 5 standard solutions prepared from the mother solution. The concentration of the calibration points used in the range of  $2 \cdot 10^{-3}$  to  $50 \cdot 10^{-3}$  mmol/l. This calibration curve is established using the Beer-Lambert law:

$$A = \epsilon lc \quad (16)$$

Where A is the absorbance,  $\epsilon$  is the molar extinction coefficient (depends on the nature of the molecule used), l is the optical path length which is 1 cm in our case, and c is the concentration of the given solution.  $\epsilon$  obtained for different dyes in various solvents are placed in Table 3.

Table 3 :  $\epsilon$  ( $l/\mu\text{M}$ ) obtained for different organic dyes prepared in various solvents.

molar extinction coefficient $\epsilon$ ( $l/\mu\text{M}$ )				
Molecules Solvents	BF	C <sub>1</sub> DiA (sDiA)	C <sub>4</sub> DiA	C <sub>16</sub> DiA
Water	0.085 $\lambda_{\text{max}}$ 538 nm	0.025 $\lambda_{\text{max}}$ 447 nm	-	-
Ethanol	-	0.046 $\lambda_{\text{max}}$ 479 nm	0.049 $\lambda_{\text{max}}$ 494 nm	0.055 $\lambda_{\text{max}}$ 495 nm
DMSO	-	0.038 $\lambda_{\text{max}}$ 470 nm	-	-
Acetonitrile	-	0.043 $\lambda_{\text{max}}$ 470 nm	-	--
Methanol	-	0.047 $\lambda_{\text{max}}$ 474 nm	-	-



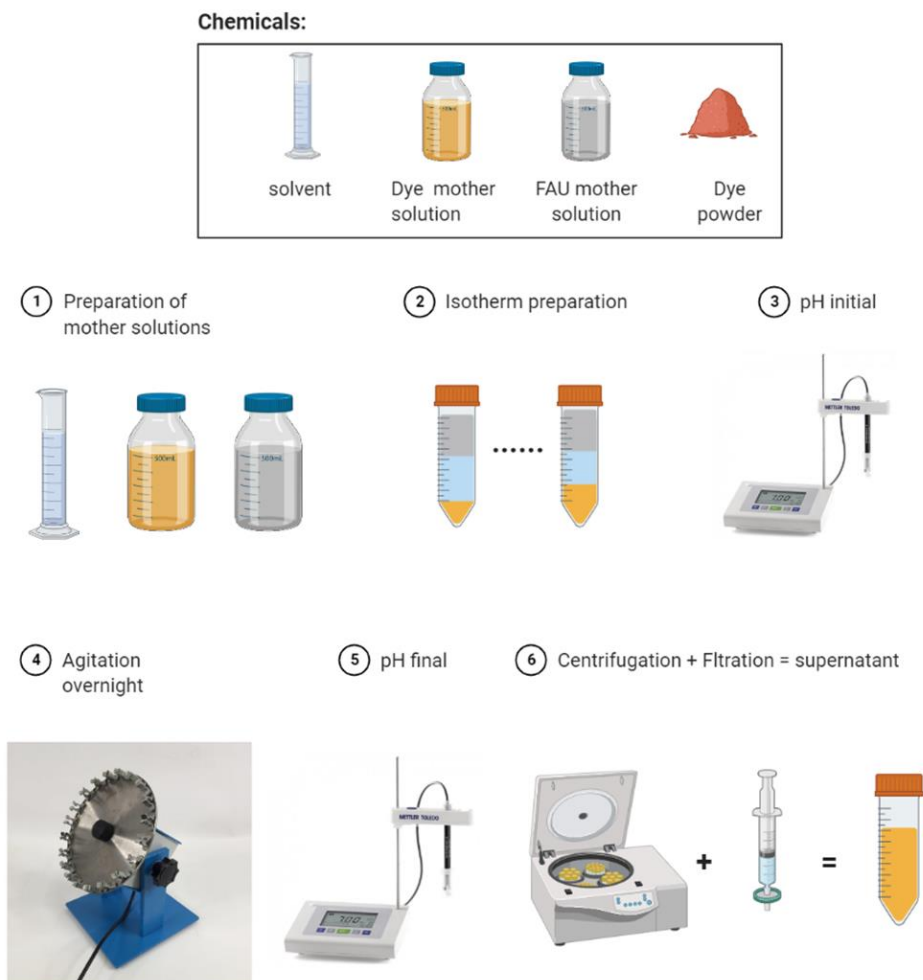


Figure 30 : Experimental procedure of adsorption isotherm

### 1.9 By SHS

Second-harmonic scattering (SHS) was also used to evaluate the adsorption capacity of different dyes onto FAU. This was done by measuring the equilibrium concentration of the supernatant obtained after filtration where it was determined from the SHS intensity obtained for each sample at 400 nm. In addition, the SHS measurement for the dye suspension in the presence of FAU was performed to determine the organization and orientation of molecules at the solid/liquid interface.

## Titration calorimetry measurements

### 1.10 Generalities

Isothermal Titration Calorimetry (ITC) is a technique that allows probing the interactions between two species by measuring the heat released or absorbed during their mixing in solution. It allows bringing new light on the nature of the interactions and complexation processes on a wide variety of systems (polyelectrolyte-polyelectrolyte, adsorbate-adsorbent, target-active principle...). ITC is the only experimental technique that allows to obtain all the thermodynamic parameters characterizing an interaction in a single experiment. In the case of homogeneous systems in purely liquid systems, it is possible to determine the interaction constant ( $K$ ), the stoichiometry ( $n$ ) and the enthalpy ( $\Delta H$ ) associated with the interaction. From  $K$  and  $\Delta H$  it is then possible to calculate the variation of Gibbs free energy ( $\Delta G$ ) and the entropy ( $\Delta S$ ) contribution. In the particular case of the solid/liquid interface, the obtained information is slightly different.

### 1.11 Theory

ITC is a powerful characterization method capable of measure with precision the heat released or absorbed by the interaction between two species. In a first step, a simple reading of this heat allows to estimate the intensity of the interaction. In a second step, the processing of the signal with the help of an adapted model allows to obtain more information about the interaction, in particular the enthalpy of adsorption.

Isothermal titration calorimetry allows the measurement of weak interactions, but in general non-specific, in particular when it concerns complexes between small molecules. Indeed, the charged species associating in electrostatic interaction, the heat involved in this process is more intense than that involved in weak interactions such as the hydrogen interaction. This is for adsorption at the solid/liquid interface. The global enthalpy that is measured using ITC is the sum of various phenomena occurring in our sorption system. The first phenomenon is the adsorption of dye molecules on an active site associated with a loss of water molecules around it and the latter contributes to the enthalpy of dehydration of the dye molecule. Protons (or other counterion) desorbing from the active sites corresponds to the enthalpy of desorption where this proton (or other counterion) undergoes a change in its surrounding water molecules when it goes from the bulk of the material and becomes free in the medium producing an enthalpy of hydration (Figure 31).



Figure 31 : Major phenomena of the global enthalpy due to adsorption, desorption and displacement (hydration – dehydration).

The notable advantage of this method is that it is extremely sensitive and thus able to detect heat variations of the order of a hundredth of a kJ/mol. Among the set of constants derived from the interpretation of the data, it is also possible to deduce much more information than with traditional techniques, in particular, the mode of interaction according to which the two chemical species present themselves to each other. The few technical difficulties come from the fact that this technique suffers from the drawbacks of its advantages. Indeed, the high sensitivity of this equipment implies that the measurement can be disturbed in the case of significant difference in external temperature, or in case of the presence of impurity or a residual air bubble, or in case of electrical instability. As for the advantages of ITC over other techniques, it is important to mention that it is a method that makes it possible to measure directly the interaction in bulk. There is no limitation related to the molecular weight of the chemical species present. Finally, this technique is "non-destructive" and therefore allows the system to be recovered after the experiment, in order to pursue further studies on the same sample.

### 1.12 Instrument

In order to measure the thermodynamic properties of an interaction between two species by measuring the heat involved in the interaction, the chosen technique is ITC for Isothermal Titration Calorimetry.

ITC device is composed of two identical cells placed in a closed adiabatic system which is maintained at a constant temperature (generally 25 ° C) for the time of the titration. It is made from a material having sufficient thermal conductivity effective for detecting low amplitude heat. The first cell filled with water, is maintained at the ambient temperature and corresponds to the reference cell. The second cell constitutes the measurement cell; it generally contains adsorbent solid suspended in water in our case. In an ITC experiment, the substrate (zeolite) in suspension is introduced into the measuring

cell, while a dye solution is placed in a syringe. The substrate suspension is titrated, by successive injections of dyes. Each addition corresponds to a characteristic heat release or absorption of the interaction between the titrant and the titrate. Depending on the endothermic or exothermic nature of the reaction, the control system decreases or increases the power of heating by applying an electrical signal, to maintain the temperature difference between the measuring cell and the reference cell. This heating power presents as a function of time a series of peaks corresponding to each of the injections, the areas of which are equal to the amount of heat released or absorbed, called the thermogram. A representative scheme is shown in the figure below.

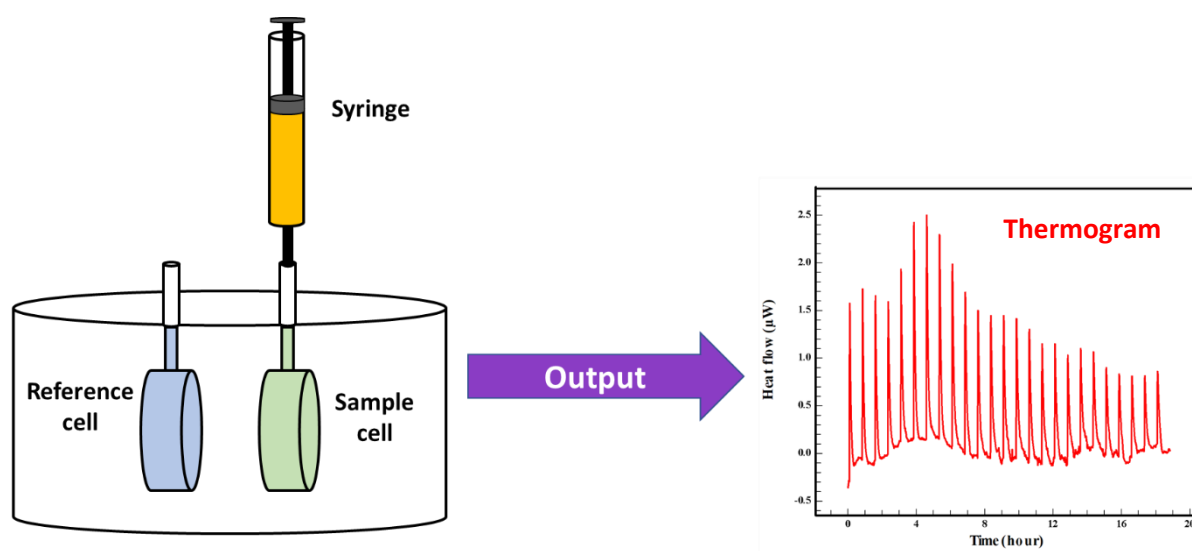


Figure 32 : Schematic representation of the ITC experiment together with the experimental thermogram obtained for sDiA adsorption onto commercial FAU.

### 1.13 Protocol

In this study, a TAM III thermostat equipped with differential nanocalorimeter operating in a heat flow mode was used to measure the enthalpy of displacement accompanying adsorption of different molecules such as ( $C_1DiA$ ) and (BF) onto commercial Faujasite (FAU-0), modified zeolites (FAU-1,2 and 3), commercial CBV-400 and CBV-780 from aqueous solutions at 298 K. 10 mg of the zeolite powder prepared in suspension with 8ml of ultrapure water were sonicated for 10 min. The 1 mL measuring ampoule containing about 0.8 mL from this suspension was placed in the nanocalorimeter. The homogeneity of the solid suspension was maintained by means of an agitation system equipped with a Gold paddle stirrer. The whole system including a reference ampoule filled with the same amount of ultrapure water was equilibrated for 2 hours. Pulse injections of an appropriate stock solution were performed making use of a computer controlled microsyringe injection device. The concentration of  $C_1DiA$  and BF stock solution was 2mM. This has been optimized, together with the amount of solids, to have: enough signal, enough adsorption, not too high dilution,

and to cover the overall range of surface coverage. The operational parameters were kept the same for all calorimetry experiments, namely: 25 injections of 10  $\mu\text{L}$  during 10 s, a stirring speed of 90 rpm and time of equilibration between two successive injections equal to 45 min. The experimental enthalpy changes were subsequently corrected for dilution effects (see below). The dilution experiments were carried out under the same experimental 25 conditions but without the zeolite powder in the measuring ampoule.

### 1.14 Data treatment

The integration of thermal peaks appearing in the thermogram (Figure 32) leads to the determination of the total enthalpy changes during successive injections,  $\Delta_{inj}H_i$  ( $i$  is the number of successive injections), which is related to the mass of solids in the measuring ampoule and can be expressed in  $\text{J}\cdot\text{g}^{-1}$ . The resulting enthalpy values were summarized to acquire the cumulative enthalpy of displacement,  $\Delta_{dpl}H_{cum}$ , per unit mass of the sample.

ITC is used to determine the enthalpy of adsorption of the dye onto faujasite. The integration of peaks appearing in this thermogram leads to the determination of the total enthalpy changes during successive injections,  $\Delta_{inj}H_i$ . The calculation of the enthalpy is shown below.

$$\frac{\Delta_{inj}H_i}{n_2^{inj}} = \Phi_H(m_2^i) + (i - 1) \cdot n_2^{inj} \cdot \frac{[\Phi_H(m_2^i) - \Phi_H(m_2^{i-1})]}{n_2^{inj}} - \Phi_H(m_2^0) \quad (17)$$

Where  $i$  is the number of successive injections,  $n_2^{inj}$  is the number of moles of the solute injected to the ampoule during each injection,  $\Phi_H(m_2)$  represents the apparent molal enthalpy of the solute corresponding to a given molality.

And  $n_2^{inj}$  depends on  $d_{pump}$ ,  $t_{inj}$ ,  $m_2^0$  according to the following equation:

$$n_2^{inj} = \frac{m_2^0 \cdot d_{pump} \cdot t_{inj}}{m_2^0 \cdot M_{solute} + 10^3} \quad (18)$$

The flow rate  $d_{pump}$  of the pump and the time  $t_{inj}$  of injection are kept constant during the experiment.

The equilibrium molality of the solution  $m_2^i$  in the cell after this injection is calculated using the following equation.

$$m_2^i = \frac{10^3 \cdot i \cdot n_2^{inj}}{M_1^0 + \frac{10^3 \cdot i \cdot n_2^{inj}}{m_2^0}} \quad (19)$$

The total change in enthalpy during the  $i^{\text{th}}$  injection in the adsorption experiment can be expressed as follows:

$$\begin{aligned} \Delta_{inj} H_i = m_s \cdot S \cdot [H_{SL}^S(m_2^i) - H_{SL}^S(m_2^{i-1})] - n_{2,i}^S \cdot \Phi_H(m_2^i) + n_{2,i-1}^S \cdot \Phi_H(m_2^{i-1}) \\ + n_2^{inj} \left\{ \Phi_H(m_2^i) + (i-1) \cdot n_2^{inj} \cdot \frac{[\Phi_H(m_2^i) - \Phi_H(m_2^{i-1})]}{n_2^{inj}} - \Phi_H(m_2^0) \right\} \end{aligned} \quad (20)$$

where  $S$  is the specific surface area of the adsorbent;  $H_{SL}^S(m_2)$  is the interfacial enthalpy for a Solid-Liquid interface in equilibrium with a bulk solution of molality  $m_2$ .

The thermal effects of successive injections can be also summarized to obtain the molar cumulative enthalpy of dilution  $\Delta_{dil} h_{cum}$  after  $k$  injections.

$$\Delta_{dil} h_{cum} = \sum_{i=1}^k \frac{\Delta_{inj} H_i}{n_2^{inj}} = k \cdot [\Phi_H(m_2^k) - \Phi_H(m_2^0)] \quad (21)$$

With  $m_2 = m_2^k$

## Second Harmonic Scattering measurement

In this part of the thesis, we will present a short description of Nonlinear optics (NLO) phenomena. Next, we will describe in more detail the second order NLO properties, which are at the origin of the Second Harmonic Generation. Finally, we will focus in particular on SHS at the microscopic level, which will allow us to better meet the challenges of specific studies on nanoparticles.

### 1.15 Introduction to non-linear optics

#### 1.15.1 Basic introduction

Nonlinear optical phenomena are due to light-matter interactions when the incident electromagnetic field is intense. A material subjected to a light wave represents a set of charges which oscillate under the effect of an incident field. This field will cause the appearance of electrical dipoles, thus creating a macroscopic polarization in the material  $\vec{P}$ . Each of these vibrating dipoles in turn emits radiation. On a macroscopic scale, the sum of these radiations is at the origin of a new electromagnetic wave which is added to the incident wave.

When the polarization generated is not proportional to the incident electric field  $\vec{E}$ , we are then in the field of nonlinear optics. Thus, nonlinear optics groups together all of the optical phenomena which have a nonlinear response with respect to the incident electric field  $\vec{E}$ . In other words, linear optics corresponds to optical phenomena having a polarization proportional to the incident electric field, in this case, the polarization is written as:

$$\vec{P}(\text{linear}) = \epsilon_0 \chi \vec{E} \quad (22)$$

With  $\chi$  the electrical susceptibility of the material and  $\epsilon_0$  the dielectric permittivity of the vacuum.

In nonlinear optical phenomena, the macroscopic polarization includes nonlinear components which are added to the initial component. The polarization is therefore written:

$$\vec{P} = \vec{P}(\text{linear}) + \vec{P}(\text{non linear}) = \epsilon_0 [\chi(1)\vec{E} + \chi(2)\vec{E} \cdot \vec{E} + \chi(3)\vec{E} \cdot \vec{E} \cdot \vec{E} + \dots] \quad (23)$$

With  $\epsilon_0$  the dielectric permittivity of the vacuum,  $\chi(1)$  the susceptibility tensor of order 1 with 3 components and  $\chi(2)$  the susceptibility tensor of order 2 with 9 components. The quadratic susceptibility tensor has more components than the linear susceptibility tensor and therefore the latter is richer in information.

### 1.15.2 Molecular view

The equations shown above describe information relating to macroscopic quantities such as the susceptibility tensor.<sup>140</sup> To access microscopic information, it is necessary to switch from macroscopic quantities to microscopic quantities. Considering a molecular system such as molecular dyes, the SHG signal emitted by the latter comes from the anharmonic oscillations of the electrons which are excited by an intense electric field. From a molecular point of view, we are interested in the dipole moment  $\mu$  which is written:

$$\mu = \mu_0 + \alpha E + \beta EE + \dots \quad (24)$$

With  $\vec{\mu}_0$  the static dipole of the molecule,  $\alpha$  is the polarizability of the molecule, and  $\beta$  is the hyperpolarizability of the molecule. The hyperpolarizability depends on the frequency of the applied field and the shape of the electronic cloud of the molecule. Here we will focus more specifically on  $\beta$ . It is a rank three tensor that characterizes the first nonlinear response of the molecule.<sup>141, 142</sup> The polarization measurements make it possible, thanks to mathematical calculations, to determine the

elements of the hyperpolarizability tensor  $\beta$  and thus to deduce the organization and the molecular interactions.

The DiA molecule and other chromophore molecules have both amphiphilic and "push-pull" acceptor-donor properties that permit them to be good probe molecules for SHS. These dyes are chosen in particular since they have a high hyperpolarizability value which characterizes their SHS efficiency.

### 1.16 Second Harmonic Generation (SHG)

In a particular phenomenon, Second Harmonic Generation (SHG) is a nonlinear optical process in which two incident photons at the fundamental frequency  $\omega$  are converted into a single photon at the harmonic frequency  $2\omega$ . A representative schema is shown in Figure 33. Indeed, in a material the centroid of positive and negative charges coincides at rest. However, this is no longer the case when an electromagnetic wave propagates in the material. This is what causes an electrical dipole to appear within the material. The resulting polarization will therefore have harmonic frequencies which will be superimposed on the fundamental frequency. Thus, in the second harmonic generation, we are interested in the response of the material comprising the double frequency, we then speak of non-linear optics of order one. As stated above, the properties of symmetry of the tensor  $\chi(2)$  are related to the properties of symmetry of the material. In fact, these polarizability tensors are constant for the same transformations which leave the material medium studied constant. Let us consider a centrosymmetric medium, which therefore has a center of symmetry. SHG is prohibited in any medium having a center of inversion in the context of the electric dipole approximation.

Indeed, the rule of centrosymmetry applies to the point source itself because it cannot act as a non-linear dipole if it is centrosymmetric. This is how this rule has been widely used to characterize the interfaces between two centrosymmetric material media such as air/liquid, liquid/liquid or solid/liquid interfaces. All this is possible at the interface of two media because the symmetry is broken, thus allowing the generation of second harmonics in the interfacial region. In other words, the second harmonic generation is used as a probe for the study of surfaces and interfaces.

The second harmonic generation (SHG) is a coherent second order optical process essentially related to the symmetry of the molecules thus it is highly sensitive to surface/interface. Coherency comes from the organized molecules at the interface thus it gives information about the supramolecular structure. However, incoherency comes from the randomly orientated molecule so it provides information about the molecules alone. Although, it can be used to probe the interface (solid/liquid and liquid/liquid) and even to probe molecules inside the colloid itself.<sup>109</sup>



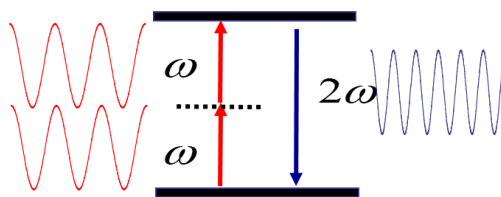


Figure 33 : Representative scheme of SHG where two photons at the fundamental frequency produce one photon at doubled frequency.

## 1.17 Hyper-Rayleigh Scattering (HRS)

### 1.17.1 HRS Principle

In HRS measurement, a molecular solution is excited by an intense laser beam of frequency  $\omega$ . Each molecule is thus subjected to this excitation and then scatters a second harmonic signal. The HRS signal is the **incoherent** sum of all these SH signals.

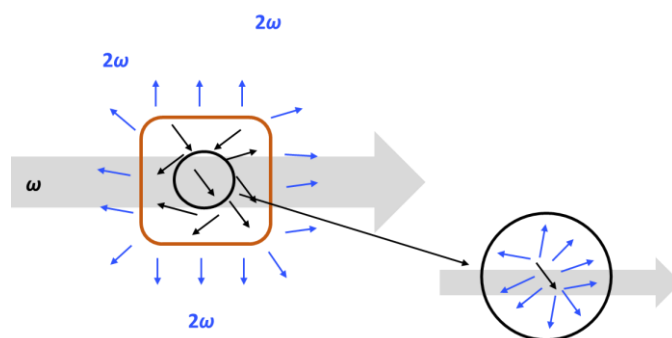


Figure 34 : Principle of Hyper Rayleigh Scattering (HRS)

This HRS signal is characterized by different parameters related to the sample but also to the experimental system. As for the SHG, the HRS signal varies quadratically with the incident intensity  $I_\omega$ . Moreover, since it is an overall measurement, the optical response depends on the concentration  $N$  of the solution and varies linearly with it since it is the sum of **incoherently scattered signals**. Furthermore, the SH scattering of the molecules is directly related to their average hyperpolarizability  $\langle\beta\rangle$ , corrected by the local field factors  $F_i$ . Finally, we must also consider an experimental factor  $G$ .

In the case where different species  $i$  are present, the HRS signal intensity is defined by Revillod<sup>143</sup>

$$I_{2\omega} = G(N_i F_i \langle\beta_i^2\rangle) I_\omega^2 \quad (25)$$

If the sample corresponds to a molecular solution consisting of a solvent and a single species of molecule, we have then:

$$I_{2\omega} = G(N_s F_s \langle\beta_s^2\rangle + N_m F_m \langle\beta_m^2\rangle) I_\omega^2 \quad (26)$$

where the indices  $s$  and  $m$  correspond respectively to the solvent and the molecules in solution.

The following paragraph details the study of the nonlinear optical response which is carried out by measurements of second harmonic scattering (SHS).

## 1.18 Second Harmonic Scattering (SHS)

### 1.18.1 SHS Principle

The conventional non-linear optical methods in transmission or reflection geometry have the drawback of being difficult to apply to the study of interfaces in situ due to the environmental cloud of the medium which contains particles, droplets or seeds. This is also the case for the sum frequency generation (SFG), and the second harmonic generation SHG. Second harmonic scattering SHS has the possibility of countering these limits and thus probing the nonlinear optical and interfacial properties of particles, droplets or grains in liquids.<sup>107</sup>

This is why the second harmonic scattering SHS is used as a probe for the study of surfaces and interfaces in the bulky medium. Indeed, this signal comes from structures composed of molecules comprising a break in symmetry such as interfaces, aggregates, and colloids. This non-linear analysis method provides important information on the organization of molecules but also on the different interactions involved.

### 1.18.2 Properties probed

The second harmonic scattering has the advantage of being very useful for working in situ in a colloidal liquid solution. The intensity measured after excitation of the system can be described as the sum of two contributions. The first one, called incoherent contribution, corresponds to the response of free molecules in a liquid. In this case, the molecules are not correlated to each other. The second, the coherent contribution, translates the response of a supramolecular structure composed of correlated molecules.

### 1.18.3 Coherence between molecules

In connection with the work reported in this manuscript, it is necessary to distinguish two aspects of the SHG process: the coherent process and the incoherent process. This distinction allows indeed to develop two different approaches of the light-matter interaction and consequently to be interested in very different physical effects. During the coherent SHG process, for which we will use second harmonic scattering SHS, there is a well-defined phase relation between the harmonic waves emitted by the different nonlinear point sources constituting the nonlinear medium. These sources, in

a rather formal way, can be associated with the molecules. Thus, if the conditions are fulfilled, then there is at least one direction of propagation in which the waves interfere constructively and lead to a resultant wave with high intensity. In this case, the conversion process is coherent. In the second case, the conversion process is incoherent. In the coherent case, due to the superposition of the amplitudes, the resulting intensity varies in a quadratic way according to the number of point sources present in the excitation volume.

#### 1.18.4 Experimental setup of SHS

The experimental setup used for probing the 'molecular organization at the solid/liquid interface is based on the second harmonic scattering (SHS). The measurements are carried out using a Femtosecond Ti-Sapphire laser which provides pulses with a duration of 100 fs at a repetition frequency of 80 MHz. The fundamental beam is tuned to a fixed wavelength varying from 790 to 810 nm and average power of 800 mW. The beam passes through a high pass filter before being focused by a microscopic objective (Ealing x10, numerical aperture 0.25) on the sample at 2mm near the exit window. The second harmonic light is then separated from the fundamental beam by a low pass filter and is then captured at 90 ° by a 10 cm focal length lens. Finally, the second harmonic light is detected by a water-cooled CCD camera, the latter is placed after a spectrometer. The fundamental beam is linearly polarized and the input polarization angle denoted  $\gamma$  is selected using a rotating half-wave plate. The role of the analyzer placed in front of the spectrometer is to separate the vertical and horizontal SH intensities noted on the diagram  $V_{out}$  and  $H_{out}$ . A schematic representation of the measurement is presented in Figure 35. An input polarization is chosen and the second harmonic signal is analyzed at 90 ° C according to two polarizations, one vertical and the other horizontal. Each of these polarizations provides information on the interactions and molecular organizations of the sample.

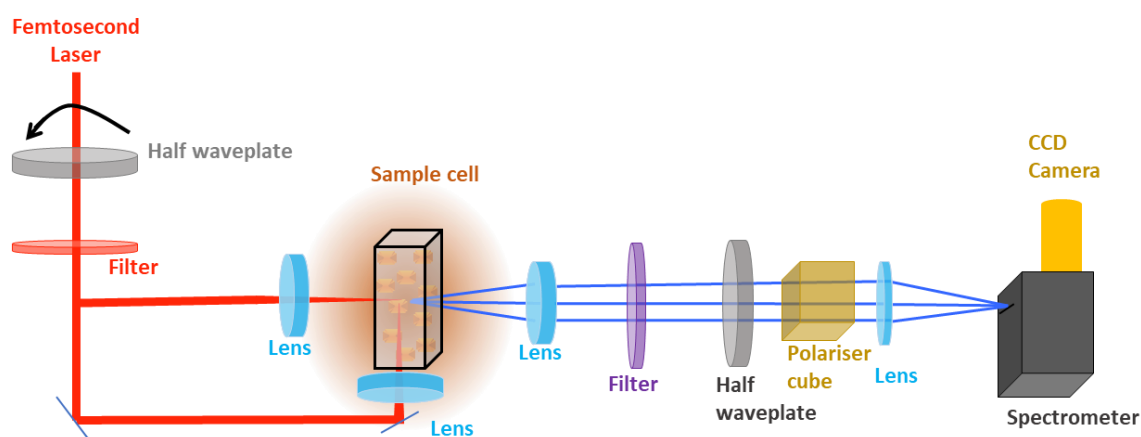


Figure 35 : Principle of SHS experimental set-up

Once the measurements have been performed, here the case of ( $C_1DiA$ ), the results are obtained in the following form (see Figure 36), with the vertical polarization (polarV) in blue and the horizontal polarization (polarH) in pink. The x-axis reveals the polarization angles (in  $^\circ$ ) and the y-axis shows the intensity of the detected second harmonic signal. From these signals, when the intensity of polarization is high, the interaction is hence strong or there is aggregation present in the suspension. In addition, if there is a modification in the shape of polarization plots (polarH and/or polarV), it could be ascribed to an organization of molecules at solid/liquid interface takes place. A more detailed explanation will be exposed in the following chapters.

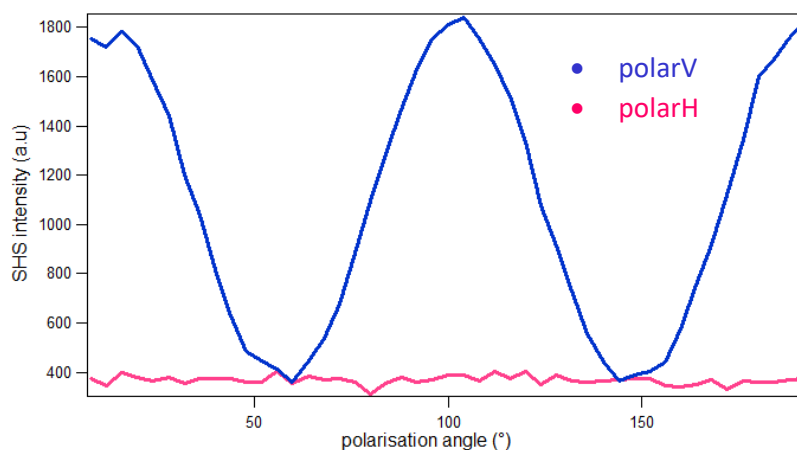


Figure 36 : Polarization-resolved SHS signal diagram sDiA alone in water medium

### Second Harmonic Scattering (SHS) data treatment

Furthermore, to have more quantitative information on SHS results, data treatment has been performed using different mathematical equations.  $C_1DiA$  onto FAU isotherm has been measured as explained previously. Suspension, supernatant, solvent, zeolite alone and dye alone contribution have

been measured by the SHS technique. The intensity of suspension comes from the contribution of the intensity of supernatant, solvent and zeolite respectively as shown in the following equation.

$$I_{suspension}^{2\omega}(\gamma) = I_{HRS,dye}^{2\omega}(\gamma) + I_{HRS,solvent}^{2\omega}(\gamma) + I_{SHS,dye+zeolite}^{2\omega}(\gamma) \quad (27)$$

With  $I_{HRS,dye}^{2\omega}$  is the Hyper Rayleigh Scattering (HRS) contribution of the dye.  $I_{HRS,solvent}^{2\omega}$  is the HRS contribution of the solvent, and  $I_{SHS,dye+materials}^{2\omega}$  is the Second Harmonic light contribution of the dye adsorbed onto and into the zeolitic material. Here, in this case, the contribution of zeolite is negligible since its intensity is equal to the intensity of water. In another word, zeolite alone has no response on SHS.

The SHS intensity of the supernatant comes from the contribution of the solvent and the free molecules present in the supernatant. The intensity can be written as:

$$I_{supernatant}^{2\omega}(\gamma) = I_{HRS,dye}^{2\omega}(\gamma) + I_{HRS,solvent}^{2\omega}(\gamma) \quad (28)$$

Therefore, the SHS intensity is due to the response of the dyes in interaction with the material. Thus, the SHS intensity can be simplified as follows:

$$I_{SHS}^{2\omega}(\gamma) = I_{suspension}^{2\omega}(\gamma) - I_{supernatant}^{2\omega}(\gamma) \quad (29)$$

The SHS results are treated according to equation (29). For some results, caution must be taken, where the re-absorption effect of  $2\omega$  photon by the solution must be considered.<sup>120</sup> Hence the intensity of suspension and the supernatant are represented as corrected intensities. The equations become as follows:

$$I_{suspension\_corrected}^{2\omega}(\gamma) = I_{suspension}^{2\omega}(\gamma) \times 10^{(Abs_{2\omega} * l/L)} \quad (30)$$

$$I_{supernatant\_corrected}^{2\omega}(\gamma) = I_{supernatant}^{2\omega}(\gamma) \times 10^{(Abs_{2\omega} * l/L)} \quad (31)$$

Altogether form the final equation that can be written as:

$$I_{SHS}^{2\omega}(\gamma) = I_{suspension\_corrected}^{2\omega}(\gamma) - I_{supernatant\_corrected}^{2\omega}(\gamma) \quad (32)$$

Where  $Abs_{2\omega}$  is the Absorbance of the suspension and supernatant at 400 nm measured by UV-vis apparatus with  $L=1\text{cm}$  is the length cell and  $l=1\text{ mm}$  is the optical path length of the second harmonic photons.

In order to have information about the organization of molecules at the solid/liquid interface, and to indicate the presence of correlation between molecule, these data are analyzed according to the following expression<sup>122, 144</sup>:

$$I_{SHS}(\gamma) = i_0 + i_2 \cos(2\gamma) + i_4 \cos(4\gamma) \quad (33)$$

where  $i_0$ ,  $i_2$  and  $i_4$  are the amplitudes of the constant, the harmonic  $2\gamma$  and the harmonic  $4\gamma$  terms respectively. In Eq. (33), the parameters  $i_0$  and  $i_2$  are related to the local microscopic structure, i.e. the first hyperpolarizability of the dye and  $i_4$  to the long-range correlations. To quantify the term of correlation, the normalized parameter  $I_4$  is introduced in eq.(34). In the case of uncorrelated species, SHS is a purely incoherent phenomenon, with no correlation between molecules and  $I_4 = 0$ <sup>122</sup>. On the contrary, when molecular orientations are correlated, the scattered photons have a well-defined phase relationship and  $i_4$  differs from 0.

$$I_4 = \frac{i_4}{i_0} \quad (34)$$

And the normalized parameter  $I_2$  is written as:

$$I_2 = \frac{i_2}{i_0} \quad (35)$$

## Conclusions

In this chapter, we present the molecules, the materials and the methods carried out to characterize the material and also the approaches used to study the adsorption phenomena at the solid/liquid interface. Zeolite Y of type faujasite has been chosen as a starting material due to their properties, then porosity of FAU has been modified to investigate their effects on the adsorption behavior.

Modification of FAU by postsynthesis was done using desilication treatment in the presence of a structuring agent (CTAB). It is an efficient way to produce hierarchical FAU by postsynthesis design since it enhances the diffusion by building mesopores homogenous in nature and size and change the elemental composition, while preserving the intrinsic properties of pristine FAU.

The characterization techniques involved in this thesis were also described. A review of the theoretical background of each technique and its operating principle was also done. The purpose of all these techniques is to analyze the structure, texture, morphology, composition, chemical environment, surface chemistry and reactivity of the material used in this thesis. This was to

understand more the properties of the material and the capability to correlate with their behavior in the adsorption performance.

This chapter also described the protocol of adsorption, stability of the suspension and the measurement of the global enthalpy by ITC as a macroscopical approach. In addition to that, the isotherm was studied at a local scale using SHS measurements where in addition to calculate the adsorption capacity from it, it allows to identify the organization and/or orientation of molecules at solid/liquid interface and also evidencing the correlation between the adsorbed molecules themselves. Finally, the combination of the two techniques will allow us to have a complete image of the phenomena of confinement of organic molecules in zeolites at different scales (macroscopic and local scale).

## References

1. Galarneau, A.; Mehlhorn, D.; Guenneau, F.; Coasne, B.; Villemot, F.; Minoux, D.; Aquino, C.; Dath, J.-P., Specific Surface Area Determination for Microporous/Mesoporous Materials: The Case of Mesoporous FAU-Y Zeolites. *Langmuir* **2018**, *34* (47), 14134-14142.
2. Zhou, W.; Apkarian, R. P.; Wang, Z. L.; Joy, D., Fundamentals of Scanning Electron Microscopy.
3. Hendricks, D. W., *Water treatment unit processes: physical and chemical*. CRC press: 2018.
4. Tengku Mohd, T. A.; Jaafar, M. Z.; Ali Rasol, A. A.; Hamid, M. F., Measurement of Streaming Potential in Downhole Application: An Insight for Enhanced Oil Recovery Monitoring. *MATEC Web Conf.* **2017**, *87*.
5. Mahira, S.; Rayapolu, R. G.; Khan, W., Chapter 4 - Nanoscale characterization of nanocarriers. In *Smart Nanocontainers*, Nguyen-Tri, P.; Do, T.-O.; Nguyen, T. A., Eds. Elsevier: 2020; pp 49-65.
6. Mehlhorn, D.; Rodriguez, J.; Cacciaguerra, T.; Andrei, R.-D.; Cammarano, C.; Guenneau, F.; Gedeon, A.; Coasne, B.; Thommes, M.; Minoux, D.; Aquino, C.; Dath, J.-P.; Fajula, F.; Galarneau, A., Revelation on the Complex Nature of Mesoporous Hierarchical FAU-Y Zeolites. *Langmuir* **2018**, *34* (38), 11414-11423.
7. Barber, D. J., J. P. Eberhart Structural and Chemical Analysis of Materials—X-ray, electron and neutron diffraction—X-ray, electron and ion spectroscopy—Electron microscopy. (Translated by J. P. Eberhart), Chichester and New York (J. Wiley and Sons), 1991, xxx + 545 pp. Price £95.00. *Mineralogical Magazine* **1992**, *56* (382), 135-135.
8. Sing, K. S. W., Reporting physisorption data for gas/solid systems with special reference to the determination of surface area and porosity (Recommendations 1984). *Pure and Applied Chemistry* **1985**, *57* (4), 603-619.
9. Cychosz, K. A.; Thommes, M., Progress in the Physisorption Characterization of Nanoporous Gas Storage Materials. *Engineering* **2018**, *4* (4), 559-566.
10. Alshameri, A.; Xinghu, W.; Dawood, A. S.; Xin, C.; Yan, C.; Assabri, A. M., Characterization of Yemeni Natural Zeolite (Al-Ahyuq Area) and its Environment Applications: A Review. *J. Ecol. Eng.* **2019**, *20* (4), 157-166.
11. Maurin, G., 6 - Modelling of Physisorption in Porous Solids. In *Adsorption by Powders and Porous Solids (Second Edition)*, Rouquerol, F.; Rouquerol, J.; Sing, K. S. W.; Llewellyn, P.; Maurin, G., Eds. Academic Press: Oxford, 2014; pp 191-235.
12. Derouane, E. G., On the physical state of molecules in microporous solids. *Microporous and Mesoporous Materials* **2007**, *104* (1), 46-51.
13. Rouquerol, J.; Llewellyn, P.; Rouquerol, F., Is the bet equation applicable to microporous adsorbents. *Studies in Surface Science and Catalysis* **2007**, *160*, 49-56.
14. Thommes, M.; Kaneko, K.; Neimark, A. V.; Olivier, J. P.; Rodriguez-Reinoso, F.; Rouquerol, J.; Sing, K. S. W., Physisorption of gases, with special reference to the evaluation of surface area and pore size distribution (IUPAC Technical Report). *Pure and Applied Chemistry* **2015**, *87* (9-10), 1051-1069.
15. Galarneau, A.; Villemot, F.; Rodriguez, J.; Fajula, F.; Coasne, B., Validity of the t-plot Method to Assess Microporosity in Hierarchical Micro/Mesoporous Materials. *Langmuir* **2014**, *30* (44), 13266-13274.
16. Thomas, J. M.; Thomas, W. J., *Principles and practice of heterogeneous catalysis*. John Wiley & Sons: 2014.
17. Tekely, P., Exploiting  $1\text{H} \rightarrow 29\text{Si}$  Cross-Polarization Features for Structural Characterization of Inorganic Materials. In *Modern Magnetic Resonance*, Webb, G. A., Ed. Springer Netherlands: Dordrecht, 2006; pp 197-203.
18. Shen, Y. R., *The principles of nonlinear optics*. 1984.
19. Maurice, A. Second harmonic scattering in liquids media : comparison between volume and surface. Université de Lyon, 2016.
20. Hsieh, C.-L. Imaging with Second-Harmonic Generation Nanoparticles. California Institute of Technology, 2011.



21. Gonella, G.; Dai, H.-L., Second Harmonic Light Scattering from the Surface of Colloidal Objects: Theory and Applications. *Langmuir* **2014**, *30* (10), 2588-2599.
22. Revillod, G. Diffusion hyper Rayleigh des assemblages moléculaires. Université Claude Bernard-Lyon I, 2006.
23. Roke, S.; Gonella, G., Nonlinear Light Scattering and Spectroscopy of Particles and Droplets in Liquids. *Annual Review of Physical Chemistry* **2012**, *63* (1), 353-378.
24. Gassin, P.-M.; Bellini, S.; Zajac, J.; Martin-Gassin, G., Adsorbed Dyes onto Nanoparticles: Large Wavelength Dependence in Second Harmonic Scattering. *The Journal of Physical Chemistry C* **2017**, *121* (27), 14566-14571.
25. Duboisset, J.; Brevet, P.-F., Salt-induced Long-to-Short Range Orientational Transition in Water. *Physical Review Letters* **2018**, *120* (26), 263001.
26. Duboisset, J.; Brevet, P.-F., Second-Harmonic Scattering-Defined Topological Classes for Nano-Objects. *The Journal of Physical Chemistry C* **2019**, *123* (41), 25303-25308.





## Chapter III: Characterization of zeolite and selection of the conditions for the adsorption process

In this part of the manuscript, we will evaluate the performance of the FAU for the adsorption of organic molecules in various physicochemical or experimental conditions. We start with the characterization of the selected materials. We then detail the different conditions of analysis used to evaluate the performance of the zeolites used.

Subsequently, we detail the results of each adsorption test on commercial FAU, in order to study the influence of solvent, in the presence of water, ethanol, 50% water 50% ethanol having various conditions.

Afterward, in order to study the effect of modification of porosity on the structural, textural properties and their sorption performances, it is important to compare it with material that is mesoporous in origin. For this reason, Al-MCM-41 material was chosen for this comparison.

Finally, in some systems, different dyes tend to have similar adsorption capacity, and thus we cannot compare their interaction with the material. For this reason, a thermodynamic study using ITC measurement for two dyes/FAU was performed to gain more information about the strength of the interaction in this system.

### 1 Characterization techniques of zeolitic materials

This section presents the analysis of different materials which are FAU, hierarchical FAU, and Al-MCM-41. The analysis was done using XRF, TGA, N<sub>2</sub>-sorption isotherm, XRD, and Si-NMR.

#### 1.1 X-Ray fluorescence

In the aim of studying the effect of the Si/Al ratio on the sorption capacity, CBV-400 and CBV-780 were chosen as materials to understand this effect due to the fact that they have different Si/Al ratios. These materials were purchased from international Zeolyst. To quantify the elemental composition of the samples X-Ray fluorescence (XRF) was applied. The composition of these materials is collected in Table 4. Si/Al evaluated by XRF for CBV-400 and CBV-780 is lower than the Si/Al ratio given by the supplier. This difference in Si/Al ratio is probably due to the difference between the experimental and supplier theoretical calculation. The experimental error for CBV-400 is higher than CBV-780. This might be due to the error in the sample preparation or calibration curve for the sample analysis.

Table 4 : The material composition for zeolite-Y and Si/Al ratio obtained from XRF and supplier.

Zeolite-Y	Si	Al	Si/Al calculated by XRF	Si/Al given by the supplier	% error
CBV-400	29.076	14.251	2.04	2.55	20
CBV-780	38.217	1.077	35.48	40	11.3

## 1.2 Thermogravimetric analysis (TGA)

Thermogravimetric analysis (TGA) measurements were done to investigate the thermal stability of the zeolite Y (FAU), sDiA dye alone, and after adsorption onto FAU. Figure 37 represents the thermogravimetric analysis curves of these samples. In the case of FAU alone, the loss of mass below 100°C with -14.7% mass variation can be ascribed to the desorption of the physically adsorbed water. Between 100°C and 550°C, there is a very small loss -2.6% mass variation which is considered negligible. No loss is obtained at a higher temperature which revealed its higher stability. The procedure of sDiA adsorption onto FAU is shown in the footnote below.<sup>1</sup> In the case of sDiA alone, the dye is stable below 235°C then degradation occurs at a high rate at a temperature higher than 235°C until reaching a complete loss of the dye. While in the case of FAU loaded with sDiA, there is a decrease in mass below 100°C of -3.41% corresponds to water desorption. Between 100 and 670°C corresponds to the desorption of chemically adsorbed water and dye and its degradation. Then, at higher temperature > 670°C, no loss is observed which corresponds to the property of the loaded material. The difference in degradation temperature between sDiA alone and sDiA adsorbed onto FAU suggests that the material protects the dye from degradation since the dye is confined in the pores because the quantity of dyes used is high enough to reach equilibrium.

<sup>1</sup> 200 µM sDiA were adsorbed onto 5 mg FAU in a total volume of 20 ml in water medium then it is left overnight to reach equilibrium. This suspension is centrifuged at 11000 rpm for 60 min followed by drying overnight in the oven at 50°C.

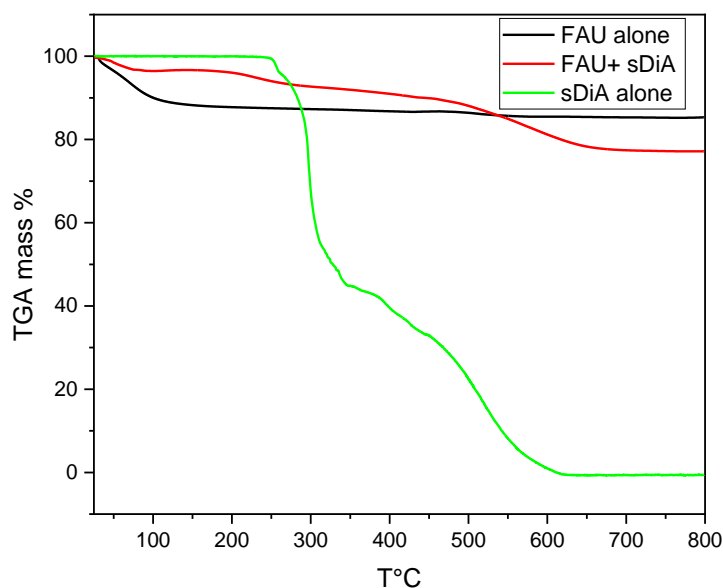


Figure 37 : TGA thermograms recorded on material (FAU; the black curve), material after dye adsorption (FAU + sDiA; the red curve) and dye alone (sDiA alone; the green curve).

### 1.3 $N_2$ -sorption isotherm

Modification of FAU by desilication-recrystallization route was carried out to obtain a material with different mesoporosity. Material modification and characterization for other FAUs were explained in chapter II. FAU-2a and FAU-2b were obtained by postsynthesis starting from commercial FAU using NaOH/Si ratios of 0.125 and 0.15 respectively. The sample preparation and the technical conditions of these materials were also stated in chapter II. FAU-2a and FAU-2b in comparison with other modified are shown in Table 5. The obtained isotherms (Figure 38) are classified as type I and type IV according to IUPAC with a sharp step of adsorption at  $P/P_0 = 0.4$  that relates to the capillary condensation into the ordered homogeneous mesopores of 4 nm diameter.<sup>145</sup> FAU-2a and FAU-2b have similar BET surface areas. As NaOH/Si ratio increases, the microporous volume decreases while mesoporous volume increases. This means that the crystalline domains remain unchanged for these modified materials.<sup>30</sup>

Table 5 :  $N_2$ -sorption isotherm of FAU after modification of the porosity using different NaOH/Si by t-plot.

FAU	NaOH/Si	$S_{BET}$ ( $m^2/g$ )	$V_{micro}$ ( $cm^3/g$ )	$V_{meso}$ ( $cm^3/g$ )
FAU-2	0.095	916	0.223	0.386

FAU-2a	0.125	916	0.161	0.515
FAU-2b	0.15	917	0.124	0.577
FAU-3	0.25	860	0.048	0.679
Al-MCM-41	-	608	-	0.52

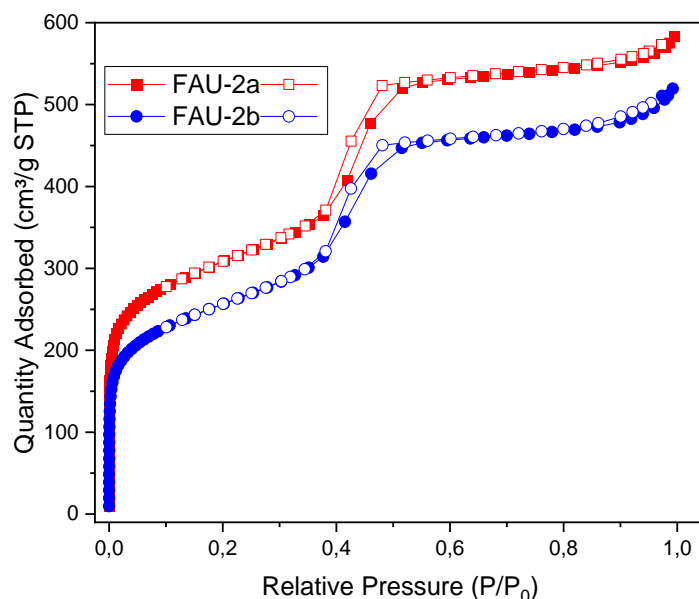
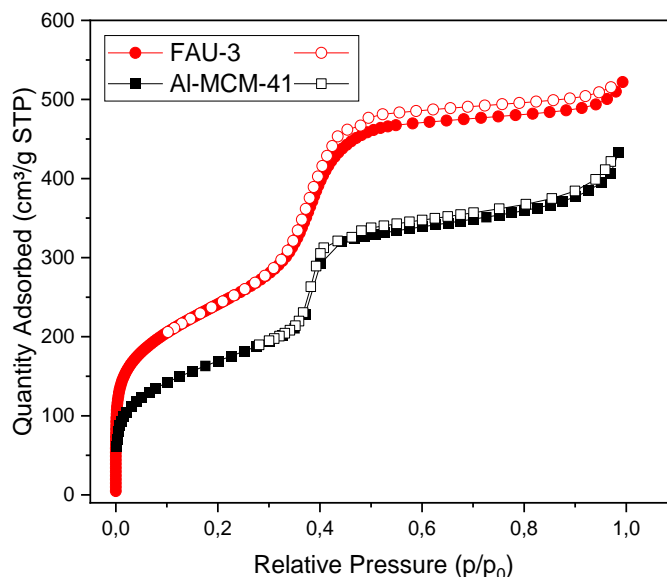


Figure 38 : Nitrogen sorption isotherm for modified FAU, FAU-0.125 (FAU-2a; red points) and FAU-0.15 (FAU-2b; blue points). The filled and empty symbols correspond to the adsorption and desorption branches, respectively.

Mesoporous silicas, including MCM-41, are silicates consisting of a system of one-dimensional cylindrical mesopores. Al-MCM-41 is ordered hexagonal mesoporous material with a well-defined pore structure. The pore diameter of these materials is 4 nm. FAU-3 is the product of highly modified FAU. It has both micro and mesopores with the majority of mesopores while Al-MCM-41 has only mesopores. The obtained isotherms are classified as a combination of type I and type IV with the majority of type IV for FAU-3 material, and type IV for Al-MCM-41 according to IUPAC. The textural properties of these two materials are placed in Table 5. The BET surface and mesoporous volume of FAU-3 are higher than that of Al-MCM-41.

Therefore, as the modification (Si/NaOH ratio) increases, the microporous volume decreases while the mesoporous volume increases. In the case of highly modified FAU (FAU-3), the predominant

pores are mesopores. Therefore FAU-3 is seen as an MCM-41-type architecture of mesopores built with amorphous zeolite walls of FAU-Y.



*Figure 39 : Nitrogen sorption isotherm for modified FAU, FAU-0.25 (red points) and Al-MCM-41 (black points). The filled and empty symbols correspond to the adsorption and desorption branches, respectively.*

#### **1.4 X-Ray diffraction**

X-Ray diffraction (XRD) studied in this work aimed to determine the identification of crystalline phases and the determination of certain structural properties such as the identification of defects in the structure. The measurements were carried out according to the powder method explained in the experimental chapter. Figure 40 presents the diffractograms of FAU-2a and FAU-2b at a large and small angle (a) and (b) respectively. According to the diagrams obtained at a large angle, these two FAU present a composition almost identical to each other and commercial material. This reveals that the crystallinity is retained after modification of porosity by alkaline treatment. In addition, the XRD pattern shows at a small angle the appearance of a broad peak at  $2\theta = 2.1^\circ$  for both materials FAU-2a and FAU-2b. This corresponds to the presence of ordered mesopores as in the case of MCM-41 type materials.

We have thus succeeded in identifying the operating conditions allowing the creation of FAU, for which micro and mesopores are present in the same material. We have shown that the presence of the mesoporous organized phase in our recrystallized materials is characterized in XRD by the presence of a small angle diffraction peak.



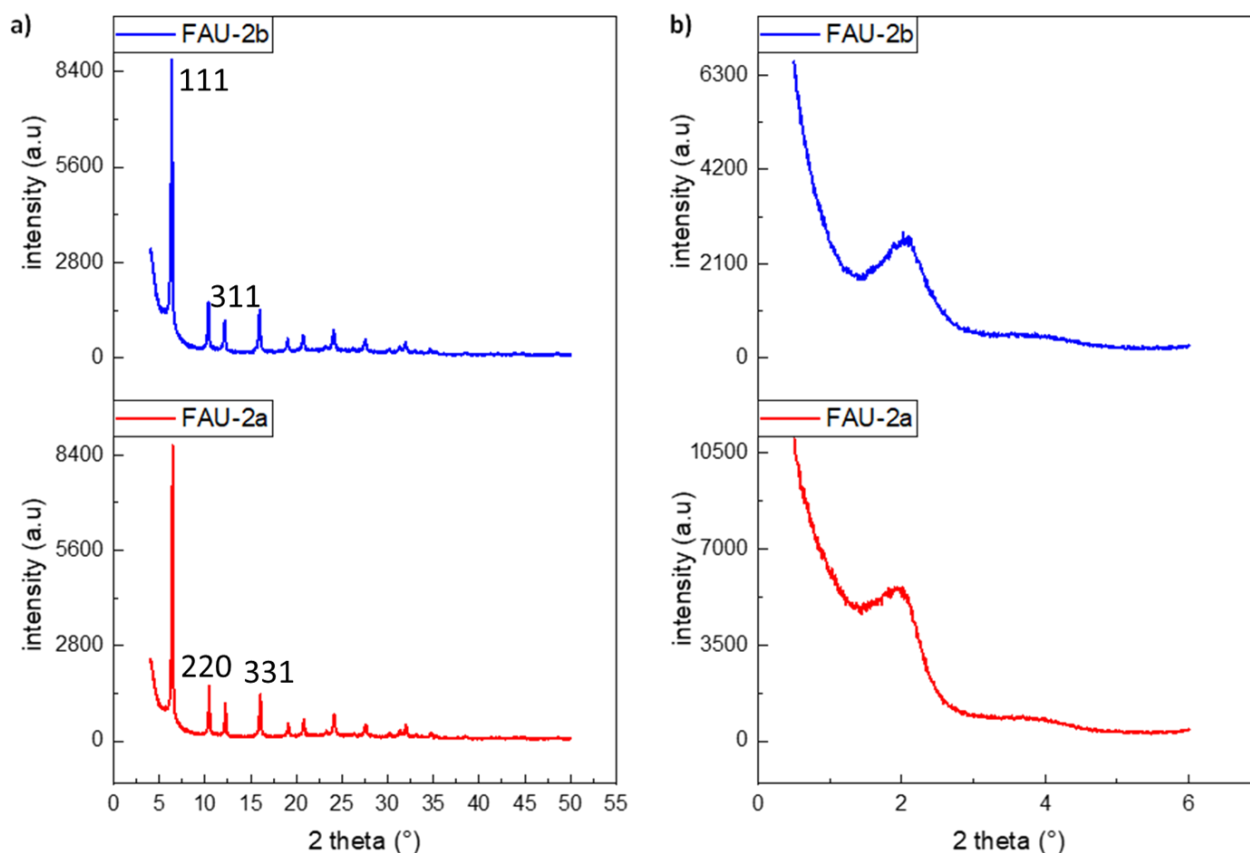


Figure 40 : Diffractogram for FAU-2a and FAU-2b with NaOH/Si = 0.125 and 0.15 respectively at a) large angle and b) small angle.

### 1.5 $^{29}\text{Si-NMR}$

Silicon NMR was carried out on FAU-2a and FAU-2b to see the Si environment of FAU. The spectra and the % of  $Q^n$  for both FAU are shown in Figure 41 and Table 6, respectively. The spectra of FAU-2a and FAU-2b show the standard peaks of FAU at -108 ppm corresponding to  $\text{Si}(4\text{Si}, 0\text{Al})$ , abbreviated  $Q^4$  environment, and -102 ppm that related to  $\text{Si}(3\text{Si}, 1\text{Al})$ , abbreviated  $Q^3$  environment. Another additional peak at -110 ppm, corresponds to the  $Q^4_{\text{amp}}$  environment.<sup>146</sup> It is attributed to the formation of a large amount of amorphous material by such alkaline treatment.<sup>147</sup> As the FAU modification increases by increasing the NaOH/Si ratio, the % of  $Q^3$  and  $Q^4_{\text{amp}}$  increases while  $Q^4_{\text{crys}}$  decreases. This shows that the transformation from  $Q^4$  to  $Q^3$  occurs on the one hand and an increase in  $Q^4_{\text{amp}}$  on the other hand which reveals an increase in amorphous phase due to the partial destruction of structure upon alkaline treatment. These results confirm that FAU-2a and 2b are *transition* samples between FAU-2 and FAU-3. This is also confirmed by XRD that stated in the experimental chapter.

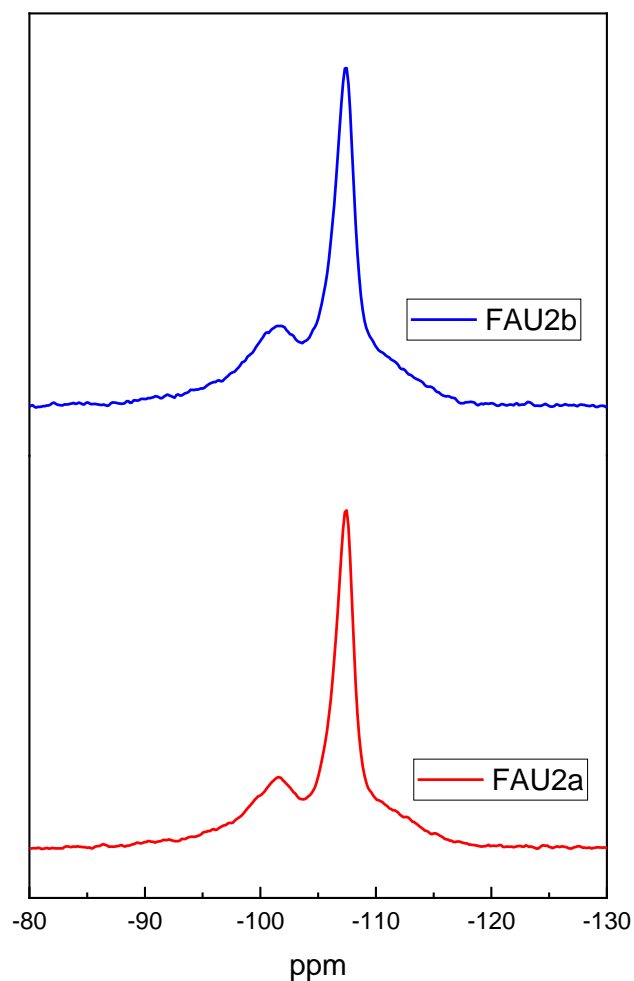


Figure 41 : Si-NMR spectra for FAU-2a and FAU-2b.

Table 6 : Si-NMR Q<sup>n</sup> entities for FAU-2a and FAU-2b in comparison with other FAU.

Modified FAU	NaOH/Si	Q <sup>3</sup> %	Q <sup>4</sup> %	Q <sup>4</sup> <sub>amp</sub> %
FAU-2	0.095	12	61.5	15
FAU-2a	0.125	17	51.5	20
FAU-2b	0.15	16.5	50.5	19
FAU-3	0.25	33	31.5	28.5

In summary, the characterization techniques for the materials obtained after desilication showed the presence of microporosity and mesoporosity in the same material by retaining the crystallinity and forming ordered mesopores except for the highly modified material. The possibility to

control the porosity of the material, maintaining close chemical properties at the solid surface, is a very interesting opportunity to study the organization of molecules and different phenomena that occurs at the interface.

## 2 Selection of experimental conditions of the procedure performed for sDiA adsorption onto commercial Faujasite

Heterogeneities in the solution affect the SHS signal either by changing its intensity or by producing large fluctuation in the SHS plots. For this purpose, protocols had to be adapted to be possible in the non-linear optic. Typically, isotherms of sDiA towards FAU (CBV-720) have been performed using two different ways of zeolite addition (Figure 42).

- Firstly, a definite amount of FAU is added directly to the tubes in the form of powder then followed by the addition of dye/water ratio. Then these tubes are stirred on a planetary rotative system overnight to ensure the equilibrium (top of the figure).
- In a second way, FAU is prepared as a suspension using a definite solid to liquid ratio (bottom of the figure). This suspension is well sonicated for 10 min to achieve homogeneity and stability of the suspension and prevent aggregation. Isotherm is then performed by adding a definite volume of the prepared suspension with different dye/water ratios following the same procedure mentioned above.

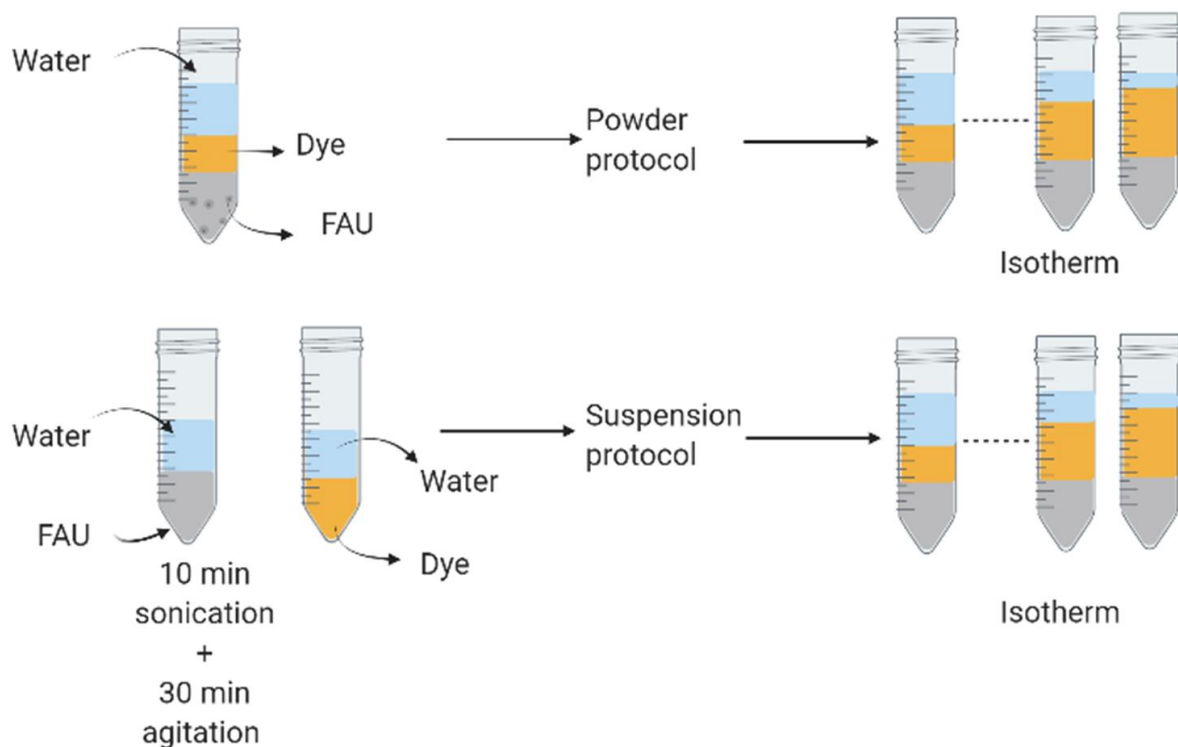


Figure 42 : Schematic representation showing two different protocols to prepare adsorption isotherm.

The effect of FAU mass, adsorption equilibrium time, solid/liquid ratio, and contact time between the solid and the solvent for the suspension preparation have been also studied in this thesis using the suspension form. We wanted to check if the isotherm prepared using FAU suspension will have the advantage over the powdered one by being homogenous without any aggregation because of sonication. Otherwise, it prevents the high fluorescence resulting from SHS experiments.

## 2.1 Effect of isotherm preparation

In order to see the influence of the isotherm preparation way on the adsorption capacity, two experiments were performed. The first experiment was prepared using powdered FAU while the second was performed using the FAU suspension in water to see its effect on the sorption capacity.

To find out the study of the effect of the various steps of the protocol on the adsorption efficiency, the same experimental conditions were applied. The experiment prepared with powder FAU of 5 mg in 20 ml total volume is equivalent to the suspension one of 0.25 g/l (same solid/liquid ratio). The adsorption isotherms of these systems are shown in Figure 43. The adsorption capacity of sDiA toward FAU for the isotherm prepared by FAU powder (5 mg), 600  $\mu\text{mol/g}$ , is higher than the one when the sample is prepared by FAU suspension (0.25 g/l) 510  $\mu\text{mol/g}$  with high affinity for both isotherms.

The difference between both capacities is due to the difference in the way of preparation of the initial mixture of solid and water. This difference might be due to the formation of aggregates due to the fact that the FAU suspension is not well sonicated or the suspension is exposed for a long time i.e. the suspension was not fresh enough which leads to a decrease in accessibility and in the sorption capacity. To validate this hypothesis, the time effect on the isotherms will be stated later in paragraph 2.3.

After that experiment, we conclude that the powder protocol using FAU powder is more adapted and reproducible.

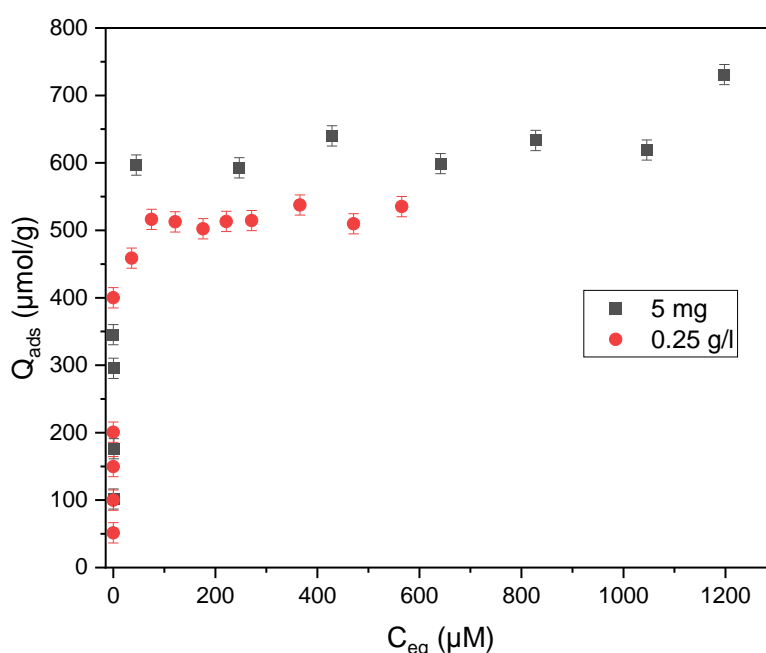


Figure 43 : Adsorption isotherm of sDiA onto commercial FAU (Si/Al = 15) prepared using the powdered form of 5 mg in 20 ml system and suspension form for 0.25 g/l in water solvent.

## 2.2 Effect of solid/liquid ratio (S/L ratio)

The adsorption isotherm was performed using the suspension protocol prepared from FAU suspension with four different FAU S/L ratios. They were prepared using following the same procedure described previously in water and ethanol medium.

### 2.2.1 In water medium

The adsorption isotherms having different FAU S/L ratios were prepared in a similar way using FAU suspension. The adsorption isotherms of these systems are shown in Figure 43. The shape of the curve at low concentration reveals that all isotherms have a high affinity of sDiA toward FAU. The

adsorption capacity of sDiA toward 0.05 g/l is similar to that of 0.15 g/l. However, these two isotherms show slightly higher adsorption capacity compared to 0.25 g/l FAU which is 510  $\mu\text{mol/g}$ . The decrease in the adsorption capacity of sDiA toward 0.25 g/l FAU compared to other isotherms is might be due to the presence of aggregate of FAU particles resulting from a high solid/liquid ratio i.e the suspension is not well dispersed due to exposing the suspension to a long time i.e. the FAU suspension was not 'fresh' enough. Accordingly, the FAU of suspension with S/L equal to 0.05 g/l seems to be the appropriate ratio for our system. This is due to the well dispersed system at the local scale, which provides the high sorption capacity at the macroscopical scale. However, at a high S/L ratio, the sorption capacity is lower probably due to the presence of aggregate that can cause a low diffusion in SHS experiments thus a fluctuation in SHS plots might be observed.

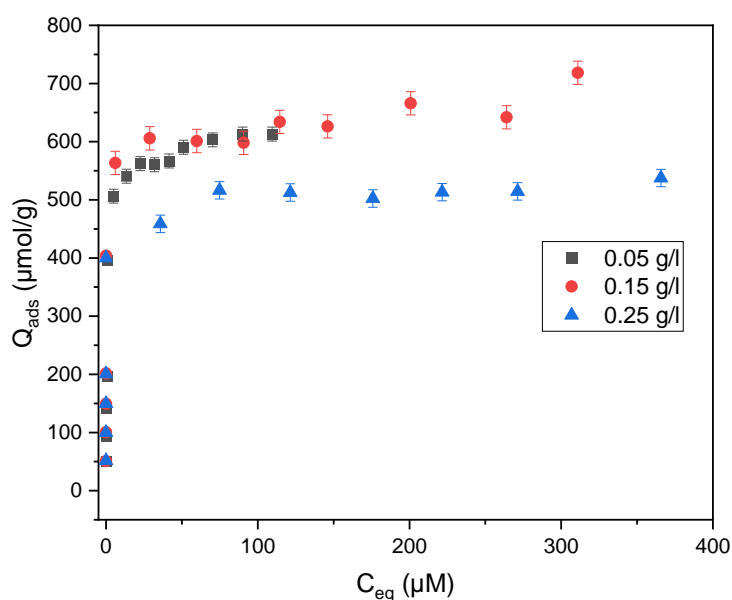


Figure 44 : Adsorption isotherm of sDiA onto commercial FAU (Si/Al = 15) prepared using the suspension form for 0.05, 0.15 and 0.25 g/l experiments in water solvent with their corresponding error bar.

In order to confirm this result and to see the effect of the S/L ratio of zeolite on the adsorption isotherm, four sDiA concentrations in the presence of different S/L ratios were measured at a local scale using the SHS technique.

## 2.2.2 In ethanol medium

To see the effect of different FAU solid/liquid (S/L) ratios on the sorption isotherm in ethanol medium, similar experiments to that in water were carried out in ethanol. The adsorption isotherms of sDiA onto FAU having different FAU S/L ratios prepared using FAU suspension are depicted in Figure

45. The adsorption capacity of sDiA onto FAU for 0.05, 0.15, and 0.25 g/l is similar and equal to 250  $\mu\text{mol/g}$  with similar affinity. The sorption capacity is lower in ethanol than in water due to the fact that the Bronsted acid in water is more active.

No effect of the S/L ratio of FAU suspension is obtained in the case of ethanol medium which opposes the results obtained in the case of water medium. This is due to the fact that well-dispersed particles in ethanol solvent as already explained by DLS measurement. At the low sDiA concentration, the adsorption capacities for the three ratios are similar (zoomed figure) with the same range of error evaluated from the standard deviation.

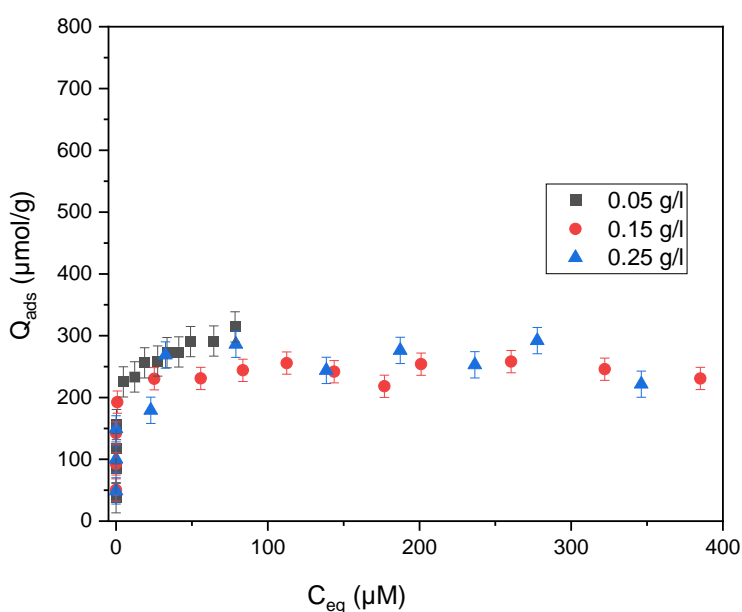


Figure 45 : Adsorption isotherm of sDiA onto commercial FAU (Si/Al = 15) prepared using the suspension form for 0.05, 0.15 and 0.25 g/l experiments in ethanol solvent with evaluation of the error bar.

### 2.2.3 By SHS

We then analyze simultaneously the effect of initial dye concentration and S/L ratio. Different suspensions prepared from various S/L ratio (0.05, 0.1, 0.15, 0.2 and 0.25 g/l), and in contact with different initial dye concentration (10, 20, 40 and 60 $\mu\text{M}$ ). These samples were measured using SHS. SHS polarization plots as a function of polarization angle for each S/L ratio of FAU suspension are reported in Figure 46. The dots are experimental data and the solid lines are the results of the best fit. Actually, in order to clearly illustrate these plots, a mathematical model explained in the experimental chapter was used to fit the experimental results. For each initial concentration of dye, the various S/L ratios of FAU are superimposed.

Generally, it is seen that the maximum SHS intensity increases as the concentration of dye increases. However, for a given sDiA concentration, the SHS intensity is lower when the S/L ratio of FAU suspension is higher. This can be interpreted by high adsorption between dye and FAU. At a low dye concentration, 10  $\mu\text{M}$ , the maximum value of horizontal polarization ( $0^\circ_{\text{in}}, H_{\text{out}}$ ) measurement is higher than the minimum value of vertical polarization measurement ( $90^\circ_{\text{in}}, V_{\text{out}}$ ). This shift increases more and more as the concentration of dye increases in addition to the enlargement in vertical polarization with a  $\cos(4\gamma)$  contribution increasing.

Concerning the evolution in solid concentration (Faujasite suspension), in the case of 0.1 g/l at a high concentration, we notice a shift between the intensity at ( $0^\circ_{\text{in}}, H_{\text{out}}$ ) and at ( $90^\circ_{\text{in}}, V_{\text{out}}$ ). Moreover, the SHS absolute intensity is the highest compared to others. So, 0.1 g/l shows the highest interaction compared to others.

In addition, the high enlargement in vertical polarization reveals the strong interaction between molecules and particles. The ratio 0.05 g/l and 0.1 g/l gave similar results. So, the low concentration is considered as the most favorable concentration in the present study, since the rediffusion effect by particle that might be produced at high concentration is avoided. Therefore, 0.1 g/l and not 0.05 g/l is considered as an appropriate S/L ratio for the sorption isotherm procedure, since in the system of 0.05 g/l, the quantity of material is too low to adsorb enough high amount of dye, and this case, the risk is that free molecules are mainly present in the system.

To confirm the obtained results on the effect of S/L on the adsorption process and SHS plots, isotherms with various conditions were performed and explained later.

To conclude in this part, a high S/L ratio leads to a decrease in the sorption capacity, therefore, affects negatively the SHS plots by causing the diffusivity of the particles in the medium. Therefore, optimal conditions must be appropriate to the system used including the S/L ratio and the protocol in order to obtain well dispersed particles in the system.



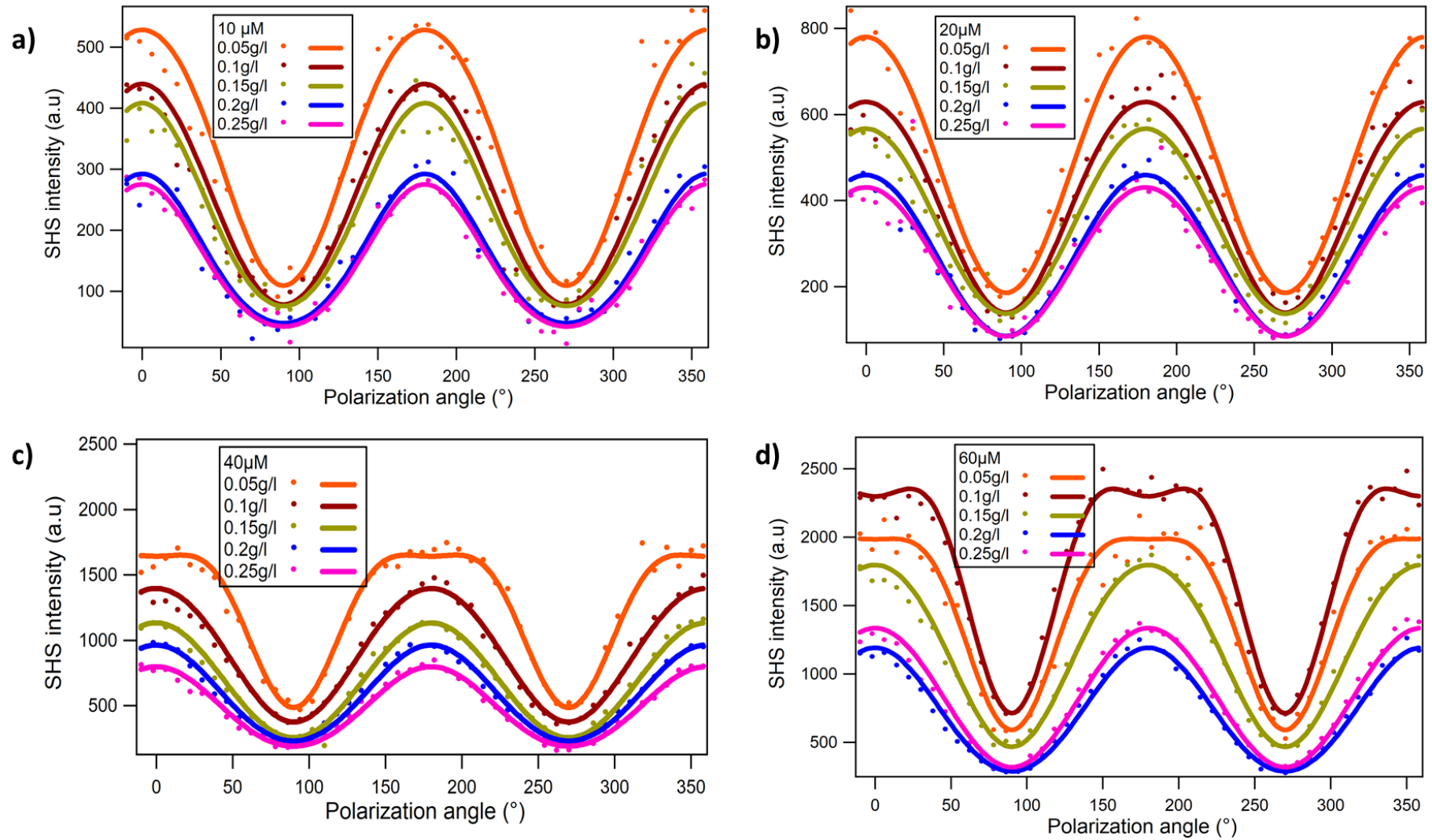


Figure 46 : Effect of S/L ratio of FAU on the adsorption of sDiA onto commercial FAU (Si/Al = 15) 0.05 g/l (orange), 0.1 g/l (red), 0.15 g/l (green), 0.2 g/l (blue), 0.25 g/l (pink) in aqueous medium at sDiA different concentrations. a) 10  $\mu$ M b) 20  $\mu$ M c) 40  $\mu$ M d) 60  $\mu$ M.

## 2.3 Effect of time on the stability of FAU suspension

### 2.3.1 In water for solid/liquid ratio 0.25 g/l

The effect of time between the FAU in suspension with water solvent was studied by performing three experiments using the protocol with the FAU suspension of S/L ratio 0.25 g/l. The sDiA adsorption isotherms were carried out by preparing the FAU suspension with the various duration of 30 min, 2 hours, and 24 hours in a water medium (and with identical experimental conditions to those previously used). The supernatant of these experiments was measured using UV-Vis spectroscopy. The isotherms are presented in Figure 47. The isotherm after 30 min exhibits the highest adsorption capacity (700  $\mu\text{mol/g}$ ) with high affinity. A small decrease is obtained after 30 min and then 24 hours to reach the capacity of 550  $\mu\text{mol/g}$ . This decrease is might be due to the formation aggregates of FAU with the solvent as a function of time.

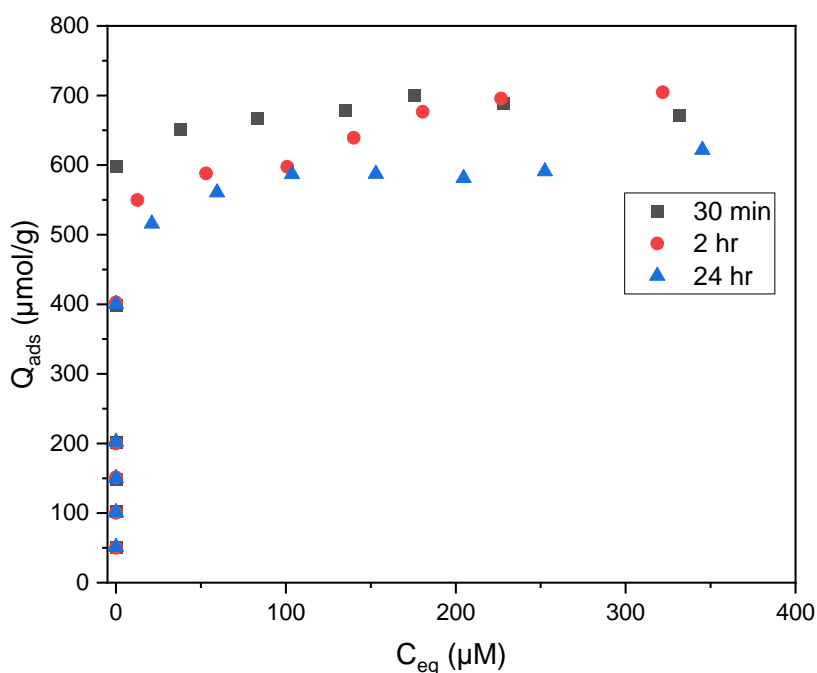


Figure 47 : Adsorption isotherm of sDiA onto 0.25 g/l commercial FAU (Si/Al=15) prepared in water medium at different contact time between FAU and water 30 min, 2 hr and 24 hr.

It has been shown that the time between solid and liquid for the preparation of the mother suspension decrease the adsorption capacity. Other experiments with different conditions such as the contact time of the isotherm after adsorption, sonication, ionic strength are also tested. Their results will be presented in the following paragraph.

### 2.3.2 For solid / liquid ratio 0.05 g/l in water and in ethanol

Other experiments with different S/L ratios of FAU suspension were proceeded to ascertain this effect on the sorption capacity. The experimental conditions are identical to those previously used with a S/L ratio of 0.05 g/l in water and ethanol medium. Adsorption isotherms of sDiA dye toward FAU were performed at two different times of contact time. The first one is made after 30 min while the latter is after two days. Both suspension and supernatant were measured using UV-Vis spectroscopy and SHS techniques at the macroscopic and local scale, respectively. In addition, the influence of solvent has been tested, using water and ethanol.

#### 2.3.2.1 Measurements using UV-Vis spectrometry

The adsorption isotherms of sDiA in water and ethanol prepared at different contact times are shown in Figure 49 a). This is done with the evaluation of dye concentration using UV-Vis spectrometry. Adsorption capacity in water decreases from 600 to 200  $\mu\text{mol/g}$  with instability in the plateau, and also the affinity seems lower. This instability in the plateau is due to the experimental error. On the contrary in ethanol, the isotherms are similar (capacity and affinity) which equal to 350  $\mu\text{mol/g}$ .

This means that in these conditions (in ethanol), there is no effect of time of the FAU suspension. This can be explained by the fact of formation of aggregates of FAU particles in the presence of water solvent after a definite time while in ethanol no effect of the time is observed on the particle aggregation. It agrees with the DLS results stated in Figure 48 in which two populations of particles appeared after 30 min and 2 days in ethanol medium. However, in the case of water medium, only one population is observed after 30 min and 2 populations are obtained after 2 days. Therefore, no effect

of time is observed in the case of ethanol in contrast to water medium where the aggregation is formed after time that leads to a decrease in the accessibility, and thus in the sorption capacity.

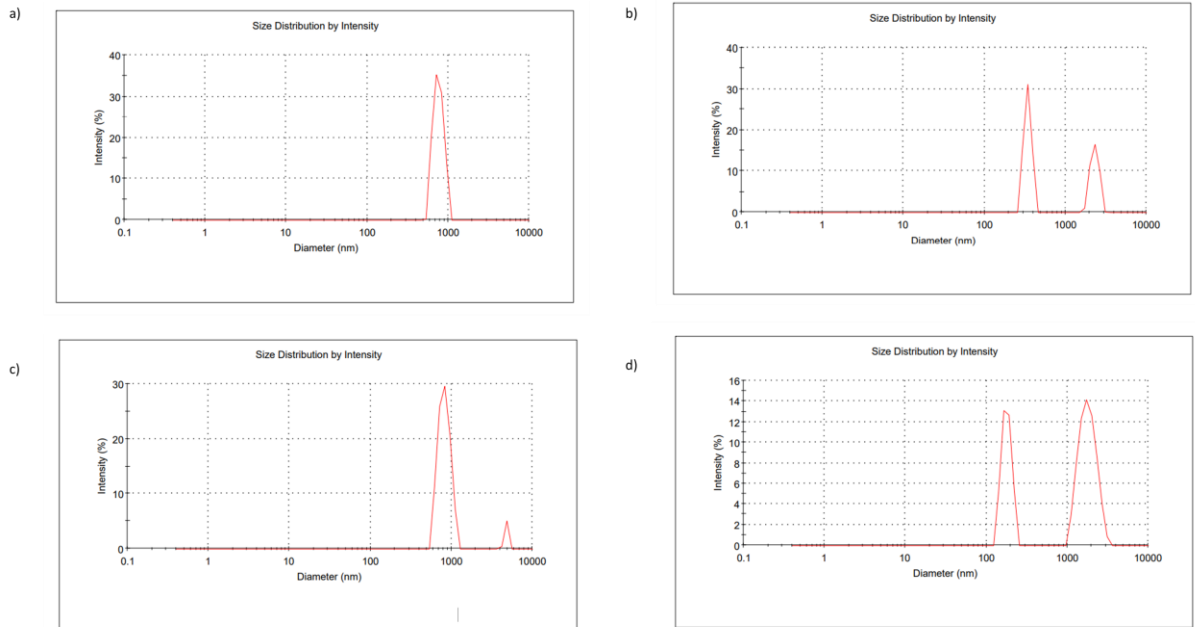


Figure 48 : DLS measurements of 0.1 g/l FAU (Si/Al = 15) prepared after 30 min and night in water a) and c) and ethanol medium b) and d) respectively.

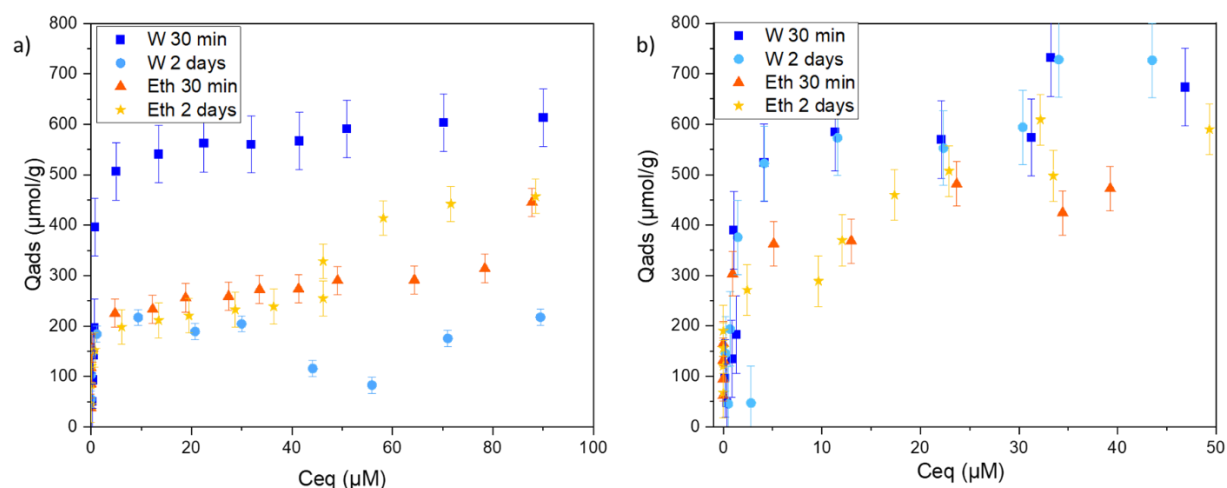


Figure 49 : Effect of contact time between commercial FAU ( $Si/Al = 15$ ) and solvent on the adsorption capacity of sDiA dye after 30 min and 2 days in water (W) and ethanol (Eth) using a) UV-Vis spectroscopy and b) SHS.

One concentration of sDiA dye at different conditions (duration, solvent) is measured and their spectra are depicted in Figure 50. In water medium, the spectrum of the supernatant after 30 min is similar to that of the dye alone while a shift to a higher wavelength has appeared after 2 days. In ethanol, the spectrum after 30 min and 2 days is similar to the spectrum of dye alone.

The shift in Figure 50 a), i.e. in water, corresponds to dyes in the presence of particles. The presence of particles after filtration is due to the fact that the filtration may not be efficient to remove all the particles of zeolite from the medium. However, in Figure 50 b) i.e. in ethanol, there is no shift and the spectrum after filtration is the same as dye alone since the zeolite is well dispersed in water than in ethanol. This is due to the different interactions between the solvent and the particles.

To understand more about this effect at the local scale, SHS has been used.

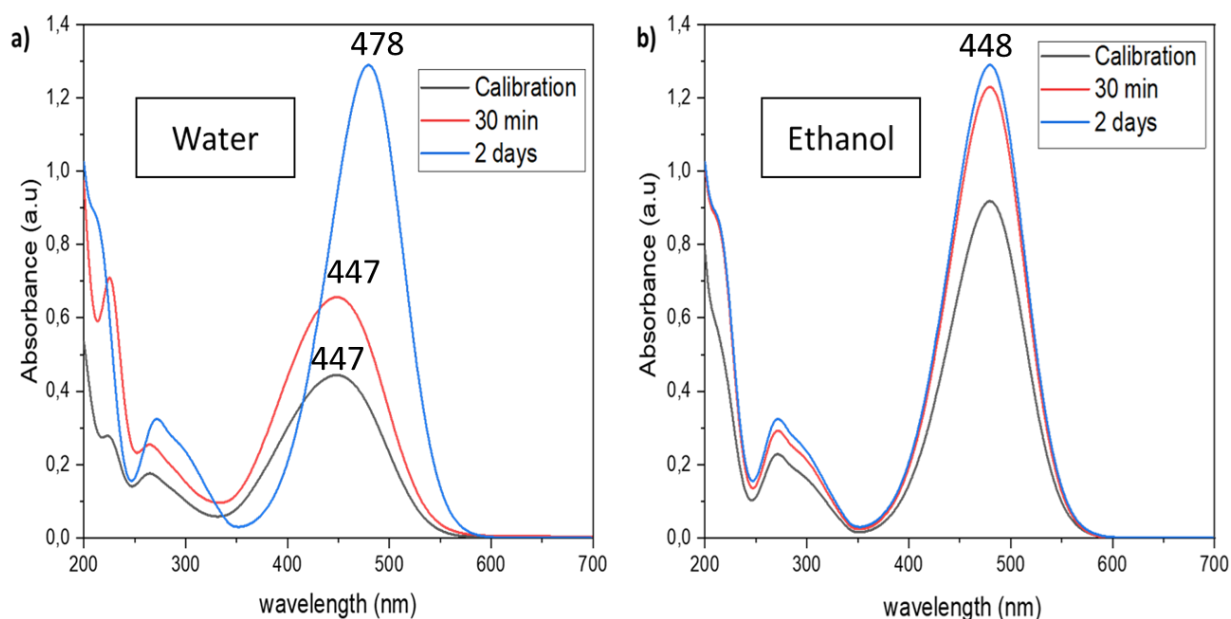


Figure 50 : Spectra of 100  $\mu\text{M}$  sDiA dye alone (calibration) (black spectrum), supernatant after 30 min (red spectrum) and 2 days (blue spectrum) of contact time between 0.05 g/l commercial FAU (Si/Al = 15) suspension in a) water solvent and b) ethanol solvent obtained by UV-Vis spectroscopy.

### 2.3.2.2 Measurements using SHS

The isotherm is plotted using SHS measurement and the curves are shown in Figure 49 b). Adsorption isotherm of sDiA onto FAU in water medium and ethanol after 30 min and two days are in complete agreement with the isotherms calculated using UV-Vis. However, the isotherm of sDiA in water after two days gave a similar result compared to the isotherm obtained after 30 min which contradicts the result acquired from UV-Vis. Moreover, Figure 51 displayed the SHS plots for sDiA with FAU in water and ethanol after 30 min and two days. These SHS plots show a decrease in SHS intensity for the solution that was measured after 2 days. This decrease in SHS intensity reveals a decrease in the sorption capacity which is related to the formation of aggregates.

In order to analyze more in details and quantitatively these results, the correlation between molecules will be determined. As usual, the data treatment of these SHS plots is performed by subtracting the SHS intensity of supernatant from the suspension and then fitted by a mathematical model to obtain the correlation parameter ( $I_4$ ). These calculations are stated in detail in the previous

chapter (experimental chapter).  $I_4$  parameter is calculated for both systems and the results are plotted in Figure 52.

At low dye concentration in a water medium, the value of the  $I_4$  parameter is -0.08 for 30 min system which is higher in absolute value compared to the system after 2 days ( $I_4$  parameter = 0). As the concentration increases, the absolute value of the  $I_4$  parameter increases in both systems to be -0.12 and -0.1 for 30 min and 2 days, respectively. However, in the case of ethanol, this parameter is zero for both systems, 30 min and 2 days at low and high concentrations. When the absolute value of  $I_4$  is high, the dye molecules are correlated. This stands for the conclusion that the molecules are not correlated in the case of ethanol in contrast to the case of water. In the case of a fresh solution in water,  $I_4$  is higher compared to that of an old solution which signifies a strong correlation. The lower correlation in the system can be explained by the aggregation of the FAU particles observed after a prolonged contact. Therefore, the molecules are less organized due to low correlation in the system.

This can be explained by the different interactions of materials with the solvent. In the case of water, the Bronsted acid is more active than in ethanol which leads to low sorption capacity and low correlation between molecules in ethanol medium.

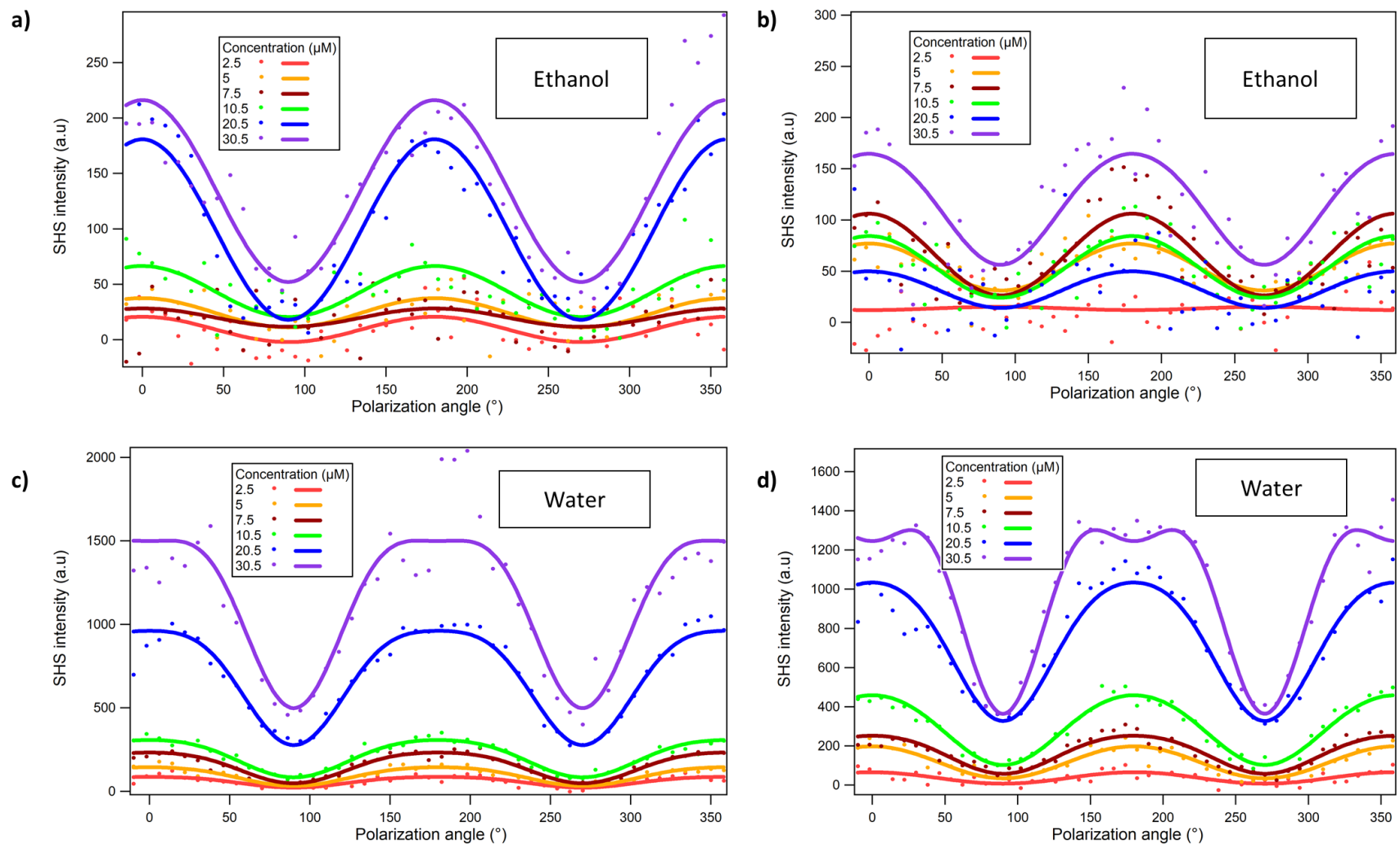


Figure 51 : SHS plots for sDiA with 0.05 g/l commercial FAU ( $Si/Al = 15$ ) in ethanol after 30 min and 2 days on a) and b) respectively and in water after 30 min and 2 days on c) and d) respectively.



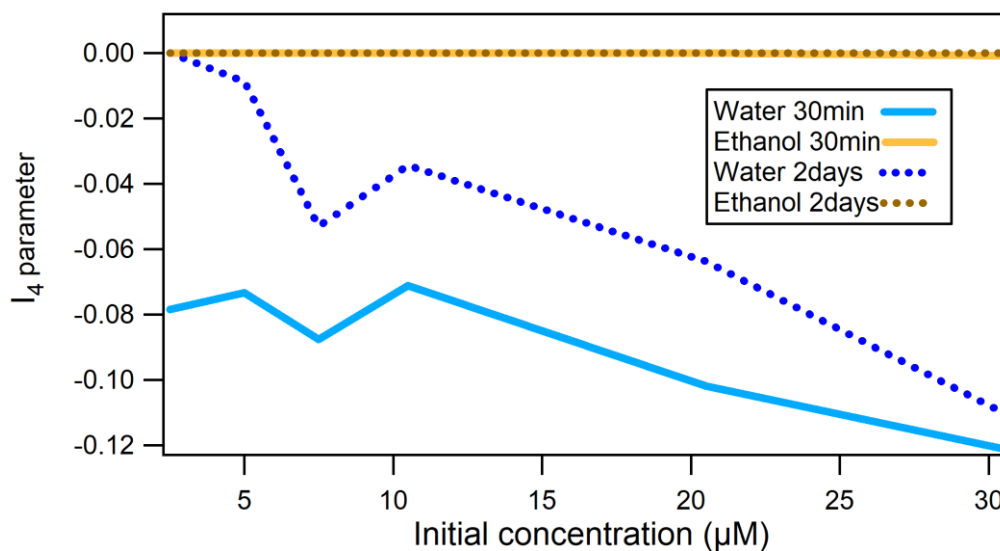


Figure 52 :  $I_4$  parameter calculated for sDiA adsorbed onto commercial FAU ( $Si/Al = 15$ ) (blue and dark blue dotted curve) in water and in ethanol (orange and brown dotted curve) after 30 min and 2 days, respectively.

## 2.4 Effect of contact time on sDiA and FAU suspension

Various experiments were carried out under different conditions to study the effect of contact time on the adsorption behavior. Four different concentrations 10, 20, 40, and 60  $\mu\text{M}$  of sDiA were adsorbed onto 0.05 g/l FAU. Suspension of FAU is used after 30 min of contact including 10 min of sonication to ensure the homogeneity of FAU-solvent suspension and to prevent particle aggregation. Both suspension and supernatant of those samples were analyzed at different times in different media, water, ethanol, and a mixture of 50%-50% water-ethanol. These experiments were prepared using the suspension protocol with the same procedure as the one mentioned on Figure 42.

### 2.4.1 In water medium

The adsorption quantity of sDiA onto FAU was characterized using two different scales, macroscopic and local scale.

- UV-Vis spectroscopy

The maximum adsorption capacities of sDiA towards FAU after different equilibrium times were evaluated. As shown on Figure 53, the quantity of dye adsorbed increases with increasing the equilibrium concentration until reaching the maximum adsorption capacity. The maximum adsorption

capacities are constant (500  $\mu\text{mol/g}$ ) for all the durations tested, and stable after 2, 5, 7, and 23 hours of adsorption.

Therefore, the equilibrium is considered to be reached after 2 hours or even less. This means that the active sites responsible for the dye adsorption reach a maximum occupation after 2 hours with respect to the initial concentration. This is similar to the result obtained with Akgül et al.<sup>148</sup> and Xiao et al.<sup>149</sup> where the adsorption equilibrium reached after 1h of methylene blue onto clinoptilolite and Cd-MOF, respectively. But in this thesis, the isotherms were kept with an equilibrium time overnight in order to have constant conditions with other dyes.

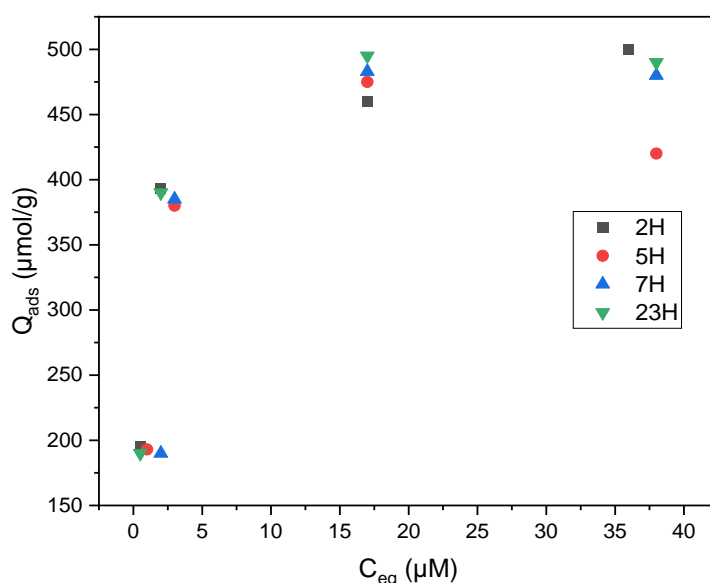


Figure 53 : Effect of time on the adsorption capacity of sDiA onto 0.05 g/l commercial FAU (Si/Al = 15) in water medium using UV-Vis spectrometry.

- SHS

The adsorption isotherms of sDiA at different times 2, 5, 8, 22H20, 46, and 70 hours were characterized using SHS and reported in Figure 54. The isotherms were calculated from the maximum vertical polarization of the supernatant (detailed calculations were shown in the experimental chapter). These isotherms gave similar results compared to UV-Vis with the maximum sorption capacity of 450  $\mu\text{mol/g}$  except for the result obtained for 70 hours where a decrease in the sorption capacity is observed and the sorption capacity becomes 300  $\mu\text{mol/g}$ . The adsorption equilibrium is reached at 2h, which is similar to the MB study toward negatively charged material Cd-MOF and clinoptilolite reported by Xiao et al.<sup>149</sup> and Akgül et al.<sup>148</sup> respectively. Moreover, suspension samples

were also measured and gave similar observations as shown in Figure 55. As moving from lower concentration to higher concentration evolution in the SHS plots is clearly seen in vertical polarization (enlargement) and horizontal polarization (increase in the intensity), mainly for 20 to 60  $\mu\text{M}$ . At 10  $\mu\text{M}$  the SHS plots are the same for various duration. However, for the other concentrations, the SHS plots were different at various equilibrium times. The SHS intensity is maximum after being exposed to a longer time, 46h and 70h.

This increase in the intensity can be explained by the formation of aggregates of FAU particles present in the solution. This high intensity might be due to the molecular organization in the FAU or around the FAU aggregates. This could be an open question to be solved in the future. Since the presence of aggregates leads to a lower adsorption capacity as explained previously thus a decrease in the SHS intensity must be observed. And we explained in detail in chapter IV in which the organized system (the correlated system) gave the high SHS intensity compared to the non-organized system. Also, we showed that the particle aggregation was observed after time.

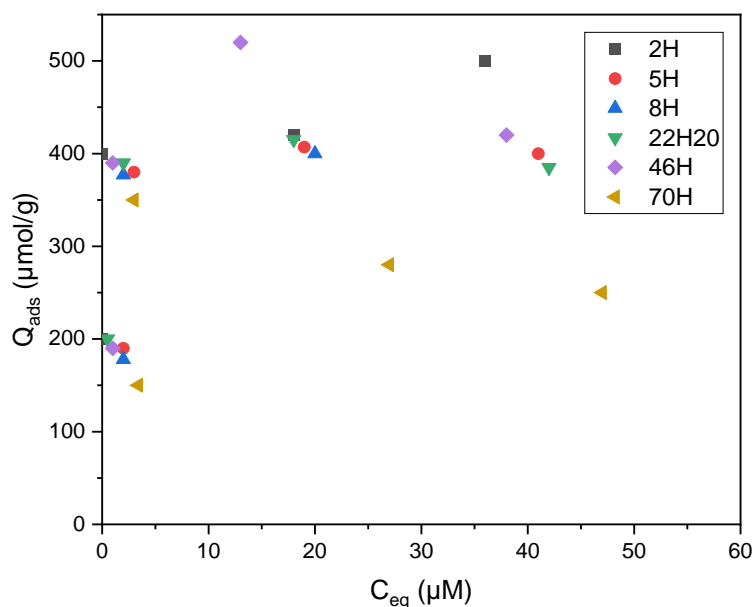


Figure 54 : Effect of time on the adsorption capacity of sDiA onto 0.05 g/l commercial FAU (Si/Al = 15) in water medium using SHS.

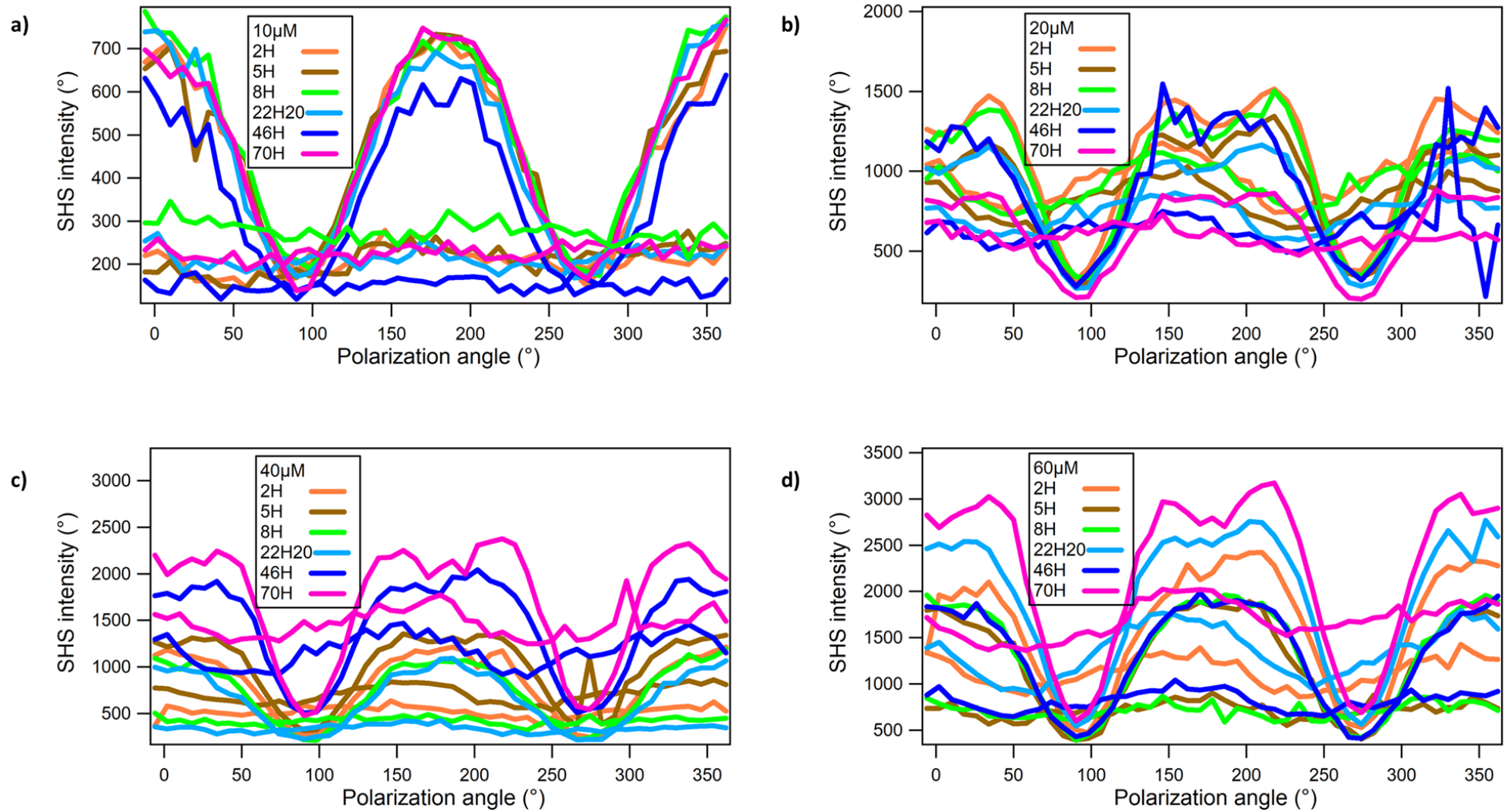


Figure 55 : SHS plots of four different concentration of sDiA adsorbed onto 0.05 g/l commercial FAU (Si/Al = 15) measured at different time in water medium; a) 10 μM, b) 20 μM, c) 40 μM and d) 60 μM.

## 2.4.2 In ethanol medium

Similar measurements were done in ethanol solvent using only SHS as a characterization tool. Figure 56 displays the various adsorption capacities. Despite the experimental error, a general tendency is observed, with a value that range from 250 to 400  $\mu\text{mol/g}$  for all isotherms at different time. The dispersity of points renders the evaluation of  $Q_{\text{max}}$  difficult. The dispersity comes from the successive experimental error that are added at the various steps of the protocol. In this particular case, the amount adsorbed is estimated from the maximum intensity of vertical polarization of the supernatant, which might be very sensitive and subject of numerous un controllable and sometimes unexplained variations. In addition, SHS plots for the suspensions are presented in Figure 57. These plots give similar polarization plots with similar intensity. Therefore, no variation is observed in the SHS plots for sDiA in suspension with FAU at different times. This means that the FAU is stable with time in the case of ethanol which means that there is no aggregation of particles present in the solution as discussed above in contrast to the case of water that form aggregates with time. Aggregation is formed directly when FAU is placed in contact with ethanol. This is also confirmed by DLS stated in the previous part.

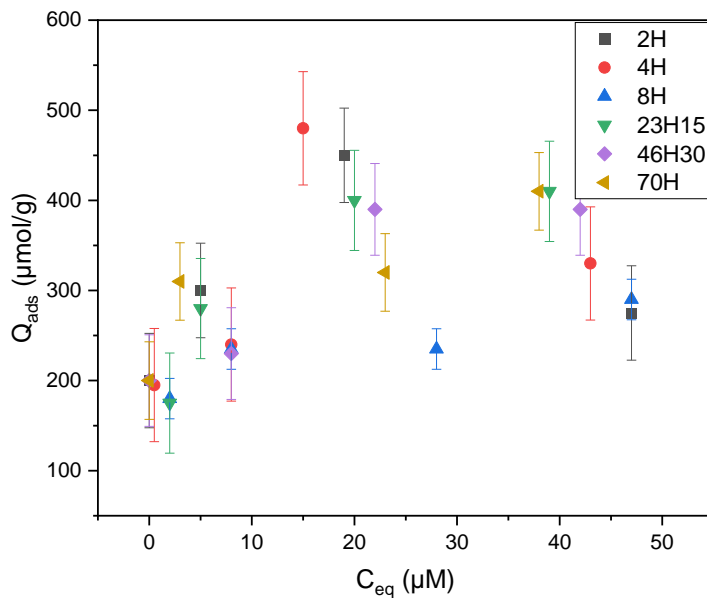


Figure 56 : Effect of time on the adsorption capacity of sDiA onto 0.05 g/l commercial FAU (Si/Al = 15) in ethanol medium using SHS.

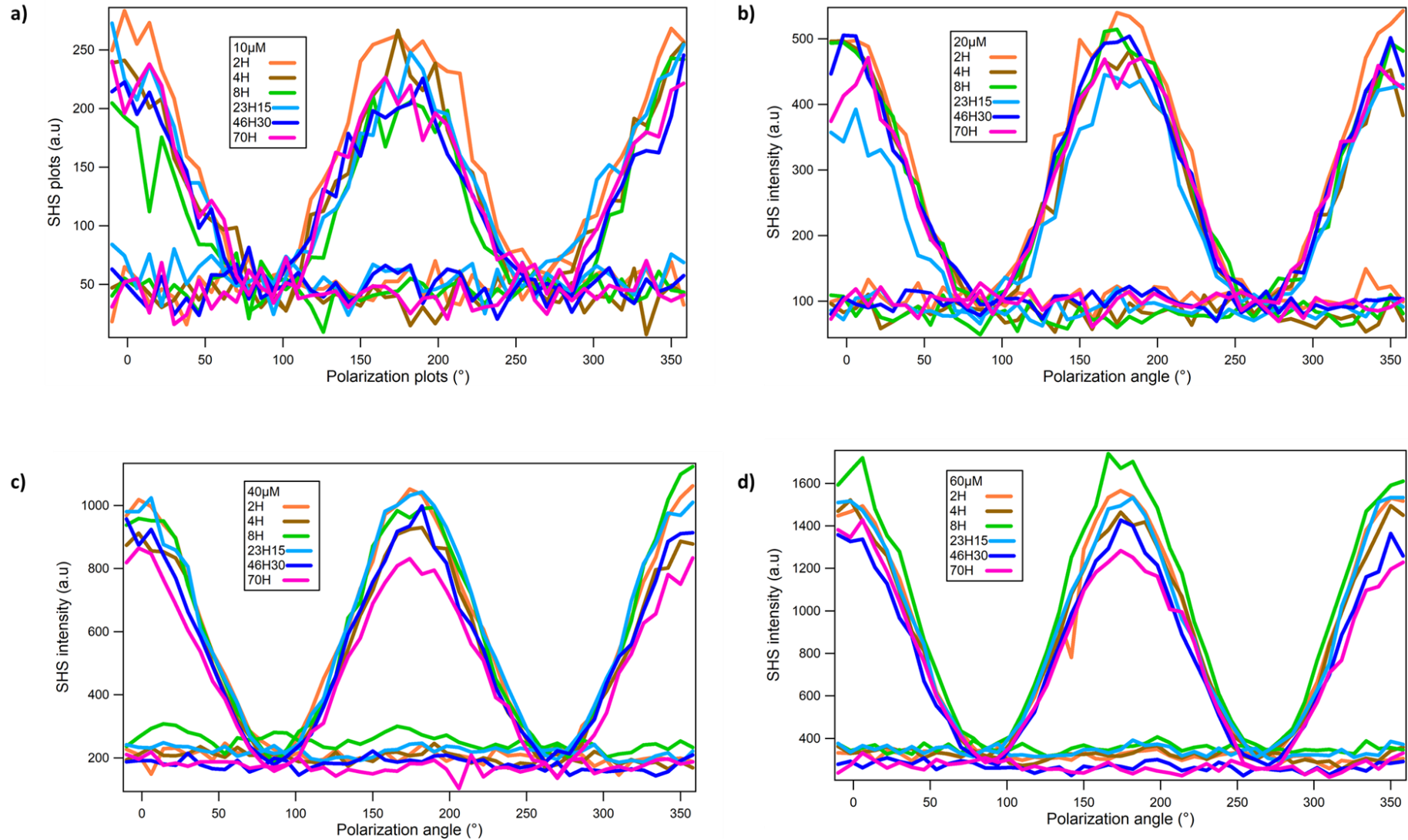


Figure 57 : SHS plots of four different concentration of sDiA adsorbed onto 0.05 g/l commercial FAU ( $Si/Al = 15$ ) measured at different time in ethanol medium; a) 10  $\mu M$ , b) 20  $\mu M$ , c) 40  $\mu M$  and d) 60  $\mu M$ .

### 2.4.3 In 50% water- 50% ethanol medium

As stated before, it seems that aggregation of particles with time appears only in water medium and not in ethanol. To evaluate the ethanol effect on the aggregation and the impact on adsorption capacity, similar experiments were repeated in the presence of a mixture of 50% water and 50% ethanol. The adsorption capacity of sDiA toward FAU in the solvent mixture is reported in Figure 58. The adsorption capacity ranges between 380 and 200  $\mu\text{mol/g}$  which is in the range between the value obtained in water and the one in ethanol medium. In addition, the Figure 59 shows the polarization plots and their fluctuations. For example, at a low concentration, 10  $\mu\text{M}$ , the SHS intensity is maximum for 2H and minimum for 70H. However, at 20  $\mu\text{M}$  the maximum intensity is obtained in the case of 7H30. No clear tendency is observed in the mixture of water and ethanol. This can be explained by the competition between the adsorption of sDiA and adsorption of ethanol since sDiA is more soluble in ethanol (16 g/l) than in water (2.6 g/l). This implies that sDiA prefers to be with ethanol instead of being adsorbed. To have a clear conclusion, an isotherm at a fixed time will be performed and explained later to clarify this point.

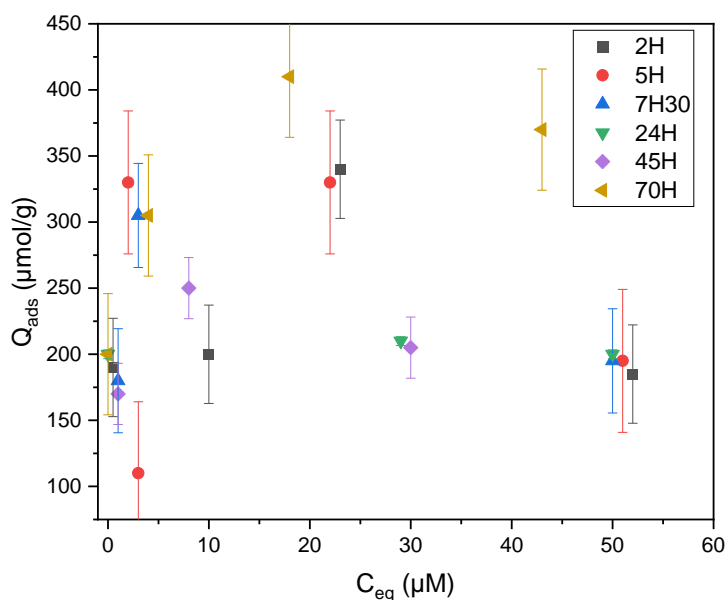


Figure 58 : Effect of time on the adsorption capacity of sDiA onto 0.05 g/l commercial FAU (Si/Al = 15) in mixture of 50% water-50% ethanol medium using SHS.



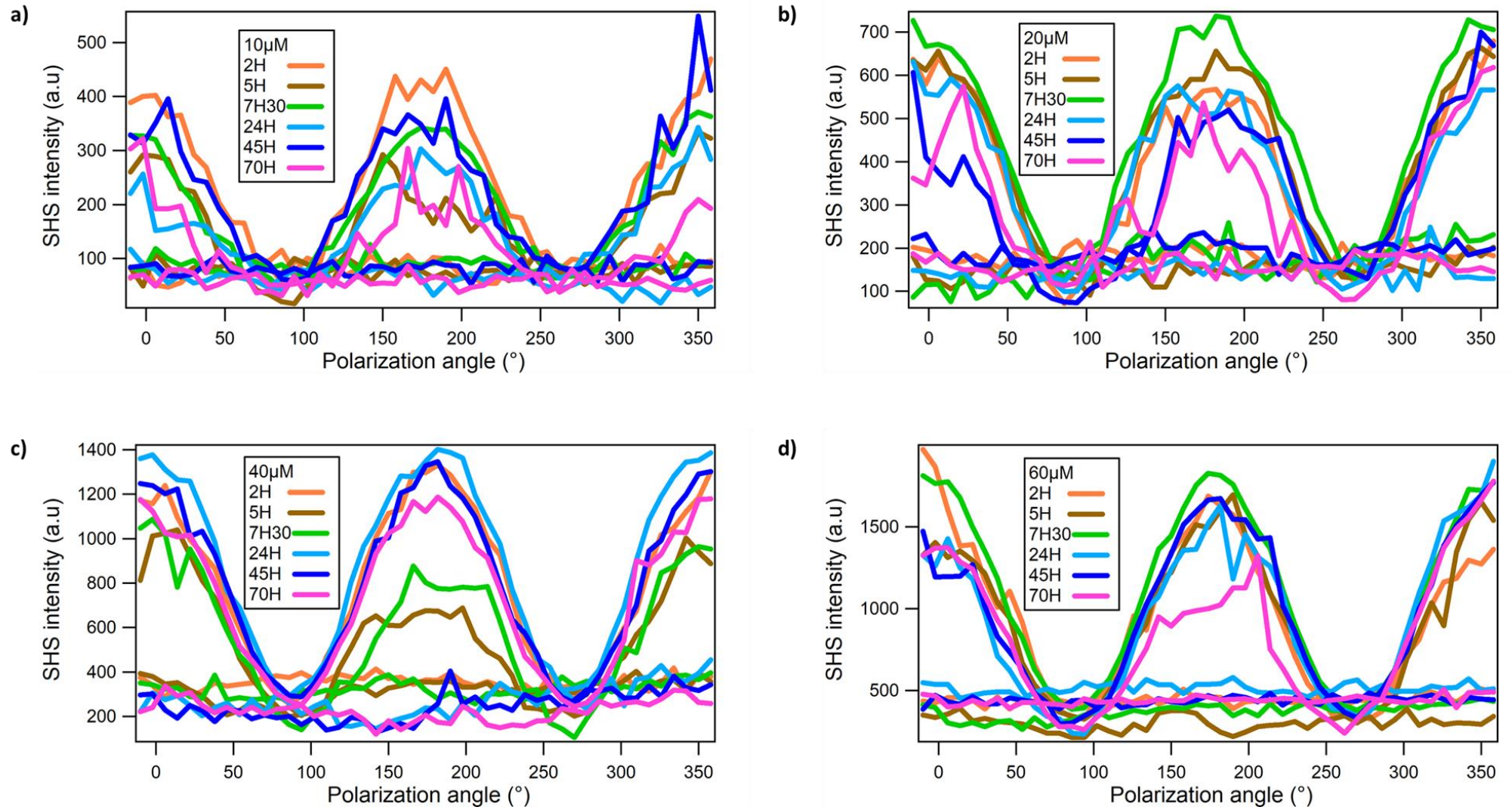


Figure 59 : SHS plots of four different concentration of sDiA adsorbed onto 0.05 g/l commercial FAU (Si/Al = 15) measured at different time in mixture of 50% water- 50% ethanol medium; a) 10 μM, b) 20 μM, c) 40 μM and d) 60 μM.

## 2.5 Effect of sonication

A fluctuation in the SHS plots and a modification in the intensity of vertical and horizontal polarization were observed in the system due to the presence of aggregates of FAU particles as already observed by DLS measurements. For this reason, sonication of the suspension was applied to disperse the aggregates and to check if this fluctuation is due to the presence of aggregates. The sonication effect was studied by preparing several samples and studying sDiA adsorption onto 0.05 g/l FAU at different sDiA concentrations with and without sonication. Suspensions were sonicated for 10 minutes and then kept under constant stirring at 25 °C. The results of the samples measured by SHS are shown in Figure 60. The SHS plots of samples with the same concentration of sDiA with and without sonication show similar behavior with the same SHS intensity for both suspension and supernatant. Therefore, no effect of sonication is observed on SHS plots but sonication is a better to ensure dispersion the aggregates formed with time.

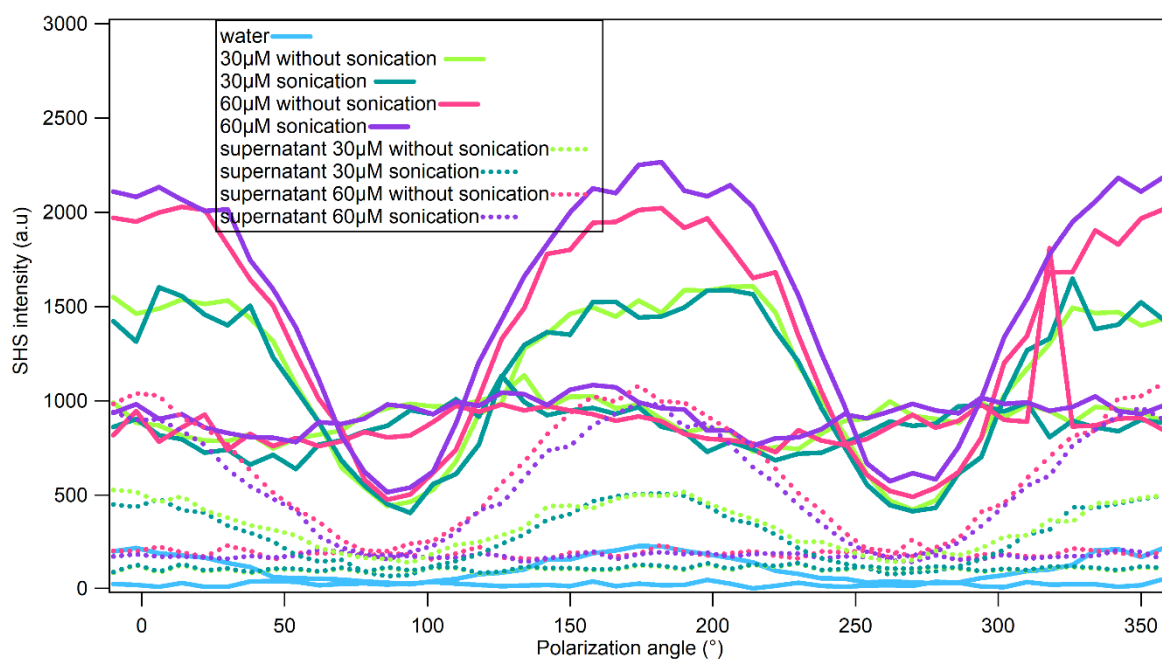


Figure 60 : SHS plot of sDiA adsorbed onto 0.05 g/l commercial FAU (Si/Al = 15) prepared in water medium at two different sDiA concentrations with and without sonication. The measurement done for suspension and supernatant, the solid line and the dotted line respectively.

## 2.6 Effect of ionic strength

The presence of salt in the solution might change ionic strength when the concentration varies a lot. This modification of ionic strength may induce changes in the surface charge concerning the surface sites with variable charge (in opposition to permanent charge), and then contribute to modification of the adsorption process depending on the electrostatic forces between the adsorbent surface and adsorbate ions. If the electrostatic forces are attractive, the adsorption capacity will decrease by increasing the ionic strength.

- UV-Vis approach

To study this effect, the adsorption isotherm of sDiA was determined using  $\text{NaNO}_3$  at various concentrations as a background electrolyte. These isotherms were carried out using the powdered form protocol described previously with 1 mM of sDiA mother solution prepared in 0.01 and 10 mM of  $\text{NaNO}_3$  background electrolyte. The pH was free and constant and equal to 4.5. The adsorption capacity of sDiA are shown on Figure 61. It is noticed that the sorption efficiencies in water and at the 2 various ionic strengths ( $\text{NaNO}_3$  0.01 and 10 mM) are similar. The effect of ionic strength is considered negligible at both concentrations. This corresponds with the results from Han et al.<sup>150</sup> where they didn't observe any effect of ionic strength on the adsorption of methylene green by Z9-600 using NaCl salt at various concentrations. Miyah et al.<sup>151</sup> also considered the small decrease in the adsorption capacity of MB on low-cost adsorbent (walnut shells powder) in the presence of KCl, NaCl, and  $\text{CaCl}_2$  negligible. This is due to the competition between the metal ions and MB cationic dyes from an aqueous solution.

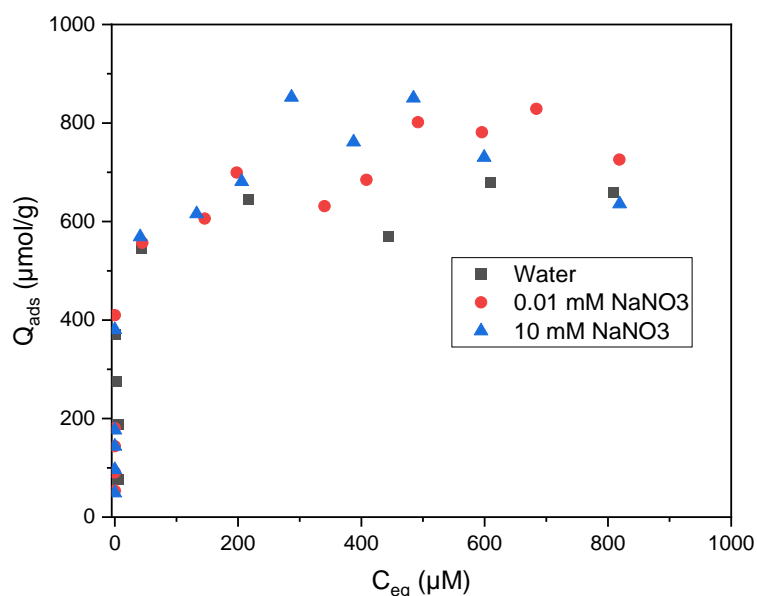


Figure 61 : Adsorption isotherm of sDiA on commercial FAU (Si/Al = 15) prepared in Ultra-Pure water or in sodium nitrate ( $\text{NaNO}_3$ ) at various ionic strengths.

- SHS approach

Only one concentration of sDiA with a different concentration of  $\text{NaNO}_3$  is measured in suspension with 0.05 g/l commercial FAU. It is clearly seen in Figure 62 that for the same concentration of sDiA the ionic strength decreases the SHS intensity especially at a high concentration of  $\text{NaNO}_3$ . For 2.5 and 10 mM  $\text{NaNO}_3$ , there is no effect of the ionic strength which is in line with the isotherm characterized previously using UV. However, at a very high concentration of  $\text{NaNO}_3$ , 100 mM, the ionic strength slightly decreases the SHS intensity. Therefore, the adsorption capacity is slightly decreased with increasing ionic strength. This can be explained by the shielding effect of the FAU surface charge due to the presence of ionic strength that diminishes the adsorption of dyes. This has also been observed by Huang et al.<sup>152</sup> who have evidenced that when increasing ionic strength ( $\text{NaCl}$ ) the adsorption capacity of MB onto zeolite is reduced. Nevertheless, the adsorption capacity can be enhanced in the presence of ionic strength as in the work of Goswami et al.<sup>153</sup> which reported the enhancement of Rhodamine-B and orange-G adsorption onto modified activated carbon. This is due to the fact that ionic strength may allow the dyes dissociation by helping their protonation. Chiou et al.<sup>154</sup> and Jiang et al.<sup>155</sup> also observed a decrease in the adsorption of methyl orange by chitosan/maghemite nanocomposites in the presence of different electrolytes. They explained this

decrease by the competitive adsorption between the inorganic anions and the anionic dye on the surface of the adsorbent. Therefore, the effect of the ionic strength on the adsorption process depends on the host and the guest interaction. In some cases, no effect can be observed, while in other cases, the ionic strength can influence the adsorption capacity either by increasing or decreasing it.

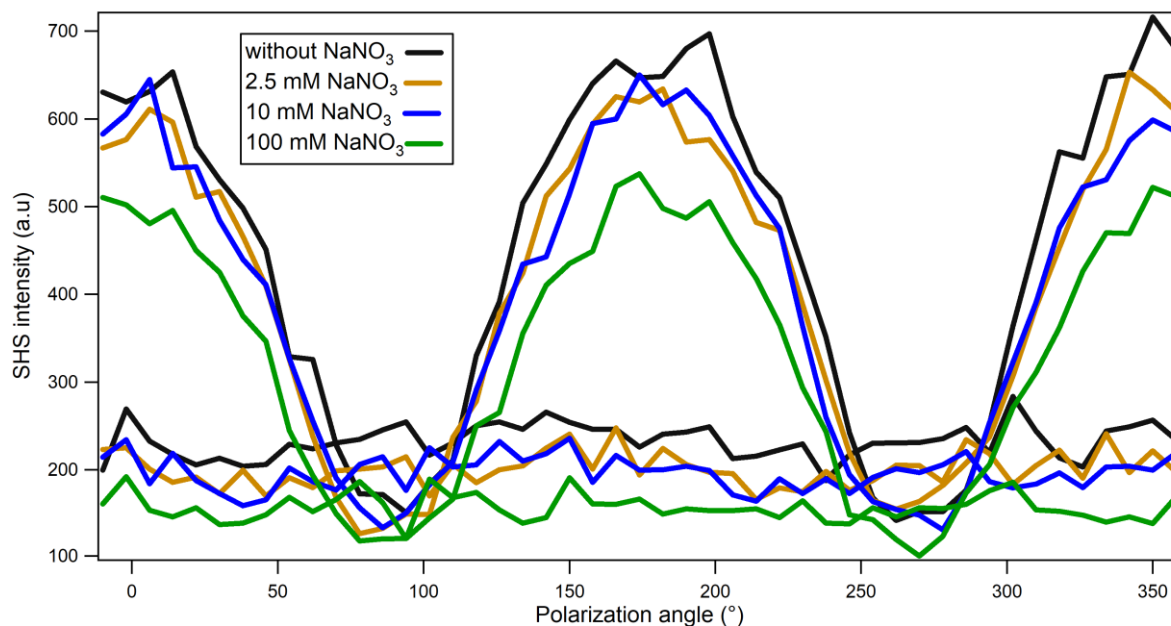


Figure 62 : SHS for sDiA 20  $\mu\text{M}$  in suspension with 0.05 g/l commercial FAU (Si/Al = 15) prepared in Ultra-Pure water or in sodium nitrate ( $\text{NaNO}_3$ ) at various ionic strengths.

## 2.7 Effect of the presence of particles on SHS plot

A modification in the intensity of vertical and horizontal polarization leads to a difference between both polarization in which these polarizations must intersect at the minimum intensity vertical polarization and maximum intensity of horizontal polarization. To check the source of this modification, different ways of filtration were tested.

SHS measurements were performed for sDiA dyes adsorbed onto FAU after filtration. The SHS plots are depicted in Figure 63. Usually, filtration is done using a PP filter of 25 mm pores 0.22  $\mu\text{m}$ . The result of the SHS measurement for the PP filter shows a higher intensity for the minimum vertical polarization that gave a difference between both polarization (vertical and horizontal). This is probably due to the presence of particles remaining after filtration. In order to solve this problem, two ways are provided using different types of filters. The first way is done by using other filters having the following specifications: GHP membrane, 13 mm pores 0.20  $\mu\text{m}$  were used to separate the solution. This filter

differs from the first one by the type of polymer used and the pore size. The SHS plots obtained using this filter doesn't show a shift between the minimum intensity of horizontal polarization and the maximum intensity of vertical polarization. This filter solves completely the problem, however, due to its high cost we have looked at other alternatives. Therefore, the other way was to centrifuge the solution for 1 hour then filter it with a syringe filter with the following specification: PP, 25 mm pores 0.22  $\mu\text{m}$ . The test gives a similar result to that of the GHP filter. In conclusion, the presence of particles in the supernatant has a great impact on the SHS plots. Although, these results agree with the results obtained by DLS measurements where fine particles are still present after filtration.

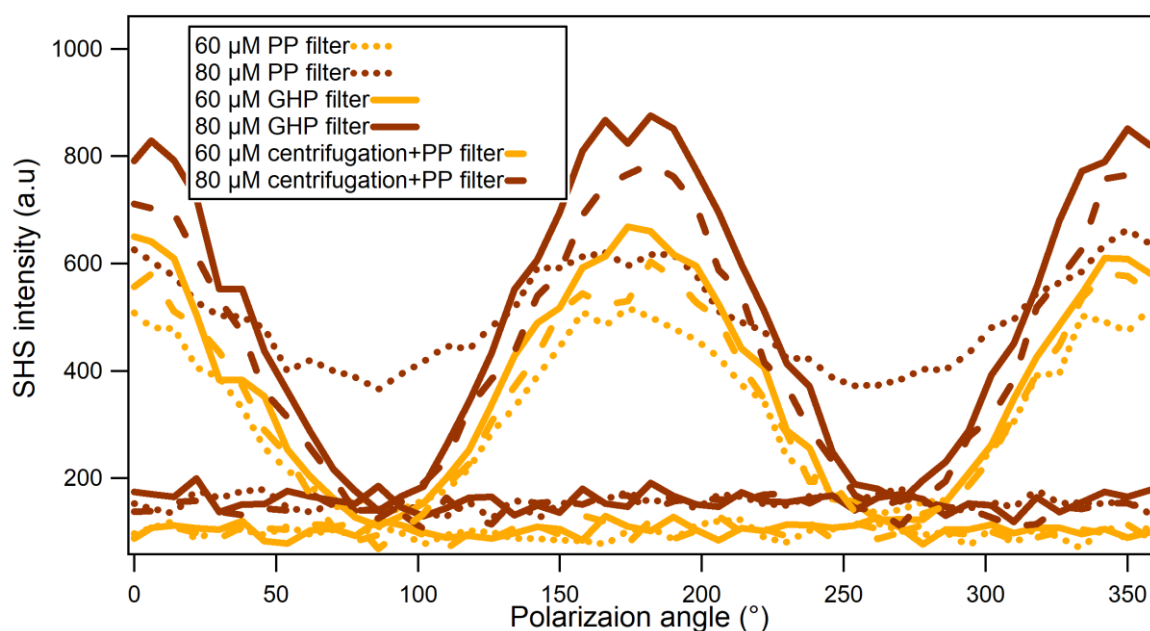


*Figure 63 : SHS plots for sDiA supernatant after filtration at different concentration.*

To summarize, the sorption process can be affected by several factors such as the presence of aggregates that formed after exposing either the FAU suspension or the sDiA and FAU suspension for a long time. In addition, it can be also affected by varying the solid/liquid ratio. These factors lead to a decrease in the sorption capacity.

### 3 Adsorption of organic molecules onto Faujasite

The aim of those studies is to understand adsorption fundamental phenomena on zeolites for a better understanding of depollution processes. In this section, we focused on the capacity of FAU to

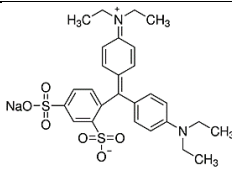
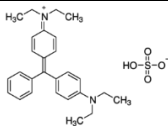
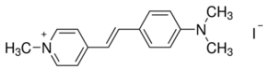
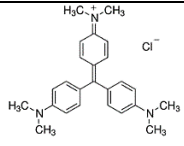
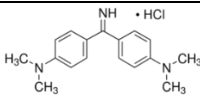
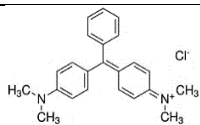
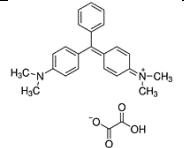
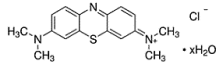
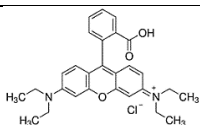


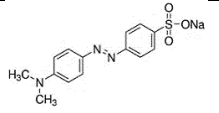
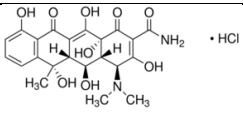
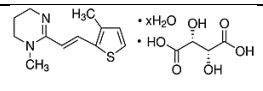
adsorb the anionic, neutral, cationic dyes, drugs, and pesticides. The adsorption isotherm has been determined in an aqueous solution using UV-Vis and SHS technique depending on the systems.

### 3.1 Organic molecules panel

Organic molecules with different charges were selected to study their adsorption capacity toward FAU. Several cationic dyes have been adsorbed onto commercial zeolite FAU bearing different functional groups of different sizes. The characteristics of these dyes are reported in Table 7.

Table 7 : Chemical properties of organic molecules.

Type	Organic molecules	Abbreviations	Structure	Purity (%)	Length (Å)	Width (Å)	ΔpH
Zwitterion	Blue patent	BP		50%	14	7	+2
Cation	Brilliant green	BG		90%	14	5	+1.5
	trans-4-[4-(Dimethylamino)styryl]-1-methylpyridinium iodide	sDiA		98%	14.5	4.3	+1.5
	Crystal violet	CV		90%	16	15	+1
	Auramine-O	AO		85%	13	8	+0.7
	Malachite green chloride	MG.Cl			15	10	+1.7
	Malachite green oxalate	MG.oxalate			15	10	+1.7
	Methylene blue	MB		97%	14	5	+1.4
	Rhodamine B	Rh-B		95%	20.5	16	+3.4

Anion	Methyl orange	MO		85%	17	4	-0.3
Neutral Drugs	Oxytetracycline HCl	OTC			17	7	+2
Neutral Pesticides	Morantel tartrate Hydrate	MT			10.5	5.5	+1.5

The adsorption isotherms for different organic molecules were established using the protocol of powdered FAU of 5 mg in a total volume of 20 ml. These isotherms are depicted in Figure 64. Each color refers to a definite molecular charge. In addition, the maximum adsorption capacity for each dye has been shown in the histogram presented in Figure 65.

Methylene blue (MB) has the highest adsorption capacity (800  $\mu\text{mol/g}$ ) compared to other dyes and organic molecules such as pesticides, and drugs. These results are in correspondence with the results obtained by Xiao et al.<sup>149</sup> where the elimination of MB by Cd-MOF is higher than other molecules, cationic having bulky sizes (crystal violet, rhodamine-B and malachite green), anionic (methyl orange) and neutral (neutral red). In this thesis, no study of the pH effect was carried out. Nevertheless, the pH changes have been measured. The pH difference between the first and the last point of the isotherm is related to pH changes induced by the mixture of the various solution, by the amount of dyes adsorbed, and the possible released of other counterions. It is indicated in Table 7 and noted as  $\Delta\text{pH}$ . As the initial concentration increases (and thus the equilibrium concentration), the proportion of the dye's mother solution is higher and higher, and the pH of the final suspension is similar to the free pH of the mother solution. The  $\Delta\text{pH}$  described in Table 7 are mainly explained by the difference between the natural pH of the suspension without dye and the free pH of the mother solution.



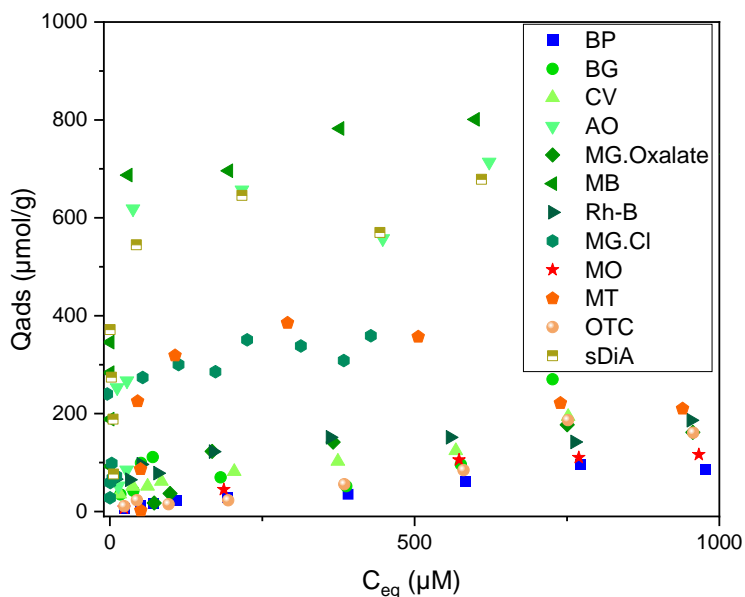


Figure 64 : Adsorption isotherms of organic molecules prepared using protocol 1 in water solvent. The symbols representing the isotherms are: ■ for BP, ● for BG, ▲ for CV, ▼ for AO, ◆ for MG.Oxalate, ◀ for MB, ▶ for Rh-B, ● for MG.Cl, ★ for MO, ◆ for MT, ● for OTC, ■ for sDiA.

The adsorption capacity of MB in comparison with other studies is depicted in Table 8. Methyl orange (MO), which is an anionic dye, shows a low adsorption capacity due to the electrostatic repulsion between the dye with the negatively charged FAU. A similar result was obtained by Kaur et al.<sup>156</sup> and Jin et al.<sup>157</sup> where they observed a low adsorption capacity for MO toward MOF and orange II toward zeolite, respectively. Additional studies on anionic dyes were not considered since the adsorption is favored by electrostatic interactions thus the size will not have a significant role in the improvement of the adsorption capacity.

In addition, the size of Morantel tartrate Hydrate (MT) is between the size of MB and auramine-O (AO) but MT is neutral. The adsorption capacity is 370 and 650  $\mu\text{mol/g}$  for MT and AO respectively. This signifies that MT has high capacity however it is still less than the capacity of MB and AO. Therefore, FAU has a high adsorption performance to cationic and neutral molecules compared to anionic molecules.

Table 8 : Maximum adsorption capacity of different adsorbent for methylene blue.

Adsorbent	Adsorption capacity (mmol/g)	Reference
Cd-MOF	1.8	149
Mordenite zeolite	0.08	158
Mordenite nanocrystal	0.12	158
Zeolite fly ash (ZFA)	0.2	159
Activated carbon	0.34	160
Modified-ZSM-5 zeolite	0.0388	157
Zeolite Y (FAU)	0.8	This study

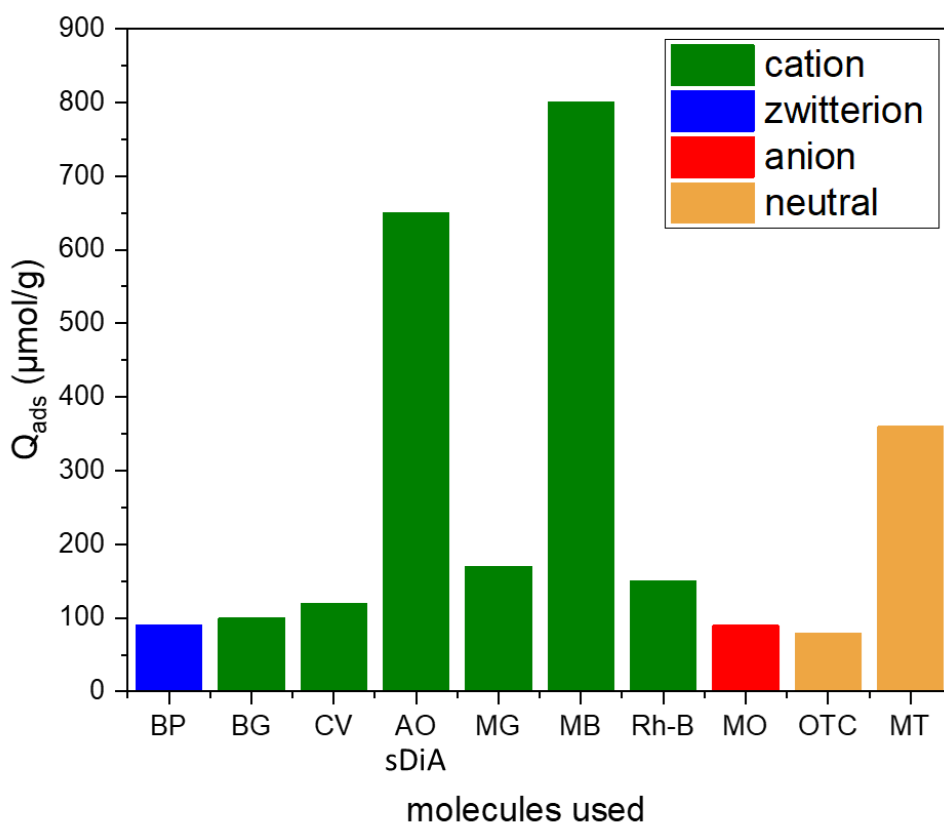


Figure 65 : Histogram showing the adsorption capacity of different organic molecules onto FAU (Si/Al=15) depending on their ionic state.

### 3.2 Charge impact

Four organic molecules were used to see the impact of the charge on the adsorption capacity. Figure 66 shows the adsorption capacity as a function of the equilibrium concentration for these four dyes. MB, the cationic molecule, shows the highest adsorption capacity which is 700  $\mu\text{mol/g}$ . It is observed that both MO and Oxytetracycline HCl (OTC), the anionic and neutral molecules, respectively, have an equal adsorption capacity of approximately 100  $\mu\text{mol/g}$  and similar affinity. This capacity is lower than that observed for the MT (neutral molecule). Therefore, cationic dyes exhibit higher

adsorption capacity towards FAU, the negatively surface charge, compared to anionic and neutral dyes. Neutral dyes also show high sorption capacity compared to the anionic ones depending on their size.

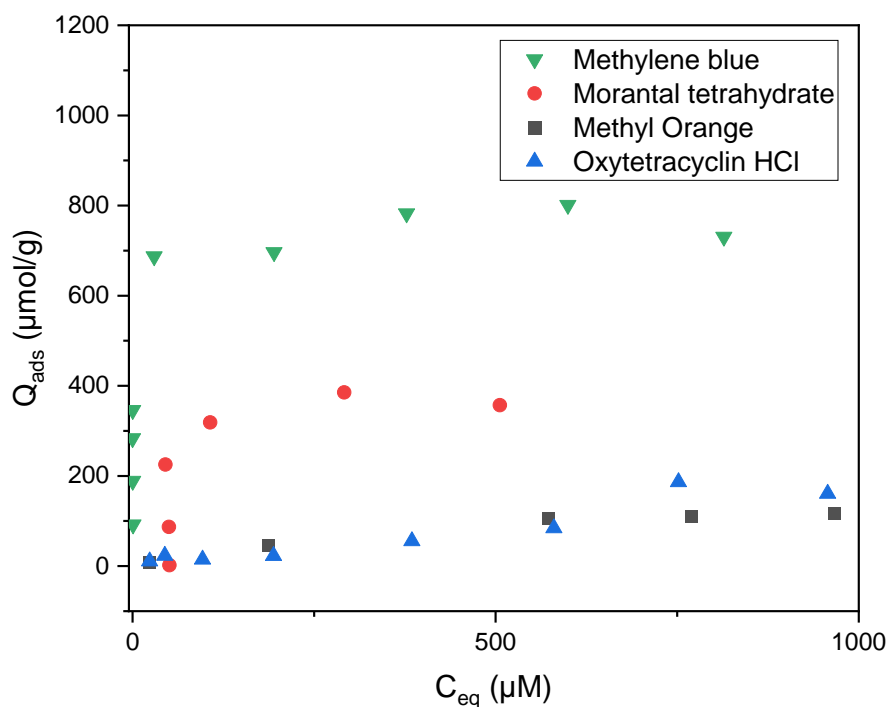


Figure 66 : Comparison between the adsorption isotherm of neutral OTC and MT and anion MO compounds towards FAU.

### 3.3 Size effect

The evolution of the adsorbing power of various molecules on FAU was studied using the protocol with powdered form. The initial concentration of these dyes was set at 1 mM. Figure 64 and Figure 65 represent the variation of the adsorption isotherm and maximum capacity of these molecules by FAU. It is notably seen that the size has a large impact on the adsorption capacity. For example, malachite green (MG), rhodamine-B (Rh-B), crystal violet (CV), and brilliant green (BG) are characterized by having three phenyl rings that differ from each other by their functional groups thus they are referred to as 3D molecules. These dyes, on one hand, have a comparable size which is bigger than the FAU supercage (13 Å). On the other hand, the size of auramine-O (AO) and MB dyes are smaller than the FAU supercage. These dyes are specified as 2D molecules. The adsorption capacity of

3D molecules is lower than the capacity of 2D molecules which is 170, 130, 120, and 100  $\mu\text{mol/g}$  for MG, Rh-B, CV, and BG respectively, and 650 and 800  $\mu\text{mol/g}$  for AO and MB respectively. Therefore, as the size becomes bulkier, the adsorption capacity becomes lower. Size effect has a large effect on the adsorption capacity. Thus, the FAU adsorbents exhibited size-selective adsorption on dye molecules that agrees with the results of Pereira et al.<sup>161</sup> where the adsorption capacity onto zeolite is larger for MB, the dye with the smallest molecular size, compared to safranin and MG.

From the bulky size of the molecules and their low sorption capacity, the adsorption of 3D dyes like CV, Rh-B ... occurs at the external surface due to pore blocking. However, the size of 2D dyes allows them to enter the pores and thus produce high adsorption capacity as well as the possibility to change their conformation or orientation during the adsorption process due to the presence of free space.

### ***3.4 Effect of counter ion on Malachite green adsorption***

Malachite green (MG) is a cationic dye used for the dyestuff industry as well as the pigment industry. MG is supplied with two anionic counterions which refer to MG chloride and MG oxalate. The anionic form does not affect the color.

The presence of different counterions bearing different properties might affect the adsorption capacity. The counterions might have different thermodynamic of solvation thus they might affect the adsorption behavior of the dye. To evaluate this impact, two isotherms were established under the same experimental conditions. These isotherms are shown in Figure 67. The characteristic of both MG and the pH variation of both isotherms are the same as shown in Table 7. The adsorption capacity of MG.Cl is 350  $\mu\text{mol/g}$  while 150 $\mu\text{mol/g}$  for MG.Oxalate. Therefore, MG.Cl has a high affinity and high adsorption capacity compared to MG.Oxalate. This can be explained by two hypotheses. The first one is the high affinity of oxalate towards MG compared to FAU towards MG. In another word, a strong interaction occurs between the oxalate group and tertiary amine group present in MG compared to that found with Cl. This hypothesis can affect indirectly the dissociation and the solubility of MG. However, MG is water soluble<sup>162</sup> in both cases, oxalate, and Cl. So, this hypothesis is under doubt. The second hypothesis depends on the size of the counterion. Oxalate has a bigger size compared to Cl, so oxalate can interact with the hydrogen, the counterion of FAU, and leads to the active site blockage. In other words, the interaction between oxalate and H may be stronger than MG and FAU due to the presence of a highly negative charge of oxalate and its four oxygen. Therefore, the adsorption capacity is lower in the case of oxalate counter ion.

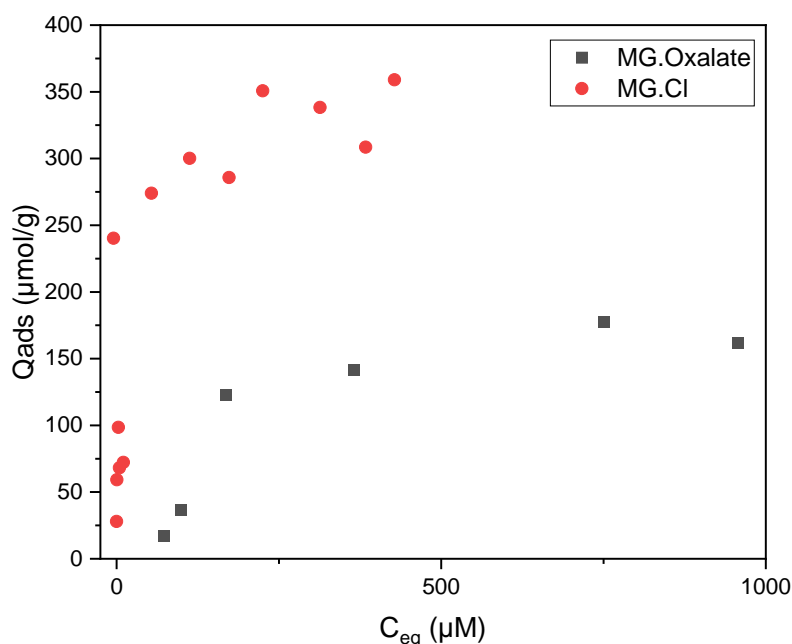


Figure 67 : Effect of counterion on the adsorption isotherm of MG towards FAU.

### 3.5 Effect of ethanol on sDiA adsorption to FAU

Adsorption isotherm for sDiA toward FAU in water, ethanol, and mixture of 50%-50% water-ethanol is depicted in Figure 68. The maximum adsorption capacity of sDiA toward FAU is 600, 470, and 250  $\mu\text{mol/g}$  in water, mixture, and ethanol respectively. In the mixture of ethanol and water, the adsorption capacity is closer to water than to ethanol. In this mixture, as the equilibrium concentration of sDiA increases, the adsorption capacity continues to increase, and the plateau cannot be reached. This can be demonstrated by two hypotheses. The first one is explained by the number of adsorption sites available depending on the solvent nature which is referred to as Bronsted acid site. These sites can be active or not depending on the solvent used. The Bronsted acid sites are more active in water than in ethanol.<sup>163</sup> Thus, the adsorption capacity is higher in the case of water. Therefore, in the presence of a mixture of water and ethanol the Bronsted acid sites are higher than ethanol alone due to the presence of water. The second hypothesis is related to the solubility of dye. sDiA is more soluble in ethanol than in water which makes sDiA prefer to be with ethanol instead of being adsorbed in the FAU material. In another word, there is a competition between sDiA and ethanol to adsorb onto FAU. Therefore, sDiA is better solvated in ethanol so it interacts less with hydrophilic zeolite which causes a decrease in the adsorption capacity onto FAU. This hypothesis can be explained by the result obtained by Zhang et al.<sup>164</sup> where the sorption capacity of ethanol/water mixture toward various zeolites increases with decreasing ethanol concentration.

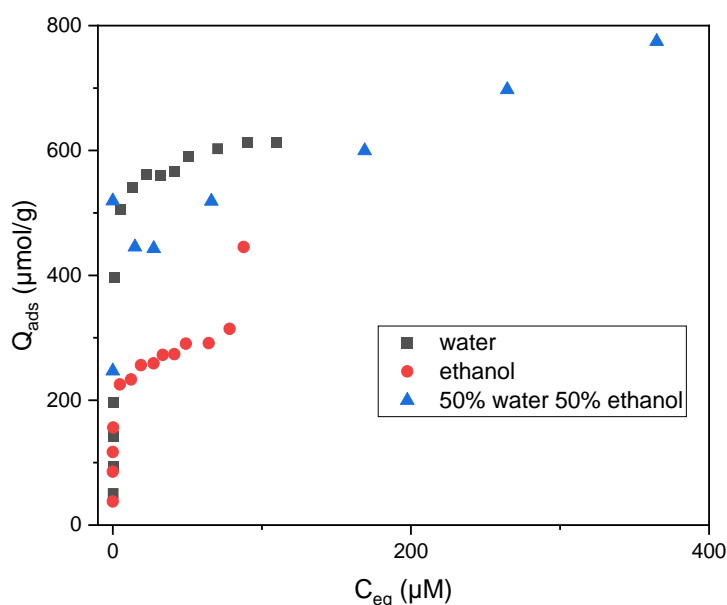


Figure 68 : Effect of solvents (water, ethanol, and mixture of 50% water 50% ethanol) on the adsorption capacity of sDiA onto commercial FAU of Si/Al ratio 15.

The surface charge and the pore diameter of the material permit the selective adsorption of molecules with cationic charge and small size (2D molecules). The solvent medium also affects the adsorption capacity depending on the solvation of the dye. If the dye is more solvated, the adsorption capacity is low.

#### 4 Comparison between FAU-3 and Al-MCM-41

Modification of FAU with dissolution-recrystallization process leads to the formation of ordered mesoporous phase with an amorphous wall as Al-MCM-41. FAU-3 is the FAU obtained after pore modification using a high concentration alkaline solution ( $\text{NaOH/Si}=0.25$ ). The microporous volume of FAU-3 obtained after modification is somehow negligible. Therefore, the majority of pores of FAU-3 are mesopores. For this reason, mesoporous material obtained from the microporous origin will be compared with the originally mesoporous material. In comparison, Al-MCM-41 has only mesopores which has been synthesized by our collaborator, Lucie Desmurs. The same protocol as for hierarchical FAU was used to synthesize MCM-41 materials by replacing FAU-Y by fumed silica and Aerosil 200, purchased from Degussa. The mesoporous volume of FAU-3 is 0.67 mL/g greater than that of Al-MCM-41 and is 0.52 mL/g. The isotherms of sDiA onto FAU-3 and Al-MCM-41 are shown in Figure 69. The affinity and the adsorption capacity are similar for both materials and the  $Q_{max}$  are around 400  $\mu\text{mol/g}$ . The mesopore diameter in both materials is around 4 nm which is mentioned by Mehlhorn et al.<sup>30</sup> FAU-

3 and Al-MCM-41 possess similar structure and textural properties which is confirmed by XRD at small angle and nitrogen sorption isotherm in addition to their sorption behavior. Therefore, they are considered as a material having the same architecture.

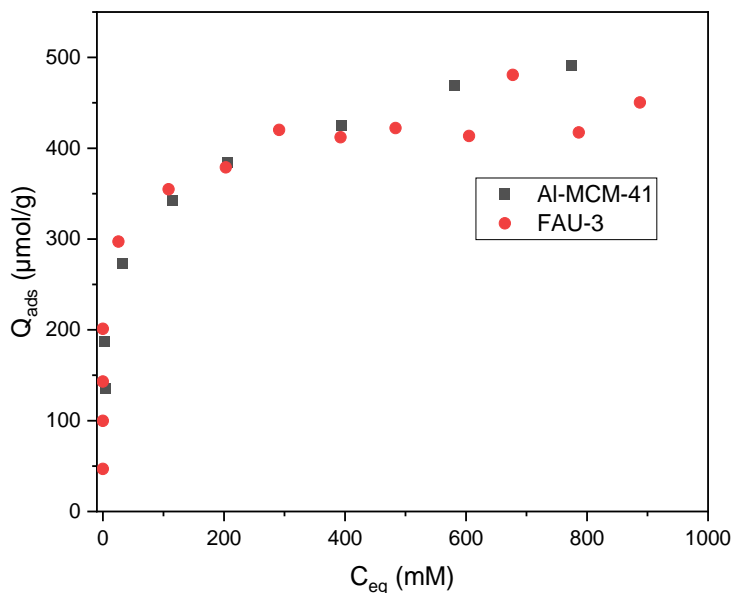


Figure 69 : Sorption isotherm for sDiA towards FAU-3 (the highly modified material) and Al-MCM-41 (mesoporous material) in water medium, red and black curves respectively.

SHS plots for both materials are shown in Figure 70. Both have similar behavior in SHS with the same SHS shape and intensity for both polarization (vertical and horizontal). So, FAU-3 and Al-MCM-41 are considered similar materials in terms of architecture, texture, and adsorption properties.

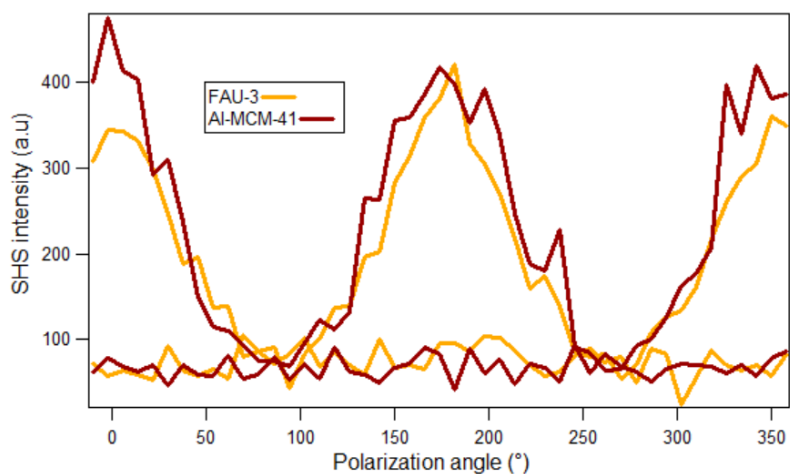


Figure 70 : SHS polarization plot for 20  $\mu\text{M}$  sDiA adsorbed onto FAU-3 and Al-MCM-41, orange and dark red plots respectively.



FAU-3 has similar architectural and textural properties compared to Al-MCM-41 which leads to a similar sorption behavior. The mesoporosity in our system is considered the same as in Al-MCM-41, therefore, Al-MCM-41 can be a reference to our system.

## 5 Comparison between adsorption of dyes using ITC approach

ITC measurements were carried out for several dyes to compare the enthalpy of adsorption with the adsorption isotherms. All ITC measurements were done in water at free pH. Malachite green, sDiA, and auramine-O were measured using high concentrations for the injection which are 14, 22, and 20 mM respectively with 5 mg of FAU in 8ml ultra-pure water. Unfortunately, due to the low solubility of these dyes, these concentrations are too high and cause sedimentation of dyes aggregates in the injection syringe during ITC measurement. To solve the insolubility problem, the measurements were repeated using lower concentration, at 2.4 mM for Auramine-O and sDiA with 1 mg of FAU, and keeping the other parameters unchanged.

The reason behind choosing specifically these dyes to do thermodynamic measurements is that they exhibit similar adsorption isotherm; i.e. similar adsorption capacity (Figure 71). From the isotherm, the affinity of both dyes toward the material is constant which means that Gibbs free energy ( $\Delta G$ ) is constant for both systems. Therefore, the thermodynamic of the system is governed by enthalpy ( $\Delta H$ ) and entropy ( $\Delta S$ ). The enthalpy change is negative for both dyes which means the adsorption process is exothermic. The enthalpy change is calculated from the slope of the heat displacement as a function of adsorption quantity (Figure 72). The graph is composed of two regimes, with two linear parts on the curves. The slope of both regimes is calculated and placed in Table 9. We assume that the first molecules are adsorbed in micropores since they are better stabilized. Thus, the first regime (adsorption quantity  $< 0.2$  mmol/g) probably corresponds to the micropores where there are more active sites and the latter to the mesopore. Since both have similar adsorption capacities so they might have different strengths of interaction. From the obtained value of the enthalpy changes and the shape of the curve, we can see that sDiA has a steeper slope than auramine-O. This shows that the strength of the interaction is stronger in the case of sDiA compared to auramine-O. Since  $\Delta H$  is higher in sDiA (in absolute value) therefore the entropy ( $\Delta S$ ) is lower. This means that the disorder is lower in sDiA than AO. Therefore, sDiA is more organized in FAU compared to AO.

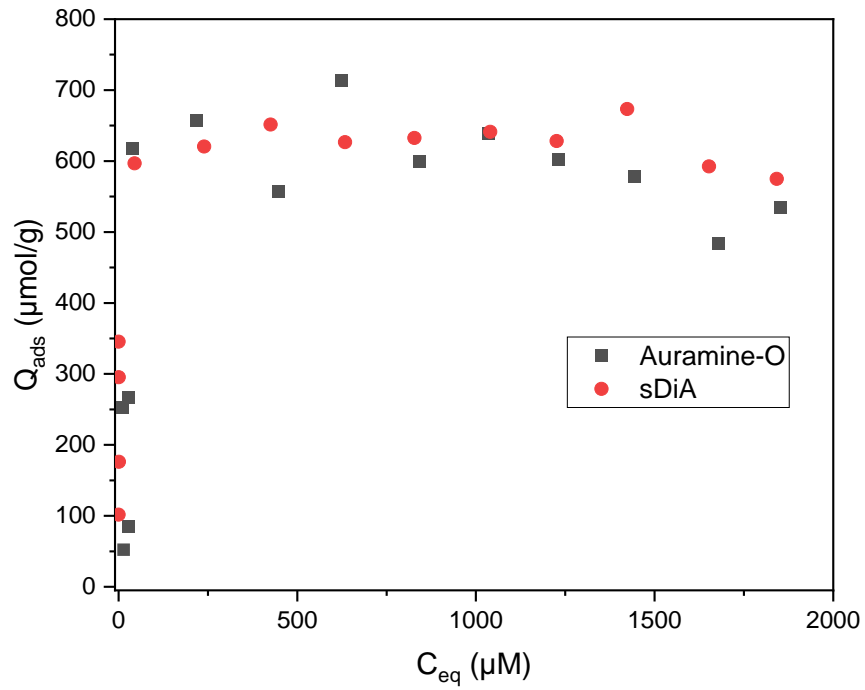


Figure 71 : Adsorption isotherm of sDiA and auramine-O with commercial FAU (Si/Al = 15).

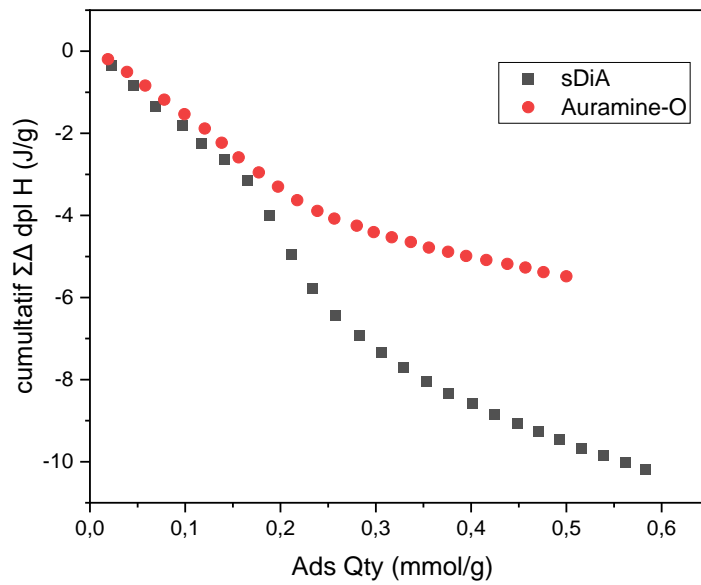


Figure 72 :The enthalpy of displacement of dyes calculated from ITC. The experimental conditions are 2.4 mM of Auramine-O (red) and sDiA (black) onto 1mg FAU at free pH.

Table 9 : Displacement enthalpy for the adsorption of dyes onto FAU having similar adsorption capacity.

Dyes / 1mg FAU	$\Delta H_{dpl}$ first regime (kJ/mol)	$\Delta H_{dpl}$ second regime (kJ/mol)
Auramine-O	-16.5	-5.5
sDiA	-22.5	-11.5

The strength of interaction varies from one molecule to another even if they have similar adsorption capacities. These modifications of the displacement enthalpy reveal the dependence of the strength of interaction with depending on the organization of these molecules at the solid/liquid interface. When the enthalpy change is higher in absolute value, the strength of the interaction is strong, and thus the highly organized system is observed.

## 6 Conclusion

The complementary analysis of FAU, FAU-2a, FAU-2b and Al-MCM-41 proves that the modification of FAU by alkaline treatment affects the surface chemistry of the material. It leads to a decrease in the microporous volume and increase in mesoporous volume as well as a decrease in  $Q^4$  environment and increase in  $Q^3$  environment. Al-MCM-41 has similar behavior including architecture, performance and sorption properties as FAU-3 (the highly modified FAU).

The results of this study show that commercial faujasite has a remarkable adsorption capacity concerning the removal of organic molecules, whether they are cations or neutral provided that it has a smaller size compared to the size of the pores.

Several parameters have an impact on the adsorption behavior. The presence of ethanol solvent leads to a decrease in the sorption capacity. Effect of solid/liquid ratio, sonication, ionic strength was also studied. Sonication prevents aggregation so it should be done in order to homogenize the suspension. The high S/L ratio leads to a decrease in the sorption capacity. However, ionic strength doesn't generate any effect except a small decrease observed at a high concentration of the ionic strength. Therefore, care must be taken to perform well adsorption isotherm.

The results of this research were compared with the results published in the same domain and judged in agreement with most of them. In this chapter 3, those unpublished systematic studies allow us to explore many parameters in order to know better our systems. It permits to be confident on publishing or submitting two papers presented in chap 4 and 5.



References

1. Goscianska, J.; Marciniak, M.; Pietrzak, R., The effect of surface modification of mesoporous carbons on Auramine-O dye removal from water. *Adsorption* **2016**, *22* (4), 531-540.
2. Mehlhorn, D.; Rodriguez, J.; Cacciaguerra, T.; Andrei, R.-D.; Cammarano, C.; Guenneau, F.; Gedeon, A.; Coasne, B.; Thommes, M.; Minoux, D.; Aquino, C.; Dath, J.-P.; Fajula, F.; Galarneau, A., Revelation on the Complex Nature of Mesoporous Hierarchical FAU-Y Zeolites. *Langmuir* **2018**, *34* (38), 11414-11423.
3. Tarach, K.; Góra-Marek, K.; Tekla, J.; Brylewska, K.; Datka, J.; Mlekodaj, K.; Makowski, W.; Iguálada López, M. C.; Martínez Triguero, J.; Rey, F., Catalytic cracking performance of alkaline-treated zeolite Beta in the terms of acid sites properties and their accessibility. *Journal of Catalysis* **2014**, *312*, 46-57.
4. Gackowski, M.; Datka, J., Acid Properties of Hierarchical Zeolites Y. *Molecules* **2020**, *25* (5).
5. Akgül, M.; Karabakan, A., Promoted dye adsorption performance over desilicated natural zeolite. *Microporous and Mesoporous Materials* **2011**, *145* (1), 157-164.
6. Xiao, M.; Yue, H.-D.; Feng, X.-J.; Wang, Y.-T.; He, M.-Y.; Chen, Q.; Zhang, Z.-H., A double-layered neutral cadmium-organic framework for selective adsorption of cationic organic dyes through electrostatic affinity. *Journal of Solid State Chemistry* **2020**, *288*, 121376.
7. Han, T.-T.; Bai, H.-L.; Liu, Y.-Y.; Ma, J.-F., Synthesis of nanoporous cobalt/carbon materials by a carbonized zeolitic imidazolate framework-9 and adsorption of dyes. *New Journal of Chemistry* **2018**, *42* (1), 717-724.
8. Miyah, Y.; Lahrichi, A.; Idrissi, M.; Khalil, A.; Zerrouq, F., Adsorption of methylene blue dye from aqueous solutions onto walnut shells powder: Equilibrium and kinetic studies. *Surfaces and Interfaces* **2018**, *11*, 74-81.
9. Huang, T.; Yan, M.; He, K.; Huang, Z.; Zeng, G.; Chen, A.; Peng, M.; Li, H.; Yuan, L.; Chen, G., Efficient removal of methylene blue from aqueous solutions using magnetic graphene oxide modified zeolite. *Journal of Colloid and Interface Science* **2019**, *543*, 43-51.
10. Goswami, M.; Phukan, P., Enhanced adsorption of cationic dyes using sulfonic acid modified activated carbon. *Journal of Environmental Chemical Engineering* **2017**, *5* (4), 3508-3517.
11. Chiou, M. S.; Li, H. Y., Adsorption behavior of reactive dye in aqueous solution on chemical cross-linked chitosan beads. *Chemosphere* **2003**, *50* (8), 1095-1105.
12. Jiang, R.; Fu, Y.-Q.; Zhu, H.-Y.; Yao, J.; Xiao, L., Removal of methyl orange from aqueous solutions by magnetic maghemite/chitosan nanocomposite films: Adsorption kinetics and equilibrium. *Journal of Applied Polymer Science* **2012**, *125* (S2), E540-E549.
13. Kaur, H.; Kumar, R.; Kumar, A.; Krishnan, V.; Koner, R. R., Trifunctional metal-organic platform for environmental remediation: structural features with peripheral hydroxyl groups facilitate adsorption, degradation and reduction processes. *Dalton Transactions* **2019**, *48* (3), 915-927.
14. Jin, X.; Jiang, M.-q.; Shan, X.-q.; Pei, Z.-g.; Chen, Z., Adsorption of methylene blue and orange II onto unmodified and surfactant-modified zeolite. *Journal of Colloid and Interface Science* **2008**, *328* (2), 243-247.
15. Sohrabnezhad, S.; Pourahmad, A., Comparison absorption of new methylene blue dye in zeolite and nanocrystal zeolite. *Desalination* **2010**, *256* (1), 84-89.
16. Sapawe, N.; Jalil, A. A.; Triwahyono, S.; Shah, M. I. A.; Jusoh, R.; Salleh, N. F. M.; Hameed, B. H.; Karim, A. H., Cost-effective microwave rapid synthesis of zeolite NaA for removal of methylene blue. *Chemical Engineering Journal* **2013**, *229*, 388-398.
17. Gerçel, Ö.; Özcan, A.; Özcan, A. S.; Gerçel, H. F., Preparation of activated carbon from a renewable bio-plant of *Euphorbia rigida* by H<sub>2</sub>SO<sub>4</sub> activation and its adsorption behavior in aqueous solutions. *Applied Surface Science* **2007**, *253* (11), 4843-4852.
18. Pereira, P. M.; Ferreira, B. F.; Oliveira, N. P.; Nassar, E. J.; Ciuffi, K. J.; Vicente, M. A.; Trujillano, R.; Rives, V.; Gil, A.; Korili, S.; De Faria, E. H., Synthesis of Zeolite A from Metakaolin and Its Application in the Adsorption of Cationic Dyes. *Applied Sciences* **2018**, *8* (4).

19. Raval, N. P.; Shah, P. U.; Shah, N. K., Malachite green “a cationic dye” and its removal from aqueous solution by adsorption. *Applied Water Science* **2017**, *7* (7), 3407-3445.
20. Gould, N. S.; Li, S.; Cho, H. J.; Landfield, H.; Caratzoulas, S.; Vlachos, D.; Bai, P.; Xu, B., Understanding solvent effects on adsorption and protonation in porous catalysts. *Nature Communications* **2020**, *11* (1), 1060.
21. Zhang, K.; Lively, R. P.; Noel, J. D.; Dose, M. E.; McCool, B. A.; Chance, R. R.; Koros, W. J., Adsorption of Water and Ethanol in MFI-Type Zeolites. *Langmuir* **2012**, *28* (23), 8664-8673.



## Chapter IV: The Driving Forces of Cationic Dye Adsorption, Confinement and Long Range Correlation in Zeolitic Materials

In this section, we present a paper submitted Langmuir Journal. The results presented concern the study of driving force of adsorption at the solid/liquid interface. Among the materials presented in the experimental part (part 2), the samples (Zeolite Y) Faujasite with different surface properties have been selected. These samples constitute a series of particles with different Si/Al ratio, from 2.55, 15 and 40 for FAU400, FAU720 and FAU780 respectively.

For these solids considered here, three probe molecules, have been chosen in order to highlight the effect of surface chemistry and the impact on the confinement of molecules within the porosity, and on the long-range correlation in Zeolite material. They are referred to as hemicyanine dyes, particularly n-DiA, which differ by the length of the alkyl chain and hydrophobic properties. Four different solvents: water, ethanol, acetonitrile and DMSO were used. The evolution of the adsorption capacity has been determined in correlation with the quantity of Bronsted acid sites involved in the cationic exchange depending on the nature of the solvent used.

The adsorption capacity is related to the cationic exchange capacity (CEC) of the material. This CEC depends on the Si/Al ratio of the material since it is equivalent to the negative charge obtained after substitution of Si by Al. In order to study the guest-host interactions of these systems, adsorption isotherms are studied as a macroscopic approach. Furthermore, SHS technique will be used to investigate the organization and correlation of the adsorbed molecules at the local scale. This approach gives a new experimental quantity called  $l_4$  that characterizes the local correlation of the adsorbed dye.



## 1 Written manuscript submitted in Langmuir Journal

# The Driving Forces of Cationic Dye Adsorption, Confinement and Long Range Correlation in Zeolitic Materials

Marwa Assaf, Gaelle Martin-Gassin, Benedicte Prelot, Pierre-Marie Gassin\*

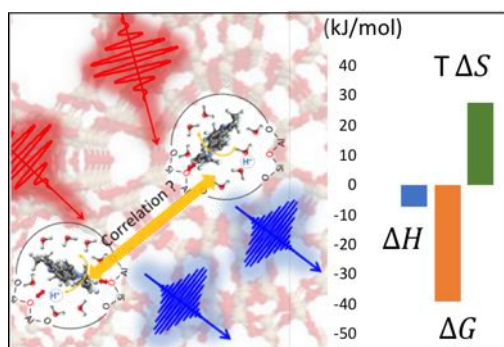
AUTHOR ADDRESS ICGM, Univ Montpellier, ENSCM, CNRS, Montpellier, France

### Corresponding Author:

\*pierre-marie.gassin@enscm.fr

KEYWORDS Faujasite – Adsorption - Second Harmonic Scattering - Solvent effect – hemicyanine dye - Cationic Exchange Capacity – Solid / Liquid Interface- Isothermal Titration Calorimetry

TOC



### ABSTRACT

Zeolitic materials are commonly used to capture emergent contaminants in water or in complex aqueous effluents. The efficiency of this adsorption depends strongly on the guest-host interactions and on the surrounding environment with possible co-adsorption of the solvent. Only few experimental techniques are available to probe in situ the sequestration processes at the solid / liquid interface. We propose in the present work to combine Second Harmonic Scattering (SHS) technique with Isothermal Titration Calorimetry (ITC) in order to investigate the adsorption and the confinement of an hemicyanine dye adsorbed inside Faujasite materials. The methodology described here permits to quantify the correlations between the confined dyes in the material, and thus give local information about the organization at the nanometer scale. Various impacts, such as the effect of solvent type, the silicon to aluminum ratio of the zeolitic adsorbent, are quantitatively estimated and discussed. This work highlights that the most correlated system matches with the higher adsorption capacity associated with the lower entropic contribution.

## Introduction

Zeolites, porous crystalline structures of Aluminum Silicate, have great potential for a wide range in technical<sup>165</sup>, industrial<sup>166, 167</sup>, agricultural<sup>168</sup>, environmental<sup>169</sup> and biomedical applications<sup>170</sup>. These applications are based on their outstanding properties for sorption, ion-exchange and catalytic processes. Numerous studies have also emphasized the ability of zeolitic material for the purification and the capture of emergent contaminants from water<sup>171-179</sup> or complex beverage like wine<sup>180</sup>. Indeed, in addition to their valuable sorption selectivity, or exchange capacity, these materials otherwise exhibit high chemical stability, good recyclability and above all non-toxicity. Zeolitic materials have been the object of numerous studies to tune their chemistry, their structure, their textural properties, to optimize their efficiency on the one hand<sup>181-183</sup> and to understand the driving force of adsorption and confinement processes on the other hand.

The porous network and the presence of confined spaces bring new properties such as chemical reactivity under nanoconfinement<sup>184</sup> in general and for the case of zeolite their use in heterogeneous catalysis. Indeed, catalytic reactions in confined spaces exhibit unique behaviors compared to those observed on bulk materials<sup>185, 186</sup>. The confinement effects thus imply modification on catalytic reaction, as well as on diffusion and on adsorption/desorption. For application on sorption, there are various properties responsible for the modification of sorption behavior, with the structural and the textural properties together with the surface chemistry. This is particularly the case at the solid / liquid interface with additional physicochemical properties, and where the sorption is indeed a displacement. This involves the influence of the nature of the solvent<sup>79, 163</sup> and the specific influence of the hydration of adsorbed and desorbed species<sup>187</sup>. For zeolites, the adsorption properties are governed by the ability of adsorbed molecules to penetrate into zeolite voids and by their surface chemistry, with hydrophilic/hydrophobic balances, surfaces acidities (Lewis and Bronsted), and mainly their permanent charge designed as the Cation Exchange Capacity (CEC), this CEC resulting from the isomorphic substitution of Silicon atoms by Aluminum within the crystallographic framework. Even if interesting theoretical results are reported concerning the understanding of the Bronsted Acid Site (BAS) role<sup>163, 188, 189</sup> in sorption and catalytic properties<sup>190</sup>, the various contributions of the mechanisms<sup>190-192</sup> are not commonly investigated from the experimental and local point of view.

The aim of this work is to investigate the guest-host interactions and to rationalize the significance of electrostatic, Van Der Waals and steric interactions in the global adsorption process. To achieve that, the adsorption of a cationic hemicyanine dye inside Faujasite materials has been chosen as reference system. The adsorption is studied by modulating the nature of the solvent and the charge

inside the material. To characterize and quantify these interactions, UV-visible absorption method is used to determine the macroscopic adsorption isotherm, Isothermal Titration Calorimetry (ITC) measurement are performed in order to get macroscopic information about the thermodynamic of the adsorption and an original approach based on Second Harmonic Scattering (SHS), is employed to probe the local organization of the dye inside the material, within the micropores. This last technique, based on Second Harmonic Generation (SHG) phenomena, in which two photons at frequency  $\omega$  are converted into a photon at the double frequency  $2\omega$ , has become increasingly popular since recent studies<sup>119, 122, 193-200</sup> demonstrated that it is suitable to obtain information about organization in long range structured system. Recent works<sup>121, 122, 201</sup> have developed a methodology to quantify the correlation between the nonlinear emitter, by analyzing the polarization resolved SHS signal. The novelty of this work is to combine these two approaches, global calorimetric measurement and local SHS measurement used until now to quantify correlation in homogeneous liquid, to probe the order of the guest molecules confinement inside the microporous host material. The hemicyanine dye is chosen because it is an efficient SHG active molecule, and previous works have demonstrated its insertion in zeolitic system<sup>199</sup>. The material studied here is a Faujasite type zeolite which consists of cubic-octahedrons called sodalite cages or  $\beta$ -cages. The assembly of these cages linked together by hexagonal prisms leads into a larger cavity of diameter 13 Å called supercage (SC) which is approximately the size of the guest hemicyanine dye molecule chosen. The  $\beta$ -cages are only accessible to solvent, whereas the supercages are accessible for solvent and organic dye<sup>192</sup>.

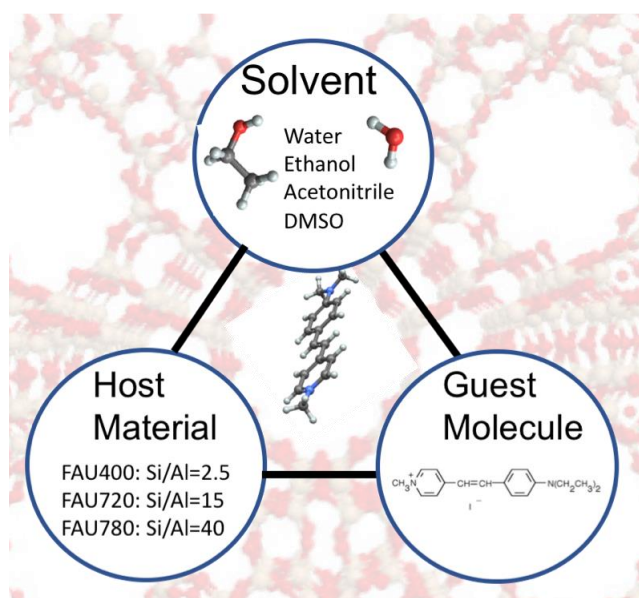


*Figure 73: Schematic representation of the three various elements (adsorbate, adsorbent and solvent) involved in the modulation of the adsorption processes and studied in the present work. The hemicyanine dye is referred as sDiA dye molecule in the following.*

## Experimental procedure

### 1°) Reagent and materials:

Faujasite Y with different Si/Al ratio were purchased from Zeolyst International: Faujasite CBV400, CBV720, and CBV780 with Si/Al ratio equal to respectively to 2.5, 15 and 40 and referred as FAU400, FAU720 and FAU780 in the following. The CEC of these different materials are theoretically deduced by the Si/Al ratio and equal to 4.7 meq.g<sup>-1</sup>, 1.0 meq.g<sup>-1</sup> and 0.4 meq.g<sup>-1</sup> respectively (additional details are given in the SI).

Acetonitrile, Ethanol, and DMSO were obtained from Sigma Aldrich at HPLC grade. Ultrapure water is 18 MOhm.cm resistivity. The hemicyanine dye is 4-(4-Diethylaminostyryl)-1-methylpyridinium iodide, M=394.29 g.mol<sup>-1</sup> also referred as sDia in the following, purchased from Sigma Aldrich. All chemicals were used as received without further purification.

Fresh suspensions of Faujasite in the considered solvent were prepared at a solid / liquid concentration of 0.1 g.L<sup>-1</sup> and used within 12h. Suspensions were sonicated 10 minutes and kept under constant stirring at 25 °C to prevent solid particles aggregation before using. The characteristic size of all the particles in all solvent is around 800 nm diameter +/- 200 nm determined with DLS (additional details in SI).

### 2°) Adsorption isotherm:

The adsorption isotherms were determined using the depletion method in batch conditions by putting in contact during 24h at 25 °C, solutions of hemicyanine at various initial concentrations with Faujasite suspension at 0.05 g.L<sup>-1</sup> coming from the fresh suspensions of Faujasite. The suspensions are centrifugated at 11000 rpm during 1h and then filtered with polypropylene 0.2µm filter. The dye adsorbed onto the material is determined according to:

$$\Gamma_{ads} = \frac{(C_0 - C_e)V}{m} \quad (1)$$

Where  $\Gamma_{ads}$  is the dye amount adsorbed into the material, V is the volume (L) of the solution, and m is the mass of the solid phase (g),  $C_0$  is the initial concentration of the dye and  $C_e$  is the equilibrium concentration in the supernatant. This  $C_e$  was measured by UV-vis absorbance (JASCO V-670) at 460 nm on the supernatant.

### 3°) ITC measurements

Isothermal Titration Calorimetry (ITC) measurements were performed with a TAM III multichannel calorimetric device with nanocalorimeters and a Micro Reaction System (TA Waters). ITC experiments were carried out in cells (hastelloy) with 800  $\mu\text{L}$  of zeolitic suspension, at 298 K and consist of 25 injections of 10 seconds with 10  $\mu\text{L}$  of the dye solution at 2 mM. The system is equipped with a gold paddle stirrer used at 90 rpm. In order to allow the system to stabilize between injections, the latter are spaced 45 min apart. The dilution effect is evaluated under similar conditions with only the solvent. The global heat effect and displacement enthalpy were calculated after appropriate subtraction of the dilution effect, and then related to the real adsorbed amount for each injection<sup>202</sup>.

4°) SHS measurement:

The polarization resolved SHS experimental setup is detailed elsewhere<sup>120</sup> and additional details are given in SI. Briefly, the SHS intensity is monitored in the right angle direction as a function of the input polarization angle  $\gamma$ , which was selected with a rotating half-wave plate and the second harmonic light was selected in the vertical state by an analyzer, placed in front of the spectrometer. All experimental data were recorded for 10 s under stirring conditions, a magnetic stirrer is operated in the cell measurement. For each system, two separate SHS measurements are performed. On the one hand, the SHS measurement of the whole suspension and on the other hand, the SHS measurement of the supernatant solution obtained after centrifugation. Formally, the SHS intensity of the suspension comes from 3 different contributions as depicted in formula (2):

$$I_{suspension}^{2\omega}(\gamma) = I_{HRS,dye}^{2\omega}(\gamma) + I_{HRS,solvent}^{2\omega}(\gamma) + I_{SHS,dye+materials}^{2\omega}(\gamma) \quad (2)$$

Where  $I_{HRS,dye}^{2\omega}$  is the incoherent Second Harmonic light coming from the free dye in solution also referred in the literature as the Hyper Rayleigh Scattering (HRS) contribution of the dye;  $I_{HRS,solvent}^{2\omega}$  is the Hyper Rayleigh Scattering contribution of the solvent, and  $I_{SHS,dye+materials}^{2\omega}$  is the Second Harmonic light contribution of the dye adsorbed onto and into the material. The contribution of the bare Faujasite can be neglected as it is shown in the additional data presented in SI. The SHS intensity of the supernatant can be written as:

$$I_{supernatant}^{2\omega}(\gamma) = I_{HRS,dye}^{2\omega}(\gamma) + I_{HRS,solvent}^{2\omega}(\gamma) \quad (3).$$

At the concentrations where the SHS experiment are performed, the re-absorption of the  $2\omega$  photon by the solution is negligible<sup>203</sup> as it is discussed in SI. Thus, the SHS signal coming from the dye adsorbed onto and into the material is obtained by the subtraction equation (2) minus equation (3):

$$I_{SHS}^{2\omega}(\gamma) = I_{suspension}^{2\omega}(\gamma) - I_{supernatant}^{2\omega}(\gamma) \quad (4)$$

All the SHS data presented in the manuscript are treated according to equation (4).

Results and discussions

1°) The Si/Al ratio effect on the adsorption

Figure 74 A shows the adsorption isotherms of sDiA in water onto the different faujasite materials. According to the nature of the initial portion of the curve and its slope, the isotherms exhibit a shape corresponding to a L type (or Langmuir type) following Giles classification. The adsorption isotherms are thus well fitted with the Langmuir like model, equation (5), even if liquid-phase adsorption of molecule into zeolites is not a situation traditionally characteristic of a Langmuir isotherm. The applicability of this model is discussed here<sup>163</sup> and results from a relatively strong interaction of the dyes with the pore walls.

$$\Gamma_{ads} = \frac{\Gamma_{max}C_eK_L}{1+C_eK_L} \quad (5)$$

Through this simplified adsorption model used in its linearized form, the maximum amount of adsorbed dye  $\Gamma_{max}$ , as well as the Langmuir constant  $K_L$  have been evaluated for sDiA sorption on the various zeolites. For the sDiA adsorption, the maximum amount capacity varies from 0.622 mmol.g<sup>-1</sup> for the FAU400 material, to 0.338 mmol.g<sup>-1</sup> for FAU780 material. This finding is explained by the number of adsorption sites available depending on the Si/Al ratio of the material. Indeed, these adsorption sites are located on the oxygen atom neighboring an aluminum atom and are thus referred as Brønsted Acid Site (BAS)<sup>163, 188, 189, 204</sup>. The different material FAU400, FAU720 and FAU780 exhibits different BAS number, or it is the same thing different CEC, which are respectively equal to 4.7 meq.g<sup>-1</sup> (6.7 sites per SC), 1.0 meq.g<sup>-1</sup> (1.5 sites per SC) and 0.4 meq.g<sup>-1</sup> (0.6 sites per SC). For FAU780 material the number of the BAS seems to be the factor which limits the adsorption because the  $\Gamma_{max}$  measured to 0.49 molecule per SC is close to the theoretical CEC of 0.59 site per SC. It confirms that the cationic exchange is the driving force of the adsorption, and that other interactions like Van der Waals interaction are not efficient to yield dye adsorption. At higher charge density in the material, the adsorption is limited by the empty space available in the pore. When the ratio of 1 molecule per SC is reached, no more adsorption can occur even if there is more BAS. The adsorption capacity  $\Gamma_{max}$  is nearly the same for FAU720 and FAU400 materials, around 1 molecule adsorbed per SC, far lower from the theoretical CEC of 6.7 sites per SC for FAU400. It shows that steric effects, *i.e.* the space available in the material for the dye is, here, the limiting factor of adsorption. In other word, increasing the number of BAS up to 1 per SC has no effect on the adsorption capacity.

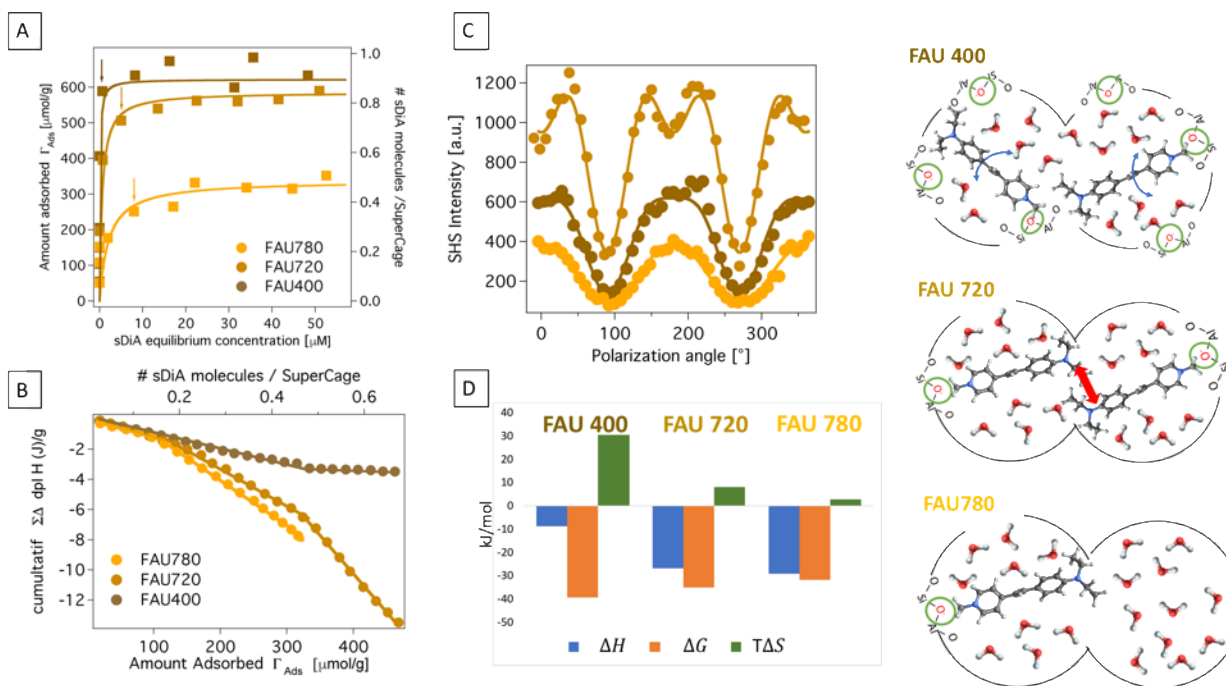


Figure 74: A) sDiA in water adsorption isotherm onto the three Faujasite, B) Corresponding ITC measurement, C) SHS polarization plot measured at the concentration given by the arrow in A), D) the adsorption thermodynamic quantities for the three Faujasite, at high coverage. On right, a microscopic picture to illustrate the interaction or not between the neighboring dyes.

Figure 74B shows the displacement enthalpy measured by ITC during the adsorption process on the three different materials. The observed behavior is different for the various considered materials. ITC approach provides the chance to measure directly the heat effect all along the isotherm. The displacement enthalpy is determined for various surface coverage corresponding to the complete loading of the materials. Three distinct areas can be observed depending on the amount adsorbed range. In the first region, at low adsorption, *i.e.* when  $\Gamma_{ads} < 0.2$  molecule per SC, the displacement enthalpy, obtained by the slope in the graphic 2B, is the same for the 3 materials with a value around  $\Delta H_{ads} = -10 \text{ kJ.mol}^{-1}$ . In the intermediate region,  $0.2 < \Gamma_{ads} < 0.5$  molecule per SC, the displacement enthalpy is nearly stable for FAU400, but it increases for FAU720 and 780 at around  $\Delta H_{ads} = -28 \text{ kJ.mol}^{-1}$ . In the high adsorption region, this quantity continues to increase for FAU720 with high  $\Delta H$  estimated at  $-50 \text{ kJ.mol}^{-1}$ , whereas it slightly decreases for FAU400. For FAU780 at sorption higher than  $0.32 \text{ mmol.g}^{-1}$ , calculation does make sense since saturation is reached and no adsorption occurs. Those results can be understood with a microscopic model which supposed that the filling of the SC is not independent from the neighboring SC. Indeed, in each Faujasite material, a SC is linked by a dodecagonal window to four other SC. In the low adsorption regime, the adsorbed dye is in average involved in a SC surrounded by four empty SC. Thus, no interaction between the dye occurs in this regime. At higher adsorption,  $0.2 < \Gamma_{ads} < 0.5$  molecule per SC, the filling of the material induces that

the dyes can begin to interact with other dyes located in neighboring SC. For FAU400 material which has a lot of BAS per SC, around five or six sites in average, various spatial configurations can be explored by the dye and probably the system should find the configuration where the dyes don't interact with the neighboring dyes, see the picture in Figure 74 right. For FAU720 and FAU780 material, which have respectively around 1.5 and 0.6 BAS per SC, the configuration of adsorption probably induced interaction between the neighboring dye. This effect is enhanced at higher adsorption. The analysis of ITC measurements highlights the link between the number of microscopic configurations available by the system and the displacement enthalpy. To go further in the thermodynamics approach, the measured enthalpy was combined with other thermodynamics values. As the system is a dilute solution of a charged adsorbate, the global free adsorption enthalpy  $\Delta G_{ads}$  can be deduced from the constant extracted from equation (5) applied to the adsorption isotherm<sup>205</sup>:

$$\Delta G_{ads} = -RT \ln(K_L) \quad (6).$$

The combination of the measured  $\Delta H_{ads}$  from ITC and the calculated  $\Delta G_{ads}$  permits to estimate the entropic term  $T\Delta S_{ads}$ . The results are given in Table 10 and Figure 74D. Two ranges on the surface coverages have been distinguished, with  $\Gamma_{ads}$  lower or higher than 0.2 molecule per SC. For low surface coverage, the entropic terms  $T\Delta S_{ads}$  is in the range of 30-20 kJ.mol<sup>-1</sup> for the 3 materials, with a slight decrease from CBV-400 to CBV-780 in line with the small decrease of  $\Delta G_{ads}$ . For higher loading, the difference in the entropic contribution between materials is more pronounced, with a high decrease of  $T\Delta S_{ads}$  for CBV-400 to CBV-780. It is interesting to discuss the FAU400 and FAU720 results. Indeed, these two materials exhibits nearly the same adsorption capacity, but the adsorption thermodynamics quantities are strongly different with a higher entropic contribution for the FAU400. This difference should be likely explained by the greater BAS number available for FAU400. To probe locally the order/disorder of the dye organization inside the material, polarization resolved SHS measurement are presented in Figure 74C. These data were analyzed as a Fourier series<sup>122</sup>:

$$I_{SHS}(\gamma) = i_0 + i_2 \cos(2\gamma) + i_4 \cos(4\gamma) \quad (7)$$

where  $i_0$ ,  $i_2$  and  $i_4$  are the amplitudes of the constant, the harmonic  $2\gamma$  and the harmonic  $4\gamma$  terms. In Eq. (7), the parameters  $i_0$  and  $i_2$  are related to the local microscopic structure, i.e. the first hyperpolarizability of the dye and  $i_4$  to the long-range correlations. In the case of uncorrelated species, SHS is a purely incoherent phenomenon and the amplitude  $i_4$  vanishes<sup>122</sup>. On the contrary, when molecular orientations are correlated, the scattered photons have well-defined phase relationship and  $i_4$  differs from 0. To quantify this term, the normalized parameter  $I_4$  is introduced as:

$$I_4 = \frac{i_4}{i_0} \quad (8)$$



$I_4$  is equal to 0 when no correlation occurs between adsorbed dyes and is different from 0 when correlations between dyes exist. The  $I_4$  parameter deduced from the fit are presented in Table 10 and its absolute value is clearly higher for FAU720 compared to FAU400 and FAU780. As discussed before, the comparison between FAU400 and FAU720 results is interesting as the filling of the material is nearly the same. The higher  $I_4$  value in the FAU720 is attributed by a more frustrated organization of the dye than in the case of FAU400. In this material, the dyes can likely move more independently because of several BAS in one SC, and the molecule may probably jump from one configuration to one other as depicted in Figure 74 right. Also, this interpretation is in agreement with a higher entropic contribution for this material. For the systems studied here, the parameter  $I_4$  which characterize the correlation between the dyes, is linked to the confinement of the dye in the material. Thus, the previous results show that the system which lead to the better dye confinement is not obtained with the system having the higher BAS, but for an optimum around 1 BAS per SC.

*Table 10 : Results of the fitting parameters extracted from macroscopic experiment adsorption of sDiA, with the  $\Gamma_{max}$ , the maximum amount adsorbed,  $K_L$  the Langmuir like constant,  $\Delta G_{ads}$  the corresponding free enthalpy obtained from equation (6),  $\Delta H_{ads}$  measured by ITC, deduced  $T\Delta S_{ads}$  and  $I_4$  the normalized SHS correlation parameter. For  $\Delta H_{ads}$  and  $T\Delta S_{ads}$ , the values are calculated for the two various regimes, with low surface coverage (in italic) and high surface coverage (in bold).*

Material	$\Gamma_{max}$ [ $\mu\text{mol.g}^{-1}$ ]	$\Gamma_{max}$ [molecule/SC]	$K_L$ [L. $\mu\text{mol}^{-1}$ ]	$\Delta G_{ads}$ [kJ.mol <sup>-1</sup> ]	$\Delta H_{ads}$ [kJ.mol <sup>-1</sup> ]		$T\Delta S_{ads}$ [kJ.mol <sup>-1</sup> ]		SHS- $I_4$ parameter
					<i>-9.3</i>	<b>-8.7</b>	<i>30.0</i>	<b>30.6</b>	
FAU400	622	0.9	10	-39.3	<i>-9.3</i>	<b>-8.7</b>	<i>30.0</i>	<b>30.6</b>	- 0.10
FAU720	588	0.85	1.7	-34.9	<i>-11.0</i>	<b>-26.7</b>	<i>23.9</i>	<b>8.2</b>	- 0.26
FAU780	338	0.49	0.5	-31.9	<i>-12.1</i>	<b>-29.2</b>	<i>19.8</i>	<b>2.7</b>	- 0.01

## 2°) The solvent effect on the adsorption

Figure 75A shows the sDiA adsorption isotherms onto the FAU720 material with different solvents. The maximum amount of adsorption varies with the solvent in the order Water>acetonitrile>Ethanol>DMSO. Those results follow the order recently published<sup>163</sup> obtained with

pyridine onto various zeolites. These findings can be explained by the active site protonation or deprotonation depending of the solvent. Indeed, probably, if the proton is solvated, as depicted in Figure 75C, the cationic exchange can occur, and if it is weakly solvated, the exchange is lesser. For water solvent results, as the  $\Gamma_{\max}$  measured reaches nearly the CEC, it means that BAS can be considered as “active” for the exchange as all proton are solvated in water. For the other solvents this  $\Gamma_{\max}$  quantity is far below from the CEC of 1 molecule per SC, which can may be explained by a partially “inactive” BAS in respect with the lower relative permittivity value of the solvent. As depicted in Figure 75C and 3D, the solvent effect observed in the whole adsorption process could be explained by this difference in proton solvation. Figure 75 B presents the SHS polarization plot for these systems. The case of water solvent exhibits a significant  $I_4$  contribution, as discussed above. All the other SHS polarization plots show a nearly zero  $I_4$  contribution as summarized in Figure 77.

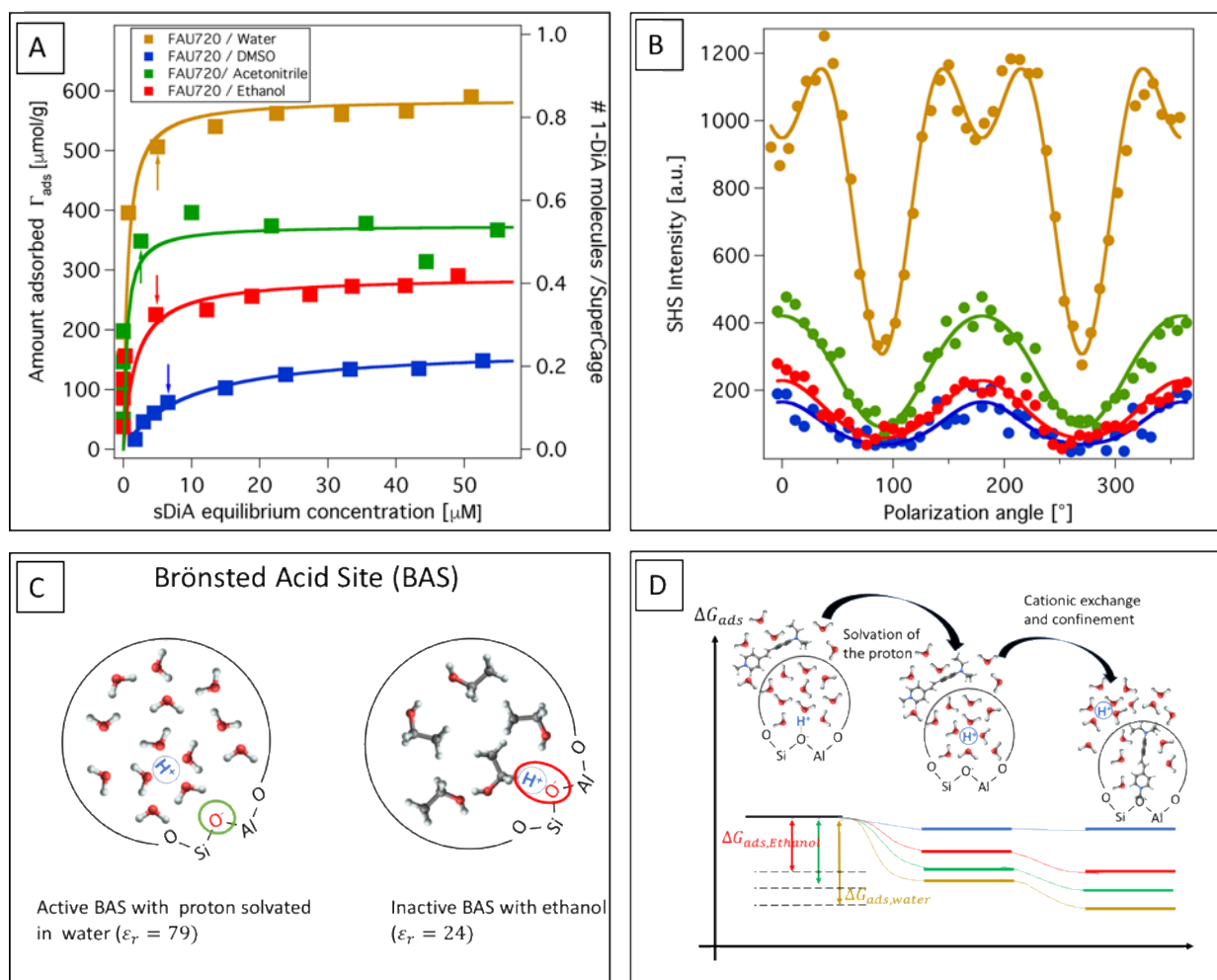


Figure 75: A) Adsorption isotherm for sDiA onto FAU720 with different solvents: water (brown), acetonitrile (green), ethanol (red) and DMSO (blue). B) SHS polarization plot performed at the isotherm shoulder, as indicated with the arrow on graph A. C) Scheme to depict active or inactive Bronsted Acid Site depending on the solvent used. D) Evolution of free enthalpy during the adsorption process.

The impact of the material for the case of ethanol solvent is presented in Figure 76A. The results greatly differ from the water solvent. The adsorption capacity follows monotonically the Si/Al ratio, which shows that the adsorption is only limited by the number of active BAS and not by the space available in the framework. Those results show that only a small fraction of the BAS is “active” with a proton solvated in ethanol. Figure 76B presents the SHS polarization plot for these systems. Those results show that when the material is few filled, no correlation is measured and that the  $I_4$  parameter increases with the filling of the material.

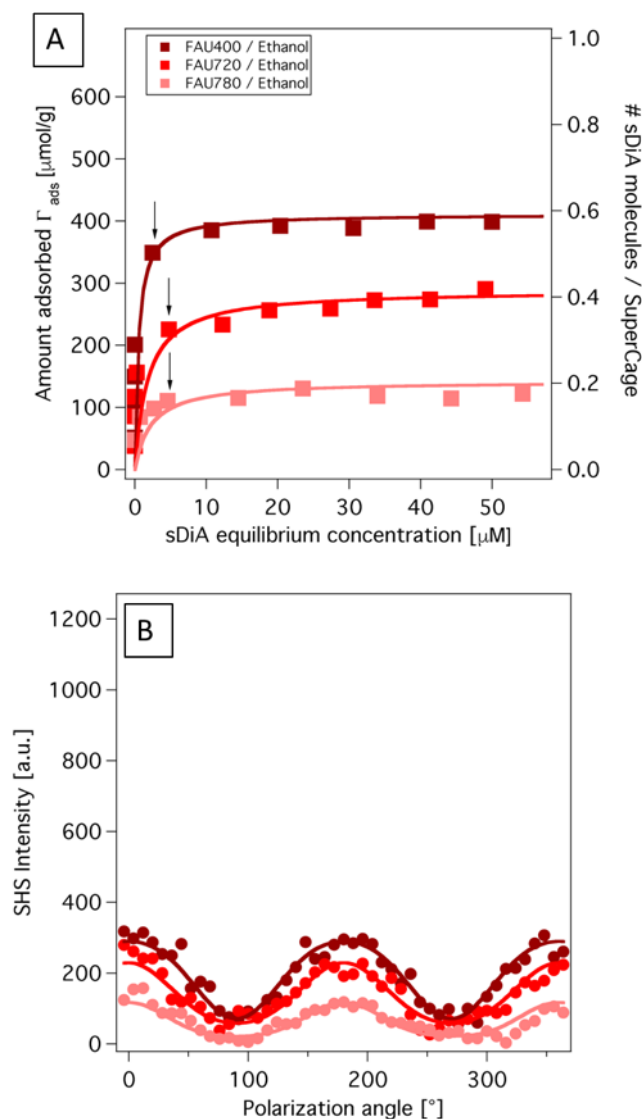


Figure 76: A) Adsorption isotherm for sDiA onto FAU400, FAU720 and FAU780 in ethanol, B) SHS polarization plot performed at the isotherm shoulder, as indicated with the arrow on graph A.

A summary presented in Figure 77 and taking into account all the SHS results presented in this work, shows that the quantification of the  $I_4$  parameter leads clearly to the distinction of three types of dyes intercalation. For the case of low adsorption with  $\Gamma_{\text{max}}$  lower than 0.5 molecule per SC, the  $I_4$  value is around 0, which means that the system exhibits no correlation between the dye. It has been

shown that the molecule is not strongly interacting with the others and thus the molecule cannot be considered strongly confined in the material. For the case of intermediate or high adsorption with  $\Gamma_{\max}$  higher than 0.5 dye per SC, the  $I_4$  value varies between -0.05 and -0.25. In such case, the system exhibits “weak correlation” or “strong correlation”. It has been highlighted in the first part of this work, that an optimum about the BAS number per SC gives the higher correlated system. It results from a balance between enough BAS to full filled the material and not too much acid sites to prevent movement or jump of the dye from one site to one other.

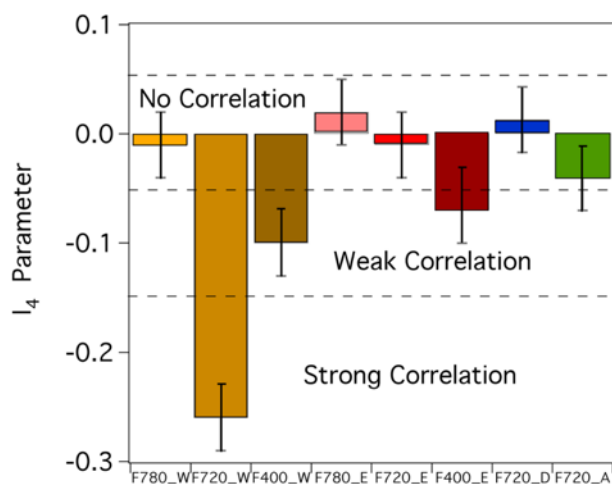


Figure 77:  $I_4$  parameters deduced from SHS experiments for sDiA adsorption onto the different Faujasites and various solvent. The acronym in horizontal axis gives the material and solvent (W=Water, E=Ethanol, D=DMSO and A=Acetonitrile).

As a conclusion, the effect of the solvent and the silicon to aluminum ratio on the dye adsorption has been investigated quantitatively with both SHS and calorimetric measurements. Firstly, it has been shown that the adsorption and organization of the dye inside the material is driven by electrostatic interaction, available voids in the material, and the number of adsorption site in the material. Secondly, increasing the number of adsorption sites in the material increases the affinity of the dye for the materials but seems to decrease the confinement of the dye. An optimum of the charge inside the material -good enough to fill all the void and not too high to completely frustrate the dye- seems to be necessary to get the better confinement of the dye and consequently larger correlations in the system. The calorimetric measurements confirm this disorder increases by a higher entropic contribution. Thirdly, the solvent effect observed in the results can be explained by the proton solvation properties. Finally, this work demonstrates the ability of SHS measurements to probe the organization in buried system. In particular, it opens new perspectives to probe the local order and confinement of molecular inclusion in other class of material, thanks to the SHS measurement of correlations.

**Supporting Information.** Additional information are given about the SHS experimental setup, the  $2\omega$  photons reabsorption, the suspension characterization by DLS measurement, and the calculus of the theoretical cationic exchange capacity. The following files are available free of charge.

#### **Funding Sources**

Financial support for this work by the ANR project **CAMOMILS (ANR-15-CE21-0002)** is greatly acknowledged.

#### **ACKNOWLEDGMENT**

We thank Lotfi Boudjema and Anne Galarneau for regular discussions about the zeolite structure.

#### **ABBREVIATIONS**

SHS, Second Harmonic Scattering; BAS, Bronsted Acid site; CEC, Cationic Exchange Capacity, SC, SuperCage.

#### **REFERENCES**

1. Li, Y.; Li, L.; Yu, J., Applications of Zeolites in Sustainable Chemistry. *Chem* **2017**, *3* (6), 928-949.
2. Stocker, K.; Ellersdorfer, M.; Lehner, M.; Raith, J. G., Characterization and Utilization of Natural Zeolites in Technical Applications. *BHM Berg- und Hüttenmännische Monatshefte* **2017**, *162* (4), 142-147.
3. Colella, C.; Gennaro, M. d.; Aiello, R., Use of Zeolitic Tuff in the Building Industry. *Reviews in Mineralogy and Geochemistry* **2001**, *45* (1), 551-587.
4. Nakhli, S. A. A.; Delkash, M.; Bakhshayesh, B. E.; Kazemian, H., Application of Zeolites for Sustainable Agriculture: a Review on Water and Nutrient Retention. *Water, Air, & Soil Pollution* **2017**, *228* (12), 464.
5. Misaelides, P., Application of natural zeolites in environmental remediation: A short review. *Microporous and Mesoporous Materials* **2011**, *144* (1), 15-18.
6. Bacakova, L.; Vandrovцова, M.; Kopova, I.; Jirka, I., Applications of zeolites in biotechnology and medicine – a review. *Biomaterials Science* **2018**, *6* (5), 974-989.
7. Shaw, R.; Sharma, R.; Tiwari, S.; Tiwari, S. K., Surface Engineered Zeolite: An Active Interface for Rapid Adsorption and Degradation of Toxic Contaminants in Water. *ACS Applied Materials & Interfaces* **2016**, *8* (19), 12520-12527.
8. Jiang, N.; Shang, R.; Heijman, S. G. J.; Rietveld, L. C., High-silica zeolites for adsorption of organic micro-pollutants in water treatment: A review. *Water Research* **2018**, *144*, 145-161.
9. Samanta, P.; Desai, A. V.; Let, S.; Ghosh, S. K., Advanced Porous Materials for Sensing, Capture and Detoxification of Organic Pollutants toward Water Remediation. *ACS Sustainable Chemistry & Engineering* **2019**, *7* (8), 7456-7478.

10. Wang, S. B.; Peng, Y. L., Natural zeolites as effective adsorbents in water and wastewater treatment. *Chem. Eng. J.* **2010**, *156* (1), 11-24.
11. Wang, S.; Li, H.; Xie, S.; Liu, S.; Xu, L., Physical and chemical regeneration of zeolitic adsorbents for dye removal in wastewater treatment. *Chemosphere* **2006**, *65* (1), 82-87.
12. De Smedt, C.; Ferrer, F.; Leus, K.; Spanoghe, P., Removal of Pesticides from Aqueous Solutions by Adsorption on Zeolites as Solid Adsorbents. *Adsorption Science & Technology* **2015**, *33* (5), 457-485.
13. Martucci, A.; Braschi, I.; Bisio, C.; Sarti, E.; Rodeghero, E.; Bagatin, R.; Pasti, L., Influence of water on the retention of methyl tertiary-butyl ether by high silica ZSM-5 and Y zeolites: a multidisciplinary study on the adsorption from liquid and gas phase. *RSC Adv.* **2015**, *5* (106), 86997-87006.
14. Wang, S. B.; Li, H.; Xu, L. Y., Application of zeolite MCM-22 for basic dye removal from wastewater. *J. Colloid Interface Sci.* **2006**, *295* (1), 71-78.
15. Sarti, E.; Chenet, T.; Stevanin, C.; Costa, V.; Cavazzini, A.; Catani, M.; Martucci, A.; Precisvalle, N.; Beltrami, G.; Pasti, L., High-Silica Zeolites as Sorbent Media for Adsorption and Pre-Concentration of Pharmaceuticals in Aqueous Solutions. *Molecules* **2020**, *25* (15).
16. Noviello, M.; Gattullo, C. E.; Allegretta, I.; Terzano, R.; Gambacorta, G.; Paradiso, V. M., Synthetic zeolite materials from recycled glass and aluminium food packaging as potential oenological adjuvant. *Food Packaging and Shelf Life* **2020**, *26*, 100572.
17. Pagis, C.; Morgado Prates, A. R.; Farrusseng, D.; Bats, N.; Tuel, A., Hollow Zeolite Structures: An Overview of Synthesis Methods. *Chemistry of Materials* **2016**, *28* (15), 5205-5223.
18. Serrano, D. P.; Escola, J. M.; Pizarro, P., Synthesis strategies in the search for hierarchical zeolites. *Chemical Society Reviews* **2013**, *42* (9), 4004-4035.
19. Shamzhy, M.; Opanasenko, M.; Concepción, P.; Martínez, A., New trends in tailoring active sites in zeolite-based catalysts. *Chemical Society Reviews* **2019**, *48* (4), 1095-1149.
20. Grommet, A. B.; Feller, M.; Klajn, R., Chemical reactivity under nanoconfinement. *Nature Nanotechnology* **2020**, *15* (4), 256-271.
21. Dai, J. J.; Zhang, H. B., Recent Advances in Catalytic Confinement Effect within Micro/Meso-Porous Crystalline Materials. *Small* **2021**, *17* (22).
22. Sastre, G.; Corma, A., The confinement effect in zeolites. *Journal of Molecular Catalysis a-Chemical* **2009**, *305* (1-2), 3-7.
23. Varghese, J. J.; Mushrif, S. H., Origins of complex solvent effects on chemical reactivity and computational tools to investigate them: a review. *Reaction Chemistry & Engineering* **2019**, *4* (2), 165-206.

24. Gould, N. S.; Li, S.; Cho, H. J.; Landfield, H.; Caratzoulas, S.; Vlachos, D.; Bai, P.; Xu, B., Understanding solvent effects on adsorption and protonation in porous catalysts. *Nature Communications* **2020**, *11* (1), 1060.
25. Prelot, B.; Lantenois, S.; Charbonnel, M.-C.; Marchandeu, F.; Douillard, J. M.; Zajac, J., What are the main contributions to the total enthalpy of displacement accompanying divalent metal adsorption at the silica-electrolyte interface? *J. Colloid Interface Sci.* **2013**, *396*, 205-209.
26. Bordiga, S.; Lamberti, C.; Bonino, F.; Travert, A.; Thibault-Starzyk, F., Probing zeolites by vibrational spectroscopies. *Chemical Society Reviews* **2015**, *44* (20), 7262-7341.
27. Vimont, A.; Thibault-Starzyk, F.; Daturi, M., Analysing and understanding the active site by IR spectroscopy. *Chemical Society Reviews* **2010**, *39* (12), 4928-4950.
28. Grifoni, E.; Piccini, G.; Lercher, J. A.; Glezakou, V.-A.; Rousseau, R.; Parrinello, M., Confinement effects and acid strength in zeolites. *Nature Communications* **2021**, *12* (1), 2630.
29. Tabacchi, G., Supramolecular Organization in Confined Nanospaces. *ChemPhysChem* **2018**, *19* (11), 1249-1297.
30. Ramamurthy, V., Controlling photochemical reactions via confinement: zeolites. *Journal of Photochemistry and Photobiology C: Photochemistry Reviews* **2000**, *1* (2), 145-166.
31. Van Cleuvenbergen, S.; Smith, Z. J.; Deschaume, O.; Bartic, C.; Wachsmann-Hogiu, S.; Verbiest, T.; van der Veen, M. A., Morphology and structure of ZIF-8 during crystallisation measured by dynamic angle-resolved second harmonic scattering. *Nature communications* **2018**, *9* (1), 3418-3418.
32. Moris, M.; Van Den Eede, M.-P.; Koeckelberghs, G.; Deschaume, O.; Bartic, C.; Van Cleuvenbergen, S.; Clays, K.; Verbiest, T., Harmonic light scattering study reveals structured clusters upon the supramolecular aggregation of regioregular poly(3-alkylthiophene). *Communications Chemistry* **2019**, *2* (1), 130.
33. Duboisset, J.; Brevet, P.-F., Salt-induced Long-to-Short Range Orientational Transition in Water. *Physical Review Letters* **2018**, *120* (26), 263001.
34. Gassin, P.-M.; Prelot, B.; Grégoire, B.; Martin-Gassin, G., Second-Harmonic Scattering in Layered Double Hydroxide Colloids: A Microscopic View of Adsorption and Intercalation. *Langmuir* **2018**, *34* (40), 12206-12213.
35. Gassin, P.-M.; Prelot, B.; Gregoire, B.; Martin-Gassin, G., Second-Harmonic Scattering Can Probe Hydration and Specific Ion Effects in Clay Particles. *The Journal of Physical Chemistry C* **2020**, *124* (7), 4109-4113.
36. Pardon, A.; Bonhomme, O.; Gaillard, C.; Brevet, P.-F.; Benichou, E., Nonlinear optical signature of nanostructural transition in ionic liquids. *Journal of Molecular Liquids* **2021**, *322*, 114976.

37. Chen, Y.; Okur, H. I.; Gomopoulos, N.; Macias-Romero, C.; Cremer, P. S.; Petersen, P. B.; Tocci, G.; Wilkins, D. M.; Liang, C.; Ceriotti, M.; Roke, S., Electrolytes induce long-range orientational order and free energy changes in the H-bond network of bulk water. *Science Advances* **2016**, *2* (4), e1501891.
38. Tocci, G.; Liang, C.; Wilkins, D. M.; Roke, S.; Ceriotti, M., Second-Harmonic Scattering as a Probe of Structural Correlations in Liquids. *The Journal of Physical Chemistry Letters* **2016**, *7* (21), 4311-4316.
39. Kim, H. S.; Lee, S. M.; Ha, K.; Jung, C.; Lee, Y.-J.; Chun, Y. S.; Kim, D.; Rhee, B. K.; Yoon, K. B., Aligned Inclusion of Hemicyanine Dyes into Silica Zeolite Films for Second Harmonic Generation. *Journal of the American Chemical Society* **2004**, *126* (2), 673-682.
40. van der Veen, M. A.; Sels, B. F.; De Vos, D. E.; Verbiest, T., Localization of p-nitroaniline chains inside zeolite ZSM-5 with second-harmonic generation microscopy. *J Am Chem Soc* **2010**, *132* (19), 6630-1.
41. Boudjema, L.; Aarrass, H.; Assaf, M.; Morille, M.; Martin-Gassin, G.; Gassin, P.-M., PySHS: Python Open Source Software for Second Harmonic Scattering. *Journal of Chemical Information and Modeling* **2020**, *60* (12), 5912-5917.
42. Duboisset, J.; Rondepierre, F.; Brevet, P.-F., Long-Range Orientational Organization of Dipolar and Steric Liquids. *The Journal of Physical Chemistry Letters* **2020**, *11* (22), 9869-9875.
43. Zajac, J., Calorimetry at the Solid–Liquid Interface. In *Calorimetry and Thermal Methods in Catalysis*, Auroux, A. E., Ed. Springer Series in Materials Science: 2013; pp 197-270.
44. Gassin, P.-M.; Bellini, S.; Zajac, J.; Martin-Gassin, G., Adsorbed Dyes onto Nanoparticles: Large Wavelength Dependence in Second Harmonic Scattering. *The Journal of Physical Chemistry C* **2017**, *121* (27), 14566-14571.
45. Houbrechts, S.; Clays, K.; Persoons, A.; Pikramenou, Z.; Lehn, J.-M., Hyper-Rayleigh scattering investigation of nitrobenzyl pyridine model compounds for optical modulation of the hyperpolarisability. *Chemical Physics Letters* **1996**, *258* (3), 485-489.
46. Kondo, J. N.; Nishitani, R.; Yoda, E.; Yokoi, T.; Tatsumi, T.; Domen, K., A comparative IR characterization of acidic sites on HY zeolite by pyridine and CO probes with silica–alumina and  $\gamma$ -alumina references. *Physical Chemistry Chemical Physics* **2010**, *12* (37), 11576-11586.
47. Liu, Y., Is the Free Energy Change of Adsorption Correctly Calculated? *Journal of Chemical & Engineering Data* **2009**, *54* (7), 1981-1985.



## Supporting Information:

# The driving forces of cationic dye adsorption, confinement and long range correlation in Zeolitic Materials

*Marwa Assaf, Gaëlle Martin-Gassin, Benedicte Prelot, Pierre-Marie Gassin\**

### 1°) SHS experimental setup details

The SHS experimental setup was built on a femtosecond Ti-sapphire oscillator laser source providing pulses with a duration of about 100 fs at a repetition rate of 80 MHz (coherent, model Chameleon ultra II). After passing through a low-pass filter, the fundamental beam, set to a fixed wavelength at 800 nm and an averaged power of 600 mW, was focused by a microscope objective (Ealing x10, numerical aperture 0.25.) onto the sample at 1 mm close to the output cell window (Hellma QS 10 mm). The SH light was collected at 90° by a 10 cm focal length lens and separated from its fundamental counterpart by a high-pass filter. The SH light was detected with a water-cooled CCD camera (Andor, Newton) placed after a spectrometer (Andor, Shamrock 193). The fundamental input beam was linearly polarized and the input polarization angle  $\gamma$  was selected with a rotating half-wave plate. An analyzer, placed in front of the spectrometer, was used to separate two polarization states: vertical output state further named  $I(\gamma, V_{out})$ , or horizontal output state referred to  $I(\gamma, H_{out})$ . All the results presented in the manuscript are obtained in the vertical output polarization state. The experimental data are recorded during 10 seconds for each point. All experiments were conducted at 25°C and under stirring condition (a magnetic stirrer operates in the cell measurement). All the data presented in the manuscript have been reproduced three times with different batches. The errors bars

in Figure 77 are obtained with the standard deviation of the  $I_4$  parameter coming from these different batches.

2°) Discussion about the  $2\omega$  photons reabsorption

To take into account the  $2\omega$  photons re-absorption by the suspension, the equation (3) of the manuscript has to be corrected with a Beer Lambert factor according to<sup>203</sup>:

$$I_{suspension\_corrected}^{2\omega}(\gamma) = I_{suspension}^{2\omega}(\gamma) \times 10^{(Abs_{2\omega} * l/L)} \quad \text{(equation S1)}$$

Where  $Abs_{2\omega}$  is the Absorbance of the suspension at 400 nm measured by UV-vis apparatus with  $L=1\text{cm}$  is the length cell and  $l=1\text{ mm}$  is the optical path length of the second harmonic photons. For all the SHS measurement presented in the manuscript, the absorbance of the suspension at 400 nm is below 0.3. Thus, the Beer Lambert term in equation (S1) is at the outside equal to 1.07 leading to a fraction inferior to 10% of photon reabsorbed. This correction has not been taken into account in the data presented in the manuscript. For sample with high reabsorption (this is not the case for the data presented in the manuscript), the following procedure may be used:

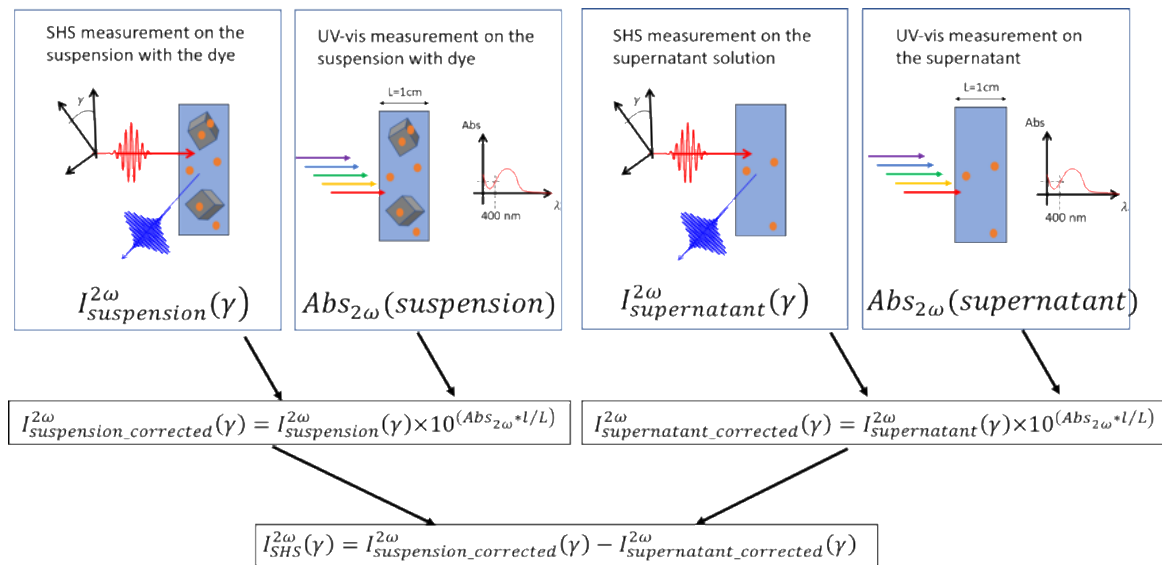


Figure S1. Procedure which may be used to take into account reabsorption.

3°) Additional SHS experimental data

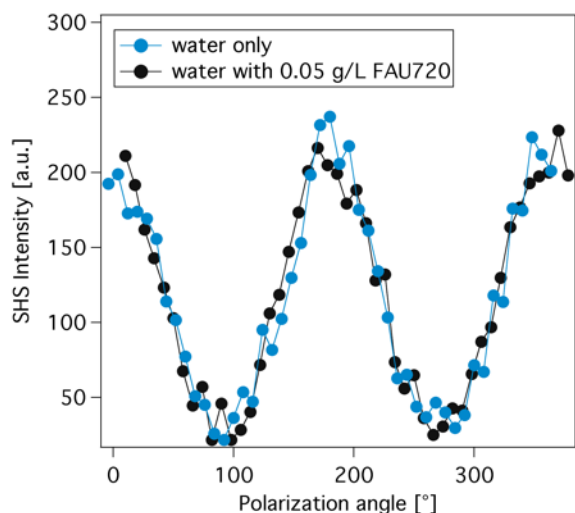


Figure S2: SHS polarization plot of pure water without (blue points) or with Faujasite FAU720 material (black points).

#### 4°) suspension characterization: Dynamic Light Scattering (DLS) measurement

Samples were prepared by suspending 1mg FAU in 10 ml either ultra-pure water or other solvent (ethanol, methanol, acetonitrile, DMSO), thus suspension is sonicated for 10 min in ultrasonic bath to homogenize the sample. The apparatus used to characterize the zeolite suspension is a NanoZS (Malvern Instrument, UK) equipped with a 633 nm He-Ne laser. The measurements were carried out at 25 ° C and at a scattering angle of 173 °. The following results have been obtained:

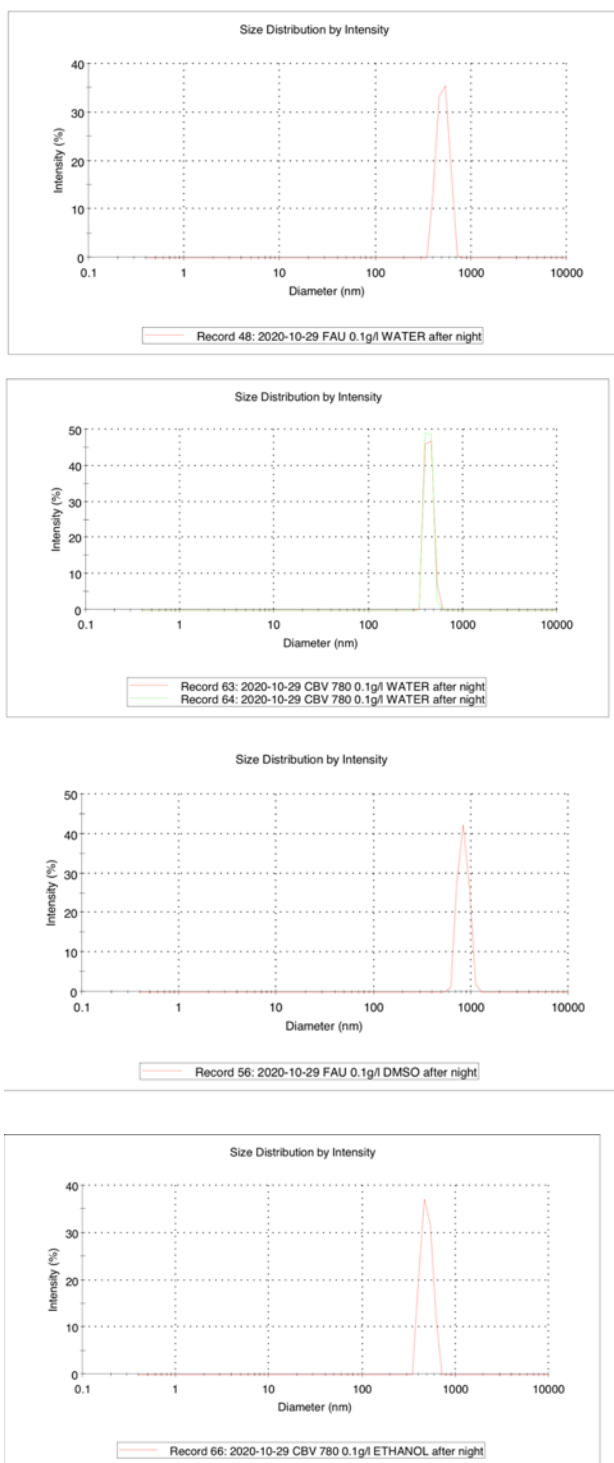


Figure S3. DLS size distribution for FAU720 with water solvent (a), for FAU780 with water solvent (b), for FAU720 with DMSO (c), for FAU 780 with ethanol solvent.

5°) Theoretical Cationic Exchange Capacity

- FAU720 :  $H_{12}Al_{12}Si_{180}O_{384}$  (ratio Si/Al=15)

$$M(\text{FAU720}) = 11520 \text{ g/mol}$$

The Cationic exchange capacity is obtained when all the H<sup>+</sup> are exchange, ie

$$\text{CEC} = 12/11520 = 1.04 \text{ mmol/g}$$

- FAU400 :  $H_{54}Al_{54}Si_{138}O_{384}$  (ratio Si/Al = 2.55)

$$M(\text{FAU400}) = 11520 \text{ g/mol}$$

$$\text{CEC} = 54/11520 = 4.69 \text{ mmol/g}$$

- FAU780  $H_{4.7}Al_{4.7}Si_{187.3}O_{384}$  (ratio Si/Al = 40)

$$M(\text{FAU400}) = 11520 \text{ g/mol}$$

$$\text{CEC} = 4.7/11520 = 0.41 \text{ mmol/g}$$

References:

1. Houbrechts, S.; Clays, K.; Persoons, A.; Pikramenou, Z.; Lehn, J.-M., Hyper-Rayleigh scattering investigation of nitrobenzyl pyridine model compounds for optical modulation of the hyperpolarisability. *Chemical Physics Letters* **1996**, *258* (3), 485-489.

## Conclusion

We have shown that the combination of a series of well-defined materials and well adapted probe molecules allows to identify the contributions of different effects. These include Si/Al ratio, length of alkyl chain of hemicyanin dye, Bronsted acid sites, and proton solvation. The high adsorption capacity reveals that the adsorption of dyes occurs inside the porosity of zeolite. Thanks to SHS measurements that permit to probe the confinement effect of dyes, thus the correlation between molecules on one hand, and the organization of molecules at solid/liquid interface on the other hand.

The adsorption capacity obtained is in the order of FAU400 > FAU720 > FAU780 which is related to the cationic exchange capacity (CEC) of the material. In addition, in the case of FAU720, this capacity varies with solvents, ranging from water, having the highest Bronsted acidity sites, to acetonitrile followed by ethanol then DMSO. This allowed us to probe the organization of dyes inside the zeolitic material using SHS measurements. It is important to note that the FAU720 shows high correlation in the presence of water solvent since it has the highest  $I_4$  parameter in absolute value.

Based on these results, we can conclude that the variation of the correlations in long range organized system is mainly related to the change of the confinement properties. Confinement effect can be explained by the frozen movement of dyes inside the pores. The movement of dyes depends on the Si/Al ratio that is related to the charge present in the material. In the confined system, the loading inside the material is optimized to fill the pores perfectly to not disrupt the dye. This leads to a high organization of molecules at solid/liquid interface thus a high correlation between molecules.



## Chapter V: Effect of modification of the porosity of Zeolite FAU on the adsorption of dyes: contribution of global and local techniques

In parallel to the previous paper, this part constitutes a second paper to be submitted in the Journal of colloid and interface science. The results presented here concern the study of the effect of modification of FAU pores on the adsorption of the dyes at the solid/liquid interface.

In this section, we studied the modification of the porosity of FAU. FAU has been prepared by alkaline treatment followed by the addition of surfactant to build mesoporosity. Various levels of mesoporosity were obtained by varying Si/NaOH ratios and noted as FAU-0 (unmodified), FAU-1, FAU-2, and FAU-3. Two molecules, sDiA and basic fuchsin, with different groups and sizes (linear and bulky dye) were chosen as probe molecules.

We sought to determine the capacity of the probe molecules as a function of the pore modification. For this purpose, adsorption isotherms were established. In addition, SHS was used to probe the organization of molecules and their correlations at the solid/liquid interface. Moreover, the global enthalpy of adsorption was also measured using direct calorimetric measurements as a function of modified porosity.

Beforehand, several characterization techniques were performed to analyze the hierarchical materials obtained after modification of porosity. Nitrogen sorption isotherm will allow determining the specific surface area, the micropore, and the mesopore volume of the hierarchical materials. The structure of these materials as well as the determination of elemental will be studied by X-ray fluorescence (XRF) and silicon NMR. X-ray diffractometry measurements will also be made to determine the crystallinity of the materials as well as the orderly organization of the mesopores.



1 Written manuscript submitted in Journal of colloid and interface science

**Effect of modification of the porosity of Zeolite FAU on the adsorption of dyes: contribution of global and local techniques**

M. Assaf, L. Desmurs, Ph Gaveau, A. Galarneau, P-M. Gassin, G. Gassin\*, B. Prelot\*

*Univ Montpellier, CNRS, ENSCM, Institute Charles Gerhardt, UMR 5253,*

*Montpellier Cedex 5, 34095, France*

**Keywords:** hierarchical faujasite, adsorption isotherm, dyes, confinement effect, Second Harmonic Scattering, Isotherm Titration Calorimetry

**Abstract**

Adsorption processes at the solid / liquid interface are driven by numerous factors coming from the adsorbate, the adsorbent, both possibly modified when in contact with the solvent. In the context of waste water treatment as well as from the strict fundamental point of view, better knowledge of interaction mechanisms could provide valuable evidences in order to optimize the materials or to better understand the driving forces of sorption. These approaches require to combine information at different scales, and including the consideration of various properties of the adsorbent / adsorbate system. Concerning the solids, not only the structural and the chemical properties of the adsorbent influence the adsorption, but the textural characteristics are also key issues, with the probable impact of different level of porosity, commonly named as confinement effects. On the other hand, various methodologies have to be combined to acquire complementary evidence of the effect of surface chemistry microporosity.

Adsorption of cationic dyes in so called hierarchical materials has been investigated through adsorption isotherms, Isothermal Titration Calorimetry (ITC) and polarization-resolved by Second Harmonic Scattering (SHS) measurements. Zeolite-Y (commercial H-FAU with Si/Al = 15) has been used as a zeolite reference material. Modification of the initial solid has been carried out to introduce mesoporosity in addition to the pristine microporosity of faujasite (FAU-0), while trying to keep the

same surface chemistry. A series of hierarchical FAU (FAU-1, FAU-2 and FAU-3) has been prepared by the dissolution-reconstruction process in alkaline conditions and by adding a structuring agent. Alkyltrimethylammonium surfactant has been used, and depending on the amount of NaOH, various degrees of modification has been obtained. The four materials have been extensively characterized using N<sub>2</sub> adsorption isotherm, <sup>29</sup>Si-NMR, X-Ray fluorescence, and X-Ray diffraction to evaluate structural and textural properties.

Two dyes have been chosen (Styryl Pyridinium sDiA and Pararosaniline or Basic Fuchsin BF) as probe molecules of the interface, because, as conjugated molecules, they exhibit high hyperpolarizability that allow them to be used in SHS, and then reveal the interfacial organization. The sorption capacity of the linear probe sDiA onto the less modified faujasites (FAU-0, FAU-1, FAU-2) was similar 600 μmol/g and decreased for the highly modified materials (FAU-3 with 400 μmol/g). On the other hand, the bulkier molecular probe BF is slightly adsorbed for purely microporous solid (FAU-0 with sorption at 50 μmol/g), while this capacity increases progressively with increasing the mesoporosity. The ITC signals exhibits two regimes, for adsorption capacity lower or higher than 400 μmol/g. For low surface coverage, the displacement enthalpies of sDiA are in the range of -16 to -28 kJ/mol, with the lowest value for the initial zeolite, and quite similar for the three mesoporous faujasites. The effect of the various level of porosities is more pronounced for higher surface coverage. The displacement enthalpy is increased to -50 kJ/mol for microporous and slightly modified solid, is stable for the intermediate material, and decreased for highly modified materials FAU-3. In the case of BF (for FAU-2 and FAU-3), the adsorption enthalpies are slightly lower for low surface coverage, in relation with the size and the steric hindrance of BF. In the second regime, it marginally increases for FAU-2 and remains stable for FAU-3.

In addition, the correlation factor evaluated from SHS plots, or normalized  $i_4$ , becomes less negative as the fraction of mesopore increases, thus the correlation between dyes molecule decreases. The confinement effect on the adsorption of sDiA and BF has been confirmed when the enthalpy and the normalized  $i_4$  become more negative.

## 1. Introduction:

Despite 72% of the surface of the earth being covered by water, only 0.5% is freshwater. The most hazardous contamination is the organic molecules like dyes, pesticides, and toxins since they contain conjugated molecules.<sup>206</sup> Worldwide discharging of dyes has been projected at approximately 700,000 tons per year which is 70% of dye production. Dyes such as basic fuchsin, BF, crystal violet, malachite green are mainly used in textile, leather, food, paper, dyeing, and printing

industries.<sup>157, 207</sup> Particularly, a biological dye, trans-4-[4-(dibutylamino)styryl-1-methyl]pyridinium iodide, sDiA, is an interesting probe molecule because it has a unique behavior.<sup>208</sup> Dyes are complex aromatic molecules that are not biodegradable, so they may pose a threat to human health and the environment.<sup>209</sup> It has been clued up to cause mutagenesis, chromosomal fractures, carcinogenesis, respiratory toxicity and affecting the photosynthetic activity in aquatic life by reducing the availability of sunlight.<sup>210</sup>

The reduction or removal of these toxic molecules from water is a big challenge in the world. This can be achieved by various methods such as chemical extraction, electrochemical processes, membrane filtration, ozonation, radiolysis, reverse osmosis, bioleaching, and adsorption, or by combining several of these methods.<sup>101, 211</sup>

The sorption-based technology usually combines easy handling, fast operational readiness, low operating costs, low-level discharge generation, and also good chemical, thermal and mechanical stability.<sup>212</sup> Decontamination processes are often based on the use of materials with specific properties such as high adsorption capacity and accessibility which is the case of nanostructured materials such as zeolites, activated carbon or clays.

The most efficient material for dyes removal is activated carbon, but they are suffering from high costs and difficulties in regeneration<sup>209</sup>. Zeolites are providing high adsorption capacities since they display a crystalline network together with a microporosity and a large surface area. They are thus commonly used in numerous application domains such as catalysis, adsorption, separation. In addition to their advantage, there is a limitation of diffusion due to the clogging of the pore of the bulky product such as dyes which leads to a limitation of the mass transfer thus slow kinetics and the deactivation of the zeolite by causing high back pressure.<sup>213, 214</sup> The Si/Al ratio and the position of the negative charge density vary from one zeolite to another<sup>215</sup>. The exchangeable cationic sites and the porosity make the zeolite a strong adsorbent. Molecules such as dyes are selectively adsorbed onto zeolite depending on their shape, size, or electrical charge.<sup>216</sup>

Nowadays, the confinement term is used to mean a modification in the physico-chemical properties of the molecular species confined in the pores space.<sup>76</sup> Most studies were made on the water<sup>83</sup> or solvent<sup>78, 79</sup> confinement in the pore space with the help of molecular simulations.<sup>217, 218</sup> From the fundamental point of view, the different contributions in the adsorption, sequestration, and confinement processes<sup>191</sup> are still not clear especially the adsorption of dyes. There are three factors that confinement can affect the adsorption process. These factors are (i) size, (ii) shape, and (iii) interaction of guest species with the boundaries of the confined space.<sup>80</sup> When the size of molecules is comparable to the pore size, we are probably in a confined system, thus the initial heat of adsorption

increases sharply. In the case of small molecules, the initial heat of adsorption tends to rapidly decrease until reaching the plateau whereas it remains constant for the larger molecules. In the confinement model, the adsorption of small molecules firstly takes place in order to increase the Van der Waals attraction energy also to achieve the best fit between the molecules (shape and size) and intercrystalline zeolites<sup>219</sup> thus the enthalpy decrease (become more negative).<sup>80, 92, 93, 220</sup>

Furthermore, hierarchical zeolite is the primary goal to reduce or remove the limitation of diffusion in microporosity, thus resulting in additional pores that improve the accessibility for bulky molecules. Additional pores can be added using a different process such as steaming, acid leaching, and desilication. Dealumination treatment generates pores that are not homogenous in size and not connected to the external surfaces as mentioned in the literature.<sup>221</sup> However, desilication with base leaching especially NaOH has been specified as a powerful and efficient process for introducing mesoporosity connected to the exterior by maintaining the crystallinity and acidic properties of the pristine zeolite<sup>222</sup> but the mesopores are not homogenous in size.<sup>28, 223</sup> Thus, a surfactant can be added in the desilication process<sup>23</sup> to obtain more ordered mesoporosity that is homogeneous in size and can be either restricted to the external layer of the zeolite crystal or connected to the microporosity<sup>30</sup>.

The second harmonic scattering (SHS) is a powerful surface technique used as a probe to investigate the interaction and orientation of dye molecules at a flat solid/liquid interface.<sup>109, 119, 120, 224</sup> SHS is based on SHG (Second Harmonic Generation, a second nonlinear optical technique), which results in the incident light at frequency  $\omega$  scattered at  $2\omega$  after interacting with active matter. It is only applied when the inversion of symmetry is broken.<sup>224, 225</sup> This technique is well used to explore the confinement effect, diffusion, and capacity effect. A theoretical model could be applied to give a microscopic interpretation of the experimental pattern.<sup>122</sup> The SHG signal can be greatly improved if the wavelength is close to two-photon resonating molecules.<sup>226</sup>

In the present study, two cationic dyes have been chosen (sDiA and BF). They differ from each other by having different reactive groups, different sizes, and thus different interactions with the adsorbent material. These dyes are cationic organic molecules, achiral amphiphilic dyes and have been used as a probing molecule in interfacial studies using SHG because of their large second-order nonlinear hyperpolarizability.<sup>227, 228</sup> sDiA dye is known as an efficient SHG active molecule, and Kim and co-workers demonstrate its intercalation in the zeolitic system.<sup>199, 229</sup> The organization and orientation of the molecules adsorbed at the solid/liquid interface can be determined by measuring their SHG.<sup>230</sup> The material studied here is a Faujasite type zeolite which consists of cubic-octahedrons called sodalite cages or  $\beta$ -cages. The assembly of these cages linked together by hexagonal prisms leads to windows of 7.4 Å and a larger cavity of diameter 13 Å called supercage (SC), which is close to the size of the guest sDiA dye molecule (4.3 Å x 14.5 Å) chosen.<sup>231</sup> However, the size of the BF dye molecule (11.9 Å x

10.6 Å) is too large to enter Faujasite cavities. The hierarchical Faujasites prepared by micelle-templating feature additional mesopores of 40 Å pore diameter accessible for both probe molecules.

Various characterization methods have been performed on the prepared hierarchical Faujasite such as X-ray diffraction, X-ray fluorescence, N<sub>2</sub> Sorption Isotherm, and <sup>29</sup>Si solid state NMR. Adsorption has been studied by combining macroscopical and local approaches. To that purpose, standard adsorption isotherms were determined using the depletion method and classical analytical tools such as UV. In addition, the original methodology has been developed to study orientation and correlation between dyes or within the materials. Non-linear optics, in particular, Second Harmonic Generation (SHG) measurements were carried out. In the end, direct calorimetric studies at the solid/liquid interface along the adsorption were performed to evaluate the adsorption molar enthalpy ( $\Delta H_{ads}$ ) accompanying dye adsorption on FAU in order to correlate the thermodynamics and the local adsorption mechanism.

## 2. Materials and methods

### 2.1 Materials and Faujasite modifications

H-Faujasite (Si/Al = 15) under the trade name CBV720 was purchased from Zeolyst International. Sodium hydroxide pellets (NaOH); octadecyltrimethylammonium bromide (C<sub>18</sub>TAB), MW = 329.50 g.mol<sup>-1</sup> and 98% purity; trans-4-[4-(dibutylamino)styryl-1-methyl]pyridinium iodide (sDiA), C<sub>16</sub>H<sub>19</sub>IN<sub>2</sub>, MW= 366.24 g.mol<sup>-1</sup> and 98% purity and Basic Fuchsin (BF) C<sub>19</sub>H<sub>17</sub>N<sub>3</sub>.HCl, MW= 323.82 g.mol<sup>-1</sup> and purity > 85%, was purchased from Sigma Aldrich. The structures are shown in Table 11. The solution was prepared using ultra-pure water (18MΩ). All materials were used without any further purification.

A series of modified faujasites (FAU) were synthesized using CBV720 as starting material following the methodology previously developed by Galarneau et al.<sup>123</sup> The procedure is based on the use of a base as a leaching agent (NaOH) and then the addition of a structuring agent (octadecyltrimethylammonium bromide, named C<sub>18</sub>TAB) to generate an ordered mesoporosity of 40 Å diameter. Different quantity of NaOH pellets (0.3495; 0.8854; 1.1655 g for NaOH/Si ratio 0, 0.075, 0.095 and 0.25 respectively) was used depending on the expected additional mesoporous volume. By increasing the quantity of NaOH, the volume of mesopores increases and the volume of micropores decreases (Table 12). NaOH was added with 104.86 g of H<sub>2</sub>O into a 250 ml beaker in the presence of a magnetic stirrer to achieve total dissolution. 4.573 g of C<sub>18</sub>TAB was then added to the mixture by keeping the stirring until total dissolution. When the homogeneity of the mixture is verified, the magnetic stirrer was replaced by an endless screw stirrer, which is gentler and necessary to keep the particle size and shape of the initial particles. Then 7 g of pristine FAU (Si/Al = 15) was added to the mixture and stirred for 1-2 h at ambient temperature (25 °C) to get a white homogeneous suspension.

After that, the slurry was transferred into a 250 ml Teflon-lined stainless-steel autoclave for 20 hours at 115 °C. Finally, the mixture was filtered and washed several times until the pH becomes neutral followed by drying at 80°C in the oven for 12 h and calcination at 550 °C for 8 h with a heating rate of 5 °C/min. These materials were denoted as FAU-0, 1, 2 and 3 for Si/NaOH ratio 0, 0.075, 0.095 and 0.25, respectively.

## 2.2 Materials characterization

Crystallographic identification and relative crystallinity were determined by X-Ray powder diffractometer (XRD) at room temperature using the Malvern Panalytical Empyrean apparatus with Cu Ka radiation ( $\lambda = 1.5405980 \text{ \AA}$ ). The  $2\theta$  diffraction angles were recorded at a scan rate of  $0.025^\circ$  and a time step of 5 s in the  $2\theta$  range from  $3^\circ$  to  $40^\circ$ .

The nature of different elements, their concentration and the Si/Al ratio were evaluated by Wavelength Dispersive X-ray Fluorescence (WDXRF). The spectrometer applied for the XRF analyses was a PANalytical AXIOS Max with an SST-mAX50 X-ray source specially adapted for the detection of light elements.

Adsorption isotherms for gaseous nitrogen at 77 K were measured using a Micromeritics 3 flex sorption instrument. Each sample was degassed overnight at 200 °C under vacuum prior to analysis. Brunauer–Emmett– Teller (BET) model and corrected t-plots<sup>123</sup> were applied to estimate the external surface area, micropore and mesopore volumes and surface areas.

BET model is used to determine the total surface areas. However, the BET model is valid for microporous materials, as in the case of zeolites, only if the Rouquerol criteria, also called consistency criteria, is used to choose the pressure domain for the BET linearization.<sup>232</sup> The microporous and mesoporous volumes in porous materials were determined by the t-plot method. This method depends on the thickness of the adsorbed layer (t) as the function of pressure for the same adsorbate and temperature. Generally, t values (in nm) are estimated using the following equations:<sup>137</sup>

$$\left(0.009 < \frac{P}{P_0} < 0.12\right) \quad (36)$$

$$t = 1.62973 + 76.4748(P/P_0) - 2171.7914 \left(\frac{P}{P_0}\right)^2 + 41734.77357 \left(\frac{P}{P_0}\right)^3 - 465290.41181 \left(\frac{P}{P_0}\right)^4 + 2.72432.106 \left(\frac{P}{P_0}\right)^5 + 6.43708.106 \left(\frac{P}{P_0}\right)^6$$

$$\left(0.13 \leq \frac{P}{P_0} < 0.6\right) \quad (37)$$

$$t = 3.07721 + 5.64019(P/P_0)$$

$$\left(0.60 \leq \frac{P}{P_0} < 0.80\right) \quad (38)$$

$$t = 4592.05803 - 38\,117.31548(P/P_0) - 131\,602.19741 \left(\frac{P}{P_0}\right)^2 - 241\,680.40239 \left(\frac{P}{P_0}\right)^3 \\ - 249\,079.8569 \left(\frac{P}{P_0}\right)^4 - 136\,632.44762 \left(\frac{P}{P_0}\right)^5 + 31\,182.4149 \left(\frac{P}{P_0}\right)^6$$

For faujasite and hierarchical faujasite, it was demonstrated that classical t-plot underestimated micropore volume and overestimated mesopore surface area. Corrections of micropore volume and mesopore surface area were provided by a corrected t-plot method as a function of  $V_{mic}$  and  $V_{total}$  defined by classical t-plot analysis  $((V_{mic}/V_{tot})_{tpt})$  for hierarchical faujasite following the equations.<sup>55,57</sup>

$$(V_{mic}/V_{tot})_{tpt} < 30\%: \\ (S_{mes+ext})_{real} / (S_{mes+ext})_{tpt} = 1 \quad (39)$$

$$30 < (V_{mic}/V_{tot})_{tpt} < 55\%: \\ (S_{mes+ext})_{real} / (S_{mes+ext})_{tpt} = 1.6 - 0.02138(V_{mic}/V_{tot})_{tpt} \quad (40)$$

$$(V_{mic}/V_{tot})_{tpt} > 55\%: \\ (S_{mes+ext})_{real} / (S_{mes+ext})_{tpt} = 0.38 \quad (41)$$

$$(V_{mic}/V_{tot})_{tpt} < 7\% : \\ (V_{mic})_{real} / (V_{mic})_{tpt} = 1 \quad (42)$$

$$7\% < (V_{mic}/V_{tot})_{tpt} < 45\% : \\ (V_{mic})_{real} / (V_{mic})_{tpt} = 0.52947 (V_{mic}/V_{tot})_{tpt}^{0.25334} \quad (43)$$

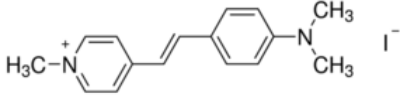
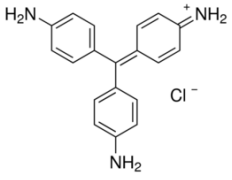
$$(V_{mic}/V_{tot})_{tpt} > 45\% : \\ (V_{mic})_{real} / (V_{mic})_{tpt} = 1.40 \quad (44)$$

with  $(V_{mic}/V_{tot})_{tpt}$  expressed in %.

<sup>29</sup>Si solid state NMR spectra have been recorded on a VARIAN 400MHz VNMRs spectrometer (Wide Bore magnet at 9.4 Tesla) using a T<sub>3</sub>MAS (Magic Angle Spinning) probe with 7.5mm ZrO<sub>2</sub> rotors. Spectra have been acquired using quantitative single pulse technique with <sup>1</sup>H decoupling: recycle delay of 60s,  $\pi/6$  pulse of 2  $\mu$ s and spinning rate of 5 kHz. Q8M8H (octakis(dimethylsiloxy)octasilsesquioxane) has been used as a secondary reference (left peak at -2.25 ppm). The spectra were fitted using DMFit software<sup>233</sup> to extract quantitative contributions of the different <sup>29</sup>Si environment.

**Chapter V: Effect of modification of the porosity of Zeolite FAU on the adsorption of dyes: contribution of global and local techniques**

Table 11 : sDiA and BF structures and their general characteristics.

Dye	structure	Length Å	Width Å	Depth Å	Wavelength nm
sDiA		14.5	4.3	1.80	443
BF		11.847	10.611	6.260	538

### 2.3 Second Harmonic Scattering Setup

The Second Harmonic Scattering (SHS) was constructed from a femtosecond Ti-sapphire oscillator laser source delivering pulses with a duration of  $\sim 100$  fs at a repetition rate of 80 MHz (Spectra-Physics, model Mai Tai). The initial beam in the presence of a low-pass filter is used to extract the undesirable harmonic light that cannot be produced by the interface. This beam was directed to the sample through the lens with a focal length of 10 cm at 800 nm wavelength and a standard power of 600 mW. The second harmonic light (SH) was collected at  $90^\circ$  and detected with a water-cooled CCD camera (Andor, Newton) placed after a spectrometer (Andor, Shamrock 193). Separation of vertical output (V\_out) or horizontal output (H\_out) SH intensities was performed with an analyzer which was placed in advance of the spectrometer. Both suspension and supernatant were measured in a cuvette of 3ml. The experiments were carried out at  $20^\circ\text{C}$  and under stirring conditions (a magnetic stirrer is operated in the cell measurement)<sup>119, 195, 228, 234</sup>.

At high concentration, the absorption is maximum with respect to the solid capacity. Many additional molecules keep free in the bulk. Consequently, the SHS signal is partially reduced by the reabsorption of those free colored molecule at the second harmonic wavelength in the light path.<sup>227</sup> The reabsorption effect of molecules at 400 nm (harmonic wavelength) was considered for the correction of second harmonic intensity.

$$I^{2\omega}(\gamma, \Gamma) = I_{measured}^{2\omega}(\gamma, \Gamma) \times 10^{(Abs_{2\omega} * l/L)} \quad (45)$$

$I_{measured}^{2\omega}$  is the second harmonic light effectively detected and  $A_{2\omega}$  is the linear absorbance at  $2\omega$ <sup>120</sup>.



The SHS signal is resolved in polarization to study molecular orientation.<sup>122</sup> In the present work, the experimental work is compared with the theoretical model (fitting the SHS curve) to obtain valuable information about the interaction between molecules.

The SHS signal can be calculated using the following mathematical expression:

$$I_{SHS} = i_0 + i_2 \cos(2\alpha) + i_4 \cos(4(\alpha - \alpha_0)) \quad (46)$$

where  $i_0$ ,  $i_2$ , and  $i_4$  are the magnitude of the constant, the  $2\alpha$  harmonic and the  $4\alpha$  harmonic, respectively, and  $\alpha_0$  is the phase shift of the  $4\alpha$  frequency with respect to the  $2\alpha$  frequency. The first hyperpolarizability of the molecule is determined by  $i_0$  and  $i_2$ , while the long-range term (correlation effect) from  $i_4$  is evaluated by the following formula.

$$\text{normalized } i_4 = \frac{i_4}{i_0} \quad (47)$$

#### 2.4 Isothermal titration Calorimetry (ITC)

The displacement enthalpy associated with the adsorption of the dye molecules at 298 K was measured using an Isothermal Titration Calorimetry setup, installed in a nanocalorimeter in a long-term stability thermostat (TAM III). The titration was ensured with 25 injections of a stock solution containing 2 mM sDiA (or BF) added using a Hamilton micro-syringe. The 1 mL measuring ampoule containing approximately 1 mg of powder and 0.8 mL of ultrapure water (prepared as a suspension of 10 mg of powder with 8 ml of ultrapure water sonicated for 10 min) was placed in the nanocalorimeter. The homogeneity of the solid suspension was maintained by means of an agitation system equipped with a gold paddle stirrer. 10  $\mu$ L of the stock solution was successively injected during 10 s under a stirring speed of 90 rpm with an equilibration time of 45 min between two successive injections. The experimental enthalpy changes were then corrected for dilution effects.<sup>235, 236</sup> The dilution experiments were performed under the same experimental conditions but without the zeolite powder in the measuring ampoule.

The heat, in kJ, has been obtained from each injection  $i$  in the experiment by integrating the thermograms provided by the equipment and the enthalpy change produced from the adsorption ( $\Delta H_{ads}$ ), in kJ/mol was achieved using the following equation:<sup>237</sup>

$$\Delta_{\alpha} H_{cum} = \sum_{j=1}^k \frac{\Delta_{inj} H_j - n_{inj} \Delta_{dil} H(C_e)}{Q_e^j - Q_e^{j-1}} \quad (48)$$

Where  $\Delta_a H_{cum}$  is the total enthalpy change recorded during the  $i^{th}$  injection; is the number of moles of anions introduced into the calorimetric ampoule; is the molar enthalpy effect of dilution of the same stock solution to an equilibrium concentration  $C_e$ ; indicates the corresponding change in the amount of solute adsorbed at the solid-liquid interface.

### 2.5 Adsorption isotherms

Batch adsorption tests were performed using the depletion method. Faujasite suspension (0.1 g/l) was prepared from faujasite material suspended in ultra-pure water sonicated for 10 min to assure homogeneity. The mixture was added to 14 tubes with different ratios of a concentrated mother solution of dyes and EUP with a constant amount of solution. The pH of the solid/liquid suspension measured without any modification of the pH. The tubes were then stirred at ambient temperature ( $25 \pm 2^\circ\text{C}$ ) for 18 h to ensure adsorption equilibrium. After that, the pH was measured again to monitor the pH evolution. The particles were then separated from the liquid phase by centrifugation at 11000 rpm for 60 minutes, followed by the filtration of the supernatant using a syringe filter (Polypropylene membrane  $0.22\mu\text{m}$  porosity). The equilibrium concentration of the dyes was measured using UV-Vis spectrometer and Second Harmonic Scattering (SHS) for both suspension and supernatant. These experiments were done at free pH.

The adsorption capacity of molecules  $Q_e$  (mmol/g) was calculated using the following equation:

$$Q_e = \frac{(C_i - C_e)}{C_{ads}} \quad (49)$$

Where  $C_i$  is the initial concentration (mmol/L),  $C_e$  is the equilibrium concentration (mmol/L) and  $C_{ads}$  is the concentration of adsorbent (g/l).

Table 12 : Textural and structural properties of commercial FAU hierarchical FAU-Y synthesized with different NaOH/Si ratio.

Material	NaOH/Si	Si/Al ratio	% Relative Crystallinity	S <sub>BET</sub> (m <sup>2</sup> /g)	V <sub>micro</sub> (cm <sup>3</sup> /g)	V <sub>meso</sub> (cm <sup>3</sup> /g)	S <sub>micro</sub> (m <sup>2</sup> /g)	S <sub>meso+ext</sub> (m <sup>2</sup> /g)	S <sub>ext</sub> (m <sup>2</sup> /g)
		XRF	XRD		Corrected t-plot	Corrected t-plot	Corrected t-plot	Corrected t-plot	t-plot
FAU-0	0	15	100	944	0.371	0.020	832	105	99
FAU-1	0.075	15	96	924	0.292	0.244	596	298	29
FAU-2	0.095	15	75	916	0.223	0.386	417	509	30
FAU-3	0.25	13	12.5	860	0.048	0.679	127	827	34

## 3. Results and discussions

### 3.1 Characteristic of faujasite

The XRD patterns for modified faujasite are shown in Figure 78. The characteristic diffraction peaks that ranged between 3-40° exist in FAU-0, 1, 2, and 3, indicating the faujasite structure, implying that the FAU structure was retained after modification with alkaline treatment.<sup>238, 239</sup> It should be noted that the intensity of XRD patterns for modified FAU (FAU-1 and 2) decreased slightly, while a significant decrease is shown for FAU-3.<sup>222, 240</sup> When passing from FAU-0 to FAU-1, -2, -3, the XRD pattern shows at a small angle the appearance of a broad peak at  $2\theta = 2.15^\circ$  for FAU-1,2 and  $2^\circ$  for FAU-3 (supplementary figure-S3). This corresponds to the presence of ordered mesopores as in the case of MCM-41 type materials with a cell parameter of 6.3 nm for FAU-1, -2, and 4.9 nm for FAU-3. As shown previously,<sup>68</sup> this indicates that FAU-1, -2 are ordered mesoporous materials with walls (thickness 2.2 nm) that can accommodate a FAU cell, so walls can be zeolite walls, while FAU-3 is an ordered mesoporous material with walls too thin (1.4 nm) to accommodate a FAU cell and are therefore amorphous. FAU-1,2 presents also zeolite nanodomains of 100-200 nm, whereas for FAU-3 the size of the zeolite nanodomains decrease below 60 nm.<sup>30</sup>

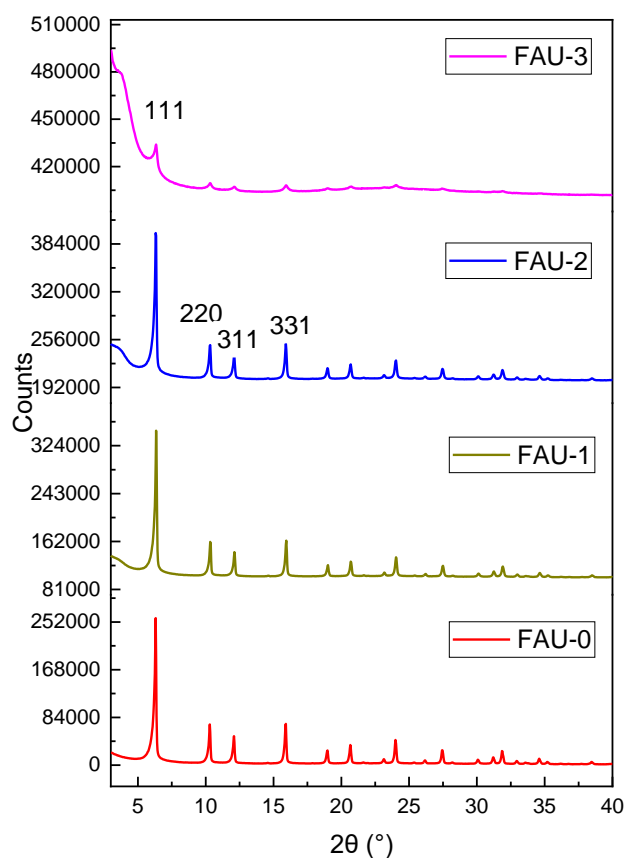


Figure 78: XRD patterns (high angles) of commercial H-FAU-Y (FAU-0) and hierarchical faujasite named FAU-1,2 and 3, XRD pattern (high angles) of FAUmes prepared with different NaOH/Si ratios. Inset, magnification of (220) XRD peak of FAU-Y.

The relative crystallinity of FAU was calculated from the intensity of the peaks at 6.5°, 10.5°, 12° and 16° and reported in Table 12.<sup>241, 242</sup> The calculated values decrease from 100 to 12.5 % when passing from FAU-0 to FAU-3. This confirms that there is a decrease in zeolite nanodomains size with the increase of NaOH treatment.<sup>68</sup>

The Nitrogen adsorption-desorption isotherms at 77K for initial and modified faujasites are shown in Figure 79. Referring to International Union from Pure and Applied Chemistry (IUPAC), the obtained isotherms are classified as the majority of type I (microporous materials) with few mesoporosities for FAU-0 and a combination of type I and type IV for the others with a sharp step of adsorption at around  $p/p_0 = 0.4$  relatives to the capillary condensation into the ordered homogeneous mesopores of 4 nm diameter.<sup>68</sup> This is obvious for the initial material FAU-0 which is pure microporous zeolite. For the others, there is an ongoing evolution of the curves with the NaOH modification, with the increase of total pore volume from FAU-1 to FAU-3.

The textural parameters are calculated and shown in detail in Table 12. The microporous and mesoporous volumes and surface areas were determined using the corrected t-plot method and the BET equation to calculate the total surface area.<sup>55,57</sup> The microporous surface decreases, and the mesoporous surface area increases with the increase of NaOH/Si ratio in the synthesis and are similar for FAU-2 (NaOH/Si ratio = 0.095). The microporous volume gradually decreases from 0.37 to 0.048 cm<sup>3</sup>/g as the NaOH/Si ratio increases in the synthesis, while the mesoporous volume strongly increases from 0.02 to 0.679 cm<sup>3</sup>/g. The micropore and mesopore volumes are similar for FAU-1 (NaOH/Si ratio = 0.075). The external surface area is higher for FAU-0 (99 m<sup>2</sup>/g) in comparison to the modified faujasite (FAU-1, -2, -3) (30 m<sup>2</sup>/g). The formation of mesopores and the increase in mesoporous volume are comparable to the results obtained from the previous studies.<sup>55,57,68</sup> These properties make the hierarchical FAU attractive for their adsorption properties and the removal efficiency of pollutants such as cationic dyes due to the presence of cationic exchange-sites naturally present in zeolites and of additional mesopores of 4 nm diameter large enough to adsorb most organic pollutants<sup>243</sup>.

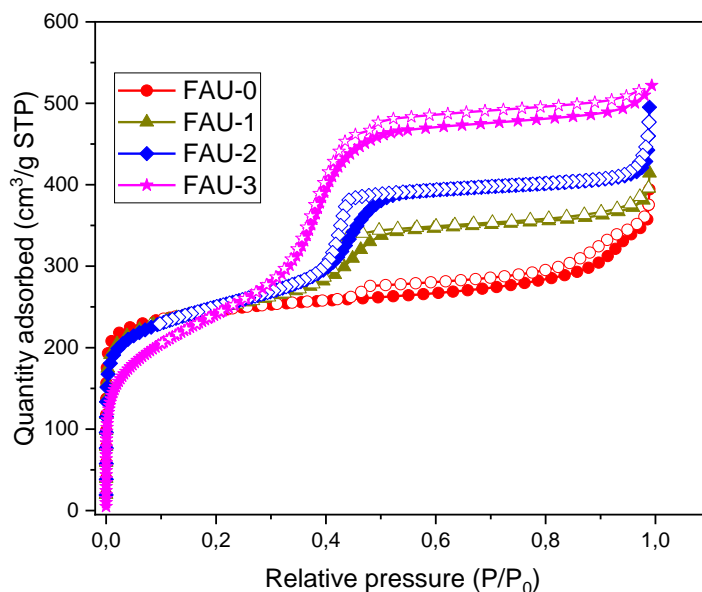


Figure 79: Nitrogen sorption isotherm at 77 K for commercial H-FAU-Y (Si/Al = 15) (CBV720) named FAU-0 and hierarchical FAU named FAU-1, 2 and 3, synthesized from H-FAU-Y and  $C_{18}TAB$  surfactants with NaOH/Si ratios 0.075, 0.095 and 0.25 respectively. The filled and empty symbols correspond to the adsorption and desorption isotherms, respectively.

X-Ray fluorescence (XRF) results are reported in Table 12. The Si/Al ratio is kept constant as for FAU-0 (Si/Al = 15) for the least modified FAU while for highly modified FAU-3, the Si/Al ratio decreased from 15 to 13. The Si amount of FAU-3 decreases with respect to the Al content. The percentage of Al content is constant for the FAU-0, 1, and 2 which is equal to 2.6 %, however, an increase in Al percentage is obtained for FAU-3 from 2.6 to 3.1 %. This reveals that alkaline treatment removes the silicon from the faujasite framework and relative realumination takes place.<sup>28, 239</sup> The decrease in Si/Al ratio also decreases the Brønsted acidity and increases the Lewis acidity<sup>29</sup>.

The  $^{29}Si$  solid-state NMR spectra of commercial FAU and modified FAU are shown in Figure 80. The spectrum of FAU-0 shows results similar to the reference.<sup>75, 146</sup> Contributions, obtained using DMFIT<sup>233</sup>, can be attributed as followed: line at -110.7 ppm correspond to amorphous Si(4Si,0Al) environment, abbreviated  $Q^4_{am}$ , the line at -107.2 ppm correspond to crystalline Si(4Si,0Al) environment, abbreviated  $Q^4_{crys}$ , the line at -101.8 correspond to Si(3Si,1Al) environment, abbreviated  $Q^3_{Al}$ , and finally others at -95.8 ppm and -91.3 ppm correspond to different  $Q^2$  environments.

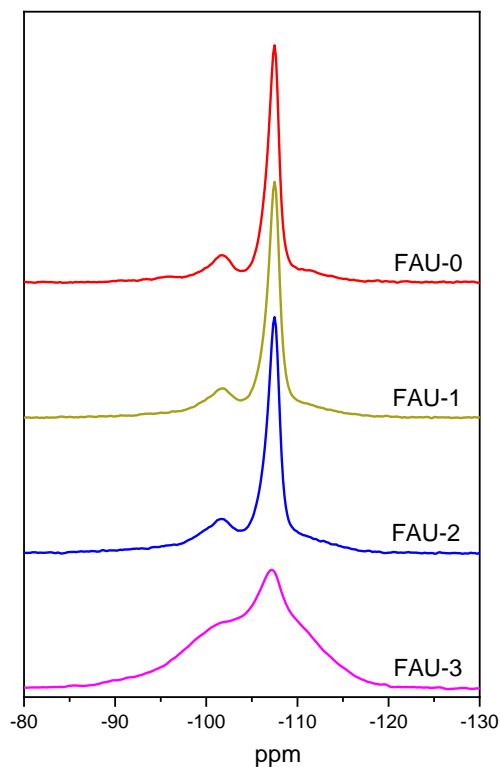


Figure 80:  $^{29}\text{Si}$ -NMR spectra for parent FAU (FAU-0) and modified FAU (FAU-1, 2 and 3).

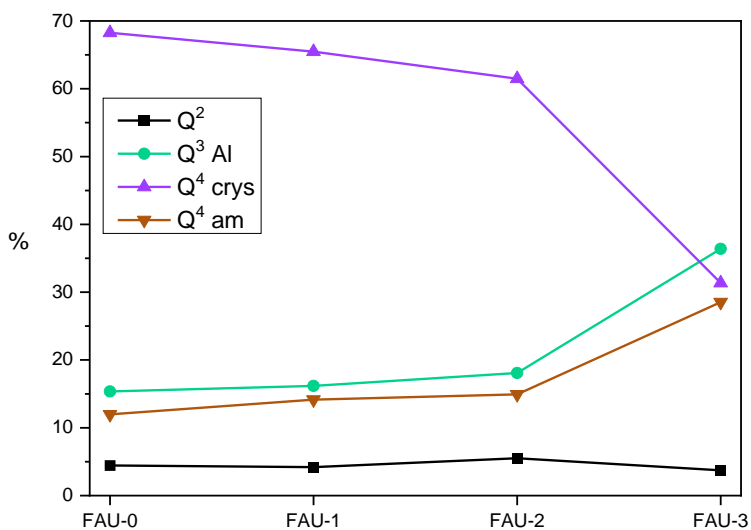


Figure 81:  $Q^n$  contribution corresponds to  $\text{Si}(n\text{Si}, n-1\text{Al})$  environment obtained from Si-NMR analysis using DMFIT.

The Figure 81 shows the evolution of all of these contributions from FAU-0 to FAU-3. For FAU-1 and FAU-2 (lower NaOH/Si concentration), there is a decrease of the  $Q^4_{crys}$  contribution and an increase of both  $Q^4_{am}$  and  $Q^3_{al}$ , thus indicating a transformation of the silicon environment. This effect is drastically seen for the most modified FAU-3. This suggests that both an amorphization ( $Q^4_{crys}$  to  $Q^4_{am}$ ) and a desilication ( $Q^4_{crys}/Q^4_{am}$  to  $Q^3_{al}$ ) of the material are due to the alkaline treatment<sup>146</sup>. The last process leads to an increase of the Al content in the framework and, thus a decrease of the Si/Al ratio, leading to a distortion of the zeolitic structure, in other words, a local transformation from crystalline FAU to a FAU with lower crystallinity or amorphous aluminosilicate<sup>28, 244</sup>.

### 3.2 Adsorption isotherm

The adsorption isotherms of sDiA and BF towards FAU-0 and hierarchical FAU are shown in Figure 82. These figures show that the quantity of adsorbed dye increased with the equilibrium concentration of the dye, meaning favorable adsorption takes place. For sDiA dye (linear molecule) with all materials, the amount adsorbed sharply increases even for very low concentrations. This stands for the high affinity between the dye and the materials, whatever the extent of the modification and the generated hierarchical porosity. Similar maximum adsorption capacity is reported for FAU-0, -1 and -2, which is about 600  $\mu\text{mol/g}$ , while it decreases to be 400  $\mu\text{mol/g}$  for FAU-3.

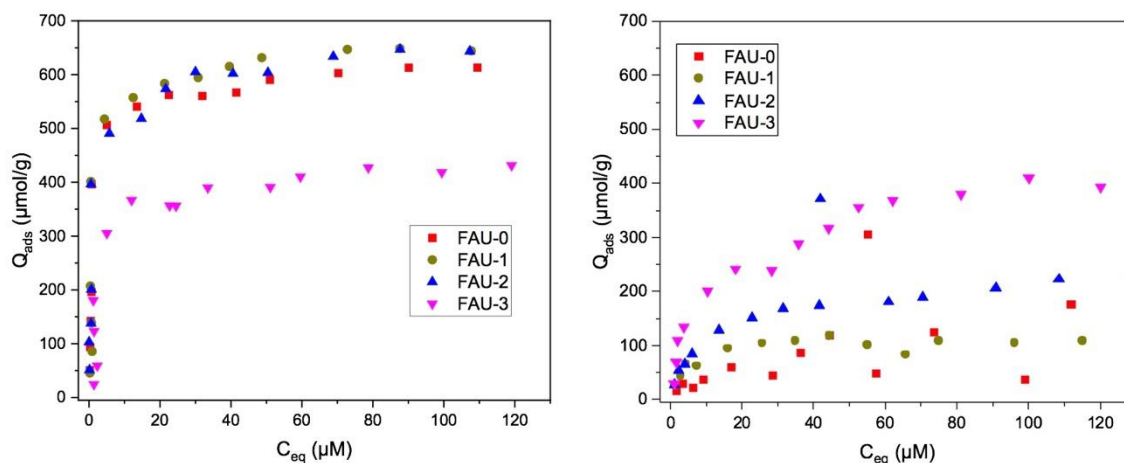


Figure 82: Adsorption isotherm for sDiA (left) and BF (right) onto hierarchical FAU with water solvent using UV-Vis spectrometer.

In the case of bulky dye BF, the shape of the curves is different. The slope of the first part of the isotherm, i.e. the affinity, is less pronounced. The adsorption capacity was 50  $\mu\text{mol/g}$  for the initial

zeolite FAU-0 (micropores) and increased progressively with increasing mesopore volume and surface area from 100  $\mu\text{mol/g}$  for FAU-1 to FAU-3 to 400  $\mu\text{mol/g}$ . This could be explained by the size of the molecule, which is too large (Table 11) compared to sDiA, and it might be assumed that it can not penetrate in zeolite windows and cages.

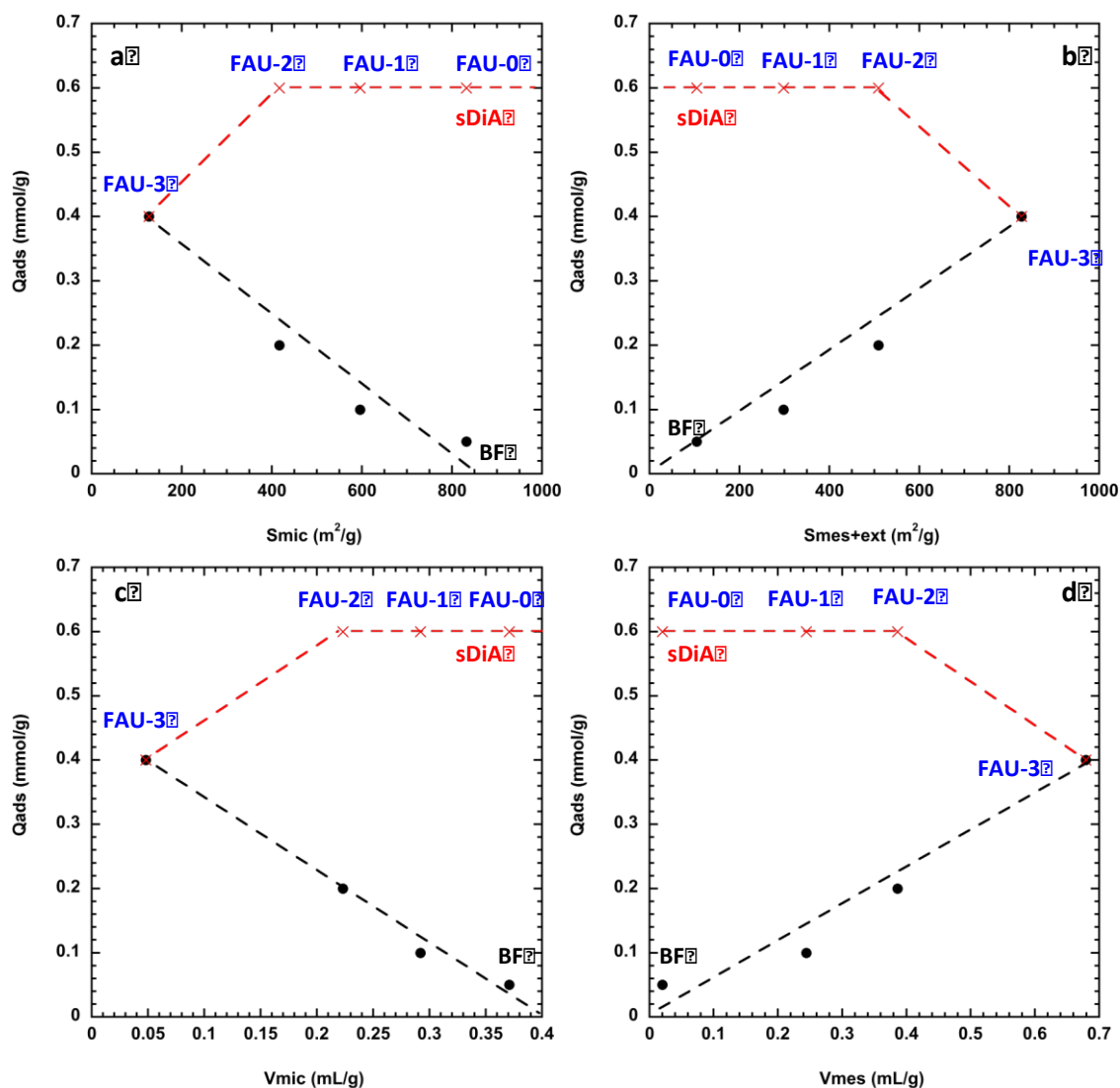


Figure 83: Adsorbed amount of dyes (sDiA and BF) as a function of (a) micropore surface areas, (b) mesopore and external surface areas, (c) micropore volumes and (d) mesopore volumes for FAU-0, FAU -1, FAU-2, FAU-3.

The Figure 83 summarizes the correlation between textural properties (microporous surface areas, mesopore and external surface areas, micropore volumes and mesopore volumes), with the maximum adsorption capacity. It has to be mentioned that FAU-3 exhibits similar adsorption capacity for BF and sDiA whereas the sorption efficiency is influenced by the presence of hierarchical porosity. The comparison between BF and sDiA suggests that adsorption of sDiA occurs within the micropores with higher capacity, while it is limited for BF to mesopore and external surface areas. The amount of



adsorbed BF increases linearly with the increase of mesopore + external surface area (Figure 83) and reaches the maximum at 400  $\mu\text{mol/g}$  for FAU-3. The adsorption of sDiA is independent of the variation of micropore and mesopore volume for FAU-0, FAU-1, and FAU-2, featuring an adsorption capacity of 600  $\mu\text{mol/g}$ . This is surprising since the microporous volume is decreasing from 0.37 to 0.22  $\text{cm}^3/\text{g}$  from FAU-0 to FAU-2. However, the volume of FAU supercages is theoretically equal to 0.28  $\text{cm}^3/\text{g}$  and it was found experimentally to be between 0.16 and 0.27  $\text{cm}^3/\text{g}$  with hexane adsorption. Previously, hexane adsorption on FAU-0 was calculated to be 0.20  $\text{cm}^3/\text{g}$ .<sup>214</sup> Therefore, we can suggest that sDiA fully occupied FAU supercages in FAU-0, FAU-1, and FAU-2 and that the micelle-templating modification of FAU-0 in alkaline medium destroy or distort SOD cages in a way that nitrogen molecules can no more penetrate in these cages.

The decrease in adsorption capacity from 600 to 400  $\mu\text{mol/g}$  for FAU-3 is probably due to the change in the surface properties. XRF analysis has evidenced the decrease of the Si/Al ratio. This is commonly correlated to the increase of the cationic exchange capacity (CEC) and hence the adsorption capacity. This is not the case in the present study, where the adsorption capacity decreases for FAU-3. As a matter of fact, in addition to the CEC modification, the hydrophilicity of the material is also modified as determined with <sup>29</sup>Si NMR where the intensity of the Q<sup>3</sup> signal increases with modification, especially for FAU-3. Due to the local transformation from Q<sup>4</sup> to Q<sup>3</sup>, the hydrophilic character increases due to the increase of the silanol group (Q<sup>3</sup>). This can be confirmed with the recent study by Luo et al.<sup>245</sup> in which they observed that the synthesis of pure Si-Beta zeolites produces the highest intensity of Q<sup>4</sup> compared to the weak intensity of Q<sup>3</sup> in using Si-NMR in combination with TG-DTA which reveals that the material is highly hydrophobic. Another study was done by Galarneau et al.<sup>123</sup> on the same materials where they evaluate the hydrophilic character by estimating the orientation of nitrogen molecules using Ar isotherm. They observed a progressive increase in the hydrophilicity with increasing the FAU modification (increasing NaOH/Si ratio) due to the increase in silanol groups. Thus, the decrease of adsorption capacity could be explained by the competition between the adsorption of the dye molecule and the solvent (water), for the hydrophilic surface of FAU-3<sup>246</sup>. If the hydrophobicity/hydrophilicity balance varies, electrostatic interaction and ionic exchange might not be the predominant mechanism<sup>247</sup>.

The maximum adsorption capacities of modified FAU for BF dyes and sDiA were compared to various materials reported in the literature (Table 13). From this table, it can be concluded that modified FAU even the commercial FAU shows high adsorption capacity compared to other materials. This indicates that from applications point of view, such materials are good candidates for dyes removal.

**Chapter V: Effect of modification of the porosity of Zeolite FAU on the adsorption of dyes: contribution of global and local techniques**

Table 13 : Comparison of modified FAU with other materials reported in the literature for BF and sDiA adsorption .

	Adsorbent	Q <sub>max</sub> (mg/g)	References
BF	SBA-16	40	248
	Al-SBA-16	70	248
	Al-MCM-41	54	249
	Fe(III) and Mn(II) modified activated carbons derived	238	250
	FAU-0	17	This study
	FAU-1	33	This study
	FAU-2	65	This study
	FAU-3	130	This study
sDiA	BeWo cell	22	251
	FAU-0	220	This study
	FAU-1	220	This study
	FAU-2	220	This study
	FAU-3	147	This study

### 3.3 Second Harmonic Scattering (SHS)

The adsorption isotherm is generated to a large extent by the SHS method. SHS curves show the plot of SHS intensity versus polarization angle, described as H<sub>out</sub> and polarV, corresponding to a horizontal and vertical curve, respectively. The SHS plots for sDiA are reported in Figure 84 while for BF the plots can be found in the ESI part (Figure-S6). The SHS signal from free BF and sDiA alone in solution is due to hyper-Rayleigh scattering.<sup>252</sup> The I<sub>4</sub> values are calculated from equation 47 and are plotted in Figure 84 b) for sDiA.

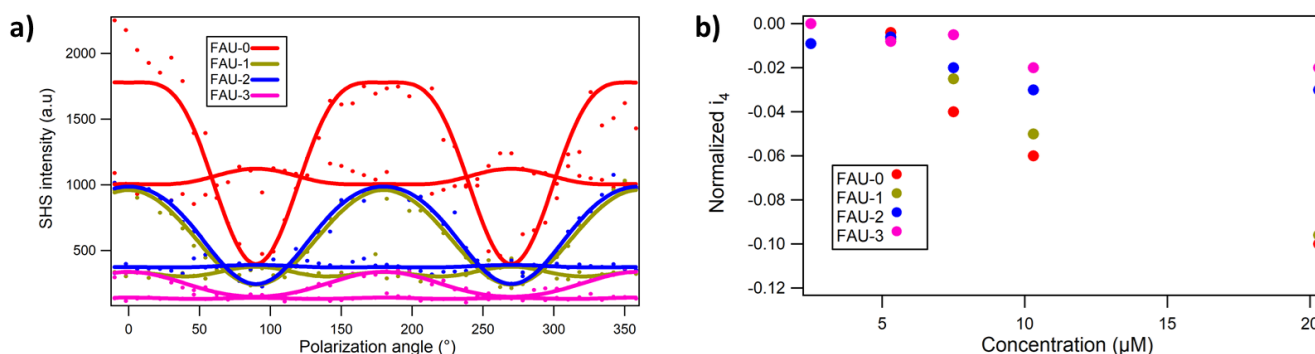


Figure 84: a) SHS polarization plot for sDiA adsorbed onto FAU-0 and hierarchical FAU; b) normalized  $i_4$  ( $I_4$  parameters) deduced from SHS experiment for sDiA adsorption onto pristine FAU and hierarchical FAU.

The  $I_4$  value increases in negative value. By increasing the porosity level, the  $I_4$  parameter reaches lower values, corresponding to higher correlations in the molecular system. This  $I_4$  parameter introduced by Duboisset et al.<sup>122</sup> gives the strength of correlation, and is interpreted as strong interactions between molecules in the solid environment.

In Figure 84a), the intensity of SHS increases probably related to the interactions between the molecule and the material. The high value of  $I_4$  (Figure 84-b) indicates the high interaction with a strong correlation between sDiA molecules in the case of FAU-0. However, with increasing the porosity level, the intensity of SHS decreases as well as the  $I_4$  value is reduced in absolute. This reveals a decrease in interaction between sDiA and the materials (FAU-1 and FAU-2) even though the adsorption capacity is similar for FAU-0, FAU-1 and FAU-2, which contributes to the decrease in correlation between the molecules. This is due to the formation of free space leading to a different orientation of the molecules within the pores<sup>253</sup>. Thus, in the case of FAU-0, where the majority of the pores are micropores, the molecules are confined and give an indication in the form of  $V_{out}$ . This observation holds for all FAU due to the presence of microporosity (enlargement of  $V_{out}$  and increasing intensity of  $H_{out}$ ). However, for modified FAU the modification in the polarization plots becomes less significant with mesoporosity. This reveals that the sDiA molecules are confined and organized in the microporosity.

For BF molecules in FAU-0, FAU-1, and FAU-2, FAU-3, difficulties were encountered to properly determine the values of the  $I_4$  parameter. The signals are bothered by the low intensity and fluctuation of SHS plots (Figure-S6). This do not permit any appropriate data treatment nor confident interpretation. One of the reasons for FAU-0 and 1–could be that the samples exhibit very low adsorption capacity. However, when the sorption capacity increases from 100 to 200 and 400  $\mu\text{mol/g}$  for FAU-2 and 3, respectively), the adsorption process occurs within the mesopores. In this case, the  $I_4$  parameter is expected to increase in absolute value but it is not the case since the mesoporous diameter is larger than the size of BF which leads to adsorption of BF in the presence of free space.

This reveals that BF is not organized, thus the molecules are not correlated as in the case of sDiA in FAU-3.

### *3.4 Isothermal calorimetric titration (ITC)*

In the previous section of this study, the first insight into the interaction between dye and adsorbent has been described from a qualitative point of view. Nevertheless, in order to understand in detail, the driving force behind the dye adsorption, quantitative evidence is required. The enthalpy change of adsorption on hierarchical adsorbent materials has been measured using Isothermal Titration Calorimetry (ITC). In this work, ITC was applied to measure the enthalpy change (adsorption or displacement)  $\Delta_{\text{dpl}}H_{\text{cum}}$  of dyes onto FAU with different porosity as a function of the quantity adsorbed. The enthalpy changes ( $\Delta_{\text{dpl}}H_{\text{cum}}$ ) are displayed in Figure 85. The  $\Delta_{\text{dpl}}H_{\text{cum}}$  values for sDiA (Figure 85 a) and BF (Figure 85 b) are negative, revealing that the adsorption is exothermic.<sup>216</sup>

For all materials, as the dyes adsorption increases,  $\Delta_{\text{dpl}}H_{\text{cum}}$  is divided into two regimes, the first regime is ranged from 0 to 0.2 mmol/g and the second regime for the amount adsorbed higher than 0.2 mmol/g. To analyze quantitatively the obtained curves, the slope of the plot of  $\Delta_{\text{dpl}}H_{\text{cum}}$  versus amount adsorbed corresponding to the molar enthalpy was calculated. The calculation of the slope was performed in the two adsorption capacity regimes and the results are summarized in Table 14. The cumulative enthalpy represents a global effect combining various contributions involved in the overall sorption process. This includes such different contributions as the insertion-sorption of the adsorbed species, the displacement of other species (*e.g.* release of proton or sodium), different types of interaction depending on the molecule to be adsorbed, and the nature of the sorption sites, together with the rehydration/dehydration of the exchanged species or the surface.<sup>187</sup>

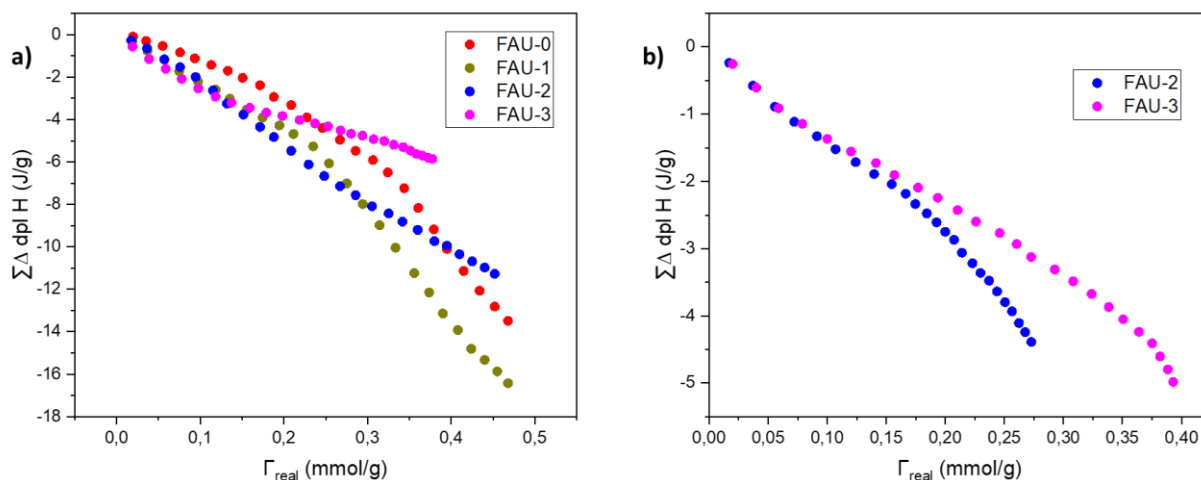


Figure 85: Curves of heat displacement change against the equilibrium adsorbed amount for adsorption of a) sDiA dye and b) BF on the parent FAU and hierarchical FAU adsorbent at free pH values at 25 °C

For the microporous FAU-0, the  $\Delta_{dpl}H_{cum}$  in the first regime is -16.4 kJ/mol which is lower than the values observed for modified FAU (FAU-1, 2, and 3) that are similar (between -24.3 and -28.5 kJ/mol) for sDiA molecule. In the case of BF (bulky molecule), the  $\Delta_{dpl}H_{cum}$  is not determined due to the lower adsorption capacity for FAU-0 and FAU-1 (50 and 100  $\mu\text{mol/g}$  respectively).  $\Delta_{dpl}H_{cum}$  is -14.1 kJ/mol and -12.8 kJ/mol for FAU-2 and FAU-3, respectively, which are similar. The first adsorbed sDiA molecule in microporous FAU-0 exhibits a less exothermic contribution. It has to be mentioned here that FAU-0 is in proton form, whereas FAU-1, 2, and 3 are in sodium form. The first species to be adsorbed at low concentration are generally sorbed onto the most reactive sites of the materials, within the microporosity.<sup>96, 254</sup> Since the microporous part is present in all materials, the observed difference in the first regime is probably to the different cation in FAU-0 compared to FAU-1, 2, and 3. The cost in energy is similar for the sDiA adsorption contribution but is different for the contribution of the counter-ions (desorption and rehydration of proton or sodium).

Table 14 : enthalpy displacement for the adsorption of dyes onto hierarchical FAU.

Material	sDiA		BF	
	$\Delta H_{dpl}$ first regime (kJ/mol)	$\Delta H_{dpl}$ second regime (kJ/mol)	$\Delta H_{ads}$ first regime (KJ/mol)	$\Delta H_{ads}$ second regime (KJ/mol)
FAU-0	-16.4	-47.9	-	-
FAU-1	-24.3	-50.3	-	-

**Chapter V: Effect of modification of the porosity of Zeolite FAU on the adsorption of dyes:  
contribution of global and local techniques**

FAU-2	-28.5	-24.1	-14.15	-20.56
FAU-3	-24.3	-12.1	-12.8	-12.11

For the second regime, two different tendencies are noticed, with an increase or a decrease of the cumulative enthalpy for surface coverage higher than 0.2 mmol/g. For all FAU materials, the affinity of dyes toward the material is quite constant which means that Gibbs free energy ( $\Delta G$ ) is constant for all systems. Therefore, the thermodynamic of the system is governed by the enthalpy ( $\Delta H$ ) and the entropy ( $\Delta S$ ). For FAU-0 and FAU-1, there is clearly higher enthalpy (triple or twice the value in the first regime). Generally speaking, the values of adsorption enthalpy are relatively high as observed in other studies on dyes on titania–silica mesoporous materials<sup>255</sup>. This indicates that the interaction between dyes and FAU is not only physisorption but not far from chemisorption, even if the limit between physisorption and chemisorption is still under debate.<sup>212, 216, 243</sup> From FAU-0 to FAU-1, a small decrease in  $\Delta H$  is observed (from -47.9 to -50.3 kJ/mol) which leads to a decrease in entropy. This means that the disorder decrease (the system becomes more ordered), but the nature of compensating cation is different. This can be explained by the different hydration of hydrogen and sodium cations. For the highly mesoporous materials, the cumulative enthalpy is similar (for FAU-2), or less negative (for FAU-3) for sDiA. This means that the entropy is similar or slightly higher, which reveals that the disorder of the system becomes higher. This agrees with the  $I_4$  parameter obtained by SHS measurements where it decreases with modification leading to a more disordered system. However, concerning the BF molecule, the cumulative enthalpy is less exothermic for FAU-3 (-12.1 kJ/mol) than for FAU-2 (-20.6 kJ/mol). A similar observation is seen as in the case of sDiA where the disorder become more intense as for the obtained  $I_4$  parameter. It is necessary to consider here that the adsorption enthalpies are the outcome of chemical interaction including electrostatic interaction, but also non-polar interaction, water bridging, and hydrogen-type bonding between the dye molecules and the adsorbent structure and between adsorbed dye molecules<sup>256</sup>. Although, the higher enthalpy for FAU-0 and FAU-1 is due to the confinement effect since the size of dye is highly fitted with the size of the FAU supercages, thus the electrostatic interaction is enhanced as reported in the previous result.<sup>92</sup> Whereas, in the case of FAU-2 and FAU-3 there is more void so greater freedom of movement that impacts in lowering the enthalpy (less negative) thus the confinement effect becomes weak. Therefore, the enthalpy is higher in the confined system i.e highly matching between the size of the guest molecule and the pore size of the host material, thus the electrostatic interaction is enhanced.<sup>78, 93, 94, 100</sup>

### 3.5 Dyes adsorption as hierarchical FAU characterization techniques

To characterize the hierarchical FAU (FAU-1, -2, -3) different techniques have been used and results have been compared to native zeolite FAU-0. Besides classical techniques as XRD, nitrogen sorption isotherms at 77K and  $^{29}\text{Si}$  MAS NMR, dyes adsorption constitutes a source of complementary information. XRD pattern has shown the presence of FAU structure for all materials, with a high decrease in peak intensity for FAU-3, which is close to a mesoporous material as Al-MCM-41 with some dispersed FAU nanocrystals of 50 nm. Low angle XRD pattern of FAU-1, -2, -3, show the presence of ordered mesopores with wall thicknesses large enough to accommodate a FAU cell for FAU-1 and FAU-2, but not for FAU-3.  $^{29}\text{Si}$  MAS NMR shows similar spectra for FAU-0, -1, -2, indicating that FAU-1 and FAU-2 are built entirely by FAU structure, mesopores are dug in the zeolite structure, while FAU-3 is mainly an amorphous structure. A slight change in  $Q^3/Q^4$  ratio is observed for FAU-2 with a slight increase of  $Q^3$  suggesting a distortion or some degradation of the zeolite network in FAU-2. The nitrogen adsorption isotherm shows a continuous decrease of micropore volume and in parallel a continuous increase of mesopore volume going from FAU-0 to FAU-3.

The adsorption of a cationic dye as BF, which is too large ( $11.9 \text{ \AA} \times 10.6 \text{ \AA} \times 6.2 \text{ \AA}$ ) to penetrate the micropores of the FAU structure (windows  $7.4 \text{ \AA}$ , cavities  $13 \text{ \AA}$ ), shows low affinity with the surface of FAU-0 and hierarchical FAU. However, a linear increase of the adsorbed amount of dyes from 0.05 to 0.4 mmol/g is observed with the increase of mesopore and external surface areas for FAU-0 to FAU-3, respectively, corresponding to a constant density of cationic dye at the surface of around 0.29 molecules/nm<sup>2</sup>. Mesopores feature a diameter large enough (4 nm) to adsorb BF molecules. The heat of adsorption is low around -12/-25 kJ/mol revealing weak interactions with the surface. SHS measurements through  $I_4$  values show very low interactions in between dyes (Values of  $I_4$  for FAU-0, -1, -2, -3,  $I_4 = -0.1, -0.096, -0.03, -0.02$ , respectively), suggesting a large degree of freedom of the molecules at the surface of the mesopores. Therefore, the adsorption of a large cationic dye on the mesopore surface (and external surface) is characterized by a low enthalpy of adsorption and a low interaction between the molecules with similar space in between molecules corresponding to a dye density around 0.29 molecules/nm<sup>2</sup> for all materials, certainly corresponding to the density of  $\text{Na}^+$  cations before the adsorption by cation-exchange. The dye density corresponds to 1 molecule for 3.5 nm<sup>2</sup>, which surface is larger than the larger section of BF molecule (1.3 nm<sup>2</sup>), so molecules are free to move at the surface.

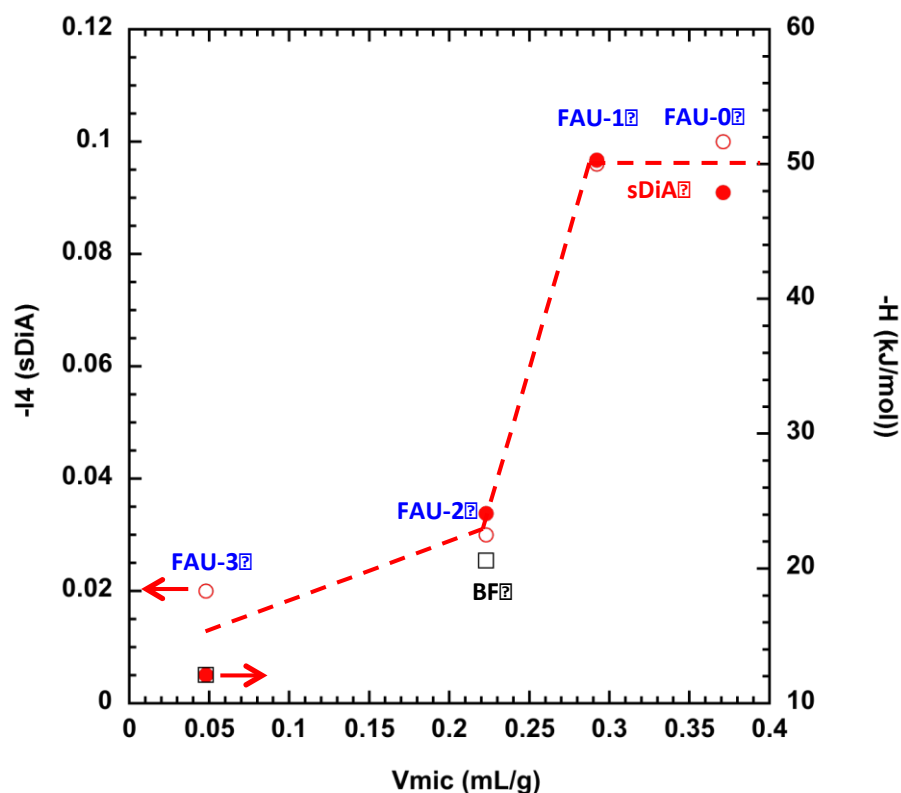


Figure 86: Enthalpies of adsorption (plain circle  $\Delta H$  for sDiA, square for BF) and  $I_4$  (empty circle  $I_4$  for sDiA) at the maximum dyes loading.

sDiA is small enough ( $14.5 \text{ \AA} \times 4.3 \text{ \AA} \times 1.8 \text{ \AA}$ ) to enter in the supercages of FAU (windows  $7.4 \text{ \AA}$ , cavities  $13 \text{ \AA}$ ), but too large to enter in SOD cages, in opposite to nitrogen (Van de Walls diameter  $3.72 \text{ \AA}$ ) that can occupy both cages. Adsorption of sDiA shows a very high affinity for FAU-0 and hierarchical FAU. Surprisingly, the maximum adsorption capacity of FAU-1 and FAU-2 is equal to the adsorption capacity of FAU-0 ( $0.6 \text{ mmol/g}$ ) although micropore volumes and external surface areas are decreasing for FAU-1 and -2, and the mesopore volumes are increasing. This suggests that no dyes are adsorbed on the external surface or mesopores surface, but only in the supercages of FAU. The constant adsorbed amount of sDiA FAU-0, -1, -2 suggests a similar micropore volume for the 3 materials and that the decrease of micropore volume observed with nitrogen as a probe from FAU-0 to FAU-2 is due to a distortion or the damage of the SOD cages, while the supercages keep their adsorption capacity. The heat of adsorption is very high for FAU-0 and FAU-1 ( $-50 \text{ kJ/mol}$ ) (Figure 86) suggesting that the probes in the supercages are in strong interactions with the surface. SHS measurements through  $I_4$  values show very strong interactions between probes in FAU-0 and FAU-1 ( $I_4 = -0.1$ ). The heat of



adsorption of sDiA in FAU-2 is lower as for FAU-3 (around -12/-25 kJ/mol) and as for BF adsorption, suggesting a weaker interaction with the surface. The SHS measurements through  $I_4$  values show very low interactions in between probes ( $I_4 = -0.02/-0.03$ ), suggesting a large degree of freedom at the surface of the supercages for FAU-2. This could probably become from a distortion of the supercages. For FAU-3, which is mainly a mesoporous material, the amount of sDiA adsorbed is equivalent to the amount of BF (0.4 mmol/g), suggesting the same density of dyes (1 molecule per 3.5 nm<sup>2</sup>) at the surface of the mesopores, as these two dyes are enough space to even lay on the surface (maximum section of sDiA is 0.62 nm<sup>2</sup>).

All of these results demonstrate that FAU-1 has very similar intrinsic properties as FAU-0 with a micropore volume of 0.29 mL/g together with an additional ordered mesoporosity (0.24 mL/g).

Cationic dyes should be highly recommended to probe hierarchical FAU. sDiA dye allows to probe the integrity of the supercages of the FAU and BF dye allows to probe the amount of mesopore and the external surface area. In the case of hierarchical FAU prepared by micelle-templating, FAU-1 prepared with NaOH/Si = 0.075 should be highly recommended in applications (adsorption or catalysis) needing the specificity of FAU with enhanced diffusion properties given by the presence of mesopores.

## 4. Conclusions

Hierarchical materials synthesized by post synthesis in basic medium (NaOH) in the presence of C<sub>18</sub>TAB surfactant formed from Faujasite as a starting material (CBV-720) comprise different materials bearing different textural properties depending on the NaOH/Si ratio. When NaOH/Si ratio increases, the mesopore volume and surface area increase and the micropore volume and surface area decreases. <sup>29</sup>Si NMR reveals the preservation of the FAU structure for NaOH/Si = 0.075 (FAU-1) and 0.095 (FAU-2) and an the amorphization of the structure for NaOH/Si = 0.25 (FAU-3).

Concerning the sorption of sDiA, the maximum adsorption capacity was observed for FAU-0, 1 and 2 (600 μmol/g) and a lower capacity for FAU-3 (400 μmol/g) for sDiA. In FAU-0, 1 and 2, sDiA totally occupies the volume of the supercages of the materials. The decrease in micropore volumes during the transformation is certainly due to the distortion of the SOD cages, avoiding the adsorption of nitrogen. The lower adsorption capacity of FAU-3 is probably due to the increase the surface hydrophilicity. However, for the case of bulky dye (BF), too large to enter the FAU supercages, the sorption capacity increases linearly with the increase of mesopore and external surface area from FAU-0 to FAU-3 (from 50 to 400 μmol/g). Those isotherms are highly generated by SHS. In addition, the SHS experiments permit to probe the confinement properties of the dye inside the pore firstly from the shape of the SHS plot and secondly from the normalized  $i_4$  values. When the SHS plots show an enlargement in the vertical polarization and higher intensity of the horizontal polarization it reveals a

higher interaction between the molecule and the material thus a higher absolute value of  $i_4$  is obtained. As a conclusion sDiA onto FAU-0 and FAU-1 exhibit better confinement, thus larger correlation. This was confirmed by the displacement enthalpy measured via ITC.

All of these results demonstrate that FAU-1 has very similar intrinsic properties as FAU-0 with an additional mesoporosity and should be highly recommended in applications (adsorption or catalysis) needed the specificity of FAU with enhanced diffusion properties. The adsorption of cationic dyes represents a powerful complementary characterization technique for hierarchical zeolites.

### **Acknowledgements**

The authors also thank the Balard Plateforme d'Analyses et de Caractérisation (PAC Balard) facilities for technical support in analysis and characterizations. The authors are grateful to Mr. Amine Geneste for his valuable help with calorimetric experiments, Nicolas Donzel for Nitrogen Adsorption and Emmanuel Fernandez for NMR measurements.

Electronic Supplementary Information (ESI)

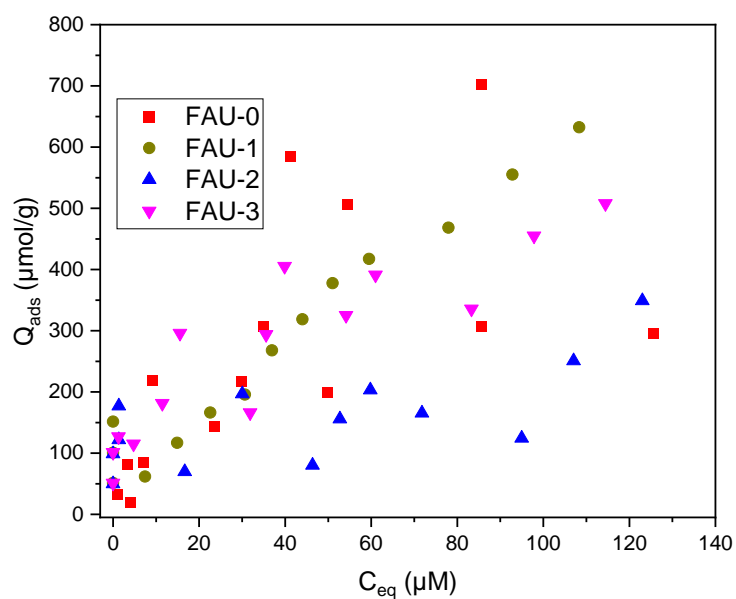


Figure-S1: Adsorption isotherm of BF by SHS

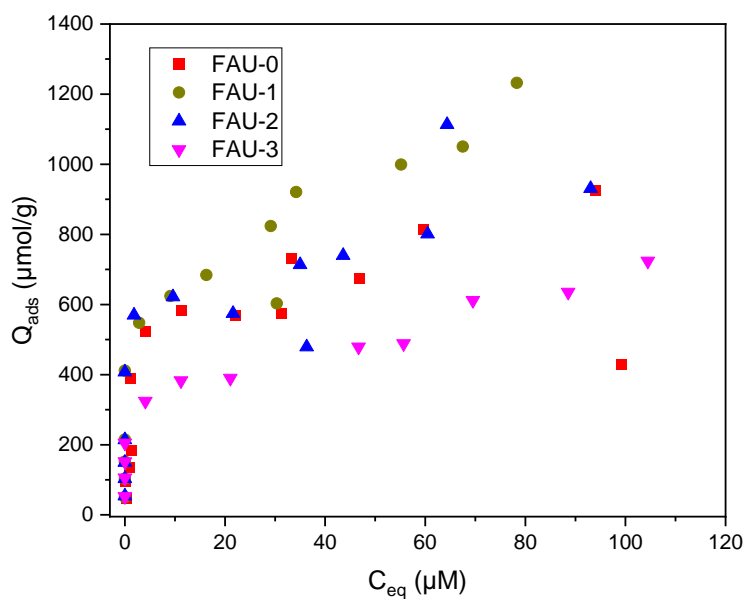


Figure-S2: Adsorption isotherm of sDiA by SHS

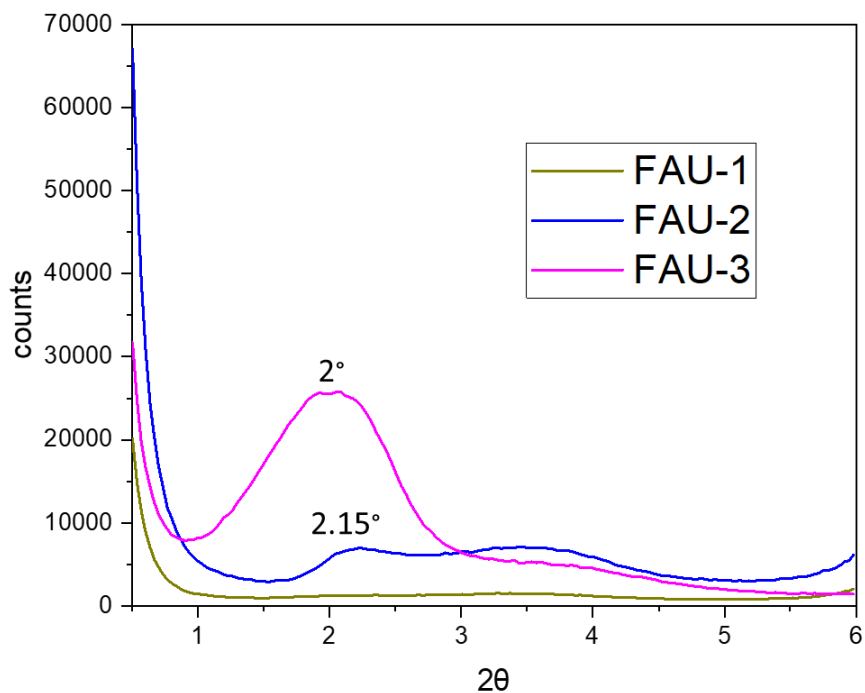


Figure-S3: XRD for hierarchical FAU at small angle

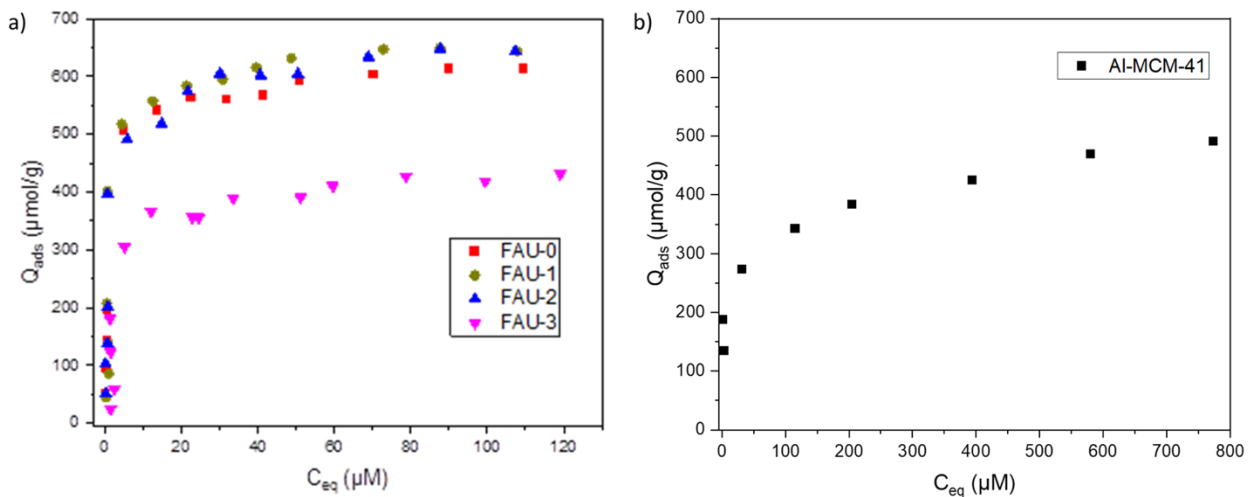


Figure-S4: Adsorption isotherm of sDiA towards hierarchical FAU and Al-MCM-41 in a) and b) respectively.

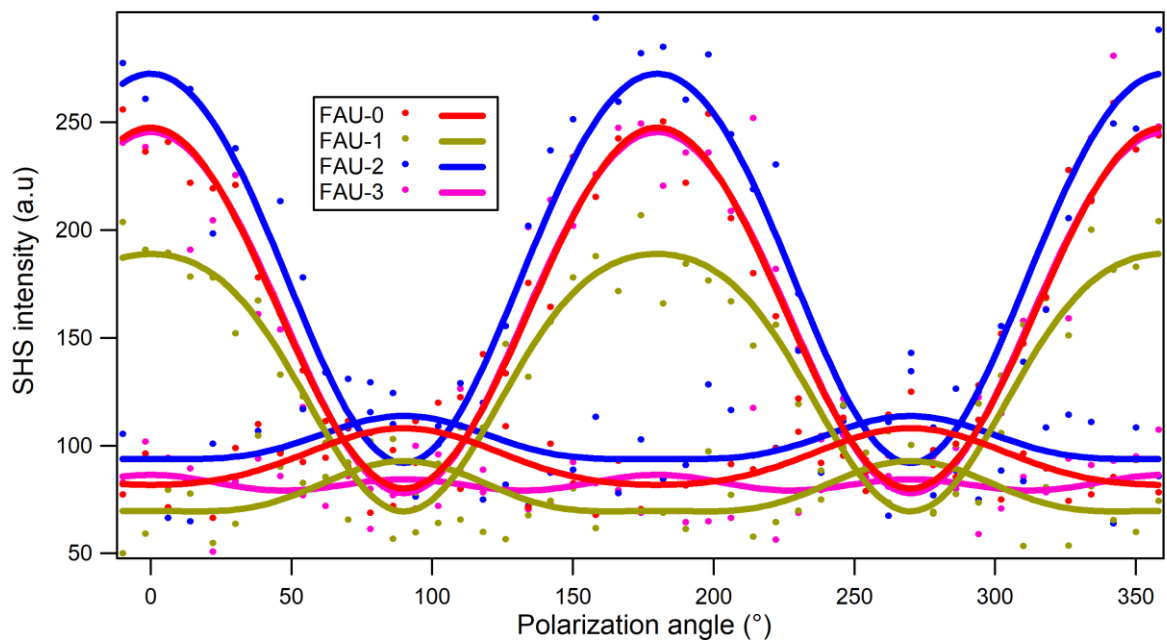


Figure-S5: SHS polarization plot for BF adsorbed onto FAU-0 and hierarchical 0.05g/l FAU

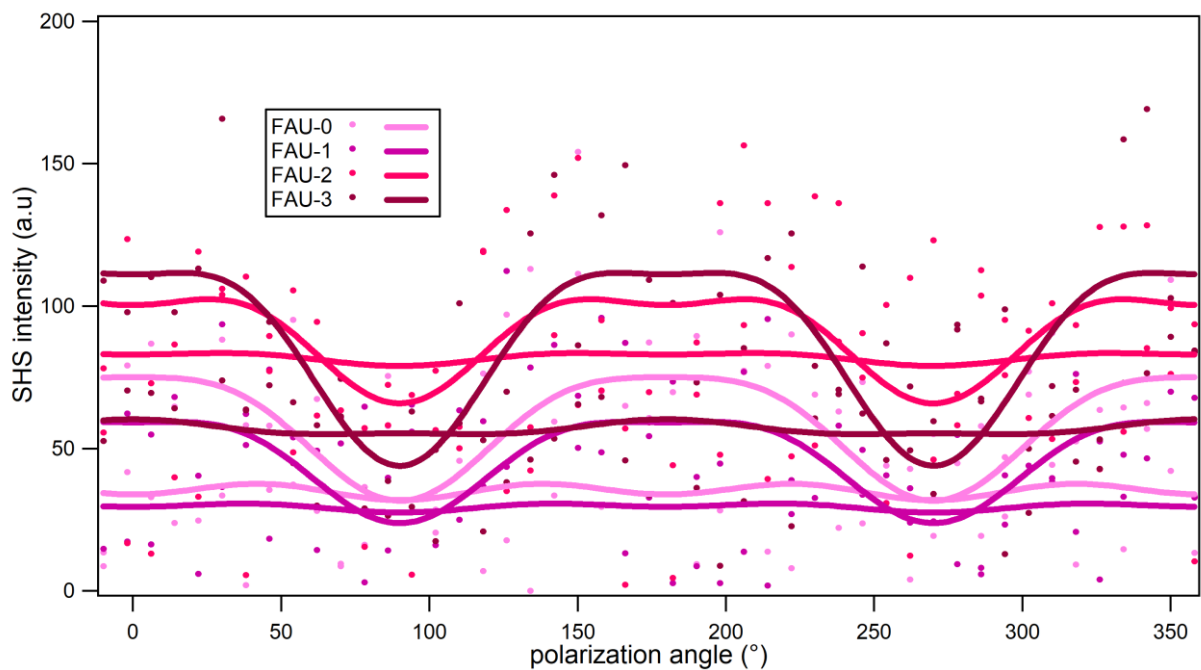


Figure-S6: SHS polarization plot for BF adsorbed onto FAU-0 and hierarchical 0.05g/l FAU

## References

1. Guivarch, E. Traitement des polluants organiques en milieux aqueux par procédé électrochimique d'oxydation avancée" Electro-Fenton": application à la minéralisation des colorants synthétiques. Université de Marne-la-Vallée, 2004.
2. Oudar, J. L.; Zyss, J., Structural dependence of nonlinear-optical properties of methyl-(2,4-dinitrophenyl)-aminopropanoate crystals. *Physical Review A* **1982**, *26* (4), 2016-2027.
3. Sing, K. S., Adsorption by active carbons. *Adsorption by powders and porous solids: principles, methodology and applications* **2013**, 321-391.
4. McKay, G.; Porter, J. F.; Prasad, G. R., The Removal of Dye Colours from Aqueous Solutions by Adsorption on Low-cost Materials. *Water, Air, and Soil Pollution* **1999**, *114* (3), 423-438.
5. Langmuir, I., The Constitution and Fundamental Properties of Solids and Liquids. part I. Solids. *Journal of the American Chemical Society* **1916**, *38* (11), 2221-2295.
6. Emmett, P. H.; Brunauer, S., The Adsorption of Nitrogen by Iron Synthetic Ammonia Catalysts. *Journal of the American Chemical Society* **1934**, *56* (1), 35-41.
7. Rouquerol, J.; Rouquerol, F.; Llewellyn, P.; Maurin, G.; Sing, K. S., *Adsorption by powders and porous solids: principles, methodology and applications*. Academic press: 2013.
8. Forgacs, E.; Cserháti, T.; Oros, G., Removal of synthetic dyes from wastewaters: a review. *Environment International* **2004**, *30* (7), 953-971.
9. Bhatnagar, A.; Hogland, W.; Marques, M.; Sillanpää, M., An overview of the modification methods of activated carbon for its water treatment applications. *Chemical Engineering Journal* **2013**, *219*, 499-511.
10. Rafatullah, M.; Sulaiman, O.; Hashim, R.; Ahmad, A., Adsorption of methylene blue on low-cost adsorbents: A review. *Journal of Hazardous Materials* **2010**, *177* (1), 70-80.
11. Dai, J.; Huang, T.; Tian, S.-q.; Xiao, Y.-j.; Yang, J.-h.; Zhang, N.; Wang, Y.; Zhou, Z.-w., High structure stability and outstanding adsorption performance of graphene oxide aerogel supported by polyvinyl alcohol for waste water treatment. *Materials & Design* **2016**, *107*, 187-197.
12. Wang, S.; Li, H.; Xu, L., Application of zeolite MCM-22 for basic dye removal from wastewater. *Journal of Colloid and Interface Science* **2006**, *295* (1), 71-78.
13. Lee, C.-K.; Liu, S.-S.; Juang, L.-C.; Wang, C.-C.; Lin, K.-S.; Lyu, M.-D., Application of MCM-41 for dyes removal from wastewater. *Journal of Hazardous Materials* **2007**, *147* (3), 997-1005.
14. Wong, T., *Handbook of zeolites: Structure, properties and applications*. Materials Science and Technolo: 2009.
15. Inglezakis, V. J., The concept of "capacity" in zeolite ion-exchange systems. *Journal of Colloid and Interface Science* **2005**, *281* (1), 68-79.
16. Waheed, A.; Baig, N.; Ullah, N.; Falath, W., Removal of hazardous dyes, toxic metal ions and organic pollutants from wastewater by using porous hyper-cross-linked polymeric materials: A review of recent advances. *Journal of Environmental Management* **2021**, *287*, 112360.
17. Townsend, R. P.; Coker, E. N., Chapter 11 Ion exchange in zeolites. In *Studies in Surface Science and Catalysis*, van Bekkum, H.; Flanigen, E. M.; Jacobs, P. A.; Jansen, J. C., Eds. Elsevier: 2001; Vol. 137, pp 467-524.
18. Lutz, W.; Löffler, E.; Zibrowius, B., Increased hydrothermal stability of highly dealuminated Y zeolites by alumination. *Zeolites* **1993**, *13* (8), 685-686.
19. Lutz, W.; Wieker, W.; Müller, D.; Schneider, M.; Rüscher, C. H.; Buhl, J. C., Phase Transformations in Alkaline and Acid Leached Y Zeolites Dealuminated by Steaming. *Zeitschrift für anorganische und allgemeine Chemie* **2000**, *626* (6), 1460-1467.
20. Ojuva, A. Processing and performance of zeolites for efficient carbon dioxide separation. Department of Materials and Environmental Chemistry, Stockholm University, 2015.
21. Tao, Y.; Kanoh, H.; Abrams, L.; Kaneko, K., Mesopore-Modified Zeolites: Preparation, Characterization, and Applications. *Chemical Reviews* **2006**, *106* (3), 896-910.

22. Schwieger, W.; Machoke, A. G.; Weissenberger, T.; Inayat, A.; Selvam, T.; Klumpp, M.; Inayat, A., Hierarchy concepts: classification and preparation strategies for zeolite containing materials with hierarchical porosity. *Chemical Society Reviews* **2016**, *45* (12), 3353-3376.
23. Pérez-Ramírez, J.; Christensen, C. H.; Egeblad, K.; Christensen, C. H.; Groen, J. C., Hierarchical zeolites: enhanced utilisation of microporous crystals in catalysis by advances in materials design. *Chemical Society Reviews* **2008**, *37* (11), 2530-2542.
24. Chal, R.; Gérardin, C.; Bulut, M.; van Donk, S., Overview and Industrial Assessment of Synthesis Strategies towards Zeolites with Mesopores. *ChemCatChem* **2011**, *3* (1), 67-81.
25. Koohsaryan, E.; Anbia, M., Nanosized and hierarchical zeolites: A short review. *Chinese Journal of Catalysis* **2016**, *37* (4), 447-467.
26. Verboekend, D.; Nuttens, N.; Locus, R.; Van Aelst, J.; Verolme, P.; Groen, J. C.; Pérez-Ramírez, J.; Sels, B. F., Synthesis, characterisation, and catalytic evaluation of hierarchical faujasite zeolites: milestones, challenges, and future directions. *Chemical Society Reviews* **2016**, *45* (12), 3331-3352.
27. Zhang, K.; Ostraat, M. L., Innovations in hierarchical zeolite synthesis. *Catalysis Today* **2016**, *264*, 3-15.
28. de Jong, K. P.; Zečević, J.; Friedrich, H.; de Jongh, P. E.; Bulut, M.; van Donk, S.; Kenmogne, R.; Finiels, A.; Hulea, V.; Fajula, F., Zeolite Y Crystals with Trimodal Porosity as Ideal Hydrocracking Catalysts. *Angewandte Chemie International Edition* **2010**, *49* (52), 10074-10078.
29. Li, W.; Zheng, J.; Luo, Y.; Da, Z., Effect of hierarchical porosity and phosphorus modification on the catalytic properties of zeolite Y. *Applied Surface Science* **2016**, *382*, 302-308.
30. Mehlhorn, D.; Rodriguez, J.; Cacciaguerra, T.; Andrei, R.-D.; Cammarano, C.; Guenneau, F.; Gedeon, A.; Coasne, B.; Thommes, M.; Minoux, D.; Aquino, C.; Dath, J.-P.; Fajula, F.; Galarneau, A., Revelation on the Complex Nature of Mesoporous Hierarchical FAU-Y Zeolites. *Langmuir* **2018**, *34* (38), 11414-11423.
31. Huang, L.; Guo, W.; Deng, P.; Xue, Z.; Li, Q., Investigation of Synthesizing MCM-41/ZSM-5 Composites. *The Journal of Physical Chemistry B* **2000**, *104* (13), 2817-2823.
32. Verhoef, M. J.; Kooyman, P. J.; van der Waal, J. C.; Rigutto, M. S.; Peters, J. A.; van Bekkum, H., Partial Transformation of MCM-41 Material into Zeolites: Formation of Nanosized MFI Type Crystallites. *Chemistry of Materials* **2001**, *13* (2), 683-687.
33. Majano, G.; Mintova, S.; Ovsitser, O.; Mihailova, B.; Bein, T., Zeolite Beta nanosized assemblies. *Microporous and Mesoporous Materials* **2005**, *80* (1), 227-235.
34. Kloetstra, K. R.; Zandbergen, H. W.; Jansen, J. C.; van Bekkum, H., Overgrowth of mesoporous MCM-41 on faujasite. *Microporous Materials* **1996**, *6* (5), 287-293.
35. Karlsson, A.; Stöcker, M.; Schmidt, R., Composites of micro- and mesoporous materials: simultaneous syntheses of MFI/MCM-41 like phases by a mixed template approach. *Microporous and Mesoporous Materials* **1999**, *27* (2), 181-192.
36. Holland, B. T.; Abrams, L.; Stein, A., Dual Templating of Macroporous Silicates with Zeolitic Microporous Frameworks. *Journal of the American Chemical Society* **1999**, *121* (17), 4308-4309.
37. Vuong, G.-T.; Do, T.-O., A New Route for the Synthesis of Uniform Nanozeolites with Hydrophobic External Surface in Organic Solvent Medium. *Journal of the American Chemical Society* **2007**, *129* (13), 3810-3811.
38. Wei, Y.; Parmentier, T. E.; de Jong, K. P.; Zečević, J., Tailoring and visualizing the pore architecture of hierarchical zeolites. *Chemical Society Reviews* **2015**, *44* (20), 7234-7261.
39. Garwood, W. E., Conversion of C<sub>2</sub>-C<sub>10</sub> to Higher Olefins over Synthetic Zeolite ZSM-5. In *Intrazeolite Chemistry*, AMERICAN CHEMICAL SOCIETY: 1983; Vol. 218, pp 383-396.
40. Tabak, S. A.; Krambeck, F. J.; Garwood, W. E., Conversion of propylene and butylene over ZSM-5 catalyst. *AIChE Journal* **1986**, *32* (9), 1526-1531.
41. Wang, S.; Dou, T.; Li, Y.; Zhang, Y.; Li, X.; Yan, Z., A novel method for the preparation of MOR/MCM-41 composite molecular sieve. *Catalysis Communications* **2005**, *6* (1), 87-91.

42. Datema, K. P.; Nowak, A. K.; van Braam Houckgeest, J.; Wielers, A. F. H., In-situ<sup>13</sup>C magic-angle-spinning NMR measurements of the conversion of ethene to aliphatic hydrocarbons over structurally different zeolites. *Catalysis Letters* **1991**, *11* (3), 267-276.
43. Yamamura, M.; Chaki, K.; Wakatsuki, T.; Okado, H.; Fujimoto, K., Synthesis of ZSM-5 zeolite with small crystal size and its catalytic performance for ethylene oligomerization. *Zeolites* **1994**, *14* (8), 643-649.
44. Fărcașiu, D.; Hutchison, J.; Li, L., An analysis of factors that influence shape selectivity in the cracking of long-chain alkanes on zeolite catalysts. *Journal of Catalysis* **1990**, *122* (1), 34-43.
45. Giudici, R.; Kouwenhoven, H. W.; Prins, R., Comparison of nitric and oxalic acid in the dealumination of mordenite. *Applied Catalysis A: General* **2000**, *203* (1), 101-110.
46. Hogan, J., Catalytic polymerization of olefins. *Phillips petroleum company, US* **1957**, 2794842.
47. Caicedo-Realpe, R.; Pérez-Ramírez, J., Mesoporous ZSM-5 zeolites prepared by a two-step route comprising sodium aluminate and acid treatments. *Microporous and Mesoporous Materials* **2010**, *128* (1), 91-100.
48. van laak, A. N. C.; Gosselink, R. W.; Sagala, S. L.; Meeldijk, J. D.; de Jongh, P. E.; de Jong, K. P., Alkaline treatment on commercially available aluminum rich mordenite. *Applied Catalysis A: General* **2010**, *382* (1), 65-72.
49. Holm, M. S.; Hansen, M. K.; Christensen, C. H., "One-Pot" Ion-Exchange and Mesopore Formation During Desilication. *European Journal of Inorganic Chemistry* **2009**, *2009* (9), 1194-1198.
50. Groen, J. C.; Abelló, S.; Villaescusa, L. A.; Pérez-Ramírez, J., Mesoporous beta zeolite obtained by desilication. *Microporous and Mesoporous Materials* **2008**, *114* (1), 93-102.
51. Ogura, M.; Shinomiya, S.-y.; Tatenó, J.; Nara, Y.; Kikuchi, E.; Matsukata, M., Formation of Uniform Mesopores in ZSM-5 Zeolite through Treatment in Alkaline Solution. *Chemistry Letters* **2000**, *29* (8), 882-883.
52. Ogura, M.; Shinomiya, S.-y.; Tatenó, J.; Nara, Y.; Nomura, M.; Kikuchi, E.; Matsukata, M., Alkali-treatment technique — new method for modification of structural and acid-catalytic properties of ZSM-5 zeolites. *Applied Catalysis A: General* **2001**, *219* (1), 33-43.
53. Paixão, V.; Carvalho, A. P.; Rocha, J.; Fernandes, A.; Martins, A., Modification of MOR by desilication treatments: Structural, textural and acidic characterization. *Microporous and Mesoporous Materials* **2010**, *131* (1), 350-357.
54. van Laak, A. N. C.; Sagala, S. L.; Zečević, J.; Friedrich, H.; de Jongh, P. E.; de Jong, K. P., Mesoporous mordenites obtained by sequential acid and alkaline treatments – Catalysts for cumene production with enhanced accessibility. *Journal of Catalysis* **2010**, *276* (1), 170-180.
55. Li, X.; Prins, R.; van Bokhoven, J. A., Synthesis and characterization of mesoporous mordenite. *Journal of Catalysis* **2009**, *262* (2), 257-265.
56. Groen, J. C.; Sano, T.; Moulijn, J. A.; Pérez-Ramírez, J., Alkaline-mediated mesoporous mordenite zeolites for acid-catalyzed conversions. *Journal of Catalysis* **2007**, *251* (1), 21-27.
57. Groen, J. C.; Peffer, L. A. A.; Moulijn, J. A.; Pérez-Ramírez, J., Mechanism of Hierarchical Porosity Development in MFI Zeolites by Desilication: The Role of Aluminium as a Pore-Directing Agent. *Chemistry – A European Journal* **2005**, *11* (17), 4983-4994.
58. Groen, J. C., Mesoporous zeolites obtained by desilication. **2007**.
59. Groen, J. C.; Moulijn, J. A.; Pérez-Ramírez, J., Desilication: on the controlled generation of mesoporosity in MFI zeolites. *Journal of Materials Chemistry* **2006**, *16* (22), 2121-2131.
60. Abelló, S.; Bonilla, A.; Pérez-Ramírez, J., Mesoporous ZSM-5 zeolite catalysts prepared by desilication with organic hydroxides and comparison with NaOH leaching. *Applied Catalysis A: General* **2009**, *364* (1), 191-198.
61. Yang, S.; Yu, C.; Yu, L.; Miao, S.; Zou, M.; Jin, C.; Zhang, D.; Xu, L.; Huang, S., Bridging Dealumination and Desilication for the Synthesis of Hierarchical MFI Zeolites. *Angewandte Chemie International Edition* **2017**, *56* (41), 12553-12556.
62. Goto, Y.; Fukushima, Y.; Ratu, P.; Imada, Y.; Kubota, Y.; Sugi, Y.; Ogura, M.; Matsukata, M., Mesoporous Material from Zeolite. *Journal of Porous Materials* **2002**, *9* (1), 43-48.



63. Ivanova, I. I.; Kuznetsov, A. S.; Yuschenko, V. V.; Knyazeva, E. E., Design of composite micro/mesoporous molecular sieve catalysts. *Pure and Applied Chemistry* **2004**, 76 (9), 1647-1657.
64. Wang, S.; Dou, T.; Li, Y.; Zhang, Y.; Li, X.; Yan, Z., Synthesis, characterization, and catalytic properties of stable mesoporous molecular sieve MCM-41 prepared from zeolite mordenite. *Journal of Solid State Chemistry* **2004**, 177 (12), 4800-4805.
65. Ordonsky, V. V.; Murzin, V. Y.; Monakhova, Y. V.; Zubavichus, Y. V.; Knyazeva, E. E.; Nesterenko, N. S.; Ivanova, I. I., Nature, strength and accessibility of acid sites in micro/mesoporous catalysts obtained by recrystallization of zeolite BEA. *Microporous and Mesoporous Materials* **2007**, 105 (1), 101-110.
66. Ivanova, I. I.; Kuznetsov, A. S.; Knyazeva, E. E.; Fajula, F.; Thibault-Starzyk, F.; Fernandez, C.; Gilson, J. P., Design of hierarchically structured catalysts by mordenites recrystallization: Application in naphthalene alkylation. *Catalysis Today* **2011**, 168 (1), 133-139.
67. J.Y. Ying, J. G. M., Mesostructured zeolitic materials, and methods of making and using the same. *Massachusetts Institute Of Technology, US*, **2005**, Patent n° US 2005/0239634 A1.
68. Chal, R.; Cacciaguerra, T.; van Donk, S.; Gérardin, C., Pseudomorphic synthesis of mesoporous zeolite Y crystals. *Chemical Communications* **2010**, 46 (41), 7840-7842.
69. Ivanova, I. I.; Knyazeva, E. E., Micro-mesoporous materials obtained by zeolite recrystallization: synthesis, characterization and catalytic applications. *Chemical Society Reviews* **2013**, 42 (9), 3671-3688.
70. Sachse, A.; García-Martínez, J., Surfactant-Templating of Zeolites: From Design to Application. *Chemistry of Materials* **2017**, 29 (9), 3827-3853.
71. Al-Ani, A.; Haslam, J. J. C.; Mordvinova, N. E.; Lebedev, O. I.; Vicente, A.; Fernandez, C.; Zholobenko, V., Synthesis of nanostructured catalysts by surfactant-templating of large-pore zeolites. *Nanoscale Advances* **2019**, 1 (5), 2029-2039.
72. Sachse, A.; Grau-Atienza, A.; Jardim, E. O.; Linares, N.; Thommes, M.; García-Martínez, J., Development of Intracrystalline Mesoporosity in Zeolites through Surfactant-Templating. *Crystal Growth & Design* **2017**, 17 (8), 4289-4305.
73. Sachse, A.; Aumond, T.; Rousseau, J.; Batonneau-Gener, I., Impact of Hierarchization on the Textural Properties of MCM-22 Based Zeolites. *Advanced Materials Interfaces* **2021**, 8 (11), 2100356.
74. Jolivet, J.-P.; Froidefond, C.; Pottier, A.; Chanéac, C.; Cassaignon, S.; Tronc, E.; Euzen, P., Size tailoring of oxide nanoparticles by precipitation in aqueous medium. A semi-quantitative modelling. *Journal of Materials Chemistry* **2004**, 14 (21), 3281-3288.
75. Auffan, M.; Rose, J.; Bottero, J.-Y.; Lowry, G. V.; Jolivet, J.-P.; Wiesner, M. R., Towards a definition of inorganic nanoparticles from an environmental, health and safety perspective. *Nature Nanotechnology* **2009**, 4 (10), 634-641.
76. Prelot, B.; Lantenois, S.; Chorro, C.; Charbonnel, M.-C.; Zajac, J.; Douillard, J. M., Effect of Nanoscale Pore Space Confinement on Cadmium Adsorption from Aqueous Solution onto Ordered Mesoporous Silica: A Combined Adsorption and Flow Calorimetry Study. *The Journal of Physical Chemistry C* **2011**, 115 (40), 19686-19695.
77. Song, B.; Chu, Y.; Li, G.; Wang, J.; Lo, A.-Y.; Zheng, A.; Deng, F., Origin of Zeolite Confinement Revisited by Energy Decomposition Analysis. *The Journal of Physical Chemistry C* **2016**, 120 (48), 27349-27363.
78. Boekfa, B.; Pantu, P.; Probst, M.; Limtrakul, J., Adsorption and Tautomerization Reaction of Acetone on Acidic Zeolites: The Confinement Effect in Different Types of Zeolites. *The Journal of Physical Chemistry C* **2010**, 114 (35), 15061-15067.
79. Varghese, J. J.; Mushrif, S. H., Origins of complex solvent effects on chemical reactivity and computational tools to investigate them: a review. *Reaction Chemistry & Engineering* **2019**, 4 (2), 165-206.
80. Boscoboinik, J. A., Chemistry in confined space through the eyes of surface science-2D porous materials. *J Phys Condens Matter* **2019**, 31 (6), 063001.

81. Derouane, E. G.; André, J.-M.; Lucas, A. A., A simple van der waals model for molecule-curved surface interactions in molecular-sized microporous solids. *Chemical Physics Letters* **1987**, *137* (4), 336-340.
82. Derouane, E. G., The energetics of sorption by molecular sieves: Surface curvature effects. *Chemical Physics Letters* **1987**, *142* (3), 200-204.
83. Senapati, S.; Chandra, A., Dielectric Constant of Water Confined in a Nanocavity. *The Journal of Physical Chemistry B* **2001**, *105* (22), 5106-5109.
84. Mizota, T.; Petrova, N. L.; Nakayama, N., Entropy of Zeolitic Water. *Journal of Thermal Analysis and Calorimetry* **2001**, *64* (1), 211-217.
85. Hureau, M.; Moissette, A.; Legrand, A.; Luchez, F.; Sliwa, M.; Bremard, C., Chemical Control of Photoinduced Charges under Confinement in Zeolites. *The Journal of Physical Chemistry C* **2012**, *116* (16), 9092-9105.
86. Luchez, F.; Carré, S.; Moissette, A.; Poizat, O., Sorption and spontaneous ionization of phenothiazine within channel type zeolites: Effect of the confinement on the electron transfers. *RSC Advances* **2011**, *1* (2), 341-350.
87. Chu, Y.; Ji, P.; Yi, X.; Li, S.; Wu, P.; Zheng, A.; Deng, F., Strong or weak acid, which is more efficient for Beckmann rearrangement reaction over solid acid catalysts? *Catalysis Science & Technology* **2015**, *5* (7), 3675-3681.
88. Derouane, E. G.; Nagy, J. B.; Fernandez, C.; Gabelica, Z.; Laurent, E.; Maljean, P., Diffusion of alkanes in molecular sieves evidence for confinement effects. *Applied Catalysis* **1988**, *40*, L1-L10.
89. Hennessy, B.; Megelski, S.; Marcolli, C.; Shklover, V.; Bärlocher, C.; Calzaferri, G., Characterization of Methyl Viologen in the Channels of Zeolite L. *The Journal of Physical Chemistry B* **1999**, *103* (17), 3340-3351.
90. Insuwan, W.; Rangsiwatananon, K.; Meeprasert, J.; Namuangruk, S.; Surakhot, Y.; Kungwan, N.; Jungsuttiwong, S., Combined experimental and theoretical investigation on Fluorescence Resonance Energy Transfer of dye loaded on LTL zeolite. *Microporous and Mesoporous Materials* **2017**, *241*, 372-382.
91. Viani, L.; Minoia, A.; Cornil, J.; Beljonne, D.; Egelhaaf, H.-J.; Gierschner, J., Resonant Energy Transport in Dye-Filled Monolithic Crystals of Zeolite L: Modeling of Inhomogeneity. *The Journal of Physical Chemistry C* **2016**, *120* (48), 27192-27199.
92. Fu, J.; Feng, X.; Liu, Y.; Yang, C., Effect of pore confinement on the adsorption of mono-branched alkanes of naphtha in ZSM-5 and Y zeolites. *Applied Surface Science* **2017**, *423*, 131-138.
93. Pantu, P.; Boekfa, B.; Limtrakul, J., The adsorption of saturated and unsaturated hydrocarbons on nanostructured zeolites (H-MOR and H-FAU): An ONIOM study. *Journal of Molecular Catalysis A: Chemical* **2007**, *277* (1), 171-179.
94. Boekfa, B.; Choomwattana, S.; Khongpracha, P.; Limtrakul, J., Effects of the Zeolite Framework on the Adsorptions and Hydrogen-Exchange Reactions of Unsaturated Aliphatic, Aromatic, and Heterocyclic Compounds in ZSM-5 Zeolite: A Combination of Perturbation Theory (MP2) and a Newly Developed Density Functional Theory (M06-2X) in ONIOM Scheme. *Langmuir* **2009**, *25* (22), 12990-12999.
95. Hsieh, C.-T.; Fan, W.-S.; Chen, W.-Y., Impact of mesoporous pore distribution on adsorption of methylene blue onto titania nanotubes in aqueous solution. *Microporous and Mesoporous Materials* **2008**, *116* (1), 677-683.
96. Eder, F.; Lercher, J. A., On the Role of the Pore Size and Tortuosity for Sorption of Alkanes in Molecular Sieves. *The Journal of Physical Chemistry B* **1997**, *101* (8), 1273-1278.
97. Gounder, R.; Iglesia, E., Catalytic Consequences of Spatial Constraints and Acid Site Location for Monomolecular Alkane Activation on Zeolites. *Journal of the American Chemical Society* **2009**, *131* (5), 1958-1971.
98. Chai, Y.; Han, X.; Li, W.; Liu, S.; Yao, S.; Wang, C.; Shi, W.; da-Silva, I.; Manuel, P.; Cheng, Y.; Daemen, L. D.; Ramirez-Cuesta, A. J.; Tang, C. C.; Jiang, L.; Yang, S.; Guan, N.; Li, L., Control of zeolite pore interior for chemoselective alkyne/olefin separations. *Science* **2020**, *368* (6494), 1002.

99. Dai, J.; Zhang, H., Recent Advances in Catalytic Confinement Effect within Micro/Meso-Porous Crystalline Materials. *Small* **2021**, *n/a* (n/a), 2005334.
100. Janda, A.; Vlaisavljevich, B.; Lin, L.-C.; Smit, B.; Bell, A. T., Effects of Zeolite Structural Confinement on Adsorption Thermodynamics and Reaction Kinetics for Monomolecular Cracking and Dehydrogenation of n-Butane. *Journal of the American Chemical Society* **2016**, *138* (14), 4739-4756.
101. Thach, U. D.; Prelot, B.; Pellet-Rostaing, S.; Zajac, J.; Hesemann, P., Surface Properties and Chemical Constitution as Crucial Parameters for the Sorption Properties of Ionosilicas: The Case of Chromate Adsorption. *ACS Applied Nano Materials* **2018**, *1* (5), 2076-2087.
102. Guil, J. M.; Perdigón-Melón, J. A.; Brotas de Carvalho, M.; Carvalho, A. P.; Pires, J., Adsorption microcalorimetry of probe molecules of different size to characterize the microporosity of pillared clays. *Microporous and Mesoporous Materials* **2002**, *51* (2), 145-154.
103. Cao, Z.; Peng, Y.; Yan, T.; Li, S.; Li, A.; Voth, G. A., Mechanism of Fast Proton Transport along One-Dimensional Water Chains Confined in Carbon Nanotubes. *Journal of the American Chemical Society* **2010**, *132* (33), 11395-11397.
104. Armstrong, J. A.; Bloembergen, N.; Ducuing, J.; Pershan, P. S., Interactions between Light Waves in a Nonlinear Dielectric. *Physical Review* **1962**, *127* (6), 1918-1939.
105. Franken, P. A.; Hill, A. E.; Peters, C. W.; Weinreich, G., Generation of Optical Harmonics. *Physical Review Letters* **1961**, *7* (4), 118-119.
106. Brevet, P.-F., *Surface second harmonic generation*. PPUR presses polytechniques: 1997.
107. Roke, S.; Gonella, G., Nonlinear Light Scattering and Spectroscopy of Particles and Droplets in Liquids. *Annual Review of Physical Chemistry* **2012**, *63* (1), 353-378.
108. Eisenthal, K. B., Liquid Interfaces Probed by Second-Harmonic and Sum-Frequency Spectroscopy. *Chemical Reviews* **1996**, *96* (4), 1343-1360.
109. Gonella, G.; Dai, H.-L., Second Harmonic Light Scattering from the Surface of Colloidal Objects: Theory and Applications. *Langmuir* **2014**, *30* (10), 2588-2599.
110. Wang, H.; Yan, E. C. Y.; Borguet, E.; Eisenthal, K. B., Second harmonic generation from the surface of centrosymmetric particles in bulk solution. *Chemical Physics Letters* **1996**, *259* (1), 15-20.
111. Wang, H.; Troxler, T.; Yeh, A.-G.; Dai, H.-L., In Situ, Nonlinear Optical Probe of Surfactant Adsorption on the Surface of Microparticles in Colloids. *Langmuir* **2000**, *16* (6), 2475-2481.
112. Eckenrode, H. M.; Dai, H.-L., Nonlinear Optical Probe of Biopolymer Adsorption on Colloidal Particle Surface: Poly-l-lysine on Polystyrene Sulfate Microspheres. *Langmuir* **2004**, *20* (21), 9202-9209.
113. Yan, E. C. Y.; Liu, Y.; Eisenthal, K. B., New Method for Determination of Surface Potential of Microscopic Particles by Second Harmonic Generation. *The Journal of Physical Chemistry B* **1998**, *102* (33), 6331-6336.
114. van der Veen, M. A.; Verbiest, T.; De Vos, D. E., Probing microporous materials with second-harmonic generation. *Microporous and Mesoporous Materials* **2013**, *166*, 102-108.
115. Eckenrode, H. M.; Jen, S.-H.; Han, J.; Yeh, A.-G.; Dai, H.-L., Adsorption of a Cationic Dye Molecule on Polystyrene Microspheres in Colloids: Effect of Surface Charge and Composition Probed by Second Harmonic Generation. *The Journal of Physical Chemistry B* **2005**, *109* (10), 4646-4653.
116. Haber, L. H.; Kwok, S. J. J.; Semeraro, M.; Eisenthal, K. B., Probing the colloidal gold nanoparticle/aqueous interface with second harmonic generation. *Chemical Physics Letters* **2011**, *507* (1), 11-14.
117. Schürer, B.; Wunderlich, S.; Sauerbeck, C.; Peschel, U.; Peukert, W., Probing colloidal interfaces by angle-resolved second harmonic light scattering. *Physical Review B* **2010**, *82* (24), 241404.
118. Revillod, G.; Duboisset, J.; Russier-Antoine, I.; Benichou, E.; Bachelier, G.; Jonin, C.; Brevet, P.-F., Multipolar Contributions to the Second Harmonic Response from Mixed DiA-SDS Molecular Aggregates. *The Journal of Physical Chemistry C* **2008**, *112* (7), 2716-2723.
119. Gassin, P.-M.; Prelot, B.; Grégoire, B.; Martin-Gassin, G., Second-Harmonic Scattering in Layered Double Hydroxide Colloids: A Microscopic View of Adsorption and Intercalation. *Langmuir* **2018**, *34* (40), 12206-12213.

120. Gassin, P.-M.; Bellini, S.; Zajac, J.; Martin-Gassin, G., Adsorbed Dyes onto Nanoparticles: Large Wavelength Dependence in Second Harmonic Scattering. *The Journal of Physical Chemistry C* **2017**, *121* (27), 14566-14571.
121. Boudjema, L.; Aarrass, H.; Assaf, M.; Morille, M.; Martin-Gassin, G.; Gassin, P.-M., PySHS: Python Open Source Software for Second Harmonic Scattering. *Journal of Chemical Information and Modeling* **2020**, *60* (12), 5912-5917.
122. Duboisset, J.; Brevet, P.-F., Salt-induced Long-to-Short Range Orientational Transition in Water. *Physical Review Letters* **2018**, *120* (26), 263001.
123. Galarneau, A.; Mehlhorn, D.; Guenneau, F.; Coasne, B.; Villemot, F.; Minoux, D.; Aquino, C.; Dath, J.-P., Specific Surface Area Determination for Microporous/Mesoporous Materials: The Case of Mesoporous FAU-Y Zeolites. *Langmuir* **2018**, *34* (47), 14134-14142.
124. Zhou, W.; Apkarian, R. P.; Wang, Z. L.; Joy, D., Fundamentals of Scanning Electron Microscopy.
125. Hendricks, D. W., *Water treatment unit processes: physical and chemical*. CRC press: 2018.
126. Tengku Mohd, T. A.; Jaafar, M. Z.; Ali Rasol, A. A.; Hamid, M. F., Measurement of Streaming Potential in Downhole Application: An Insight for Enhanced Oil Recovery Monitoring. *MATEC Web Conf.* **2017**, *87*.
127. Mahira, S.; Rayapolu, R. G.; Khan, W., Chapter 4 - Nanoscale characterization of nanocarriers. In *Smart Nanocontainers*, Nguyen-Tri, P.; Do, T.-O.; Nguyen, T. A., Eds. Elsevier: 2020; pp 49-65.
128. Barber, D. J., J. P. Eberhart Structural and Chemical Analysis of Materials—X-ray, electron and neutron diffraction—X-ray, electron and ion spectroscopy—Electron microscopy. (Translated by J. P. Eberhart), Chichester and New York (J. Wiley and Sons), 1991, xxx + 545 pp. Price £95.00. *Mineralogical Magazine* **1992**, *56* (382), 135-135.
129. Sing, K. S. W., Reporting physisorption data for gas/solid systems with special reference to the determination of surface area and porosity (Recommendations 1984). *Pure and Applied Chemistry* **1985**, *57* (4), 603-619.
130. Cychosz, K. A.; Thommes, M., Progress in the Physisorption Characterization of Nanoporous Gas Storage Materials. *Engineering* **2018**, *4* (4), 559-566.
131. Rahman, M. M.; Muttakin, M.; Pal, A.; Shafiullah, A. Z.; Saha, B. B., A Statistical Approach to Determine Optimal Models for IUPAC-Classified Adsorption Isotherms. *Energies* **2019**, *12* (23).
132. Alshameri, A.; Xinghu, W.; Dawood, A. S.; Xin, C.; Yan, C.; Assabri, A. M., Characterization of Yemeni Natural Zeolite (Al-Ahyuq Area) and its Environment Applications: A Review. *J. Ecol. Eng.* **2019**, *20* (4), 157-166.
133. Maurin, G., 6 - Modelling of Physisorption in Porous Solids. In *Adsorption by Powders and Porous Solids (Second Edition)*, Rouquerol, F.; Rouquerol, J.; Sing, K. S. W.; Llewellyn, P.; Maurin, G., Eds. Academic Press: Oxford, 2014; pp 191-235.
134. Derouane, E. G., On the physical state of molecules in microporous solids. *Microporous and Mesoporous Materials* **2007**, *104* (1), 46-51.
135. Rouquerol, J.; Llewellyn, P.; Rouquerol, F., Is the bet equation applicable to microporous adsorbents. *Studies in Surface Science and Catalysis* **2007**, *160*, 49-56.
136. Thommes, M.; Kaneko, K.; Neimark, A. V.; Olivier, J. P.; Rodriguez-Reinoso, F.; Rouquerol, J.; Sing, K. S. W., Physisorption of gases, with special reference to the evaluation of surface area and pore size distribution (IUPAC Technical Report). *Pure and Applied Chemistry* **2015**, *87* (9-10), 1051-1069.
137. Galarneau, A.; Villemot, F.; Rodriguez, J.; Fajula, F.; Coasne, B., Validity of the t-plot Method to Assess Microporosity in Hierarchical Micro/Mesoporous Materials. *Langmuir* **2014**, *30* (44), 13266-13274.
138. Thomas, J. M.; Thomas, W. J., *Principles and practice of heterogeneous catalysis*. John Wiley & Sons: 2014.
139. Tekely, P., Exploiting  $1\text{H} \rightarrow 29\text{Si}$  Cross-Polarization Features for Structural Characterization of Inorganic Materials. In *Modern Magnetic Resonance*, Webb, G. A., Ed. Springer Netherlands: Dordrecht, 2006; pp 197-203.

140. Shen, Y. R., *The principles of nonlinear optics*. 1984.
141. Maurice, A. Second harmonic scattering in liquids media : comparison between volume and surface. Université de Lyon, 2016.
142. Hsieh, C.-L. Imaging with Second-Harmonic Generation Nanoparticles. California Institute of Technology, 2011.
143. Revillod, G. Diffusion hyper Rayleigh des assemblages moléculaires. Université Claude Bernard-Lyon I, 2006.
144. Duboisset, J.; Brevet, P.-F., Second-Harmonic Scattering-Defined Topological Classes for Nano-Objects. *The Journal of Physical Chemistry C* **2019**, *123* (41), 25303-25308.
145. Goscianska, J.; Marciniak, M.; Pietrzak, R., The effect of surface modification of mesoporous carbons on Auramine-O dye removal from water. *Adsorption* **2016**, *22* (4), 531-540.
146. Tarach, K.; Góra-Marek, K.; Tekla, J.; Brylewska, K.; Datka, J.; Mlekodaj, K.; Makowski, W.; Iguálada López, M. C.; Martínez Triguero, J.; Rey, F., Catalytic cracking performance of alkaline-treated zeolite Beta in the terms of acid sites properties and their accessibility. *Journal of Catalysis* **2014**, *312*, 46-57.
147. Gackowski, M.; Datka, J., Acid Properties of Hierarchical Zeolites Y. *Molecules* **2020**, *25* (5).
148. Akgül, M.; Karabakan, A., Promoted dye adsorption performance over desilicated natural zeolite. *Microporous and Mesoporous Materials* **2011**, *145* (1), 157-164.
149. Xiao, M.; Yue, H.-D.; Feng, X.-J.; Wang, Y.-T.; He, M.-Y.; Chen, Q.; Zhang, Z.-H., A double-layered neutral cadmium-organic framework for selective adsorption of cationic organic dyes through electrostatic affinity. *Journal of Solid State Chemistry* **2020**, *288*, 121376.
150. Han, T.-T.; Bai, H.-L.; Liu, Y.-Y.; Ma, J.-F., Synthesis of nanoporous cobalt/carbon materials by a carbonized zeolitic imidazolate framework-9 and adsorption of dyes. *New Journal of Chemistry* **2018**, *42* (1), 717-724.
151. Miyah, Y.; Lahrichi, A.; Idrissi, M.; Khalil, A.; Zerrouq, F., Adsorption of methylene blue dye from aqueous solutions onto walnut shells powder: Equilibrium and kinetic studies. *Surfaces and Interfaces* **2018**, *11*, 74-81.
152. Huang, T.; Yan, M.; He, K.; Huang, Z.; Zeng, G.; Chen, A.; Peng, M.; Li, H.; Yuan, L.; Chen, G., Efficient removal of methylene blue from aqueous solutions using magnetic graphene oxide modified zeolite. *Journal of Colloid and Interface Science* **2019**, *543*, 43-51.
153. Goswami, M.; Phukan, P., Enhanced adsorption of cationic dyes using sulfonic acid modified activated carbon. *Journal of Environmental Chemical Engineering* **2017**, *5* (4), 3508-3517.
154. Chiou, M. S.; Li, H. Y., Adsorption behavior of reactive dye in aqueous solution on chemical cross-linked chitosan beads. *Chemosphere* **2003**, *50* (8), 1095-1105.
155. Jiang, R.; Fu, Y.-Q.; Zhu, H.-Y.; Yao, J.; Xiao, L., Removal of methyl orange from aqueous solutions by magnetic maghemite/chitosan nanocomposite films: Adsorption kinetics and equilibrium. *Journal of Applied Polymer Science* **2012**, *125* (S2), E540-E549.
156. Kaur, H.; Kumar, R.; Kumar, A.; Krishnan, V.; Koner, R. R., Trifunctional metal-organic platform for environmental remediation: structural features with peripheral hydroxyl groups facilitate adsorption, degradation and reduction processes. *Dalton Transactions* **2019**, *48* (3), 915-927.
157. Jin, X.; Jiang, M.-q.; Shan, X.-q.; Pei, Z.-g.; Chen, Z., Adsorption of methylene blue and orange II onto unmodified and surfactant-modified zeolite. *Journal of Colloid and Interface Science* **2008**, *328* (2), 243-247.
158. Sohrabnezhad, S.; Pourahmad, A., Comparison absorption of new methylene blue dye in zeolite and nanocrystal zeolite. *Desalination* **2010**, *256* (1), 84-89.
159. Sapawe, N.; Jalil, A. A.; Triwahyono, S.; Shah, M. I. A.; Jusoh, R.; Salleh, N. F. M.; Hameed, B. H.; Karim, A. H., Cost-effective microwave rapid synthesis of zeolite NaA for removal of methylene blue. *Chemical Engineering Journal* **2013**, *229*, 388-398.
160. Gerçel, Ö.; Özcan, A.; Özcan, A. S.; Gerçel, H. F., Preparation of activated carbon from a renewable bio-plant of *Euphorbia rigida* by H<sub>2</sub>SO<sub>4</sub> activation and its adsorption behavior in aqueous solutions. *Applied Surface Science* **2007**, *253* (11), 4843-4852.

161. Pereira, P. M.; Ferreira, B. F.; Oliveira, N. P.; Nassar, E. J.; Ciuffi, K. J.; Vicente, M. A.; Trujillano, R.; Rives, V.; Gil, A.; Korili, S.; De Faria, E. H., Synthesis of Zeolite A from Metakaolin and Its Application in the Adsorption of Cationic Dyes. *Applied Sciences* **2018**, *8* (4).
162. Raval, N. P.; Shah, P. U.; Shah, N. K., Malachite green “a cationic dye” and its removal from aqueous solution by adsorption. *Applied Water Science* **2017**, *7* (7), 3407-3445.
163. Gould, N. S.; Li, S.; Cho, H. J.; Landfield, H.; Caratzoulas, S.; Vlachos, D.; Bai, P.; Xu, B., Understanding solvent effects on adsorption and protonation in porous catalysts. *Nature Communications* **2020**, *11* (1), 1060.
164. Zhang, K.; Lively, R. P.; Noel, J. D.; Dose, M. E.; McCool, B. A.; Chance, R. R.; Koros, W. J., Adsorption of Water and Ethanol in MFI-Type Zeolites. *Langmuir* **2012**, *28* (23), 8664-8673.
165. Li, Y.; Li, L.; Yu, J., Applications of Zeolites in Sustainable Chemistry. *Chem* **2017**, *3* (6), 928-949.
166. Stocker, K.; Ellersdorfer, M.; Lehner, M.; Raith, J. G., Characterization and Utilization of Natural Zeolites in Technical Applications. *BHM Berg- und Hüttenmännische Monatshefte* **2017**, *162* (4), 142-147.
167. Colella, C.; Gennaro, M. d.; Aiello, R., Use of Zeolitic Tuff in the Building Industry. *Reviews in Mineralogy and Geochemistry* **2001**, *45* (1), 551-587.
168. Nakhli, S. A. A.; Delkash, M.; Bakhshayesh, B. E.; Kazemian, H., Application of Zeolites for Sustainable Agriculture: a Review on Water and Nutrient Retention. *Water, Air, & Soil Pollution* **2017**, *228* (12), 464.
169. Misaelides, P., Application of natural zeolites in environmental remediation: A short review. *Microporous and Mesoporous Materials* **2011**, *144* (1), 15-18.
170. Bacakova, L.; Vandrovцова, M.; Kopova, I.; Jirka, I., Applications of zeolites in biotechnology and medicine – a review. *Biomaterials Science* **2018**, *6* (5), 974-989.
171. Shaw, R.; Sharma, R.; Tiwari, S.; Tiwari, S. K., Surface Engineered Zeolite: An Active Interface for Rapid Adsorption and Degradation of Toxic Contaminants in Water. *ACS Applied Materials & Interfaces* **2016**, *8* (19), 12520-12527.
172. Jiang, N.; Shang, R.; Heijman, S. G. J.; Rietveld, L. C., High-silica zeolites for adsorption of organic micro-pollutants in water treatment: A review. *Water Research* **2018**, *144*, 145-161.
173. Samanta, P.; Desai, A. V.; Let, S.; Ghosh, S. K., Advanced Porous Materials for Sensing, Capture and Detoxification of Organic Pollutants toward Water Remediation. *ACS Sustainable Chemistry & Engineering* **2019**, *7* (8), 7456-7478.
174. Wang, S. B.; Peng, Y. L., Natural zeolites as effective adsorbents in water and wastewater treatment. *Chem. Eng. J.* **2010**, *156* (1), 11-24.
175. Wang, S.; Li, H.; Xie, S.; Liu, S.; Xu, L., Physical and chemical regeneration of zeolitic adsorbents for dye removal in wastewater treatment. *Chemosphere* **2006**, *65* (1), 82-87.
176. De Smedt, C.; Ferrer, F.; Leus, K.; Spanoghe, P., Removal of Pesticides from Aqueous Solutions by Adsorption on Zeolites as Solid Adsorbents. *Adsorption Science & Technology* **2015**, *33* (5), 457-485.
177. Martucci, A.; Braschi, I.; Bisio, C.; Sarti, E.; Rodeghero, E.; Bagatin, R.; Pasti, L., Influence of water on the retention of methyl tertiary-butyl ether by high silica ZSM-5 and Y zeolites: a multidisciplinary study on the adsorption from liquid and gas phase. *RSC Adv.* **2015**, *5* (106), 86997-87006.
178. Wang, S. B.; Li, H.; Xu, L. Y., Application of zeolite MCM-22 for basic dye removal from wastewater. *J. Colloid Interface Sci.* **2006**, *295* (1), 71-78.
179. Sarti, E.; Chenet, T.; Stevanin, C.; Costa, V.; Cavazzini, A.; Catani, M.; Martucci, A.; Precisvalle, N.; Beltrami, G.; Pasti, L., High-Silica Zeolites as Sorbent Media for Adsorption and Pre-Concentration of Pharmaceuticals in Aqueous Solutions. *Molecules* **2020**, *25* (15).
180. Noviello, M.; Gattullo, C. E.; Allegretta, I.; Terzano, R.; Gambacorta, G.; Paradiso, V. M., Synthetic zeolite materials from recycled glass and aluminium food packaging as potential oenological adjuvant. *Food Packaging and Shelf Life* **2020**, *26*, 100572.

181. Pagis, C.; Morgado Prates, A. R.; Farrusseng, D.; Bats, N.; Tuel, A., Hollow Zeolite Structures: An Overview of Synthesis Methods. *Chemistry of Materials* **2016**, *28* (15), 5205-5223.
182. Serrano, D. P.; Escola, J. M.; Pizarro, P., Synthesis strategies in the search for hierarchical zeolites. *Chemical Society Reviews* **2013**, *42* (9), 4004-4035.
183. Shamzhy, M.; Opanasenko, M.; Concepción, P.; Martínez, A., New trends in tailoring active sites in zeolite-based catalysts. *Chemical Society Reviews* **2019**, *48* (4), 1095-1149.
184. Grommet, A. B.; Feller, M.; Klajn, R., Chemical reactivity under nanoconfinement. *Nature Nanotechnology* **2020**, *15* (4), 256-271.
185. Dai, J. J.; Zhang, H. B., Recent Advances in Catalytic Confinement Effect within Micro/Meso-Porous Crystalline Materials. *Small* **2021**, *17* (22).
186. Sastre, G.; Corma, A., The confinement effect in zeolites. *Journal of Molecular Catalysis a-Chemical* **2009**, *305* (1-2), 3-7.
187. Prelot, B.; Lantenois, S.; Charbonnel, M.-C.; Marchandea, F.; Douillard, J. M.; Zajac, J., What are the main contributions to the total enthalpy of displacement accompanying divalent metal adsorption at the silica-electrolyte interface? *J. Colloid Interface Sci.* **2013**, *396*, 205-209.
188. Bordiga, S.; Lamberti, C.; Bonino, F.; Travert, A.; Thibault-Starzyk, F., Probing zeolites by vibrational spectroscopies. *Chemical Society Reviews* **2015**, *44* (20), 7262-7341.
189. Vimont, A.; Thibault-Starzyk, F.; Daturi, M., Analysing and understanding the active site by IR spectroscopy. *Chemical Society Reviews* **2010**, *39* (12), 4928-4950.
190. Grifoni, E.; Piccini, G.; Lercher, J. A.; Glezakou, V.-A.; Rousseau, R.; Parrinello, M., Confinement effects and acid strength in zeolites. *Nature Communications* **2021**, *12* (1), 2630.
191. Tabacchi, G., Supramolecular Organization in Confined Nanospaces. *ChemPhysChem* **2018**, *19* (11), 1249-1297.
192. Ramamurthy, V., Controlling photochemical reactions via confinement: zeolites. *Journal of Photochemistry and Photobiology C: Photochemistry Reviews* **2000**, *1* (2), 145-166.
193. Van Cleuvenbergen, S.; Smith, Z. J.; Deschaume, O.; Bartic, C.; Wachsmann-Hogiu, S.; Verbiest, T.; van der Veen, M. A., Morphology and structure of ZIF-8 during crystallisation measured by dynamic angle-resolved second harmonic scattering. *Nature communications* **2018**, *9* (1), 3418-3418.
194. Moris, M.; Van Den Eede, M.-P.; Koeckelberghs, G.; Deschaume, O.; Bartic, C.; Van Cleuvenbergen, S.; Clays, K.; Verbiest, T., Harmonic light scattering study reveals structured clusters upon the supramolecular aggregation of regioregular poly(3-alkylthiophene). *Communications Chemistry* **2019**, *2* (1), 130.
195. Gassin, P.-M.; Prelot, B.; Gregoire, B.; Martin-Gassin, G., Second-Harmonic Scattering Can Probe Hydration and Specific Ion Effects in Clay Particles. *The Journal of Physical Chemistry C* **2020**, *124* (7), 4109-4113.
196. Pardon, A.; Bonhomme, O.; Gaillard, C.; Brevet, P.-F.; Benichou, E., Nonlinear optical signature of nanostructural transition in ionic liquids. *Journal of Molecular Liquids* **2021**, *322*, 114976.
197. Chen, Y.; Okur, H. I.; Gomopoulos, N.; Macias-Romero, C.; Cremer, P. S.; Petersen, P. B.; Tocci, G.; Wilkins, D. M.; Liang, C.; Ceriotti, M.; Roke, S., Electrolytes induce long-range orientational order and free energy changes in the H-bond network of bulk water. *Science Advances* **2016**, *2* (4), e1501891.
198. Tocci, G.; Liang, C.; Wilkins, D. M.; Roke, S.; Ceriotti, M., Second-Harmonic Scattering as a Probe of Structural Correlations in Liquids. *The Journal of Physical Chemistry Letters* **2016**, *7* (21), 4311-4316.
199. Kim, H. S.; Lee, S. M.; Ha, K.; Jung, C.; Lee, Y.-J.; Chun, Y. S.; Kim, D.; Rhee, B. K.; Yoon, K. B., Aligned Inclusion of Hemicyanine Dyes into Silica Zeolite Films for Second Harmonic Generation. *Journal of the American Chemical Society* **2004**, *126* (2), 673-682.
200. van der Veen, M. A.; Sels, B. F.; De Vos, D. E.; Verbiest, T., Localization of p-nitroaniline chains inside zeolite ZSM-5 with second-harmonic generation microscopy. *J Am Chem Soc* **2010**, *132* (19), 6630-1.

201. Duboisset, J.; Rondepierre, F.; Brevet, P.-F., Long-Range Orientational Organization of Dipolar and Steric Liquids. *The Journal of Physical Chemistry Letters* **2020**, *11* (22), 9869-9875.
202. Zajac, J., Calorimetry at the Solid–Liquid Interface. In *Calorimetry and Thermal Methods in Catalysis*, Auroux, A. E., Ed. Springer Series in Materials Science: 2013; pp 197-270.
203. Houbrechts, S.; Clays, K.; Persoons, A.; Pikramenou, Z.; Lehn, J.-M., Hyper-Rayleigh scattering investigation of nitrobenzyl pyridine model compounds for optical modulation of the hyperpolarisability. *Chemical Physics Letters* **1996**, *258* (3), 485-489.
204. Kondo, J. N.; Nishitani, R.; Yoda, E.; Yokoi, T.; Tatsumi, T.; Domen, K., A comparative IR characterization of acidic sites on HY zeolite by pyridine and CO probes with silica–alumina and  $\gamma$ -alumina references. *Physical Chemistry Chemical Physics* **2010**, *12* (37), 11576-11586.
205. Liu, Y., Is the Free Energy Change of Adsorption Correctly Calculated? *Journal of Chemical & Engineering Data* **2009**, *54* (7), 1981-1985.
206. Teow, Y. H.; Tajudin, S. A.; Ho, K. C.; Mohammad, A. W., Synthesis and characterization of graphene shell composite from oil palm frond juice for the treatment of dye-containing wastewater. *Journal of Water Process Engineering* **2020**, *35*, 101185.
207. Wang, L.; Wang, J.; Pan, H.; Zhao, M.; Chen, J., Kinetics and removal pathway of basic fuchsin by electrochemical oxidization. *Journal of Electroanalytical Chemistry* **2021**, *880*, 114792.
208. Luna, M. A.; Correa, N. M.; Silber, J. J.; Falcone, R. D.; Moyano, F., Properties of AOT reverse micelle interfaces with different polar solvents. *Journal of Physical Organic Chemistry* **2016**, *29* (11), 580-585.
209. Sabarish, R.; Unnikrishnan, G., PVA/PDADMAC/ZSM-5 zeolite hybrid matrix membranes for dye adsorption: Fabrication, characterization, adsorption, kinetics and antimicrobial properties. *Journal of Environmental Chemical Engineering* **2018**, *6* (4), 3860-3873.
210. Yagub, M. T.; Sen, T. K.; Afroze, S.; Ang, H. M., Dye and its removal from aqueous solution by adsorption: A review. *Advances in Colloid and Interface Science* **2014**, *209*, 172-184.
211. Sabarish, R.; Unnikrishnan, G., Polyvinyl alcohol/carboxymethyl cellulose/ZSM-5 zeolite biocomposite membranes for dye adsorption applications. *Carbohydrate Polymers* **2018**, *199*, 129-140.
212. Brião, G. V.; Jahn, S. L.; Foletto, E. L.; Dotto, G. L., Highly efficient and reusable mesoporous zeolite synthesized from a biopolymer for cationic dyes adsorption. *Colloids and Surfaces A: Physicochemical and Engineering Aspects* **2018**, *556*, 43-50.
213. Satilmis, B.; Budd, P. M., Selective dye adsorption by chemically-modified and thermally-treated polymers of intrinsic microporosity. *Journal of Colloid and Interface Science* **2017**, *492*, 81-91.
214. Galarneau, A.; Guenneau, F.; Gedeon, A.; Mereib, D.; Rodriguez, J.; Fajula, F.; Coasne, B., Probing Interconnectivity in Hierarchical Microporous/Mesoporous Materials Using Adsorption and Nuclear Magnetic Resonance Diffusion. *The Journal of Physical Chemistry C* **2016**, *120* (3), 1562-1569.
215. Munthali, M. W.; Elsheikh, M. A.; Johan, E.; Matsue, N., Proton Adsorption Selectivity of Zeolites in Aqueous Media: Effect of Si/Al Ratio of Zeolites. *Molecules* **2014**, *19* (12), 20468-20481.
216. Fideles, R. A.; Ferreira, G. M. D.; Teodoro, F. S.; Adarme, O. F. H.; da Silva, L. H. M.; Gil, L. F.; Gurgel, L. V. A., Trimellitated sugarcane bagasse: A versatile adsorbent for removal of cationic dyes from aqueous solution. Part I: Batch adsorption in a monocomponent system. *Journal of Colloid and Interface Science* **2018**, *515*, 172-188.
217. Faeder, J.; Ladanyi, B. M., Molecular Dynamics Simulations of the Interior of Aqueous Reverse Micelles. *The Journal of Physical Chemistry B* **2000**, *104* (5), 1033-1046.
218. Manzano, H.; Gartzia-Rivero, L.; Bañuelos, J.; López-Arbeloa, I., Ultraviolet–Visible Dual Absorption by Single BODIPY Dye Confined in LTL Zeolite Nanochannels. *The Journal of Physical Chemistry C* **2013**, *117* (25), 13331-13336.
219. Derouane, E. G., Confinement Effects in Sorption and Catalysis by Zeolites. In *Guidelines for Mastering the Properties of Molecular Sieves: Relationship between the Physicochemical Properties of Zeolitic Systems and Their Low Dimensionality*, Barthomeuf, D.; Derouane, E. G.; Hölderich, W., Eds. Springer US: Boston, MA, 1990; pp 225-239.



220. Artioli, N.; Lobo, R. F.; Iglesia, E., Catalysis by Confinement: Enthalpic Stabilization of NO Oxidation Transition States by Microporous and Mesoporous Siliceous Materials. *The Journal of Physical Chemistry C* **2013**, *117* (40), 20666-20674.
221. Kortunov, P.; Vasenkov, S.; Kärger, J.; Valiullin, R.; Gottschalk, P.; Fé Elía, M.; Perez, M.; Stöcker, M.; Drescher, B.; McElhiney, G.; Berger, C.; Gläser, R.; Weitkamp, J., The Role of Mesopores in Intracrystalline Transport in USY Zeolite: PFG NMR Diffusion Study on Various Length Scales. *Journal of the American Chemical Society* **2005**, *127* (37), 13055-13059.
222. Van Aelst, J.; Haouas, M.; Gobechiya, E.; Houthoofd, K.; Philippaerts, A.; Sree, S. P.; Kirschhock, C. E. A.; Jacobs, P.; Martens, J. A.; Sels, B. F.; Taulelle, F., Hierarchization of USY Zeolite by NH<sub>4</sub>OH. A Postsynthetic Process Investigated by NMR and XRD. *The Journal of Physical Chemistry C* **2014**, *118* (39), 22573-22582.
223. Pérez-Ramírez, J.; Mitchell, S.; Verboekend, D.; Milina, M.; Michels, N.-L.; Krumeich, F.; Marti, N.; Erdmann, M., Expanding the Horizons of Hierarchical Zeolites: Beyond Laboratory Curiosity towards Industrial Realization. *ChemCatChem* **2011**, *3* (11), 1731-1734.
224. Shen, Y. R., Surface properties probed by second-harmonic and sum-frequency generation. *Nature* **1989**, *337* (6207), 519-525.
225. Eissenthal, K. B., Second Harmonic Spectroscopy of Aqueous Nano- and Microparticle Interfaces. *Chemical Reviews* **2006**, *106* (4), 1462-1477.
226. Sahu, K.; Eissenthal, K. B.; McNeill, V. F., Competitive Adsorption at the Air–Water Interface: A Second Harmonic Generation Study. *The Journal of Physical Chemistry C* **2011**, *115* (19), 9701-9705.
227. Kim, J. H., Two-step adsorption kinetics of malachite green on anionic polystyrene microspheres in aqueous solution probed by second harmonic generation. *Physical Chemistry Chemical Physics* **2017**, *19* (32), 21887-21892.
228. Martin-Gassin, G.; Benichou, E.; Bachelier, G.; Russier-Antoine, I.; Jonin, C.; Brevet, P. F., Compression Induced Chirality in Dense Molecular Films at the Air–Water Interface Probed by Second Harmonic Generation. *The Journal of Physical Chemistry C* **2008**, *112* (33), 12958-12965.
229. Kim, H. S.; Pham, T. C. T.; Yoon, K. B., A novel class of nonlinear optical materials based on host–guest composites: zeolites as inorganic crystalline hosts. *Chemical Communications* **2012**, *48* (39), 4659-4673.
230. Min, H.; Jeon, Y.; Sung, J.; Seok, S.; Kim, D.; Kim, H.; Yoon, K. B., Determination of Absolute Orientations of Hemicyanine Dyes Incorporated into the Channels of Silicalite-1 Films. *The Journal of Physical Chemistry C* **2007**, *111* (49), 18159-18163.
231. Kim, H. S.; Yoon, K. B., Preparation and characterization of CdS and PbS quantum dots in zeolite Y and their applications for nonlinear optical materials and solar cell. *Coordination Chemistry Reviews* **2014**, *263-264*, 239-256.
232. Bae, Y.-S.; Yazaydin, A. Ö.; Snurr, R. Q., Evaluation of the BET Method for Determining Surface Areas of MOFs and Zeolites that Contain Ultra-Micropores. *Langmuir* **2010**, *26* (8), 5475-5483.
233. Massiot, D.; Fayon, F.; Capron, M.; King, I.; Le Calvé, S.; Alonso, B.; Durand, J.-O.; Bujoli, B.; Gan, Z.; Hoatson, G., Modelling one- and two-dimensional solid-state NMR spectra. *Magnetic Resonance in Chemistry* **2002**, *40* (1), 70-76.
234. Gassin, P.-M.; Girard, L.; Martin-Gassin, G.; Brusselle, D.; Jonchère, A.; Diat, O.; Viñas, C.; Teixidor, F.; Bauduin, P., Surface Activity and Molecular Organization of Metallacarboranes at the Air–Water Interface Revealed by Nonlinear Optics. *Langmuir* **2015**, *31* (8), 2297-2303.
235. Prelot, B.; Ayed, I.; Marchandau, F.; Zajac, J., On the real performance of cation exchange resins in wastewater treatment under conditions of cation competition: the case of heavy metal pollution. *Environmental Science and Pollution Research* **2014**, *21* (15), 9334-9343.
236. Ahmad, M. A.; Prelot, B.; Zajac, J., Calorimetric screening of co-operative effects in adsorption of Co(II) on  $\gamma$ -alumina surface in the presence of Co-complexing anions in aqueous solution. *Thermochimica Acta* **2020**, *694*, 178800.

237. Sauvanier, D.; Li, W. S. J.; Ferlin, N.; Lacroix-Desmazes, P.; Prelot, B.; Hesemann, P., Simple and Straightforward Synthesis of Porous Ionosilica for Efficient Chromate Adsorption. *Israel Journal of Chemistry* **2019**, *59* (9), 843-851.
238. Verboekend, D.; Vilé, G.; Pérez-Ramírez, J., Hierarchical Y and USY Zeolites Designed by Post-Synthetic Strategies. *Advanced Functional Materials* **2012**, *22* (5), 916-928.
239. Sommer, L.; Mores, D.; Svelle, S.; Stöcker, M.; Weckhuysen, B. M.; Olsbye, U., Mesopore formation in zeolite H-SSZ-13 by desilication with NaOH. *Microporous and Mesoporous Materials* **2010**, *132* (3), 384-394.
240. Xing, C.; Yang, G.; Wu, M.; Yang, R.; Tan, L.; Zhu, P.; Wei, Q.; Li, J.; Mao, J.; Yoneyama, Y.; Tsubaki, N., Hierarchical zeolite Y supported cobalt bifunctional catalyst for facilely tuning the product distribution of Fischer–Tropsch synthesis. *Fuel* **2015**, *148*, 48-57.
241. Ji, Y.; Yang, H.; Yan, W., Effect of alkali metal cations modification on the acid/basic properties and catalytic activity of ZSM-5 in cracking of supercritical n-dodecane. *Fuel* **2019**, *243*, 155-161.
242. Ji, Y.; Yang, H.; Zhang, Q.; Yan, W., Phosphorus modification increases catalytic activity and stability of ZSM-5 zeolite on supercritical catalytic cracking of n-dodecane. *Journal of Solid State Chemistry* **2017**, *251*, 7-13.
243. Brião, G. V.; Jahn, S. L.; Foletto, E. L.; Dotto, G. L., Adsorption of crystal violet dye onto a mesoporous ZSM-5 zeolite synthesized using chitin as template. *Journal of Colloid and Interface Science* **2017**, *508*, 313-322.
244. Andreev, A. S.; Livadaris, V., Characterization of Catalytic Materials through a Facile Approach to Probe OH Groups by Solid-State NMR. *The Journal of Physical Chemistry C* **2017**, *121* (26), 14108-14119.
245. Luo, Y.; Li, M.; Lv, X.; Huang, Q.; Chen, X., Fast synthesis of hierarchical nanosized pure Si-Beta zeolite via a steam-assisted conversion method. *Microporous and Mesoporous Materials* **2020**, *293*, 109675.
246. Hailu, S. L.; Nair, B. U.; Redi-Abshiro, M.; Diaz, I.; Tessema, M., Preparation and characterization of cationic surfactant modified zeolite adsorbent material for adsorption of organic and inorganic industrial pollutants. *Journal of Environmental Chemical Engineering* **2017**, *5* (4), 3319-3329.
247. Taffarel, S. R.; Rubio, J., Adsorption of sodium dodecyl benzene sulfonate from aqueous solution using a modified natural zeolite with CTAB. *Minerals Engineering* **2010**, *23* (10), 771-779.
248. Guan, Y.; Wang, S.; Sun, C.; Yi, G.; Wu, X.; Chen, L.; Ma, X., Wet chemical extraction of silicon from natural palygorskite for preparing a mesoporous molecular sieve of Al-SBA-16. *Chemical Papers* **2019**, *73* (11), 2655-2666.
249. Guan, Y.; Wang, S.; Wang, X.; Sun, C.; Wang, Y.; Hu, L., Preparation of mesoporous Al-MCM-41 from natural palygorskite and its adsorption performance for hazardous aniline dye-basic fuchsin. *Microporous and Mesoporous Materials* **2018**, *265*, 266-274.
250. Huang, L.; Kong, J.; Wang, W.; Zhang, C.; Niu, S.; Gao, B., Study on Fe(III) and Mn(II) modified activated carbons derived from *Zizania latifolia* to removal basic fuchsin. *Desalination* **2012**, *286*, 268-276.
251. Rytting, E.; Bryan, J.; Southard, M.; Audus, K. L., Low-affinity uptake of the fluorescent organic cation 4-(4-(dimethylamino)styryl)-N-methylpyridinium iodide (4-Di-1-ASP) in BeWo cells. *Biochem Pharmacol* **2007**, *73* (6), 891-900.
252. Kumal, R. R.; Nguyenhuu, H.; Winter, J. E.; McCarley, R. L.; Haber, L. H., Impacts of Salt, Buffer, and Lipid Nature on Molecular Adsorption and Transport in Liposomes As Observed by Second Harmonic Generation. *The Journal of Physical Chemistry C* **2017**, *121* (29), 15851-15860.
253. Gassin, P.-M.; Martin-Gassin, G.; Prelot, B.; Zajac, J., How to distinguish various components of the SHG signal recorded from the solid/liquid interface? *Chemical Physics Letters* **2016**, *664*, 50-55.
254. Gounder, R.; Iglesia, E., The Roles of Entropy and Enthalpy in Stabilizing Ion-Pairs at Transition States in Zeolite Acid Catalysis. *Accounts of Chemical Research* **2012**, *45* (2), 229-238.

255. Messina, P. V.; Schulz, P. C., Adsorption of reactive dyes on titania–silica mesoporous materials. *Journal of Colloid and Interface Science* **2006**, *299* (1), 305-320.
256. Somasundaran, P.; Shrotri, S.; Huang, L., Thermodynamics of adsorption of surfactants at solid-liquid interface. *Pure and Applied Chemistry* **1998**, *70* (3), 621-626.

## Conclusion

This paper presented the results of the evolution of the adsorption of dyes at the local and global scales. The study of the solid-liquid interface at the global scale represents a key element to a better understanding of the interactions taking place between the probe molecules and the zeolite. In parallel, the organization of molecules at the solid/liquid interface has been estimated at the local scale.

The impact of the porous modification can lead to a change in the surface chemistry of the material. The crystallinity is reduced with modification. However, the Si/Al ratio remains constant for all FAU, except for the highest modification with a decrease from 15 to 13 is obtained. In addition, the microporous volume increases while the mesoporous volume decreases. A local transformation from  $Q^4$  to  $Q^3$  is also observed.

For the linear dye, sDiA, the adsorption capacity is constant for FAU-0, 1, and 2 (600  $\mu\text{mol/g}$ ) while a decrease is observed for FAU-3 (400  $\mu\text{mol/g}$ ). However, in the case of a bulky molecule, BF, the adsorption capacity increases successively with mesoporosity from 100 to 400  $\mu\text{mol/g}$ . we conclude that sDiA adsorb inside the pores whereas BF adsorb only at the external surface of the micropores. As mentioned in the previous article, the confinement effect depends on the frozen movement of the molecule. With increasing porosity, the molecular movement of the linear dye becomes freer.  $I_4$  parameter shows a high absolute value for sDiA in FAU-0. Therefore, sDiA is confined in micropores material, thus the most organized system with a strong correlation between molecules. From the calorimetric measurement, we succeeded in distinguishing the enthalpy of adsorbed molecules in micro and mesopores, the first and second regimes respectively. Furthermore, a decrease in the absolute value of the global enthalpy of sDiA and BF with increasing porosity is noticed.

This complete study has clearly shown that the organization of molecules and their correlation at the solid/liquid interface has a high contribution to the global enthalpy.



## **CONCLUSIONS and PERSPECTIVES**

The initial idea of this Ph.D. thesis was to study the adsorption and organization of molecules at solid-liquid interfaces. To carry out this work, two approaches were proposed and combined. The first approach consisted in adsorbing the dyes molecules to determine the adsorption capacity from the adsorption isotherm and determine the interaction between the molecules and the materials by measuring the global enthalpy using isothermal titration calorimetry (ITC). This approach is referred to as a macroscopic scale study. The second approach was developed to evaluate the correlation and the organization of molecules at the local scale using nonlinear optics (NLO), in particular second harmonic scattering (SHS).

Faujasites, chosen for this work, are porous materials with unique properties (acidity, large specific surface area, shape selectivity, and thermal and hydrothermal stability). Their particular microporous structure limits, however, the accessibility of the molecules to the active sites. This is one of the reasons why hierarchical materials are currently developed. Nevertheless, in such materials, the simultaneous presence of micro, meso, and macropores could modify the sorption behavior, with possible effects on the adsorption capacity, adsorption kinetics (diffusion, transport) together with impacts on the interaction of adsorbed molecules with the surface, their correlations, or even their self-assembly. Therefore, the other objective of this project was to relate the properties of confined molecules in the presence of hierarchical porosity at the interface.

Thus, to test the accessibility parameter for organic large molecules, we have modified the texture of zeolites by creating a secondary network of mesopores within their crystals. The combination of two strategies was successfully used, a demetallization technique called desilication, which creates mesopores by partial dissolution of the zeolite; and a second one, called recrystallization which allows the creation of a controlled mesoporosity using a structuring agent. Zeolites with porosity varying from 1 nm to 4 nm were made to study the adsorption of dyes on multi-porosity levels.

To make sure that the variation upon modification is just on the porosity level of the material without aiding in changing the chemical structure of it. Thus, in order to verify this, Si solid NMR measurements and other characterization techniques must be done.

During this thesis work, we have highlighted the textural and porous changes created during the treatment by  $^{29}\text{Si}$ -NMR and nitrogen adsorption/desorption, thanks to the quantitative analysis of the silicon environment, on the one hand, and of the mesoporous volume on the other hand.  $^{29}\text{Si}$ -NMR

reveals the modification of the surface chemistry can be also observed by the adsorption of organic molecules at the solid/liquid interface. The same molecule showed different adsorption behavior towards the materials with different porosity. N<sub>2</sub> sorption isotherms evidence an increase in mesoporous volume and a decrease in microporous volume. The chemical composition of the hierarchical zeolites was determined by X-ray Fluorescence. Silicon oxide is predominantly present in these materials. The aluminum oxide is found in appreciable quantity. The Si/Al ratio for FAU used is equal to 15. This ratio kept constant for almost all modifications except for a highly modified FAU where a reduction in the Si/Al ratio from 15 to 13 was observed.

The introduction of a secondary network of mesopores in faujasite by the desilication - recrystallization method further improves the adsorption capacity of the bulky molecules by enhancing the accessibility of the active sites. Basic fuchsin (BF) is a bulky dye with a bigger size compared to the FAU natural micropore size. The adsorption of BF occurs only at the external surface of FAU with a low sorption capacity, 150 µmol/g. However, with increasing the mesoporosity, this capacity increases until reaching the maximum of 400 µmol/g.

In this work, many parameters were investigated to modulate and fundamentally understand adsorption processes. The cationic exchange capacity, the solvent medium, and the ability of the molecules to enter the zeolitic pores can control the adsorption properties then we investigate the guest-host interactions by varying these conditions. The highly confined system depends on the optimum charge inside the material, thus higher correlation. 1-DiA in FAU720 in water solvent shows the highest correlation in the system. Optimization of the adsorption protocol has been developed under several conditions (solid/liquid ratio, sonication of FAU suspension, contact time between dye and FAU suspension, effect of time on stability of FAU suspension, heat, and ionic strength).

The adsorption capacity of the organic molecules varies depending on the properties of the adsorbed molecule (size, charge, and functional group), the property of the material (mesoporosity, microporosity, and Si/Al ratio), and the solvent medium. In the case of cationic bulky molecules (malachite green, crystal violet, rhodamine B), the adsorption capacity varies between 100 and 150 µmol/g while for the small molecules the sorption capacity reaches 650 and 800 µmol/g for auramine-O and methylene blue respectively. A low capacity is observed for methyl orange, a negative dye, because of the electrostatic repulsion between the FAU negative surface and the dye. However, in the case of neutral molecule, the sorption capacity varies with the size which it is 100 and 350 µmol/g for oxytetracycline HCl and morantel tartrate Hydrate respectively.

In the paper "The driving forces of cationic dye adsorption, confinement and long range correlation in Zeolitic Materials" we worked on 2D molecule in contact with a microporous faujasite.

We highlight in this works the effect of solvent and the Si/Al ratio to feature the most correlated system. The linear dye, sDiA, gives high adsorption capacity, 600  $\mu\text{mol/g}$ , which reveals an internal adsorption. This dye is confined inside the FAU pores produces high absolute enthalpy of adsorption, -47.9 KJ/mol, and a strong organization of molecules at the interface measured by the correlation parameter in SHS.

In the paper “Effect of modification of the porosity of Zeolite FAU on the adsorption of dyes: contribution of global and local techniques” we worked on two kinds of molecular geometry: linear (sDiA) and bulky (BF) dyes in contact with a various induced porosity faujasite. We highlight in this works the effect of porosity on the adsorption behavior. For the hierarchical FAU with increasing porosity, the sDiA sorption capacity kept constant except for the highly modified FAU, this capacity decreases to be 400  $\mu\text{mol/g}$ . However, for the bulky dye (BF), the adsorption capacity increases with porosity from 150 to 400  $\mu\text{mol/g}$ . Thanks to the SHS measurements that permit the evaluation of the organization and correlated molecules at the interface with different porosity level. In large pores, measurements show less correlations in the system, the molecules seem to be less organized.

The schematic overview presented in Figure 87 summarizes the main conclusions obtained within the framework of this thesis. This was reflected by understanding the interfacial organization of contaminants at the solid/liquid interface using the combination of both techniques.

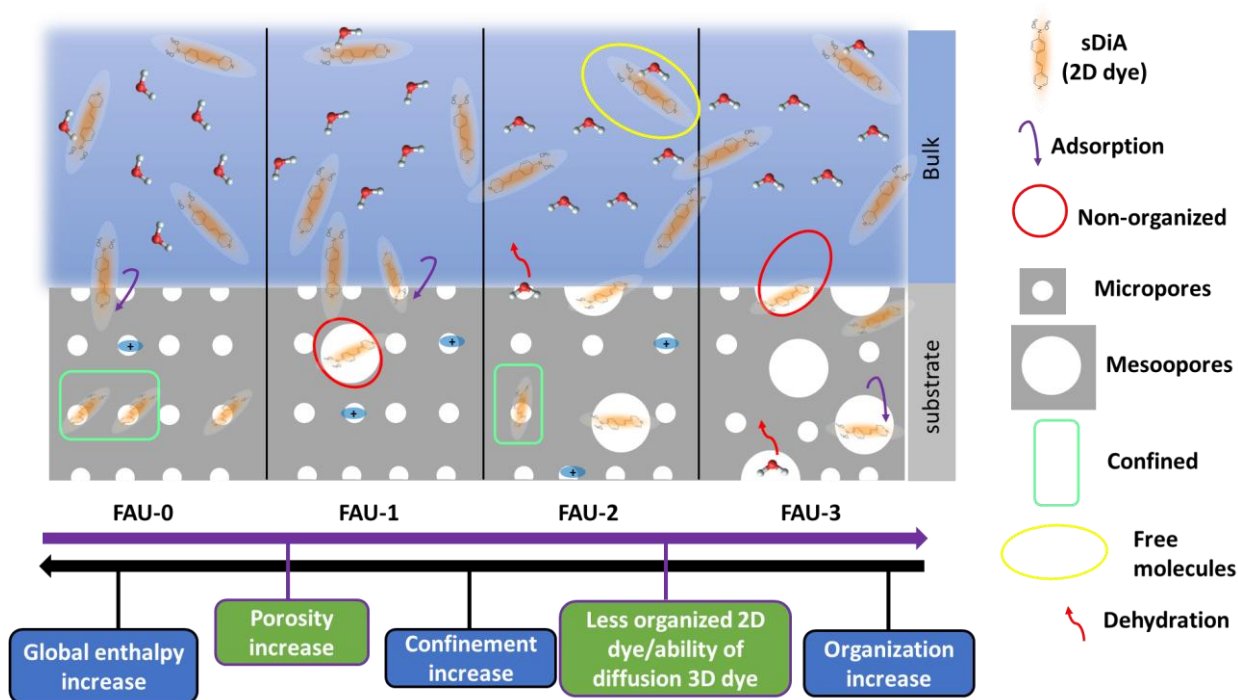


Figure 87 : Schematic overview of the objectives achieved in the framework of this PhD thesis. It shows the adsorption behavior of 2D dyes at the solid/liquid interface. The adsorption of 2D dye molecules (purple flash) on an active site is associated with a loss of water molecules around it forming an enthalpy of dehydration (red flash). These dyes, enter the



*FAU pore and become confined and thus forming the enthalpy of adsorption. The global enthalpy of adsorption, the organization of molecules as well as the confinement effect decreases with increasing FAU porosity.*

In Figure 87, the size of 2D dyes allows the entrance and confinement of molecules in the microporosity (FAU-0). In this case, the molecules are organized at the interface thus the global enthalpy of adsorption is high. Modification in the level of porosity was carried out by dissolving the commercial FAU with NaOH in the presence of a surfactant agent. Depending on the NaOH/Si ratio various porosity has been obtained. In the case of multiscale porosity, the molecules become less organized and less confined and the global enthalpy reduces in absolute value. However, this mesoporosity permits the diffusion of 3D bulky molecules.

This work was the first coupling between the thermodynamic approach and SHS approach which showed a great correlation between the two for the adsorption system (dyes-zeolite) and especially at the different scales (macro and local) however, this opens new perspectives to study on new systems the correlation between these two approaches listed before.

First, the reusability of the material will be a good idea to test. Desorption study as a function of concentration and time could be interested to evaluate the confinement effect of dyes inside the pores. The more time it takes to be desorbed, the more confined system will be, also in correlation with the strength of the interaction.

Second, Other types of molecules (malachite green, crystal violet) are to be adsorbed onto hierarchical FAU. These dyes have high polarizability as reported in the literature, therefore they are a good probe molecule to be studied in SHS in order to see their adsorption behavior at the local scale.

In addition, Malachite green with different counterions has been tested and shows different adsorption behavior towards faujasite. Many hypotheses have been reported to explain the obtained result and SHS to investigate the organization and/or orientation of these molecules. However, a complementary study like enthalpic measurement will help to evaluate the strength of interaction for both systems. Malachite green is highly dependent on the pH, so it will be also interesting to probe the pH since the ionization constant of MG change as a function of pH.

sDiA showed interesting results with hierarchical FAU in water medium. It would be attractive to see the effect of solvent as well as the different hydrophobicity levels of the molecules on the sorption behavior in the presence of different porosity. In addition, it is also interesting to perform experiments with different ethanol/water ratios since dyes are more soluble in ethanol so the hydration/dehydration effect could be different. It would be noteworthy also to measure the global

enthalpy of adsorption of these systems by ITC in the presence of ethanol solvent. This will help to produce a complete description of the sorption behavior using these two approaches.

The SHS measurements of the adsorbed dyes at the interface have proved to be an important technique at the local scale and we have proposed a software allowing the theoretical analysis of the systems. PySHS software, developed in our laboratory with Pierre-Marie Gassin, is an efficient tool to interpret and compare the SHS results with the experimental results. It would be interesting to continue this work by testing different geometries.